A network-level investigation of signalling crosstalk and drug response in aggressive breast cancer

Constance Gaya Cremers

BSc (First Class Honours)

Master of Philosophy

Biochemistry and Molecular Biology

July 2019

Department of Biochemistry and Molecular Biology

Biomedicine Discovery Institute

Monash University

Copyright notice

© Constance Gaya Cremers (*2019*)

I certify that I have made all reasonable efforts to secure copyright permissions for third-party content included in this thesis and have not knowingly added copyright content to my work without the owner's permission.

Abstract

Resistance to targeted anti-cancer drugs is a complex phenomenon and a major challenge in cancer treatment. It is becoming increasingly evident that a form of acquired drug resistance known as 'adaptive resistance' is a common cause of treatment failure and patient relapse in many cancers. Unlike classical resistance mechanisms that are acquired via genomic alterations, adaptive resistance is instead driven by non-genomic changes involving rapid and dynamic rewiring of signalling networks following therapy, enabled by complex pathway crosstalk and feedback regulation. Such network rewiring allows tumour cells to adapt to the treatment, circumvent the initial drug challenge and continue to survive in the presence of the drug. Despite its great clinical importance, adaptive resistance and drug-induced network adaptation remain largely under-studied and poorly defined. This thesis focuses on a network-level investigation of potential adaptive mechanisms to MAPK and PI3K pathway inhibitors and the use of combinational treatments in breast cancer, with an emphasis on triple-negative breast cancer (TNBC), a highly aggressive breast cancer subtype which currently has no effective targeted therapies.

To address the complexities of drug response and signalling crosstalk, our research combined experimental investigations with mathematical modelling. This integrative systems-based approach has emerged as a powerful method to capture network dynamics, allowing a quantitative understanding of the complex drug-induced network re-wiring. We were particularly interested in how loss of the tumour suppressor PTEN influences PI3K-ERK signalling and the response to PI3K and MEK inhibition. To address this, we utilised both newly genetically modified MCF10A cells and established TNBC cell lines. Specifically, a PTEN KO model was generated by CRISPR/Cas9-based gene editing to knockout PTEN in the non-tumorigenic human mammary epithelial cell line MCF10A. This approach generated isogenic PTEN KO cells, thus creating a unique model in which only PTEN was perturbed, enabling us to examine the direct effects of PTEN loss on drug response and network changes.

As expected, loss of PTEN resulted in significant upregulation of PI3K signalling in the PTEN KO cells. Interestingly, PTEN loss also led to upregulated phosphorylation of STAT3 on tyrosine 705 (Tyr705), which suggests a novel role for PTEN in regulating STAT3 activity in breast cancer cells. Importantly, PTEN loss led to reduced sensitivity to the PI3Kα inhibitor BYL719, but did not alter the response to MEK inhibition using trametinib, therefore suggesting that in this model PTEN loss influenced the PI3K pathway, but did not affect the MAPK signalling pathway. In response to treatment with selective PI3Kα isoform inhibitors, higher AKT activity was observed in the PTEN KO clones and this correlated with increased cell survival compared to WT MCF10A cells. Rescue experiments reintroducing PTEN back into these KO clones reversed this effect indicating that PTEN was driving this reduced sensitivity.

In order to examine whether the effect by PTEN loss was due to preferential activation of p110β-dependent PI3K signalling observed in many PTEN-loss tumours and cell lines, dual treatment with both selective PI3Kα (BYL719) and β (AZD6482 and TGX221) inhibitors was carried out. Our findings showed that PTEN loss as a single event did not result in a switch to the PI3Kβ as the dominant isoform in driving PI3K signalling, suggesting instead that cells harbouring PTEN loss retained parental PI3Kα isoform dominance of the wild-type MCF10A cells. Importantly, independent of PTEN status, dual PI3K p110α/β inhibition was synergistic in supressing PI3K activity in both the WT and PTEN KO MCF10A cells as well as in the TNBC cell lines, MDA-MB-468 and BT-549. Interestingly, we observe that ERK signalling is transiently inhibited by PI3K inhibition in both the WT and PTEN KO cells, and displayed a rebound in activity after 6 hours following drug treatment, thus indicating a positive link from PI3K signalling to ERK. However, when MEK was inhibited suppression of PI3K signalling was not observed suggesting the observed PI3K-ERK crosstalk occurred in a unidirectional manner. To put our experimental data in a unified context, we constructed a new mathematical model interlinking the PI3K and ERK-MAPK signalling networks, and calibrated this model using existing data. Using the model, we performed simulations to interrogate the rebound activation of ERK following PI3K inhibition, and the effect of PTEN loss on network behaviours and drug response.

In summary, the work in this thesis has provided novel systems-level insights into the crosstalk between PI3K and ERK signalling, and examines how common genetic alterations in breast cancer such as PTEN loss would influence such crosstalk to modulate response to drugs targeting these pathways. The mathematical model generated in this work further provides a quantitative framework for future investigation of adaptive drug resistance and combination treatment related to PI3K-ERK signalling in breast cancer.

Declaration

This thesis is an original work of my research and contains no material which has been accepted for the award of any other degree or diploma at any university or equivalent institution and that, to the best of my knowledge and belief, this thesis contains no material previously published or written by another person, except where due reference is made in the text of the thesis.

Author: Constance Gaya Cremers

Date: 31st July 2019

Acknowledgments

Completing my Masters as an international student was by no means an easy task and it required lots of blood, sweat and tears and tremendous amounts of grit. To all the people who helped me on this research journey and supported me along the way, I am most grateful and wish to pay my gratitude. Firstly, I wish to acknowledge and thank my main supervisor Dr Lan Nguyen for giving me this great opportunity to move to Australia to pursue a post-graduate research degree at Monash University in Melbourne. I wish to thank him for the challenges presented, and for giving me his guidance and support. I would also like to thank my co-supervisor Professor Roger Daly for his support and expert advice. I am grateful to my committee panel members; Professor David Jans, Professor Anthony Purcell and Dr Antonella Papa for their constructive feedback and guidance at milestones. I would also like to thank Mibel Aguilar and Amelia Morrison for their help and support along the way. A special thanks to Priscilla Johanesen for her support, compassionate understanding and for being generous with her time.

I would like to acknowledge and thank all the members of the Daly and Nguyen labs, both past and present, for being such friendly and helpful individuals, who together created a friendly lab environment and office space to work in. In particular, I want to thank Dr Sungyoung Shin for all his valued collaborative work and effort on the modelling component of my project. I also want to thank the postdocs in our lab both past and present; Dr Rachel Lee and Dr Hugh Ma, respectively, for their guidance and expertise.

A special thanks to Howard Chan, past lab manager and research assistant, for his unique friendship, good humour and continuous support throughout my studies. His help and encouragement both in and outside the lab helped me stay on course despite the many bumps I encountered along the way. To my friend, postdoc and fellow co-worker Dr Mimi Nguyen I would like to thank you for your lively and spirited friendship, and for reintroducing me to using Prism for data analysis. Your friendship allowed me to strike a better work-life balance and you were a constant reminder to get outdoors, enjoy the sun or do something fun.

To all the PhD students from both labs thank you for being a part of this journey and I wish you all the best in your research. To Mandy Theocharous, thanks for your help with lab duties, we made a good lab clean-up team. Also thank you for our late morning coffee runs and much needed chats, they will be missed. A special thanks to Karina Islas and her husband Erick Vargas for their friendship, support, great cooking and awesome company on all our amazing road trips together.

I would also like to thank my family back home in Ireland and the UK, for their support and for providing a safe place where my research couldn’t reach. They never fully understood exactly what it was that I was doing in the lab, but I knew they were always there if needed and supported my journey

here in Melbourne. I would like to thank all my friends, whom provided me a healthy break and happy distraction to rest my mind outside of my research. A special thanks to Mehdi Youssefi for his empathetic support during the writing process and his help with the formatting and proofreading of my thesis. He taught me many new word doc processing skills. Last, but not least, I want to thank my partner and best friend Sam Heberlein for her unconditional support and belief in me.

Table of Contents

List of Abbreviations

aa	Amino acid
ABL1	Abelson murine leukemia viral oncogene homolog 1
ALL	Acute lymphocytic leukemia
AR	Androgen receptor
ATCC	American Type Culture Collection
ATP	Adenosine triphosphate
BC	Breast cancer
BET	Bromodomain and extra-terminal motif
BFP	Blue fluorescent protein
BL-1	Basal-like 1
BL-2	Basal-like 2
bp	Base pair
BRCA1	Breast cancer 1
BRCA2	Breast cancer 2
BRD2/3/4	Bromodomain-containing proteins 2, 3 and 4
BSA	Bovine serum albumin
CDC42	Cell division cycle 42
CK2	Casein kinase 2 (also known as CSNK2)
CML	Chronic myeloid leukemia
c-MYC	Cellular myelocytomatosis proto-oncoprotein
CNV	Copy Number Variation
COSMIC	Catalogue of Somatic Mutations in Cancer
CRISPR	Clustered regularly interspaced short palindromic repeats
C-terminus	Carboxyl terminus
DMSO	Dimethyl sulfoxide
DNA	Deoxyribonucleic acid
dNTPs	Deoxyribose nucleoside triphosphates
dsRNA	Double stranded RNA
EcoR	Ecotropic receptor
EDTA	Ethylenediamine tetra-acetic acid
EGF	Epidermal growth factor
EGFR	Epidermal growth factor receptor
EMT	Epithelial to mesenchymal transition

EphA7	Ephrin type-A receptor 7
ER	Estrogen receptor
ERK	Extracellular signal-regulated kinase (also known as MAPK)
ERK1/2	Extracellular regulated kinase 1 and 2
FAK	Focal adhesion kinase
FBS	Foetal bovine serum
FOXO	Forkhead box O
Gab1	GRB2-associated-binding protein
GDP	Guanosine-diphosphate
GEF	GTPase exchange factor
GEMMS	Genetically engineered mouse models
GFP	Green fluorescent protein
GLI1	Glioma oncogene homolog
GPCR	G-protein coupled receptors
GRB2	Growth factor receptor-bound protein 2
GSK3B	Glycogen synthase kinase 3 beta
GTP	Guanosine-triphosphate
HDR	Homology directed DNA repair
HEPES	4-(2-hydroxyethyl)-1-piperazineethanesulfonic acid
HER2	Human epidermal growth factor receptor 2, also known as ERBB2
HER3	Human epidermal growth factor receptor 3, also known as ERBB3
HRP	Horse radish peroxidase
ICTV	International committee on taxonomy of viruses
IGF-1R	Insulin-like growth factor 1 receptor
IM	Immunomodulatory
INPP4B	Inositol polyphosphate-4-phosphatase type II B
IR	Insulin receptor
IRS	Insulin receptor substrate
JAK	Janus kinase
kb	Kilobase
K_d	Equilibrium dissociation constant
KD	Knockdown
kDa	Kilodalton
KO	Knockout
LAR	Luminal androgen receptor

LB	Lysogeny broth
LOH	Loss of heterozygosity
M	Mesenchymal
MAPK	Mitogen-activated protein kinase (Also known as ERK)
MEK1/2	Mitogen-activated protein kinase kinase 1/2
MM	Michaelis-Menten
MSL	Mesenchymal stem-like
mTOR	Mammalian/Mechanistic target of rapamycin
mTORC1	Mammalian/Mechanistic target of rapamycin complex 1
mTORC2	Mammalian/Mechanistic target of rapamycin complex 2
NFL	Negative feedback loop
NHEJ	Non-homologous end joining
ODEs	Ordinary differential equations
PBD	PIP2-binding domain
PBS	Phosphate buffered saline
PCR	Polymerase chain reaction
PDGFR	Platelet-derived growth factor receptor
PDK1	Pyruvate dehydrogenase kinase
PDZ	Postsynaptic density protein
PES	Phenazine ethosulfate
PEST	Proline, glutamic acid, serine, threonine
PFL	Positive feedback loop
PH	Pleckstrin homology
pH	Power of hydrogen
PI3K	Phosphoinositide 3-kinase
PIK3CA	Phosphatidylinositol-4,5-bisphosphate 3-kinase catalytic subunit alpha
PIP	Phosphatidylinositol phosphate
PIP2	Phosphatidylinositol 4,5-bisphosphate
PIP3	Phosphatidylinositol 3, 4, 5-trisphosphate
PKB	Protein kinase B also known as AKT
PMSF	Phenylmethane sulfonyl fluoride
PR	Progesterone receptor
PTB	Phosphotyrosine binding
P-TEFb	Positive transcription elongation factor b
PTEN	Phosphatase and tensin homolog deleted on chromosome 10

PYK2	Proline-rich tyrosine kinase 2
QSSA	Quasi-steady state assumption
RAS	Rapidly accelerated fibrosarcoma
RB1	Retinoblastoma protein 1
RBD	RAS-binding domain
RET	Rearranged during transfection
RhoA	RAS homolog family member A
RIPA	Radioimmunoprecipitation assay
RNA	Ribonucleic acid
RNAi	RNA interference
rpm	Revolutions per minute
RPMI	Roswell park memorial institute
RPPA	Reverse-phase protein array
rRNA	Ribosomal ribonucleic acid
RTK	Receptor-type tyrosine kinase
S6K	p70 S6 kinase
SDS-PAGE	Sodium dodecyl sulphate-Polyacrylamide gel electrophoresis
sgRNA	Single guide RNA
shRNA	Short-hairpin RNA
siRNA	Small interfering RNA
SOS	Son of Sevenless
STAT	Signal transducer and activator of transcription
TAE	Tris-acetate-EDTA
TBS	Tris buffered saline
TBST	Tris buffered saline with Tween 20
TEMED	N, N, N', N'-tetramethylethane-1,2-diamine
TNBC	Triple-negative breast cancer
Tris	Tri(hydroxymethyl) aminomethane
tRNA	Transfer ribonucleic acid
UTR	5′-Untranslated Region
UV	Ultraviolet
v/v	Volume per volume
VEGFR	Vascular endothelial growth factor receptor
w/v	Weight per volume
WT	Wild-type

Chapter 1: Literature Review

1.1 Introduction to BC and the aggressive subtype; TNBC

This research focuses on understanding how the loss of the tumour suppressor gene phosphatase and tensin homolog deleted on chromosome 10 (PTEN) influences the phosphoinositide 3-kinase (PI3K) and extracellular signal-regulated kinase (ERK) signalling pathways, and the adaptive response to PI3K and ERK inhibition in an aggressive subtype of breast cancer (BC) known as triple-negative breast cancer (TNBC). To investigate the role of PTEN loss in mediating adaptive resistance to PI3K and MEK inhibitors, drug treatment experiments were conducted on both genetically modified MCF10A cells with PTEN knockout (KO) and the TNBC cell lines MDA-MB-468 and BT-549 which harbour PTEN deletion (PTEN −/−) as well as the TNBC cell line SUM185PE which harbours a phosphatidylinositol-4,5-bisphosphate 3-kinase catalytic subunit alpha mutation (PIK3CA mut). These cells were treated with kinase inhibitors, PI3K inhibitor BYL719 or MEK inhibitor trametinib and cell growth and signalling results of both the mitogen-activated protein kinase (MAPK) and PI3K pathways were analysed. This literature review aims to highlight the importance of such work in tackling the current gaps of knowledge in drug resistant mechanisms. Treatment failure due to drug resistance is a major cause of breast cancer patient relapse and death. In order to overcome this, we need to better understand how cancer cells rewire the network in response to targeted inhibition promoting resistance. This work also aims to emphasize the power of utilizing an integrated systems-based approach which combines mathematical modelling with experimental investigations, in understanding the complexity of drug-induced network re-wiring in breast cancer cells.

1.1.2 Breast cancer: A highly heterogeneous disease with multiple subtypes

Cancer is the second most common cause of death worldwide (Mortality and Causes of Death 2016). Breast cancer accounts for almost a quarter of all cancer cases, and according to the Cancer Council Australia is the most common cancer in women and after lung cancer, the second leading cause of cancer death among women in Australia. In 2012 there were 1.7 million new cases diagnosed (Torre, Bray et al. 2015). Moreover, 1 in 8 women in Australia are at risk of developing breast cancer before the age of 85 (Youlden, Cramb et al. 2014). Breast cancer is a heterogeneous disease which can be classed into 6 main intrinsic molecular subtypes based on gene expression profiling (**Table 1.1**) These are estrogen receptor positive (ER+) luminal A and B, human epidermal growth factor receptor 2 (HER2) enriched, normal-like, basal-like breast cancer (BLBC) (Perou, Sorlie et al. 2000) and claudin-low (Prat, Parker et al. 2010). The different molecular subtypes are associated with different outcomes (Sorlie, Perou et al. 2001).

Table 1.1 Molecular classification of breast cancer subtypes and their characteristics.

Subtypes	Molecular Characteristics	Frequency
Luminal A	ER (+) and/or PR (+), HER2 (-)	40%
Luminal B	ER (+) and/or PR (+), HER2 (+)	20%
HER2+	ER (-), PR (-), HER2 (+)	10-15%
Basal-like	ER (-), PR (-), HER2 (-), cytokeratin 5/6 (+) and/or EGFR (+), high genome instability, worst prognosis, shortest survival, BRCA1/2 mutations	10-20%
Normal-like	Expressing genes characteristic of adipose tissue. p53 positive. Least characterised. Similar gene expression profile to normal breast tissue.	2-4%
Claudin-low	Low ER expression, low expression of E-cadherin, stem cell-like features, high genome instability, most undifferentiated tumour.	10-14%

Adapted from (Sorlie, Perou et al. 2001, Malhotra, Zhao et al. 2010, Gajulapalli, Malisetty et al. 2016)

1.1.3 Triple-negative breast cancer

An extremely aggressive subset of breast cancer which currently has no effective targeted therapy available for its treatment is TNBC. As the name suggests TNBC is defined histologically by low or absent expression of the hormone receptors; estrogen receptor (ER), progesterone receptor (PR) and no human epidermal growth factor receptor 2 (HER2) over-amplification. TNBC more frequently affects younger women, accounts for 10-20% of all breast cancers (Anders and Carey 2009, Chavez, Garimella et al. 2010) and has as a higher incidence in African Americans (Amirikia, Mills et al. 2011) and Hispanic women (Cintra, Teixeira et al. 2012). TNBC patients often have biologically more aggressive, larger sized tumours of higher grade with lymph node involvement at diagnosis and a poor prognosis compared to the other subtypes (Haffty, Yang et al. 2006).

TNBC is a highly heterogeneous subgroup of cancers and based on gene expression studies first shown by Lehmann et al. in 2011 (Lehmann, Bauer et al. 2011) it can be further subdivided into 6 molecular subtypes which display marked differences in responses to treatment and have different clinicopathological features. These subtypes are immunomodulatory (IM), mesenchymal (M), mesenchymal stem-like (MSL), basal-like 1 and basal-like 2 (BL1 and BL2) and a luminal androgen receptor (LAR) subtype. It is important to note that basal-like breast cancer (BLBC) and TNBC are not synonymous (Rakha, Tan et al. 2007, Gazinska, Grigoriadis et al. 2013) with about 30% discordance between the two groups. Based on gene expression analysis approximately 80% of BLBC are triple negative and about 75-80% of TNBC possess basal-like phenotype (Perou, Sorlie et al. 2000, Brenton, Aparicio et al. 2001, Carey, Perou et al. 2006) sharing common molecular features including poor prognosis (Dent, Trudeau et al. 2007) and a propensity for metastasis to the brain (Weigelt, Baehner et al. 2010, Lehmann, Bauer et al. 2011). Characteristic BLBC expression signatures are characterised by

keratins 5, 6 and 17, high expression of proliferation associated genes, and increased incidence of BRCA1/2 mutations, and/or epidermal growth factor receptor (EGFR) expression (Sorlie, Perou et al. 2001, Malhotra, Zhao et al. 2010). The remaining non-basal TNBC are associated with the other aforementioned intrinsic subtypes; IM, M, MSL and LAR.

Due to the absence of well-defined molecular targets in TNBC, no targeted therapy is available for its treatment. Thus, both early and advanced stages are treated predominantly with adjuvant chemotherapy (Brenton, Aparicio et al. 2001, Dent, Trudeau et al. 2007). Despite initial success with pre-surgical (neoadjuvant) chemotherapy, TNBC patients still have higher rates of metastasis than other subtypes (Haffty, Yang et al. 2006, Dent, Trudeau et al. 2007) with less than 30% of women with metastatic TNBC survive 5 years (Dent, Trudeau et al. 2007). Furthermore, there is also high rate of relapse due to the development of drug resistance, often leading to patient death. Thus, there is an urgent unmet medical need to identify new targetable drivers of TNBC for developing new targeted therapies.

1.1.4 PI3K and MAPK pathways in BC: key drivers of oncogenesis

Cancer is a highly complex, multi-step, multi-mechanism network disease which is in part driven by the dysfunction of signal transduction networks. This disease is characterised by the uncontrolled proliferation of genetically unstable cells which leads to tumour initiation, progression and invasion (Hanahan and Weinberg 2011). The enormous plasticity and adaptability of cancer cells can be attributed to this network dysregulation which enables them to be highly resilient against both internal and external assaults such as drug treatment. This characteristic is termed robustness and assists cancer cells in developing resistance to anti-cancer therapies.

Cancer is characterised by frequent disruption of key intracellular signal transduction pathways including the PI3K pathway also known as the PI3K-AKT-mechanistic target of rapamycin (mTOR) pathway and the MAPK pathway often known as the rapidly accelerated fibrosarcoma (RAS) -RAF-MEK-extracellular signal-regulated kinase (ERK) signal cascade, Janus kinase (JAK)-signal transducer and activator of transcription (STAT) pathway as well as the EGFR and tyrosine protein kinase MET (c-MET) pathways. An abundance of evidence exists across many different cancer types that the deregulation of these signalling pathways are key oncogenic drivers, promoting tumour initiation and progression (Smalley 2003, McCubrey, Steelman et al. 2007, Mundi, Sachdev et al. 2016). The receptor and protein kinase components of these pathways are therapeutic targets currently under investigation, with numerous drugs targeting these already developed and used in the clinic (Crown, O'Shaughnessy et al. 2012, Kalimutho, Parsons et al. 2015) (**Figure 1.1**). Yet, network rewiring and adaptive resistance represent major obstacles that limit the full clinical potential of these inhibitors.

Located downstream of receptor-type tyrosine kinases (RTKs) and G-protein coupled receptors (GPCRs) the MAPK and PI3K pathways are two highly interconnected, signalling cascades which

critically regulate oncogenesis by playing central roles in cell functions such as cell growth, proliferation, migration and survival (**Figure 1.1**). These pathways are not independent, but in fact intersect to regulate each other and co-regulate downstream functions. Such crosstalk results in a complex PI3K-MAPK signalling network, many nodes of which are targeted by inhibitors such as PI3K, AKT, ERK, mTOR and RAF inhibitors (**Figure 1.1**). In the MAPK pathway, upon activation of EGFR by growth factor binding such as EGF adaptor molecules like growth factor receptor-bound protein 2 (GRB2) associates with activated EGFR, which then recruits the guanine nucleotide exchange factor (GEF) known as Son of Sevenless (SOS), to the plasma membrane (**Figure 1.1**). This EGF-induced recruitment of the SOS-GRB2 complex to the plasma membrane is critical for the initiation of the MAPK pathway signalling (Egan, Giddings et al. 1993). SOS catalyses the exchange of membrane bound inactive RAS-guanosine-diphosphate (GDP) to activated RAS-guanosine-triphosphate (GTP) which then recruits RAF to the membrane, where it gets activated. RAF activates MEK which then activates ERK via phosphorylation (**Figure 1.1**).

In the PI3K pathway, the lipid phosphatase PTEN maintains low levels of phosphatidylinositol 3, 4, 5-tri-phosphate (PIP3), resulting in AKT inactivation. Upon binding of growth factors such as insulin and insulin-like growth factor 1 (IGF-1) to their respective RTKs, the lipid kinase PI3K is activated either directly or indirectly through the recruitment of the adaptor/docking proteins such as insulin receptor substrate (IRS) or GAB (GRB2-associated-binding protein). Activated PI3K phosphorylates phosphatidylinositol 3, 4-bisphosphate (PIP2) to generate membrane-bound PIP3 (**Figure 1.1**). PIP3 recognises and binds to the pleckstrin homology (PH) domain in the serine threonine kinase AKT translocating it to the plasma membrane (Lietzke, Bose et al. 2000). Here AKT is subsequently activated by site-specific phosphorylation at residues threonine 308 (Thr308) in the activation loop of the catalytic domain by pyruvate dehydrogenase kinase 1 (PDK1) and serine 473 (Ser473) in the carboxyl (C)-terminal hydrophobic domain by the mammalian target of rapamycin complex 2 (mTORC2) (Alessi, Andjelkovic et al. 1996).

Besides their main function of assembling complexes, scaffolding/adaptor/docking proteins are thought to mediate crosstalk between pathways (Kolch 2005) (**Figure 1.1**). Scaffold signalling proteins such as GRB2 and GAB1 are involved in both the PI3K and MAPK pathway, and help to integrate and diversify incoming mitogenic signals allowing the same or different RTKs to activate a range of downstream pathways, including the PI3K and MAPK pathways (Koyama, Nakaoka et al. 2008, Wohrle, Daly et al. 2009, Zhang, Li et al. 2019). Using experimental and computational methods, Kiyatkin et al. demonstrate that GAB1 amplifies positive interactions between survival and mitogenic pathways enhancing PI3K/AKT activation and extending the duration of RAS/MAPK signalling (Kiyatkin, Aksamitiene et al. 2006).

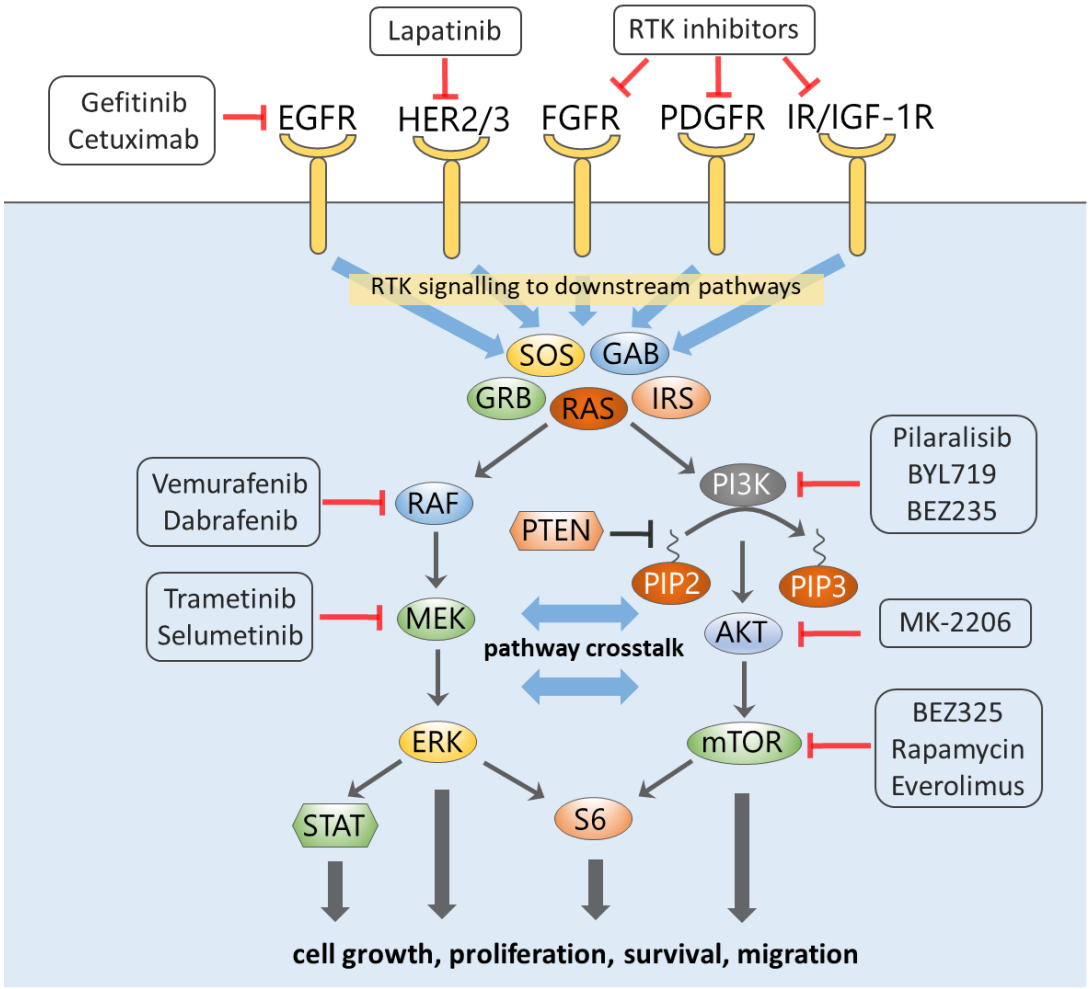

Figure 1.1 Signalling crosstalk between the PI3K (PI3K-AKT-mTOR) and MAPK (RAS-RAF-MEK-ERK) signalling pathways, showing examples of targeted inhibitors directed at the different nodes of the PI3K-MAPK network. Activation of these pathways is initiated by the binding of growth factors (GFs) such as EGF, FGF, PDGF, IGF-1 and insulin to their corresponding RTKs; EGFR, HER2/3, FGFR, PDGFR, IGFR-1 and IR. GF binding leads to subsequent RTK auto-phosphorylation generating binding sites for adaptor and scaffold signalling proteins such as GAB (GRB-associated binder), GRB (growth factor receptor-bound protein), SOS, (son of sevenless) and IRS (insulin receptor substrate). These adaptor and scaffold proteins facilitate crosstalk between the pathways and propagate the signal downstream leading to kinase cascades which regulate a diverse range of cellular functions such as growth and survival. The receptor and protein kinase components of the PI3K-MAPK signalling network are targeted by inhibitors such as EGFR inhibitor gefitinib and the HER2/3 inhibitor lapatinib as well as MEK inhibitors trametinib and selumetinib, BRAF inhibitors vemurafenib and dabrafenib, pan-PI3K inhibitor Pilaralisib and selective PI3Kα inhibitor alpelisib (BYL719), AKT inhibitor MK-2206 and mTOR inhibitors rapamycin and everolimus and dual PI3K/mTOR inhibitor BEZ325.

The PI3K-AKT-mTOR and RAS-MAPK signalling pathways are among the most frequently altered pathways across different cancer types including breast cancer (Sanchez-Vega, Mina et al. 2018). Mutations, genomic disruptions, amplifications and loss of both the MAPK (Forbes, Beare et al. 2015) and PI3K (Chalhoub and Baker 2009) pathway components are common and lead to hyper-activation of these growth pathways initiating oncogenesis. The PI3K pathway is a prototypic survival pathway and is the most frequently dysregulated pathway in breast cancer (Tokunaga, Oki et al. 2008).

Disruptive activation of the MAPK pathway occurs in more than 30% of human cancers, is associated with increased risk of metastasis (Shapiro 2002) and has been implicated in the development and progression of TNBC (Giltnane and Balko 2014). Approximately 80% of BLBC have genomic amplification of components of the EGFR-RAS-BRAF signalling network with over-activation of MAPK signalling in BLBC (Cancer Genome Atlas 2012). For example, frequent amplification of the RTK EGFR is reported in TNBC (Yu, Liu et al. 2002) and BLBC subtype (Hoadley, Weigman et al. 2007, Corkery, Crown et al. 2009). This EGFR over-expression which can amplify signals of the downstream PI3K and MAPK pathways leading to their over-activation (Cancer Genome Atlas 2012) occurs in ~ 50% of BLBC (Dent, Trudeau et al. 2007), and is associated with poor overall survival (Hoadley, Weigman et al. 2007, Corkery, Crown et al. 2009). Furthermore, EGFR mutations have been reported in up to ~ 10% of Asian TNBC patients (Teng, Tan et al. 2011). For an in-depth review on EGFR signalling in TNBC see the review paper (Masuda, Zhang et al. 2012). Together these findings provide a strong rationale for targeting both the PI3K and MAPK pathways in TNBC.

1.1.5 PTEN: a major negative regulator of the PI3K pathway

The tumour suppressor PTEN is the prime antagonist of PI3K and thus a major negative regulator of this pathway (Maehama and Dixon 1998, Stambolic, Suzuki et al. 1998). It was first characterised as a PIP_3 phosphatase by Dixon (Maehama and Dixon 1998). After the p53 tumour suppressor, PTEN is the most frequently disrupted gene in human cancers. PTEN inactivation is associated with tumorigenesis in multiple human cancers, including breast cancer. Loss of PTEN expression occurs in approximately 30% of breast cancer (Stemke-Hale, Gonzalez-Angulo et al. 2008). PTEN loss is mediated through a variety of mechanisms including mutations, particularly in the catalytic domain of the PTEN phosphatase, deletions, transcriptional silencing, and protein instability or through loss of heterozygosity (LOH) (Singh, Ittmann et al. 1998, Holohan, Van Schaeybroeck et al.) and/or epigenetic silencing mechanisms such as promoter methylation (Stemke-Hale, Gonzalez-Angulo et al. 2008). Interestingly, research by Papa et al. (Papa, Wan et al. 2014) revealed that PTEN mutation and loss are not synonymous. They found that single-allele mutation of PTEN was more oncogenic than loss of one PTEN allele since these mutant PTEN forms could heterodimerize with wild-type PTEN and in doing so supress its activity.

PTEN functions as a dual-specificity phosphatase (Myers, Stolarov et al. 1997) since it can dephosphorylate both lipids and proteins which antagonizes activated PI3K signalling to maintain normal cell growth or arrest, survival or apoptosis (Lee, Chen et al. 2018). PTEN negatively regulates the PI3K pathway by dephosphorylating the 3′ end of the triphosphate lipid second messenger PIP3, the product of the lipid kinase PI3K, producing PIP2 (Maehama and Dixon 1998, Stambolic, Suzuki et al. 1998) (**Figure 1.1**).

This inhibits activation of the serine threonine kinase AKT, also known as protein kinase B (PKB) and the AKT-dependent downstream signalling pathways, since PIP3 binds to the PH domain on AKT (Lietzke, Bose et al. 2000). PIP3 binding to AKT is essential for the translocation of AKT to the plasma membrane where it is subsequently activated by phosphorylation. Therefore, PTEN loss or inactivation leads to constitutively active PI3K-AKT signalling resulting in uncontrolled proliferation, genomic instability and tumorigenesis. However, it should be noted that PTEN loss can also disrupt PIP3-dependent processes which are mediated by AKT-independent pathways. In addition to AKT and PDK1, there are a range of other PH domain-containing proteins that bind to PIP3 and are subsequently recruited to the plasma membrane (Park, Heo et al. 2008). PIP3-regulated PH domain-containing proteins are involved in a diverse array of cellular functions and include regulators of small GTPases, signalling adaptor proteins, kinases and phosphatases (Park, Heo et al. 2008). Taken together, this suggests that PIP3 acts as a hub in the cellular signalling network, and loss of PTEN can lead to the disruption and upregulation of pathways in an AKT-independent manner.

Although PTEN was previously thought to function primarily as a PIP3 3-phosphatase which limits activation of PI3K signalling pathway, recent findings reveal an important and widespread role for PTEN as a PIP2 3-phosphatase (Malek, Kielkowska et al. 2017). They showed that both *in vitro* and *in vivo*, PTEN also functions as a PIP2 phosphatase dephosphorylating it to PIP. In the cytosol of MCF10A cells PTEN was a major PIP2 3-phosphatase and they showed that loss of PTEN together with INPP4B, a known PIP2 4-phosphatase, leads to synergistic PIP2 accumulation which correlated with increased invadopodia in epidermal growth factor (EGF)-stimulated cells. The authors state that it is likely that this function of PTEN has been overlooked because measuring PIP2 levels in cellular extracts was technically difficult. Hence this potential role of PTEN as a PIP2 phosphatase under normal physiological conditions, within both class I and class II PI3K-signalling pathways, as well as the contribution of PIP2-specific processes in PTEN-dependent tumorigenesis and metastasis clearly now demands further attention and investigation.

1.1.6 PTEN protein structure and regulation

PTEN consists of 9 exons and encodes a 47 kilodalton (kDa) 403 amino acid (aa) polypeptide. PTEN protein consists of 5 functional domains; a PIP2-binding domain (PBD), an N-terminal phosphatase domain (from aa 1 to 185) encoded by exons 1-5 with the catalytic core domain encoded by exon 5, a C2 domain, a C-terminal tail which contains multiple phosphorylation sites as well as two peptide sequences rich in proline (P), glutamic acid (E), serine (S), and threonine (T) (Bromberg, Wrzeszczynska et al.) domains for degradation, and a postsynaptic density protein (PDZ) domain-binding sequence for protein-protein interactions (**Figure 1.2**).

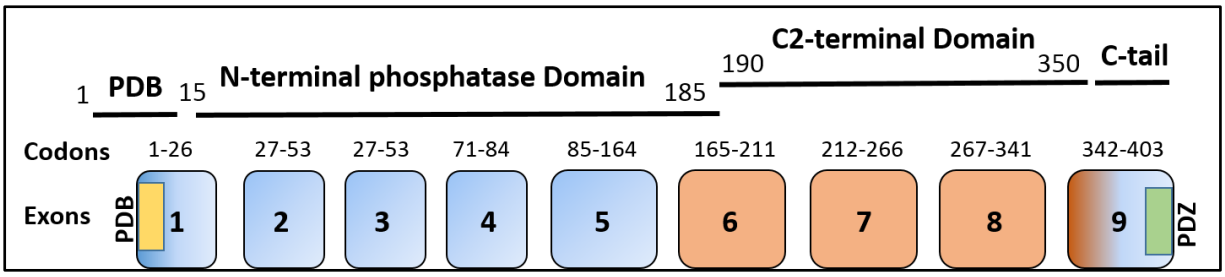

Figure 1.2 PTEN protein structure. This figure highlights the 5 functional domains, the 9 exons which encode it and their positions. Domains are; PIP2-binding domain (PBD), an N-terminal phosphatase domain, C2 domain, a carboxyl-terminal tail and a PDZ domain. Inspired by (Gbelcova, Bakes et al. 2015) and (Chalhoub and Baker 2009).

PTEN is modified and regulated at many levels including subcellular localization, binding partners and post-translational modifications such as acetylation, phosphorylation, ubiquitination and oxidation (Tamguney and Stokoe 2007). Numerous studies exist showing that the C-terminal tail of PTEN is necessary for PTEN stability and phosphatase activity. The C-terminal tail contains many phosphorylation sites which may regulate activity, stability and recruitment to the membrane (Vazquez and Devreotes 2006). Phosphorylation of the C-terminal tail of PTEN stabilizes the phosphatase and reduces its activity to PIP3. It does this by blocking interactions with PDZ domain-containing proteins and by keeping it in the cytosol and away from the membrane where PIP3 is located. In contrast, dephosphorylation of the C-terminal tail causes increased enzymatic activity followed by rapid degradation, thus tightly regulating PTEN activity. Kinases capable of phosphorylating its tail include glycogen synthase kinase 3 beta (GSK3β) (Al-Khouri, Ma et al. 2005), as RAS homolog family member A (RhoA)-associated kinase (Li, Dong et al. 2005) and casein kinase 2 (CK2, also known as CSNK2) (Torres and Pulido 2001).

1.1.7 PTEN loss is associated with TNBC and poor prognosis in breast cancer

Previous studies from several groups investigating the relationship between loss of PTEN expression and prognostic significance have been conflicting and controversial. Some studies have revealed that PTEN loss or downregulation is associated with poor prognosis in breast cancer patients such as increased breast cancer related death and lymph node spread (Depowski, Rosenthal et al. 2001). Another research group revealed that reduced PTEN expression correlated with high-grade tumour, distant tumour-node metastasis, lymph node status and reduced survival (Lee, Kim et al. 2004) whereas this prognostic significance could not be confirmed in other studies (Knudsen, Pajak et al. 2012).

To clarify these conflicting findings, a meta-analysis was conducted in 2017 evaluating the associations of PTEN expression with clinicopathological characteristics and prognosis in breast cancer (Li, Shen et al. 2017). This meta-analysis was the first of its kind and its published findings concluded that PTEN was indeed associated with poor prognosis in breast cancer. Pooled results from 27 studies showed that

PTEN loss was more frequent in breast cancer than normal tissue, was associated with larger tumour size, lymph node metastasis, poor differentiation, and the TNBC phenotype. Furthermore, breast cancer patients with PTEN loss had poorer disease-free as well as overall survival. Based on these findings the authors concluded that PTEN loss could be predictive of worst outcomes and more aggressive behaviour in breast cancer patients. In addition, a study by Beg et al. in 2015 showed that PTEN loss is associated with poor prognosis in Middle-Eastern patients with TNBC (Beg, Siraj et al. 2015). Moreover, heterozygous inactivation of PTEN in mice leads to the rapid formation of mammary tumours which resemble the BLBC phenotype suggesting that PTEN loss is directly involved in the transformation of basal-like progenitor cells (Saal, Gruvberger-Saal et al. 2008).

1.1.8 Over-activation of PI3K signalling by PTEN loss and PIK3CA mutations

PTEN and PI3K exist in a tightly regulated loop. Either PTEN loss or reduction, or PI3K activating mutations can lead to hyper-activation of the PI3K pathway and both are among the most frequent genetic disruptions in breast cancer, occurring in approximately 50–75% of breast cancers (Saal, Holm et al. 2005). Furthermore, PI3K pathway over-activation is reported in 60% of TNBC patients, supporting the important role this pathway plays in TNBC (Cancer Genome Atlas 2012). Alterations in the PI3K pathway include mutation and/or amplification of the genes encoding the PI3K catalytic subunits p110α (*PIK3CA*) and p110β (*PIK3CB*), the PI3K regulatory subunit p85α (*PIK3R1*), the PI3K effectors AKT1, AKT2, and PDK1, and loss of the phosphatases PTEN and INPP4B (Engelman 2009). The most common genetic alteration of this pathway is activating mutations in PIK3CA gene which encodes the catalytic subunit p110α of PI3K. PIK3CA mutations have a reported frequency rate of 20-40% in breast cancer (Bachman, Argani et al. 2004, Abramson, Cooper Lloyd et al. 2014) and copy number gain of this gene have been identified in 1-14% of breast cancers. Of these 80% or more occur within the helical (E542K, E545K) and kinase (H1047R) domains of p110α (Cancer Genome Atlas 2012). These mutations confer increased catalytic activity for the generation of the second lipid messenger PIP3, leading to hyper-activation of AKT signalling. Data compiled on the frequency of alterations using the CBioPortal Cancer Genomics shows that ~ 40% of breast cancer patients had PIK3CA alterations, followed by 11% having PTEN deletion (**Figure 1.3**). Interestingly, while alterations in PIK3CA are primarily missense mutations and occur mostly in luminal A/B or HER2+ patients, loss of PTEN prominently happens in basal-like/TNBC patients.

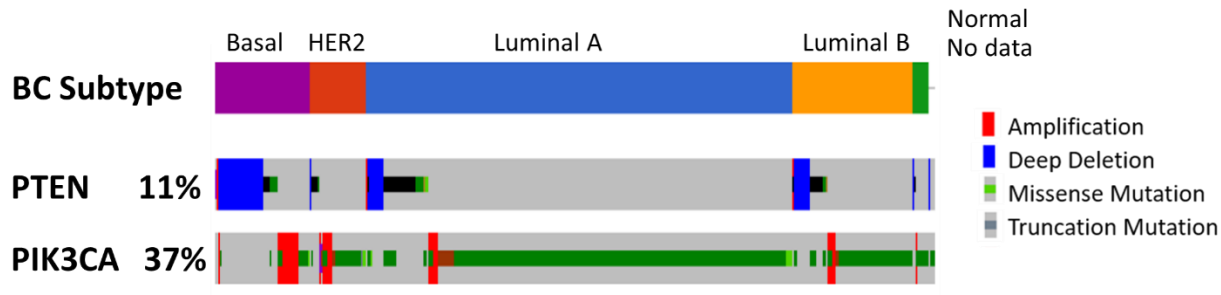

Figure 1.3 PTEN and PIK3CA gene alteration frequency in breast cancer patients by subtype. Data shows the frequency of PTEN and PIK3CA gene alterations by BC subtype and was analysed using the Pan-cancer Atlas dataset (n=994) from The Cancer Genome Atlas (TCGA) program (www.cbioportal.org).

1.1.9 Disease progression and drug resistance is mediated by PTEN loss and PIK3CA mutations

It has been demonstrated that over-activation of the PI3K pathway through PIK3CA mutations, PTEN loss, or both contribute to therapy resistance and disease progression. For instance, PIK3CA mutations or PTEN loss conferred resistance to trastuzumab, a monoclonal antibody directed against the HER2 receptor, and was associated with increased disease progression and decreased survival in trastuzumab-treated metastatic breast cancer patients (Razis, Bobos et al. 2011). Furthermore, reduced PTEN activity or increased AKT activity in breast cancer cells has been shown to confer resistance to tamoxifen-induced apoptosis (Shoman, Klassen et al. 2005). In melanoma, loss of PTEN activity in cancer cells confers resistance to the anti-growth and anti-angiogenic effects of MEK inhibitors (Ciuffreda, Di Sanza et al. 2012). In addition, this same research group discovered a novel crosstalk mechanism whereby inhibition of constitutively active MEK signalling by pharmacological or genetic means restored PTEN expression both *in vitro* and *in vivo*, leading to downstream inhibition of signalling through AKT and mTOR (Ciuffreda, Di Sanza et al. 2012). A 2016 study (Ebbesen, Scaltriti et al. 2016) using genetically engineered mouse models (GEMMs) showed that PTEN loss led to upregulation of not only the PI3K pathway, but also the MAPK signalling pathway likely through cross-activation mechanisms. Restoration of PTEN led to downregulation of both the PI3K and MAPK pathways and caused dramatic tumour regression. Importantly, they found that MAPK pathway signalling was required for maintenance of advanced breast cancer's harbouring PTEN loss since pharmacological inhibition of MAPK pathway with the MEK inhibitor, trametinib had potent anti-tumour response. This implies a rationale for using MEK inhibitors to treat therapy-resistant breast cancer patients acquiring PTEN mutations (Ebbesen, Scaltriti et al. 2016).

Although the PIK3CA gene is more frequently mutated in ER/PR positive breast cancer compared to TNBC or BLBC (ranging from 5 to 13%), the PI3K pathway is revealed as frequently over-activated in TNBC and BLBC (Cancer Genome Atlas 2012, Cossu-Rocca, Orru et al. 2015). This apparent

disconnect between the mutation of pathway genes and pathway activation is not uncommon and has been previously observed for PIK3CA mutations (Stemke-Hale, Gonzalez-Angulo et al. 2008). However, frequent over-activation of the PI3K pathway in the absence of PIK3CA mutations is likely due to the frequent loss of both PTEN and INPP4B in BLBC or TNBC which is most common in these subtypes (Hoadley, Weigman et al. 2007, Hennessy, Gonzalez-Angulo et al. 2009).

1.1.10 Despite less frequent PIK3CA mutations amplification of the PI3K pathway components is common in TNBC

A pinnacle genome study (Cancer Genome Atlas 2012) which carried out whole genome sequencing from tumour and germline deoxyribonucleic acid (Doudna and Charpentier) from 825 breast cancer patients showed that after TP53 mutations, which were the highest in basal like cancers (80%), PIK3CA was the next most commonly mutated gene at (9%). Although this was far lower than the other breast cancer subtypes, with luminal A and luminal B breast cancer having the highest level of PIK3CA mutations, 49% and 32% respectively, the PI3K pathway was most activated in the BLBC as shown by high levels of typical markers of the pathway, such as phosphorylated S6 and AKT (Cancer Genome Atlas 2012). In further support of this, many of the components of the PI3K and RAS-RAF-MEK pathways are amplified in BLBC including PIK3CA (49%), KRAS (32%), BRAF (30%) and EGFR (23%) suggesting alternative mechanisms for activation of these pathways such as through loss of PTEN and INPP4B another phosphatase implicated in cancer (Cancer Genome Atlas 2012). Indeed, PTEN mutation/loss (35%) was highest in this subtype of breast cancer compared to luminal A (13%), luminal B (24%) and HER2 (19%). In addition, INPP4B loss was highest in the basal like and HER2+ subtypes occurring in 30% of tumour samples of both subtypes (Cancer Genome Atlas 2012). Another study (Cossu-Rocca, Orru et al. 2015) focused on the mutation frequency in TNBC observed that 23.7% of TNBC had PIK3CA mutations and PTEN loss was observed in 11.3% of cancers and similarly with BLBC the TNBC showed an over-activated PI3K pathway.

1.1.11 Different pathophysiological effects of PTEN loss and PIK3CA mutations

Loss of PTEN expression and PIK3CA mutation has been shown in some papers to be a mutually exclusive event in breast cancer (Saal, Holm et al. 2005), likely because either genetic disruption would lead to increased levels of PIP3 and over activation of the PI3K pathway. However, other studies show that both PTEN loss and PIK3CA activating mutations were frequently concordant suggesting that these aberrations contribute differently to pathophysiology (Stemke-Hale, Gonzalez-Angulo et al. 2008) and occurring together can have an additive or synergistic effect in promoting tumorigenesis as seen in endometrial cancer where these genetic aberrations frequently coexist (Oda, Stokoe et al. 2005). PTEN knockdown leads to phenotype alterations associated with oncogenesis. It has been shown that PTEN knockdown (KD) in MCF10A cells using siRNA led to increased activation of both the PI3K and MAPK pathways as shown by increased levels of phosphorylated AKT and ERK (Vitolo, Weiss et al.

2009). This in turn led to EGF-independent proliferation which was blocked by pharmacological inhibition with either PI3K or MAPK inhibitors. Treatment with EGFR inhibitors gefitinib and erlotinib revealed that the PTEN KD cells were more resistant to growth inhibition than the WT MCF10As suggesting a decreased dependence on EGF for proliferation. This was further supported by the PTEN homozygous PTEN KD cells continuing to survive and proliferate in minimal media serum without EGF whereas WT MCF10A cells had reduced growth. They confirmed using flow cytometry that this increased viability and growth in PTEN KD cells was due to resistance to apoptosis.

PTEN loss also increased anchorage-independent survival (protection from anoikis - apoptosis that results from loss of attachment), but not anchorage-independent growth. In addition, PTEN loss led to increased sensitivity to the chemotherapeutic drug doxorubicin, but not Paclitaxel. Taken together their data supports the notion that PTEN deletion contributes to cancer cell survival and tumour dormancy (Vitolo, Weiss et al. 2009). However, the authors found that PTEN loss was not sufficient to promote complete tumorigenic transformation of the MCF10A cells indicating that other oncogenic events are needed. Indeed, research by Hopkins et al. using these same PTEN KD clones generated by the previous study (Vitolo, Weiss et al. 2009) revealed that EGFR over-expression, together with p53 and PTEN inactivation, genetic alterations frequently observed in BLBC (Sorlie, Tibshirani et al. 2003, Saal, Gruvberger-Saal et al. 2008), were required for promotion of complete MCF10A transformation as measured by anchorage-independent colony formation (Pires, Hopkins et al. 2013).

1.2 Drug resistance in breast cancer: the current challenge

Drug resistance is a complex phenomenon and a major challenge in cancer therapy. It is the main cause of treatment failure and patient relapse leading to disease progression and frequently patient death (Rueff and Rodrigues 2016). It is believed to be responsible for treatment failure in over 90% of metastatic cancer patients (Longley and Johnston 2005). Therefore, it is clear that overcoming drug resistance would significantly improve cancer patient survival.

Broadly, resistance to anti-cancer therapies can be divided into two categories: *intrinsic* or *acquired*. In intrinsic resistance the tumour has inherited pre-existing resistance prior to drug administration and thus the treatment is ineffective from the start. In contrast, acquired resistance is where the treatment is often initially effective, but the cancer develops resistance during the course of the treatment. To date, multiple direct and indirect mechanisms underlying drug resistance have been identified, including - poor drug influx or excessive efflux, DNA damage repair, inherent cellular heterogeneity within the tumour, cellular signalling and cell death inhibition, drug inactivation and alterations of the drug targets, which can act independently or in combination through various signal transduction pathways to limit drug efficacy (Housman, Byler et al. 2014).

Among the mechanisms of acquired resistance, development of secondary mutations of the drug targets that compromise binding or inhibition of the drug to the target has probably been the most well studied. Notable examples include the emergence of T790M mutation in EGFR leading to resistance to gefitinib in EGFR-mutant lung cancer (Kobayashi, Boggon et al. 2005), T315 in Abelson murine leukemia viral oncogene homolog 1 (ABL1) causing imatinib/dasatinib resistance in acute lymphocytic leukemia (ALL) and chronic myeloid leukemia (CML) (Gorre, Mohammed et al. 2001, Shah, Tran et al. 2004); and HER2/ERBB2 truncation leading to Trastuzumab resistance in ERBB2-positive breast cancer (Recupero, Daniele et al. 2013).

In addition to these genetic mechanisms, it has become increasingly clear that tumour cells also rely on a non-genetic and highly adaptive mechanism of drug resistance involving dynamic rewiring of cell signalling networks to circumvent the initial drug blockade. A distinguishing and remarkable feature of drug-induced 'network rewiring' and ensuing 'adaptive resistance', compared to classical resistance mechanisms, is that they can occur extremely quickly and have been commonly observed within hours or days following drug treatment in cell and animal tumour models (Duncan, Whittle et al. 2012) as well as in cancer patients (Zawistowski, Bevill et al. 2017). These bypass mechanisms enable tumour cells to adapt to their treatment, thus evading the action of single agents, such as kinase inhibitors, by activating alternative and/or compensatory survival pathways. Thereby, circumventing the initial blockade and driving drug resistance. It is becoming increasingly apparent that these early adaptive responses are critical to tumour survival and are key in driving the development of resistance. Despite this, adaptive resistance remains under-explored and often poorly understood. My research is focused on these adaptive bypass mechanisms of acquired drug resistance.

1.2.2 Adaptive bypass mechanisms of drug resistance: network rewiring

All living systems are equipped to adapt to a constantly changing environmental conditions while maintaining homeostasis. Crosstalk and feedback loops help maintain homeostasis and dynamic plasticity of the signal transduction networks and modulate drug responses often conferring resistance. Studying this feedback control and crosstalk between signalling pathways is critical for successful drug treatment and to understand the drug-induced network changes. Homeostatic crosstalk between the MAPK and PI3K pathways have been extensively studied and are well known. This crosstalk includes cross-inhibition from ERK to GAB1 (Yu, Liu et al. 2002, Lehr, Kotzka et al. 2004) and from AKT to RAF (Guan, Figueroa et al. 2000). Crosstalk between the MAPK and PI3K pathways and subsequent drug resistance is a major cause of the limited clinical benefits of drugs which target these pathways (Mendoza, Er et al. 2011).

1.3 Combination therapy as a promising strategy to overcome resistance

The success of targeted single agent therapies like kinase inhibitors in cancer treatment has been severely limited by drug resistance. A promising strategy to try and overcome this resistance to monotherapies, and which is increasingly being explored in all cancers, is the use of effective combination therapies. Combination therapy is considered the best anti-cancer treatment option since it is hypothesised that it should prevent the development of drug resistance and be more effective than any one drug used alone (Csermely, Agoston et al. 2005, Yap, Omlin et al. 2013).

For instance, in BRAF-mutant melanoma (V600E) BRAF inhibitors vemurafenib or dabrafenib in combination with trametinib, a selective MEK inhibitor led to longer progression-free survival and increased the incidence of complete response. Almost 50% of melanoma patients harbor this V600E mutation which is a valine to glutamine substitution in codon 600 of the serine-threonine kinase BRAF (Davies, Bignell et al. 2002). Despite the initial success, resistance ultimately occurs due to acquired mutations and network rewiring restoring cell growth (Eroglu and Ribas 2016). However, another research group, showed that this resistance to BRAF inhibition could be overcome by co-treatment with insulin-like growth factor 1 receptor (IGF-1R)/PI3K and MEK inhibitors, highlighting the potential of multi-targeted drug therapy as an effective treatment strategy (Villanueva, Vultur et al. 2010).

1.4 Network dynamics in the PI3K and MAPK pathways mediate adaptive drug resistance

1.4.2 Positive and negative feedback loops

Positive and negative feedback loops regulate cellular signal transduction. Positive feedback can amplify input signals and often creates a switch-like dynamic time-course response allowing phenotypic transitions to occur in an “all or nothing manner” (Nguyen and Kholodenko 2016). Negative feedback brings about robustness to noise and adaptations to perturbations such as drug-induced inhibition. The levels of the drug target protein are decreased and this leads to activation of upstream components of the pathway. Dynamically, negative feedback enables adaptive and transient responses to sustained input signals (Nguyen and Kholodenko 2016).

1.4.3 Overview of pathway adaptations in response to MEK and PI3K inhibition

Network dynamics such as negative feedback and crosstalk activation of alternative pathways have been shown to mediate resistance against drugs that target the MAPK and the PI3K pathways. In response to drugs, feedback loops can be upregulated or lost either directly rendering the drug ineffective or indirectly leading to the activation of compensatory and/or alternative pro-survival pathways ultimately causing drug resistance. Crosstalk activation of AKT in response to inhibition of

the MAPK pathway components has been observed across many different cancers, including breast cancer, suggesting a strong ERK to receptor feedback exists (Nguyen and Kholodenko 2016).

In the MAPK pathway, ERK can phosphorylate and inactivate upstream components including GAB1, SOS, RAF and EGFR (Fritsche-Guenther, Witzel et al. 2011). Negative feedback between ERK and RAF and between ERK and EGFR are well established and mediate resistance to MEK inhibitors (Mirzoeva, Das et al. 2009). MEK inhibition is tolerated by the ERK pathway because MEK inhibitors remove or weaken the negative feedback signal leading to upregulation of RAF-ERK signalling (**Figure 1.4A-B**) which compensates for the initial loss of ERK activity. Thus, enabling robust steady-state ERK signalling despite decreased ERK protein levels. Alternatively, MEK inhibition can lead to hyper-activation of EGFR signalling triggering alternative signalling pathways such as the PI3K pathway and partially restoring ERK signalling (**Figure 1.4C-D**).

Negative feedback such as an p70 S6 kinase (S6K) to IRS negative feedback loop has also been found to mediate resistance against drugs targeting the PI3K pathway (Haruta, Uno et al. 2000) (**Figure 1.4E**). Inhibitors of mammalian target of rapamycin complex 1 or mechanistic target of rapamycin complex 1 (mTORC1) remove this S6K-IRS negative feedback loop which can lead to PI3K and/or AKT activation (O'Reilly, Rojo et al. 2006) (**Figure 1.4F**). Interestingly, in response to PI3K inhibitors TNBC cells have been shown to act by stimulating the IR/IGF-1R which in turn leads to JAK/STAT pathway activation and eventually reactivation of PI3K signalling thus circumventing the drugs initial blockade (Britschgi, Andraos et al. 2012) (**Figure 1.4H**). A negative feedback loop involving the transcription factor forkhead box O (FOXO) mediates cross-pathway feedback between the IR/IGFR/AKT/mTOR and RTKs/RAF/MEK/ERK (**Figure 1.4I**). Resistance to AKT inhibitors is mediated by the drug-induced loss of the negative feedback loops S6K-IRS and AKT-FOXO-RTKs causing RTK upregulation and subsequent reactivation of the upstream kinases PI3K and ERK (Chandarlapaty, Sawai et al. 2011) (**Figure 1.4G, J**).

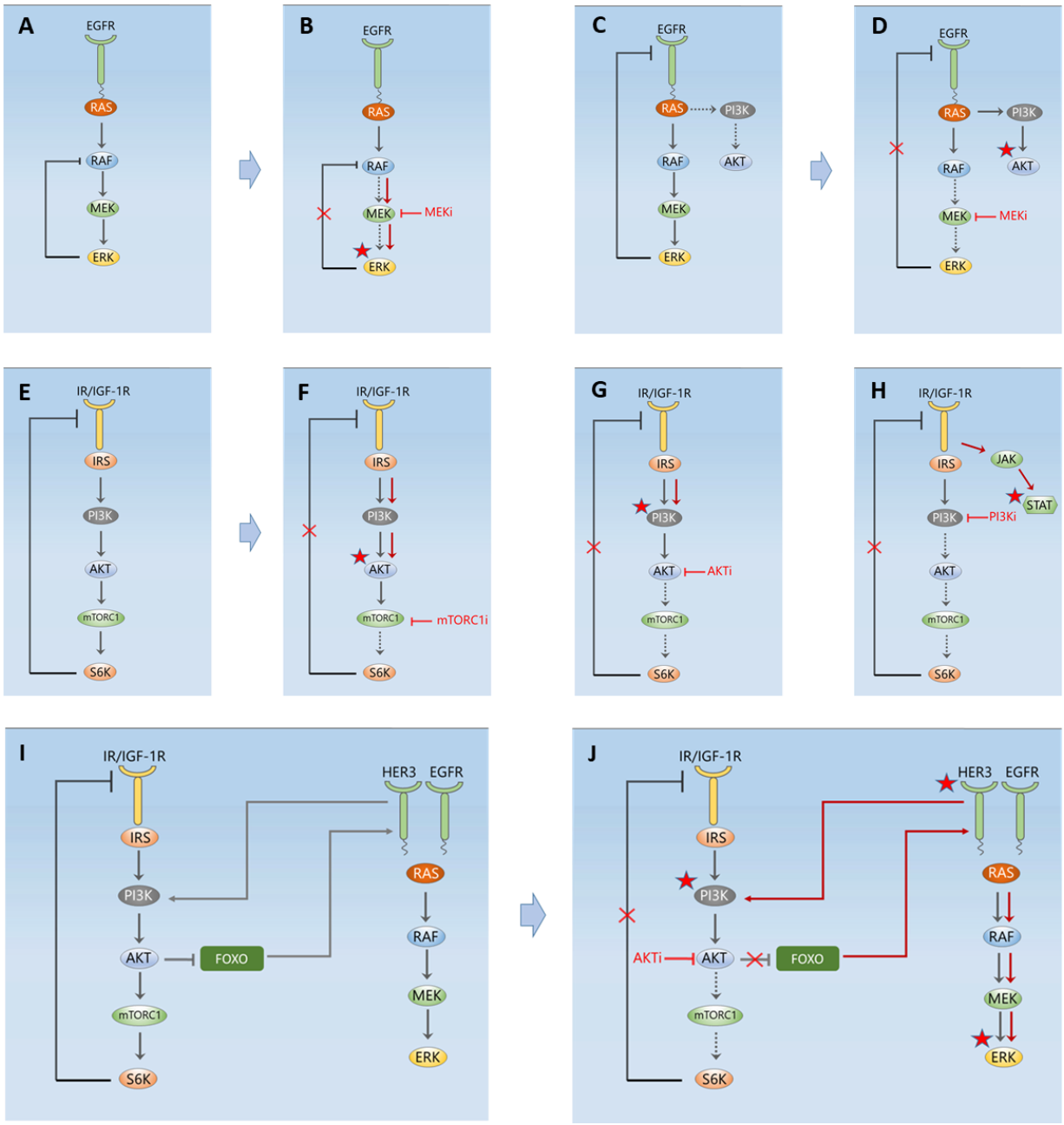

Figure 1.4 Different mechanisms of adaptive drug resistance caused by drug-induced loss of negative feedback loops in the MAPK, PI3K, JAK/STAT and RTK pathways leading to upstream activation of the pathway components and crosstalk between pathways. (**A-B**) MEK or RAF inhibition breaks the ERK-to-RAF negative feedback loop, leading to re-activation of ERK (active protein is indicated by the red star). (**C-D**) MEK inhibition breaks the ERK to EGFR negative feedback loop and stimulates alternative signalling via the PI3K/AKT pathway. (**E**) A schematic diagram showing an intact S6K-IRS negative feedback loop. Inhibition of mTORC1 (**F**), AKT (**G**) or PI3K (**H**) all break the S6K-IRS negative feedback, but lead to either AKT activation (**F**), PI3K activation (**G**) or activation of the JAK/STAT pathway (**H**). (**I**) Crosstalk between the PI3K (IR/IGFR-AKT/mTORC1) and MAPK (RTKs/RAF/MEK/ERK) pathway is mediated via a negative feedback loop involving FOXO. (**J**) AKT suppression breaks the S6K-to-IRS negative feedback and relieves its inhibition on the transcription factor FOXO leading to activation of PI3K and RTKs/ERK signalling. (Nguyen and Kholodenko 2016).

1.5 Network rewiring in response to RAS-MAPK pathway inhibition adaptive resistance mechanisms and proposed combination therapies

1.5.1 MEK inhibition activates PI3K-AKT signalling by relieving negative feedback on ERBBs

As a central node within the RAS-MAPK signalling cascade, MEK represents a promising therapeutic target; however clinical studies of MEK inhibitors (MEKi) have shown only limited anti-tumour activity (Rinehart, Adjei et al. 2004, Adjei, Cohen et al. 2008). The earliest evidence of adaptive response to MEK inhibition in breast cancer was reported almost a decade ago by independent groups (Hoeflich, O'Brien et al. 2009, Mirzoeva, Das et al. 2009), where they found inhibition of MEK led to unexpected and rapid activation of PI3K-AKT signalling. To determine how this actually happened, Mirzoeva et al. (Mirzoeva, Das et al. 2009) performed a targeted reverse-phase protein array (RPPA) allowing for temporal response of ~30 pan-pathway signalling nodes to the MEK inhibitor U0126, using the TNBC MDA-MB-231 cells as a model system. Besides activated AKT which occurred as soon as 1 hour after drug treatment, RPPA revealed the inhibitor also induced marked activation of EGFR within the same time frame, which was even more pronounced in the presence of EGF. MEK inhibition-induced -AKT activation was confirmed in 5 (out of 8 tested) cell lines including TNBC and Luminal lines, suggesting this is a common, yet cell-specific phenomenon. Since EGFR is an upstream input of PI3K signalling and ERK is a known negative regulator of EGFR (Li, Huang et al. 2008), the authors hypothesized that resistance to MEK inhibition is mediated by feedback activation of the PI3K pathway following relief of a negative feedback from MEK/ERK to PI3K/AKT via EGFR. Such feedback has been described previously (Yu, Liu et al. 2002). In further support of this hypothesis, inhibition of EGFR effectively abolished the adverse AKT activation caused by MEK inhibition alone; and combined MEK-PI3K inhibition down-regulation of cyclin D1 levels synergistically suppressed growth in 4 of the 11 breast cancer cell lines tested (Mirzoeva, Das et al. 2009). Dual inhibition only led to apoptosis in a subset of the cell lines. Interestingly, they found the cells which underwent apoptosis following combination treatment with PI3K and MEK inhibitors, harbour wild-type tumour suppressor p53. In contrast, cell lines which resulted in synergistic cell cycle arrest harboured mutant p53 suggesting a role for p53 as a predictive marker for synergistic combination therapy.

Similar findings were reported around the same time by Hoeflich et al. (Hoeflich, O'Brien et al. 2009), who provided additional *in vivo* evidence that dual MEK-PI3K inhibition was synergistic in reducing tumour growth in an MDA-MB-231 derived xenograft model of TNBC. A common conclusion reached by both studies was that basal-like/TNBC is particularly susceptible to MEK inhibition as compared to other breast cancer subtypes such as luminal and HER2-amplified tumours, this however, seemed to be a weak association rather than a general rule as several TNBC cell lines in the large panel of breast cancer cell lines examined, including MDA-MB-231, were among the most resistant lines against MEK inhibitors (Hoeflich, O'Brien et al. 2009, Mirzoeva, Das et al. 2009). Lack of PTEN, which occurs in a

subset of subset of BLBC cell lines and promotes basal PI3K-AKT signalling, was attributed to enhanced resistance to MEKi-based therapy (Hoeflich, O'Brien et al. 2009). In support of PTEN loss as a predictor of reduced sensitivity to MEK inhibition, siRNA mediated deletion of PTEN in cell lines which had previously been responsive, blocked the drug's cell cycle arrest and anti-proliferative effects (Hoeflich, O'Brien et al. 2009). This included enhanced downregulation of cyclin D1 and increased apoptosis. Furthermore, *in vitro* and *in vivo* combinations of selective PI3K and MEK inhibitors resulted in synergistic effects in the BLBC models with both intact and deleted PTEN suggesting that PTEN loss was indeed mediating resistance to MEK inhibition via PI3K pathway activation. While MEKi-induced AKT activation tends to occur in breast cancer cell lines having normal PTEN in these studies, it remains unclear if such adaptive response also happens in a PTEN-null background or if the already enhanced basal AKT activation would buffer the potential effect coming from breaking the MEK-EGFR-PI3K negative feedback.

The network rewiring induced by MEK inhibition that led to AKT activation is not exclusive to TNBC or HER2-negative breast cancer. A few years later, a study from the Engelman group showed that this signalling remodelling also occurs in a range of HER2-driven cancers (Turke, Song et al. 2012), including breast and lung cancer. Importantly, this work provided critical mechanistic insights into the functioning of the MEK/ERK-to-PI3K feedback loop, which turned out to be mediated by the tyrosine-protein kinase ERRB3, also known as HER3, rather than EGFR directly. Specifically, MEK inhibition activates AKT by inhibiting ERK activity, which blocks an inhibitory threonine phosphorylation on the juxtamembrane domains of EGFR (T669) and HER2 (T677), thereby suppressing trans-phosphorylation and activation of receptor. Inhibition of MEK using another potent inhibitor AZD6244 (selumetinib) triggered dramatic upregulation of HER3 activity, enhanced HER3 binding to GAB1 and PI3K, and phosphorylated AKT (Turke, Song et al. 2012). Consistently, knockdown of HER3 abrogates this feedback and re-sensitises cancer cells to AZD6244 treatment. Although, the previous studies did not look into HER3 (Hoeflich, O'Brien et al. 2009, Mirzoeva, Das et al. 2009), in hindsight the feedback activation of AKT seen in this work was likely to also be mediated by HER3, in addition to EGFR.

The above findings, collectively, may suggest that feedback activation of AKT is a common theme among breast and other cancers addicted to EGFR/HER2 and/or displaying over-activation of ERK signalling (Hoeflich, O'Brien et al. 2009, Mirzoeva, Das et al. 2009, Yoon, Kim et al. 2009), this however, is not the case. Indeed, when treating a panel of KRAS-mutant cell lines to MEK inhibitor, Turke et al (Turke, Song et al. 2012) found that AKT was not adversely activated despite potent upregulation of phosphorylated HER3, indicating the MEK/ERK-HER3-PI3K feedback loop was not working under these conditions. This may be due to low levels of EGFR and HER2 in these cells, which were not sufficient to transactivate HER3 to a level sufficient/ high enough for AKT activation. Another reason may be because the network circuitry is different and HER3 did not drive PI3K in these KRAS-

mut cell lines. In support of this, IGF-IR/IRS has been shown to be the major PI3K input in these cells (Ebi, Corcoran et al. 2011). While the exact cause(s) for the disconnect between HER3 and AKT activation requires further investigation, the above studies have demonstrated a highly dynamic and context-specific network rewiring mechanism to MEK inhibition, involving the PI3K/AKT pathway, which underlies adaptive resistance to MEKi-based therapy.

Together, these studies provide strong rationale for treating TNBC with a combination of PI3K and MEK inhibitors thus targeting both the PI3K and MAPK pathways. Moreover, they suggest that the activation status of these pathways including whether or not the tumours harbour loss of PTEN and/or EGFR over-expression can influence the response to therapeutics. In support of this, a recently published study (Sato, Wakabayashi et al. 2017) demonstrated that sensitivity to the MEKi (trametinib) and the PI3Ki (Wortmannin) in TNBC cells lines could be predicted by the catalytic activity of MEK and PI3K which showed strong positive correlation. MEK and PI3K activity can be used as indicators of the MAPK and PI3K pathway activation respectively and these activities may reflect crosstalk between these pathways. The authors demonstrated that this model prediction to drug sensitivity could be applied to a TNBC cell line xenograft model.

1.5.2 MEK inhibition drives extensive rewiring of the kinome epigenomic networks

While inhibition of MEK had been known to acutely reprogram specific signalling networks, the extent and complexity of such reprogramming was only truly revealed in a seminal study in 2013 (Duncan, Whittle et al. 2012), thanks to advances in mass-spectrometry (MS)-based proteomics. Using a chemical proteomics approach that coupled kinase affinity capture with quantitative mass spectrometry, Duncan et al (Duncan, Whittle et al. 2012) was able to elucidate for the first time the kinome changes in response to MEK inhibition at a global level, in both cultured cells and genetically modified mouse models of TNBC. Remarkably, MEK inhibition by AZD6244 (and U0126) induced an extensive and dynamic remodelling of the cell signalling systems that extended far beyond ERBB/PI3K signalling, evident by large changes in expression and/or activation of >140 kinases, from all major kinase subfamilies, within 24 hours of treatment. These include a variety of pro-survival RTKs; platelet-derived growth factor receptor beta (PDGFRβ), vascular endothelial growth factor receptor (VEGFR), AXL, HER2/3 and discoidin domain receptor family, member 1 (DDR1). This inhibitor-induced RTK remodelling was accompanied by increased oncogenic signalling through the PI3K/AKT, JAK/STAT and MEK/ERK pathways, consistent with previous observations (Mirzoeva, Das et al. 2009). The results by Duncan et al. (Duncan, Whittle et al. 2012) were significant as it revealed that selective perturbation of even a single node can trigger an extensive and rapid global response by the cancer cell signalling machinery, which counteracts the inhibitor's effect.

While defining the changes of signalling responses to targeted inhibitors is, nowadays, relatively straightforward with modern MS-based technologies like quantitative chemical proteomics, elucidating the underlying mechanisms of network rewiring is, however, far more challenging. In addressing this, Duncan et al. (Duncan, Whittle et al. 2012) found that the induced RTK expression/activation was due to disruption of a repressing transcriptional program exerted by the transcriptional factor c-MYC on the RTKs. As ERK phosphorylates c-MYC on S62 and enhances its stability, acute loss of ERK activity by MEKi treatment with AZD6244 led to rapid c-MYC degradation and hence transcriptional de-repression of RTKs and their ligands that are negatively regulated by c-MYC. This led to dramatic epigenetically driven transcriptomic changes with genome-wide enhancer and promoter remodelling promoting resistance. In support of this, RNAi-mediated knockdown of ERK or c-MYC induced similar RTKs as seen with MEK inhibitors, and blocking c-MYC degradation prevented the kinome reprogramming. Given c-MYC is not the only transcriptional factor regulating the induced RTKs, it is unlikely c-MYC degradation is the sole mechanism responsible for their transcriptional induction, yet this mechanistic insight offered valuable guidance for rational choice of combination therapy. For example, future selective inhibition of the E3 ligase(s) responsible for c-MYC degradation may help stabilize c-MYC and thus revert the MEKi-induced kinome remodelling. Until this is possible, the authors demonstrated proof of principle that combined treatment of MEK inhibitor AZD6244 with a pan-RTK inhibitor sorafenib synergistically reduced tumour growth in a mouse model of TNBC; albeit this combination is unlikely to be clinically useful due to the extensive off-target profile of sorafenib, which also targets RAF kinases.

To overcome this issue, a recent follow-up study (Zawistowski, Bevill et al. 2017) has demonstrated that rather than trying to combat RTK upregulation using a secondary kinase inhibitor like sorafenib, the use of bromodomain and extra-terminal motif (BET) inhibitors (BETi), which targets bromodomain-containing proteins 2, 3 and 4 (BRD2/3/4), effectively and broadly prevented MEKi-induced transcriptional adaptation. This happened not only in TNBC cell lines, but also in patients following a small 7-day window-of-opportunity clinical trial of MEKi trametinib treatment, highlighting the significant clinical relevance of the findings. Critically this study validated the clinical significance of its previous work by Duncan et al. (Duncan, Whittle et al. 2012). Mechanistically, the authors found MEKi induced an expansive, genome-wide and rapid remodelling of the epigenomic landscape (Zawistowski, Bevill et al. 2017). BET family bromodomain proteins such as BRD4, bind to acetylated lysines of histone subunits or transcriptional factors to regulate transcriptional elongation through recruitment of positive transcription elongation factor (P-TEFb), an RNA polymerase II complex containing cyclin-dependent kinase 9 (CDK9) and Cyclin T1. Within 1-4 h of trametinib treatment, enhancers with pronounced BRD4 density co-occupied with typical enhancer marks were formed genome-wide, including at sites proximal to RTK loci including *PDGFRB*, fibroblast growth factor receptor 2 (*FGFR2*), and *DDR1*, explaining their induced upregulation. Remarkably, BETi

reduced the total number of MEKi-induced enhancers near baseline level; and combined BETi JQ1 with trametinib durably and synergistically inhibited tumour growth in both orthotropic and syngeneic mouse models of TNBC (Zawistowski, Bevill et al. 2017). Consistent with the proposed model of RTK upregulation, small-molecule inhibition of P-TEFb constituent CDK9, or BRD4-assocated factor p300 prevented epigenomic remodelling by reversing the upregulation of adaptive response genes, including RTKs, thus abrogating adaptive RTK induction.

Overall, the above studies together have unveiled extraordinary adaptive reprogramming of cancer cells to targeted MEK inhibition at both epigenomic and signalling levels, the former initially triggered the latter, which in turn likely fuelled further epigenomic changes in a positive-feedback manner. Although they have provided major insights in our understanding of inhibitor-induced acute adaptation, key questions remain to be answered. For example, given that the discussed work has utilised only a handful of TNBC cell models, are the observed rewiring mechanisms conserved across different TNBC cells, and if so do they occur to a similar extent? Clues to these questions came from (Zawistowski, Bevill et al. 2017) where they found that cells of a basal-like subtype of TNBC failed to remodel the BRD4 epigenome following MEK inhibition, while cells of the claudin-low subtype displayed comprehensive *de novo* enhancer formation, suggesting remodelling is likely cell type and context specific. Are the observed transcriptional and signalling rewiring and their mechanisms unique to MEKi? Or will different sets of RTKs be induced by inhibitors targeting other kinases, e.g. PI3K or mTOR? We believe in-depth answers to these questions will require more systematic efforts involving the use of large cell line panels and diverse drug agents, which will aim to illuminate the level and extent of tumour context-specific plasticity in response to targeted treatment. For an in-depth review on other adaptive mechanisms to MEK inhibition see our review paper in appendix 1.

1.6 Network rewiring in response to PI3K pathway inhibition: adaptive resistance mechanisms and proposed combination therapies

1.6.2 Non-redundant functional roles of PI3K isoforms in normal and transformed cells

The PI3Ks generate lipid second messengers inside cells, which are essential for controlling cellular functions including cell survival, proliferation, metabolism and migration. The complexity of PI3K signalling is in part due to existence of a large number (Dogruluk, Tsang et al.) of PI3K isoforms, grouped into three classes: class I, II and III, each generates different lipids in cells and controls different cell biological aspects. While the reason remains unclear, class I PI3Ks are the main PI3K genes found to be mutated in cancer, often at high frequency, and thus are the main PI3K isoforms currently pursued in anti-cancer drug development (Vanhaesebroeck, Guillermet-Guibert et al. 2010). These PI3Ks are stimulated by tyrosine kinases, RAS and GPCRs; and as such are often recruited by tyrosine kinase-based signalling networks such as those activated by insulin and EGF. The class IA PI3Ks (PIK3Cα,

PIK3Cβ, PIK3Cδ) exist as heterodimeric proteins made up of a regulatory p85 subunit (derived from three genes, *p85a*, *p85b* and *p55*) bound to one of three p110 catalytic subunits (p110α, p110β or p110δ, encoded by *PIK3CA*, *PIK3CB*, and *PIK3CD*, respectively).

The critical role of PI3K signalling in normal physiology and its frequent disruption in cancer has led to a major effort in developing inhibitors targeting the key kinase components of this pathway, in particular class I PI3Ks, AKT and mTORC1/2. To date, over 40 PI3K-signalling targeted inhibitors have been developed, which include isoform-selective PI3K inhibitors, pan-PI3K inhibitors, dual pan-PI3K and mTORC1/2 inhibitors, as well as specific mTORC1 and AKT inhibitors. Although some of these agents such as the mTOR inhibitors (temsirolimus and everolimus) have already been approved for use in a number of cancers (Kwitkowski, Prowell et al. 2010, Roskoski 2019), undue toxicities and emergence of resistance including adaptive resistance to these inhibitors have significantly hampered their full clinical potential as single-agent therapy (Massacesi, di Tomaso et al. 2013). Clinical translation is further complicated by the poorly-understood observations that different p110 isozymes play non-redundant roles in cell transformation. For examples, while p110α is predominantly required for growth of tumours driven by RTKs, mutant RAS, and/or PIK3CA mutations, p110β is the dominant isoform in PTEN-deficient tumours (Torbett, Luna-Moran et al. 2008, Wee, Wiederschain et al. 2008). Thus, compared to pan-PI3K inhibitors, isoform-selective PI3K inhibitors are likely less toxic to normal tissues. On the downside, the use of isoform-selective inhibitors may lead to compensatory upregulation of other PI3K isoforms that reactivate the pathway and limit the drug efficacy. Striking the right balance between efficacy and toxicity is a major challenge in translating PI3K inhibitors into the clinic.

1.6.3 PI3K pathway inhibition reactivates AKT signalling through feedback upregulation of HER3 and other RTKs

In 2006, O'Reilly and colleagues provided one of the first pieces of evidence of a feedback bypass mechanism in response to PI3K signalling inhibition (O'Reilly, Rojo et al. 2006). They showed that in breast cancer cell lines with hyper-activated PI3K signalling, mTOR inhibition by rapamycin released the mTORC1-dependent suppression of IGF-1R and the insulin receptor (IR), thus upregulating IRS1 and restoring PI3K/AKT signalling (O'Reilly, Rojo et al. 2006). This drug-induced relief of the mTORC1-to-IRS1 negative feedback largely explained the modest anti-tumour activity by rapamycin and mTOR inhibitor analogues seen in the clinic. A few years later, Chakrabarty et al. (Chakrabarty, Sanchez et al. 2012) demonstrated that inhibition of PI3K by XL147 (Pilaralisib), a highly selective pan-inhibitor of class I PI3Ks (α, β, γ, and δ), induced upregulation and activation of HER3 and other RTKs, including IR, IGF1R and FGFRs in HER2-overexpressing breast cancer cell lines, which eventually reactivated PI3K/AKT signalling. The same changes were not due to off-target effects as they were also observed with another pan-PI3K inhibitor BKM120. The induction of these RTKs is explained in - part by relief of a negative feedback from AKT to the RTKs via the FOXO family of

transcription factors. Specifically, since AKT phosphorylates and inhibits FOXO via cytoplasmic sequestration (Brunet, Bonni et al. 1999), AKT inhibition by XL147 released FOXO to the nucleus which was then able to transcribe the RTKs (Chakrabarty, Sanchez et al. 2012). Importantly, because in HER2+ cell lines, HER2 is a major activator of HER3, the upregulation of HER3 expression resulted in significant HER2-mediated increase in its activity, ultimately triggering PI3K reactivation and limiting XL147's efficacy. The authors went on to show that combinations of XL147 with HER2 antagonists (trastuzumab or lapatinib) were synergistic in delaying tumour growth in mice bearing xenografts derived from BT474, a HER2+/PIK3CA-mt breast cancer cell line. By utilising the same breast cancer experimental models, very similar observations were also reported by Chandarlapaty and colleagues (Chandarlapaty, Sawai et al. 2011), but using AKT inhibitors instead of pan-class I PI3K inhibitors as in (Chakrabarty, Sanchez et al. 2012). This similarity probably came from the fact that AKT is a common downstream node of the class I PI3Ks. While the above studies both suggested HER2 induced PI3K signalling via HER3, recent work showed HER2, when overexpressed, can directly activate PI3K/AKT signalling independent of HER3 (Ruiz-Saenz, Dreyer et al. 2018). Regardless, these studies together highlight that combined PI3K/HER2 inhibition may be a potentially effective treatment for HER2-overexpresing breast cancer patients.

Would PI3K/HER2 co-inhibition be useful even in non HER2-dependent tumours? There are several clues to this question. First, PI3K/AKT and FOXO-dependent upregulation of HER3 was found even following HER2 inhibition by lapatinib (Chakrabarty, Rexer et al. 2010, Chakrabarty, Sanchez et al. 2012). Remarkably, even dual blockade of HER2 with trastuzumab and lapatinib did not entirely eliminate the compensatory upregulation of HER3 (Garrett, Sutton et al. 2013). These studies suggest that -low levels of residual HER2 comparable to that in non HER2-amplified tumours may be sufficient to phosphorylate and activate HER3, subsequently causing PI3K/AKT activation after PI3K/AKT or HER2 inhibition. Further, strong induction of common RTKs including IGF-1R, IR, HER3, ephrin type-A receptor 7 (EphA7), and rearranged during transfection (RET) were seen following AKT inhibition in both HER2+ and non-HER2+ cell lines (Chandarlapaty, Sawai et al. 2011). Collectively, these findings suggest that dual blockade of AKT and HER2 signalling may also be useful in non-HER2+ contexts. Indeed, combined AKT/HER2 inhibition was synergistic in supressing tumour growth in mice bearing xenograft established from NCI-H292, a non-HER2 amplified lung tumour cell lines (Chandarlapaty, Sawai et al. 2011). Provided toxicity is tolerable, dual combination of either PI3K or AKT inhibitors with HER3-neutralizing monoclonal antibody, or triple combination of PI3K/AKT, HER2 inhibitors and a HER3 antibody may be fruitful therapeutics for HER2+, as well as non-HER2+ cancers, as these combinations would more completely eliminate HER2-mediated HER3 activation. In support of this notion, combination of LJM716 (a HER3 neutralizing antibody) and BYL719 (a PI3Kα-specific inhibitor) inhibited AKT phosphorylation more potently than LJM716 or BYL719 alone and synergistically inhibited growth in a panel of HER2-overexpressing breast and gastric cancer cells

(Garrett, Sutton et al. 2013). Furthermore, in HER2-normal tumours where PI3K signalling is likely not driven by HER2 alone, depending on which upregulated RTKs, discussed above, are the primary input into PI3K/AKT signalling, co-inhibition of PI3K/AKT and such RTK(s) could also provide potentially effective therapies. Nonetheless such avenues clearly warrant further investigation in future research.

What about breast cancer with co-alteration of HER2 and PI3K? Our analysis of data from TCGA (using CBioPortal) showed that almost one third of HER2-amplified breast cancer patients also harbour PIK3CA mutation and/or amplification (**Figure 1.3**). In another important study (Chakrabarty, Rexer et al. 2010), Chakrabarty and colleagues found that expression of H1047R PI3K (the most common PI3K mutation) in MCF10A human mammary epithelial cells, but not E545K PI3K, markedly upregulated the HER3/HER4 ligand heregulin (HRG). This provides, yet another mechanism where specific PI3K mutations further fuel the activation of HER3 mediated by HER2. As expected, the dual PI3K/mTOR inhibitor BEZ235 markedly inhibited HRG and p-AKT levels and, in combination with lapatinib, completely inhibited growth of cells expressing H1047R PI3K (Chakrabarty, Rexer et al. 2010). These findings suggest that selection of drug combinations would need to consider the specific mutation status of PIK3CA, as direct PI3K inhibitors may be required to inhibit the unwanted mutation-induced upregulation of ERBB ligands (Rexer, Chanthaphaychith et al. 2014). These results also point to the combined use of PI3K inhibitors and ERBB1-3-neutralizing antibody mixtures, such as a Pan-HER that can simultaneously block targeted ERBB receptor and ligands (Schwarz, Hutchinson et al. 2017), as a potential therapy for breast cancer tumours with HER2/PIK3CA co-alteration.

In summary, drug induced-RTK upregulation leading to resistance has been observed by many studies to kinase inhibitors of both MAPK and PI3K pathways (Nazarian, Shi et al. 2010, Villanueva, Vultur et al. 2010, Chandarlapaty, Sawai et al. 2011). These findings provide a framework for understanding ways in which resistance to agents that target single nodes in a signalling network can occur, as well as how one can rationally use this information to guide choices for combination therapy.

1.6.4 PI3K pathway inhibition rewires ERK signalling through multiple mechanisms

While the above studies have primarily demonstrated that the PI3K/AKT pathway itself is a major escape mechanism to inhibitors targeting PI3K signalling, other studies also found that compensatory activation of ERK signalling provides another escape route. First, Carracedo et al. (Carracedo, Ma et al. 2008) showed that inhibition of mTORC1 with rapamycin not only activated PI3K-AKT signalling, but also induced ERK phosphorylation in breast cancer cell lines and tumour biopsies from patients treated with the drug. Rapamycin-induced ERK activation occurred in both normal and cancer cells lines, due to interference of a negative feedback from mTORC1/S6K to PI3K/RAS, most likely mediated via IRS1 (Carracedo, Ma et al. 2008). Later, Serra and colleagues (Serra, Scaltriti et al. 2011) demonstrated treatment with the dual PI3K/mTOR inhibitor BEZ235 in HER2+ breast cancer cells also led to potent

ERK activation, but primarily through upregulation of the RTKs, particularly ERBB signalling. This mechanism of ERBB-induced ERK activity was confirmed as combined treatment BEZ235 with HER2/3 antagonists (lapatinib or trastuzumab) or MEK inhibitor (selumetinib) led to decreased ERK activity and improved anti-tumour activity *in vivo* compared to BEZ235 treatment alone (Carracedo, Ma et al. 2008).

Does ERK activation depend on the inhibitor target? While BEZ235 was used mainly, Serra and colleagues also demonstrated ERK activation in response to diverse agents including pan-PI3K inhibitor (GDC-0941), p110α inhibitor (PIK-90), AKT inhibitor (MK-2206), as well as mTOR inhibitor (RAD001 and Torin1) in a couple of HER2+ breast cancer cell lines including BT474, suggesting ERK activation is a broad consequence of PI3K signalling inhibition regardless of the targeted node (Serra, Scaltriti et al. 2011). This, however, is at odds with results from (Chakrabarty, Sanchez et al. 2012), which reported no consistent ERK activation in BT474 cell line in response to pan-PI3K inhibition. Because the data related to ERK activation in BT474 was discussed but 'not shown' in (Carracedo, Ma et al. 2008), we could not further check/analyse these findings. Additional clues to the above question came from Will et al. (Will, Qin et al. 2014) who showed that inhibition of PI3K, but not AKT, leads to the rapid, but transient inhibition of the RAS-ERK signalling axis in HER2+ breast cancer cells; and this inhibition, though transient, is critical for the enhanced cell death caused by PI3K over AKT inhibitors. The authors posited that inhibiting PI3K causes the rapid inhibition of both AKT-mTOR and RAS-ERK signalling, whereas AKT inhibitors suppress only the former and, in fact, activate the latter. The discrepancies among the above studies deserve more investigation, which will offer more clarity on how dependent ERK activation is with regard to the specific inhibitors and/or the targets they inhibit.

In line with the above observations, a more recent study also reported induced ERK activation following prolonged HER2 inhibition with lapatinib in HER2+ breast cancer cells, which was partially dependent on FOXO transcription factors (Matkar, An et al. 2017). Interestingly, the lapatinib-induced increase in ERK phosphorylation is correlated with increased stability of c-MYC, suggesting that, in this case, ERK activation was probably due to disruption of both the AKT/FOXO and ERK/c-MYC negative feedbacks to the ERBB receptor family caused by lapatinib-mediated acute AKT and ERK inhibition. Further, compensatory ERK activation was observed *in vivo* in a genetically modified mouse model of HER2+ breast tumour with coexisting PIK3CA(H1047R) following inactivation of the oncogenic PI3K (Cheng, Liu et al. 2016). Collectively, the studies discussed here provide a strong rationale for targeting both the PI3K and ERK pathways in HER2+ breast cancer. Activation status of these pathways, including whether or not the tumours harbour loss of PTEN and/or RTK overexpression, can influence therapeutic response and serve as useful biomarkers for therapy selection (Sato, Wakabayashi et al. 2017).

1.6.5 Overcoming adaptive kinome response to PI3K inhibition through BET inhibition

It has become clear from the above studies that similar to MEK inhibition, inhibition of the PI3K signalling pathway also triggers induction of a whole host of RTKs, many of which are also induced by MEKi. In light of the effectiveness of BET inhibition as a way to prevent RTK programming following MEKi, the use of BET inhibitors as part of combination therapy have been also explored in PI3K-driven tumours. Consistent with previous work, Stratikopoulos et al. (Stratikopoulos, Dendy et al. 2015) showed that PI3K inhibition induces feedback activation of upstream RTKs and quick rebound of PI3K pathway activity. Importantly, they showed that BRD4 is key for these RTKs activation, with increased BRD4 occupancy observed at conserved regions upstream from the transcriptional start site of multiple RTKs and MYC, which was blocked by treatment with the BET inhibitor MS417. Consequently, BET inhibitors inhibited the activation of AKT, mTOR, and MYC due to PI3K inhibition, and combined PI3K-BET inhibition sustained PI3K pathway inhibition and enhanced tumour cell killing in a variety of tumour models, including prostate cancer, melanoma and TNBC (Stratikopoulos, Dendy et al. 2015). In another study, BET inhibition was also able to supress lapatinib-induced transcriptional induction of a large portion of tyrosine kinases including those identified to contribute to growth (HER3, DDR1, FGFR2 and MET) in HER2+ breast cancer cells (Stuhlmiller, Miller et al. 2015), preventing downstream SRC/FAK signalling and AKT reactivation.

Taken together, these findings suggest that combined kinase and epigenetic targeting can be a broader, more efficacious strategy to circumvent feedback-mediated resistance from inhibition of other kinases besides PI3K. This approach prevents adaptive resistance via kinome reprogramming by blocking transcription, generating the necessary sustained pathway inhibition as well as overcoming the issue of heterogeneity in the adaptive kinome reprogramming response. Despite these promising results, further work will be required in additional models and in human clinical trials to determine the efficacy and safety of combining BET and PI3K inhibitors. For an in-depth review on other adaptive resistance mechanisms to PI3K-AKT-mTOR signalling inhibition see the review paper in appendix 1.

1.7 Integrated network modelling: a powerful approach for drug combination model predictions with promising results

Biological processes occur at different time scales ranging from milliseconds (conformational changes) and minutes (post-translational changes), to hours, days (gene expression) and years (epigenetic changes). Many studies investigating network signalling soley focus on one pathway in isolation at single points in time. In doing so, the research fails to reflect or incorporate the complex interconnectivity of pathways and the network crosstalk of cells. This static approach misses the valuable dynamic changes that occur in the pathway over time which greatly limits our understanding of the network behaviour as a whole. Understanding the dynamic circuitry of signal transduction

networks that regulate functions such as cell proliferation and survival are key to understanding tumourigenesis and cancer cell behaviour including drug resistance (Kolch, Halasz et al. 2015). Due to the complexity of drug resistance, effective insight and understanding into drug resistance mechanisms, identifying new drug targets, predicting effective drug combinations and therapeutic outcomes, requires the integration of both mathematical modelling and experimental investigations. As a result computational modelling is highly instrumental and increasingly being utilised as a powerful quantitative tool to complement experimental data. Computer simulations of signalling networks produce a model which is guided and validated by the experimental data. In turn these computational models aid in validating and providing a mechanistic explanation for observed experimental data (Nguyen and Kholodenko 2016).

Moreover, mathematical modelling and model-based analysis can rationally inform suitable therapeutic targets and new drug combinations. While it is much more costly and practically challenging to screen vast number of possible target/drug combinations experimentally, predictive modelling, in principle, can be exploited to narrow down myriad possibilities and prioritise optimal combinations, thereby focusing experimental efforts only on these lead candidates (Fitzgerald, Schoeberl et al. 2006). We have recently demonstrated the validity of these concepts through model-based analysis of drug-induced signalling rebound in TNBC cells, and development of a computational drug combinations identification pipeline that enables *in silico* screening of numerous pair-wise drug combinations directed at signalling nodes and the ability to rank them by synergistic potential (Shin, Muller et al. 2018). Applying this pipeline to a new mathematical model of EGFR signalling in TNBC led to predictions that combined inhibition of EGFR with proline-rich tyrosine kinase 2 (PYK2), and to a lesser extent c-MET, displayed potent synergistic effects in suppressing oncogenic signalling. Experimental validation in TNBC cell lines and tumour xenograft confirmed these model predictions (Verma, Muller et al. 2017, Shin, Muller et al. 2018). Further, unlike machine learning based approaches to drug combination discovery which often treat the target system as black-boxes (Feala, Cortes et al. 2010), dynamic modelling has the ability to offer mechanistic reasoning behind the synergistic effect of effective drug combinations, which are critical for assessing their application under different cellular contexts. Integrated analysis of both the modelling and experimental data revealed a link between the observed switch-like responses to single-drug inhibition at both cell proliferation and signalling levels, and the synergistic drug combinations. Indeed, time-course simulations showed that EGFR-PYK2 co-inhibition was synergistic because it eliminated the adverse network rewiring and reactivation of STAT3 and ERK caused by either EGFR or PYK2 inhibition alone (Shin, Muller et al. 2018). Finally, by incorporating gene expression data from TNBC patient's simulations of patient specific models were developed allowing patient stratification into subgroups with predicted sensitivity to this combination treatment based on high expression of PYK2 and EGFR/c-MET.

1.8 Current challenges

Although there is a growing shift towards using combination therapy, this approach faces many challenges, including ways to best predict which drug combinations would be most effective and for which patients. The huge heterogeneity between cancer patients and their tumours, as well as the heterogeneity in the drug-induced network response leading to adaptive resistance poses a significant challenge for personalised cancer treatment and strongly demonstrates the need for multiple sequential combinations of kinase inhibitors that would be applicable in multiple tumour settings. Predicting which selection of tyrosine kinases are activated by feedback in any given tumour has not yet been achieved. In addition, finding out how to prioritize these drug combinations for clinical trials to achieve optimal benefit by patient stratification remains a challenge. Many clinical trials combine targeted inhibition with chemotherapy, however, only a few trials have combined small-molecule inhibitors. A key issue with combination strategies is the dose-limiting toxicity that results from using multiple drugs at once, which can lead to intolerable safety profiles (Tolcher, Peng et al. 2018). Moreover, despite initial successes, resistance to combination therapies often eventually still occurs. Here, mathematical modelling of biochemical networks further provides an effective approach to capture the patient-to-patient heterogeneity through incorporation of patient-specific –omics data and generation of patient-specific models (Fey, Halasz et al. 2015, Shin, Muller et al. 2018). These models can then be used to predict drug response (Faratian, Goltsov et al. 2009, Li, Mohammad-Djafari et al. 2013, Fey, Halasz et al. 2015), design rational combination (Nguyen, Matallanas et al. 2013, Shin, Muller et al. 2018) and identify potential predictive biomarkers (Fey, Halasz et al. 2015, Shin, Muller et al. 2018) in a personalised manner. More interestingly, dynamic outputs from these computational network models can themselves serve as biomarkers (Kolch and Fey 2017) that may be integrated with classical genes or protein-centric biomarkers for better personalisation of the treatment options. While mathematical modelling has been a highly useful tool for gaining systems-level understanding of signalling networks over the past decade, we believe future research priority should be placed on harnessing the translational capability of these models.

Importantly, in the landmark study by Lee et al. (Lee, Ye et al. 2012) it was revealed that the timing of drug administration is critical in triggering synergistic effects that effectively kill TNBC cells. The authors found that time-staggered pre-treatment (at least 4 hours prior) with the EGFR inhibitor erlotinib in combination with the DNA-damaging agent, doxorubicin sensitized TNBC cells by significantly enhancing apoptosis mediated rewiring of apoptotic signalling pathways. In contrast, simultaneous co-administration antagonized doxorubicin sensitivity. The results here highlight the potential effect that the order and timing of drug administration can also have on a therapies' success. Thus, these findings highlight another layer of complexity to combination treatment strategies and need to be considered when designing future clinical trials, as it could potentially change the efficacy of combination therapies.

1.9 Conclusion

MAPK and PI3K signalling pathways are frequently disrupted in cancer, including TNBC. Either PTEN loss or activating mutations in PIK3CA lead to PI3K pathway hyper-activation and tumorigenesis. Crosstalk and feedback regulation between the MAPK and PI3K pathways in response to drug treatment enable cancer cells to acquire drug resistance through adaptive bypass mechanisms. The ways in which these intricate and complex pathway alterations come about is still not well understood. Therefore, studying these underlying mechanisms of cancer drug resistance is key to identifying new drug targets, and assisting with the discovery of predictive and synergistic drug combinations to improve therapeutic outcomes. As highlighted by this literature review, a powerful approach for understanding the complex mechanisms of drug resistance, is the combination of both mathematical modelling and experimental investigations. My project aims to utilise this innovative and integrated approach to decipher the drug-induced changes in cancer signalling network dynamics (pathway activation/suppression). In this way, this research seeks to elucidate how cancer cells hijack adaptive network-based bypass mechanisms to confer resistance to pathway inhibitors. Furthermore, by modelling the dynamic network changes in response to drug treatment this project aims to construct models to predict and experimentally validate new synergistic drug combinations. Thus, these findings provide potential for optimising treatment strategies for breast cancer patients. In conclusion, breast cancer drug resistance is a major challenge and unmet medical need. Further research in this direction is needed to improve overall understanding and treatment of resistant cancers. My project seeks to address and fill some of these existing gaps in the current understanding of adaptive drug resistance mechanisms, in particular in TNBC.

1.10 Research Aims

The overarching goal of this thesis was to gain understanding into the adaptive bypass mechanisms of drug resistance to MAPK and PI3K pathway inhibitors in breast cancer using both genetically modified MCF10A cells (PTEN -/-) and TNBC cell lines.

1.10.1 Aim 1: Establish and characterise isogenic MCF10A PTEN KO cells

- Generate MCF10A PTEN KO clones using Clustered Regularly Interspaced Short Palindromic Repeat (CRISPR)/CRISPR-associated endonuclease (Cas9)

- Characterise the PI3K and MAPK signalling pathways in the MCF10A PTEN KO clones.

1.10.2 Aim 2: Investigate how PTEN loss influences the signalling response to PI3K and MAPK pathway inhibition

- Characterise the network-level changes which influence the dynamic response to PI3K (and ERK-MAPK) inhibition in PTEN KO and wild-type MCF10A cells.

- Investigate if altered drug responsiveness due to PTEN loss is driven by PI3K-MAPK pathway crosstalk.

- Investigate if reduced drug responsiveness to BYL719 treatment due to PTEN loss is driven via preferential activation of the p110β isoform in PI3K signalling.

1.10.3 Aim 3: Develop a computational model using the kinetic experimental data

- Develop and utilise the model to obtain network-level understanding into the mechanisms driving drug response in the presence and absence of PTEN.

Chapter 2: Materials and Methods

2.1 Tissue Culture

2.1.1 Cell culture

Human tissue culture cell lines acquired from American Type Culture Collection (ATCC) were maintained in a humidified environment under 5% (v/v) CO_2 at 37℃. Vials of frozen cells from liquid nitrogen storage were revived by thawing in a 37℃-water bath and resuspension in complete media prior to centrifugation for 3 min at 1000 rpm. The supernatant was then aspirated and the cells resuspended in complete media and cultured in 10 cm/15 cm plates or T25/T75 flasks from Corning. Cells were used for experiments up until passage 20 and cells were tested regularly for mycoplasma contamination and verified to be mycoplasma negative (**Figure 2.1**). To split and maintain cells, cells were washed with 1 x phosphate buffered saline (PBS), detached from plates with 0.05% (w/v) trypsin (Gibco, #15400054) at 37℃ in a tissue culture incubator. Trypsin was then neutralized with complete media and cells passaged according to **Table 2.1**.

Table 2.1 Human tissue culture cell lines

Cell lines	Split Ratio	Passage frequency/ week	Media	Acquisition
MCF10A-EcoR	1:20	2	DMEM: F12+ ADDITIVES	Harvard Medical School
MCF10A PTEN KOs: E6-1 & E6-7	1:20	2	DMEM: F12+ ADDITIVES	Generated in the lab using CRISPR-Cas9
BT-549 (PTEN -/-)	1:6	1	10N RPMI	ATCC® HTB-122™
MDA-MB-468 (PTEN -/-)	1:4	2	10N RPMI	ATCC® HTB-132™
SUM185PE	1:4	1	10N RPMI	Asterand Bioscience

Normal mammary epithelial cell line; MCF10A cells stably expressing the murine ecotropic receptor which aids in retroviral-mediated transduction (MCF10A EcoR) were a kind gift to the Roger Daly lab from Drs. Danielle Lynch and Joan Brugge, Harvard Medical School. These MCF10A EcoR cells (MCF10A) and MCF10A PTEN KO cells; E6-1 and E6-7, were cultured in a 1:1 mixture of Dulbecco's modified Eagle's medium and Ham's F12 (DMEM/F12, Gibco/Invitrogen Life Technologies) Medium supplemented with 5% horse serum, EGF, insulin, cholera toxin and hydrocortisone as detailed in **Table 2.2**. The TNBC cell lines SUM185PE, MDA-MB-468 and BT-549 were all cultured in Roswell Park Memorial Institute (RPMI) 1640 media supplemented with 10% foetal bovine serum (FBS), 4-(2-hydroxyethyl)-1-piperazineethanesulfonic acid (HEPES) and insulin as detailed in **Table 2.3**.

Table 2.2 DMEM/F12 Media content

MCF10A MEDIA (5% Horse Serum) - (J. Debnath et al, Methods 30 (2003))			
Content of DMEM/F12	**Final Conc.**	**Manufacturer**	**Catalogue Number**
500 ml DMEM/F12		Life Technologies	#11320-033/ #11320-082
25 ml Horse Serum	5% (v/v)	Life Technologies	#16050-122
100 µl EGF (Stock 100 µg/mL)	20 ng/ml	Peprotech	#AF-100-15
500 µl Bovine Insulin (Stock 10 mg/ml)	10 µg/ml	Sigma	#I-1882
250 µl Hydrocortisone (Stock -1 mg/ml)	5 µg/ml	Sigma	#H-0888
50 µl Cholera Toxin (Stock -1 mg/ml)	100 ng/ml	Sigma	#C-8052
Optional: 5 ml Pen/Strep/Glut	100 x	Life Technologies	#15070-063

Table 2.3 10N RPMI Media content

Content of 10N RPMI (10% FBS)	**Final Conc.**	**Manufacturer**	**Catalogue Number**
500 ml RPMI		Life Technologies	#11875-093
11 ml HEPES	20 mM	Life Technologies	#15630-080
1.4 ml Actrapid Insulin	10 µg/mL	Clifford Hallam Healthcare	#1331415
54 ml FBS USA Origin	10% FBS	Assay Matrix ASFBS-U	lot #ASM1-137A11

Cell lines were tested for mycoplasma contamination using in-house polymerase chain reaction (PCR) primers (**Table 2.4**) and verified to be mycoplasma negative as shown by the absence of the 300 base pair (bp) PCR product which is a marker for mycoplasma contamination (**Figure 2.1**). Cultured media (1 ml) that had been in contact with the cells at their growth peak (100% confluence) was collected in a labelled 1.5 ml microcentrifuge tube and stored at 4°C. On the day of the mycoplasma testing the media was centrifuged at 1500 rpm/200 g for 5 min at room temperature to remove any dead cells or debris and the supernatant was retained. On ice PCR master mixes of the samples were set up according to manufacturer's protocol as shown in **Table 2.4** and a negative control with nuclease-free H2O (Promega, #P119C) instead of DNA was also prepared. The thermocycler's conditions were set up for a routine 3-step PCR as shown in **Table 2.4**. During the PCR a 2% agarose gel was prepared by adding 2 g agarose to 100 ml 1 x TAE buffer (40 mM Tris, 20 mM, acetic acid, 1 mM EDTA, pH 8.3). Using

a microwave this was heated for 30 second intervals to ensure no spillage and the contents were mixed by swirling. Once molten, the gel was allowed to cool and 5 µl/100 ml RedSafeTM DNA dye was added into the agarose. In a pre-set-up gel tray the molten agarose was cast and allowed to cool at room temperature until solidified. The PCR samples were mixed with 5 x DNA loading buffer. For DNA length comparison a 100 base pair (bp) DNA Ladder (New England Biolabs (NEB)) was loaded onto the gel lane, followed by 5 µl of each sample. The agarose gel electrophoresis machine was run at 100 V for 30 min and the PCR products were visualised under an illuminator Gel-Doc. Samples contaminated that are mycoplasma will be indicated by a PCR product at around 300 bp size.

Table 2.4 PCR Master mix and thermocycler program for mycoplasma testing

Reagent		**25 µl Reaction**
10 µM Primer Forward: GGGAGCAAACAGGATTAGATACCCT		0.5 µl
10 µM Primer Reverse: TGCACCATCTGTCACTCTGTTAACCTC		0.5 µl
Cell culture supernatant		5 µl
One Taq® Quick-Load 2X Master Mix (NEB, #M0486)		12.5 µl
Nuclease-free H_2O (Promega, #P119C)		To 25 µl
PCR thermocycler program		
Step	**Temperature**	**Time**
Initial Denaturation	95°C	2 min
30 Cycles	94°C 60°C 72°C	60 seconds 60 seconds 60 seconds
Final Extension	72°C	15 minutes
Hold	10°C	

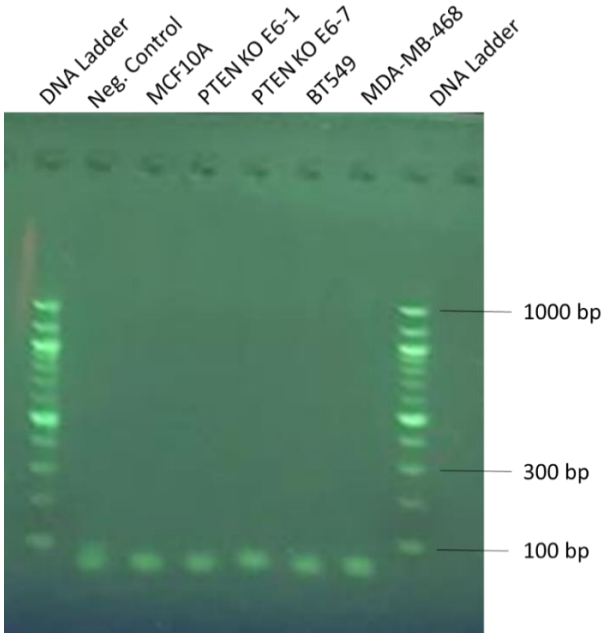

Figure 2.1 Mycoplasma testing of cell lines. Image of 2% agarose gel showing no mycoplasma contamination in WT MCF10As, PTEN KO clones (E6-1 and E6-7) and TNBC cells; BT-549 (PTEN-/-) and MDA-MB-468 cells (PTEN-/-) verified by the absence of 300bp PCR product which is a marker for mycoplasma contamination. PCR products were visualised under an illuminator Gel-Doc.

2.1.2 Cell counting

Cells were washed with 1 x PBS (136 mM NaCl, 2.6 mM KCl, 10 mM Na2HPO4, 1.76 mM KH2PO4, pH 7.4) then trypsinised at 37°C in a 5% CO_2 atmosphere to allow detachment. Trypsinised cells were then resuspended in complete media to neutralize the trypsin and mixed thoroughly by pipetting up and down. Resuspended cells were then centrifuged at 1000 rpm for 5 min and the supernatant aspirated. Cells were resuspended in 1-6 ml complete media and stained with Trypan blue (NanoTEK, #EVS-1000) and counted with the EVE automatic cell counter (EVE-MC-DEMO) according to the manufacturer's protocol.

2.1.3 Cell viability: MTS assay

Cell proliferation and viability was measured using (3-(4, 5-dimethylthiazol-2-yl)-5-(3-carboxymethoxyphenyl)-2-(4-sulfophenyl)-2H-tetrazolium, inner salt) MTS and an electron coupling reagent (phenazine ethosulfate; PES), which measure mitochondrial activity of viable cells. Cells were trypsinised as usual and counted. Cells were seeded 3000 cells in 100 µl cell/media mixture per well of a 96-well plate and allowed to adhere overnight in the incubator. Plates were incubated at 37°C in 5% CO_2 atmosphere. Day 1 post seeding cells were treated with MEK/PI3K inhibitor, Dimethyl sulfoxide (DMSO) vehicle control or media only. For each condition there was 5 technical replicates used. Media was added as a blank control to 5 wells and 200 µl PBS was added to all wells on the outer

edge. MTS cell assays were performed on separate plates for day 0 (no treatment), 1 and 2. At 0, 1- and 2-days post-treatment 20 ul MTS reagent, (Promega, #G3581) was added to each well and incubated for 1 h at 37°C. MTS absorbance readings were measured at 490 nanometre (nm) on the CLARIOstar (BMG, Labtech) or PHERAstar (BMG, Labtech) plate readers. Sample replicates were averaged and the blank was subtracted from them. Cell viability was depicted as a percentage of untreated DMSO control cells and data is represented as the mean values of three independent biological replicates.

2.2 PTEN KO using CRISPR/Cas9 gene editing

CRISPR/Cas9 gene editing technology was utilised to induce PTEN gene knock out using the CRISPR vector; pU6-(BbsI) CBh-Cas9-T2A-blue fluorescent protein (BFP) (Addgene plasmid, #64323) (Chu, Weber et al. 2015). Single guide RNA (sgRNA) oligos (**Table 2.5**) targeting exon 4 and exon 6 of PTEN gene were designed using CHOPCHOP (http://chopchop.cbu.uib.no) (Labun, Montague et al. 2016), an online CRISPR construction tool.

Table 2.5 Customised sgRNA oligos targeting Exon 6 of PTEN

Bioneer	Sequence 5-3′	GC content	Tm°C	MW (g/mole)	Vol. for 100 pmoles/µl
PTEN sgRNA Exon 6 Top strand	CACCGTGGGAATAG TTACTCCCTGG	56%	63.4	7657.8	76.2 µl
PTEN sgRNA Exon 6 Bottom strand	AAACCCAGGGAGTA ACTATTCCCAC	48%	61	7603.8	72.9 µl

2.2.1 CRISPR oligoduplex formation and vector ligation of sgRNA insert

The exon 4 and exon 6 PTEN sgRNA oligos (Bioneer) were diluted in nuclease-free H_2O to a concentration of 100 µM using the volumes given in **Table 2.5**. The sgRNA oligo inserts were set up for annealing with its top/bottom strand as shown in **Table 2.6**. sgRNA oligo inserts were then incubated at 37°C for 30 minutes in a PCR thermocycler, followed by heating to 95°C for 5 min; then slowly cooled down to 25°C at 5°C/minute, then held at 4°C. Cycling conditions were set up to enable the formation of CRISPR oligoduplexes. The cycling at 95°C allowed for the CRISPR primers (100 µM) to become phosphorylated at the 5' (allowing future ligation) by T4 polynucleotide and a subsequent decrease to 25°C results in the formation of the CRISPR oligoduplex. The annealed sgRNA oligos were diluted to 1:200 using nuclease-free H_2O and the CRISPR backbone vector; pU6-(BbsI) CBh-Cas9-T2A-BFP was digested with BbsI restriction enzyme for 2 h at 37°C on either a heat block or the thermomixer (**Table 2.7**). The digested vector was then purified as per instructions of the DNA clean-up kit; Wizard® SV Gel and PCR Clean-Up System (Promega, #A9281**,**). The purified CRISPR vector was then dephosphorylated with antarctic phosphatase by setting up the reaction as per **Table 2.8**. This was followed by another purification step using the PCR Clean-Up System as instructed

before. Finally, the newly phosphorylated sgRNA duplex insert created with sticky ends during the PCR reaction is subsequently ligated into the digested CRISPR vector; pU6-(BbsI) CBh-Cas9-T2A-BFP backbone by an overnight ligation reaction at 16°C as per **Table 2.9**. A no-insert reaction was set up as a negative control.

Table 2.6 Annealing and 5' phosphorylation of sgRNA oligos

Reagents added	Volume (µl)	Manufacturer	Catalogue Number
sgRNA (Exon 4/6) top (100µM)	1	Bioneer	N/A
sgRNA (Exon 4/6) bottom (100µM)	1	Bioneer	N/A
T4 Polynucleotide Kinase Buffer 10 x	1	NEB	#B0201S
T4 Polynucleotide Kinase (PNK) ligase	1	NEB	#M0201S
Nuclease-free H_2O	6	Promega	#P119C
Total	10		

Table 2.7 BbsI digestion of CRISPR plasmid vector (pU6-BFP)

Reagents added	Volume	Manufacturer	Catalogue Number
BbsI Restriction Enzyme	1	NEB	#R0539S
DNA template (CRISPR plasmid vector)	Vol for 1 µg DNA	Addgene	#64323
10 x NE Buffer 2.1	5 µl	NEB	#B7202S
Nuclease-free H_2O	Top up to 50 µl	Promega	#P119C
Total	50 µl		

Table 2.8 Dephosphorylation of CRISPR plasmid vector (pU6-BFP)

Reagents added	Volume	Manufacturer	Catalogue Number
pU6-(BbsI) CBh-Cas9-T2A-BFP vector	1 µg	Addgene	#64323
10 x Antarctic Phosphatase buffer	3 µl	NEB	#B0289S
Antarctic Phosphatase	1 µl	NEB	#M0289S
Nuclease-free H_2O	Top up to 30 µl	Promega	#P119C
Total	30 µl		
Set up reaction mix as follows: incubate at 37°C for 15 min. Heat inactivate for 5 min at 70°C			

Table 2.9 Overnight ligation of oligoduplex into the Bbsl digested vector (pU6-BFP)

Reagents added	Volume (µl)	Manufacturer	Catalogue Number
sgRNA oligoduplex	2	Bioneer	N/A
Bbs1 digested vector	1	Addgene	#64323
T4 Ligation Buffer 10 x + 10 mM ATP	1	NEB	#B0202S
T4 DNA Ligase	1	NEB	#M0202M
Nuclease-free H_2O	5	Promega	#P119C
Total	10		

2.2.2 Transformation of construct into *E. coli* cells

Ligation products were transformed into chemically competent DH5-alpha Escherichia coli (*E. coli*) cells. DH5α cells were thawed on ice for 5–10 min and 5 µl of the ligated construct was added to the cells. The tubes were mixed gently and incubated on ice for 30 min followed by heating to 42℃ for 1 min to heat shock the proteins. After this, cells were placed back on ice for 3 min and 500 µl of lysogeny broth (LB) media was added to the cells. The cells were then recovered by incubating on the thermomixer for 1 h at 37℃ at 350 rpm. Then the tubes were centrifuged for 5 min at 4000 rpm and 400 µl of the supernatant was taken out and the cells resuspended in 100 µl of LB media. This mixture was added onto a pre-warmed LB agar ampicillin (100 µg/ml) plates. and the DH5α cells were spread evenly across the agar plate using a sterilized spreader. Sterilise cell spreader by firstly immersing it in 100% ethanol, then let it sit in the flame for 2 seconds, and lastly let it cool for 5 seconds. The agar plate was placed into the 37℃ incubator and incubated overnight for no more than 18 h to prevent satellite colonies from forming. The following day the plates were screened for positive colonies. Selecting a single positive colony at a time, these were placed inside a round-bottom tube with pre-mixed LB media/ampicillin (3 ml LB media + 100 µg/ml ampicillin). Tubes were placed in a shaker at 220 rpm and incubated overnight at 37℃. The following day tubes were centrifuged at 4000 rpm for 5 min. Plasmids were extracted from the *E. coli* cells by use of the Wizard® Plus SV Minipreps DNA Purification System (Promega, #A1460) as per manufacturer's instructions. DNA was eluted in 40 µl nuclease-free water. The DNA was quantified in ng/µL using a Thermo Scientific NanoDrop™ 1000 Spectrophotometer. The DNA was quantified using the standard dsDNA option measurement with accepted extinction coefficient of 50 ng.cm/µl for double-strand DNA based on A260 nm absorbance.

2.2.3 Sequencing verification of sgRNA insert

The purified PCR products (400 ng of DNA) were sequenced using 10 µM U6 Forward Primer (5' GAG GGC CTA TTT CCC ATG ATT CC 3') at the Monash Micromon DNA sequencing facility to verify the sgRNA sequences were cloned correctly. The software FinchTV was used to view the DNA sequence and confirm the sgRNA was inserted correctly into the vector construct. After confirmation

of the insertion of the sgRNA sequence into the vector, the QIAGEN Plasmid plus Maxi -Kit (#12162, #12163, and #12165), and the Plasmid Buffer Set (#19046) was used as per manufacturer's instructions to produce plasmid DNA stock for future experiments. The DNA was quantified in ng/µL using a Thermo Scientific NanoDrop™ 1000 Spectrophotometer.

2.2.4 CRISPR/Cas9 vector transfection of cultured MCF10A cells by lipofection

MCF10A cells were transfected using the Lipofectamine 3000 reagent protocol (ThermoFischer Scientific) (**Table 2.10**). MCF10A cells were first seeded at 2 x 10^5 per well of a 6-well plate (approx. 50% confluency) and incubated overnight. Cells were transfected with 1.25 µg of DNA for each sgRNA construct (Exon 4 and Exon 6). A Master-Mix was prepared 5 µl of Lipofectamine 3000 reagent +250 µl optimum for each well. (x # of wells used). Mixed and incubated for 5 min at room temperature. Added 2.5 µl of p3000 reagent (2 µl/ug DNA) + 1.25 µg of DNA and made up to 250 µl with optimum for each well. Mixed together in a 1:1 ratio (250 µl) and incubated for 15 minutes at room temperature. Aspirated off previous culture medium and added 1.5 ml of fresh media (max 2 ml per well of 6-well plate). Added all 500 µl of DNA-lipid mix to cells in a drop wise fashion and incubated overnight at 37°C and 5% CO_2. Both a positive (Empty vector only) and a negative (No DNA, but all other reagents) control were prepared and the media was changed the following day.

Table 2.10 The experiment was set up as per Lipofectamine 3000 reagent protocol

Timeline	Steps	Components (6-well plate)
Day 0	Seeded cells to be 90% confluent at transfection	MCF10A-EcoR cells in DMEM/F12 media
Day 1	Diluted Lipofectamine 3000 in Opti-Mem Medium – Mix well by vortexing	Opti-MEM Medium (Millipore, #31985088)
		Lipofectamine 3000 Reagent (Invitrogen, #L3000008)
	Prepared master mix	Opti-MEM Medium (Millipore, #31985088)
		DNA (0.5-5 µg/ul)
		P3000 Reagent (2 µl/ug DNA)
	Added diluted DNA to each tube of diluted Lipofectamine 3000 reagent (1:1 ratio)	Diluted DNA (with P3000 Reagent)
		Diluted Lipofectamine
	Incubated	At room temp for 10-30 min
	Added DNA-lipid complex to cells in each well of a 6-well plate	250 µl DNA-lipid complex/well
		1500 ng DNA/well
		2.5 µl P3000 Reagent/well
		Lipofectamine 3000 5 µl
Day 2	Changed media	Incubated cells for 2-4 days then analysed transfected cells by FACS
Day 3	48 h post-transfection used FACS to sort transfected cells	

2.2.5 Fluorescent activated cell sorting (FACS) of transfected cells

At 48 hours post transfection FACS cell sorting was used to select only transfected cell populations using Blue Fluorescent Protein (BFP) generating isogenic PTEN KO cell populations. Only positively transfected MCF10A cells with the CRISPR vector pU6-(BbsI) CBh-Cas9-T2A-BFP containing the sgRNA constructs (sgRNA targeting either Exon 4 or Exon 6 of PTEN) to delete PTEN would fluoresce blue as the vector contained BFP. The transfected cells were trypsinised, spun at 1000 rpm for 5 min and the media aspirated as per usual procedure. The cells were then counted to ensure there was > 1 x 10^7 cells. Cells were resuspended in cell sorting media (1 x PBS, 2% FBS, 1 x antibiotics & antimycotics, gentamycin, 1 x pen-strep) A 96-well plate was prepared per sgRNA construct (Exon 4 and Exon 6 PTEN) with 200 µl of cells in cell sorting media/well. The samples on ice were sorted at the Flowcore cell sorting facility. At the facility, the blue cap filter was rearranged onto a polypropylene bottom and the cells were filtered through the blue capped filter unit (5 ml polypropylene tubes and blue cap strainers). The heterogeneous population of cells was sorted one cell at a time based upon the specific light scattering and fluorescent characteristics of each cell. Single cells with BFP were sorted into each

well of a 96-well plate and 1 x 96-well plate was used per sgRNA construct. Over the next 3 months PTEN KO clones were maintained and expanded up to 10 cm plates. This resulted in the generation of 22 PTEN KO cell lines.

2.2.6 PTEN KO validation using PCR and Sanger sequencing

Genomic DNA was extracted and purified from the WT and PTEN KO MCF10A cell lines using Wizard® Genomic DNA Purification Kit (Promega) as per manufacturer's protocol instructions.
Amplification of the PTEN sequence targeted by CRISPR/Cas9 constructs, in this case Exon 6 of PTEN was performed on the purified genomic DNA by PCR using the PTEN PCR primers (**Table 2.11**). These were previously designed using CHOPCHOP (http://chopchop.cbu.uib.no) (Labun, Montague et al. 2016), an online CRISPR construction tool.

Table 2.11 PTEN PCR Primers to amplify the PTEN Sequence targeted by CRISPR

Bioneer	Sequence 5-3′	GC content	Tm°C	MW (g/mole)	Vol. for 100 pmoles/µl
PTEN PCR Primer Exon 6 Left	GCTACGACCCAGTT ACCATAGC	54.6%	59.6	6664.2	143.1 µl
PTEN PCR Primer Exon 6 Right	ATCTTGTGAAACA ACAGTGCCA	40.9%	58	6727.3	136.5 µl

2.2.6.1 PCR reaction

A PCR reaction was set up as shown in **Table 2.12** using 10 mM stocks of the PCR primers and using 50 ng of genomic DNA. The thermocycler's conditions were set up for a routine PCR (3-step PCR) as shown in **Table 2.13**.

Table 2.12 PCR reaction components

Component	50 µl Reaction	Final Conc.	Manufacturer + Cat. #
Nuclease-free water	Top up to 50 µl		Promega, #P119C
5 x Phusion GC Buffer	10 µl	1 x	NEB, #B0519S
10 mM dNTPs	1 µl	200 µM	NEB, #N0447L
10 µM Forward Primer	2.5 µl	0.5 µM	Bioneer
10 µM Reverse Primer	2.5 µl	0.5 µM	Bioneer
Template genomic DNA	Vol. needed for 50 ng DNA	50 ng	N/A
100% DMSO (optional)	1.5 µl	3%	NEB, #B0515A
Phusion DNA Polymerase	0.5 µl	1.0 units/50 µl PCR	NEB, #M0530

Table 2.13 Thermocycler's conditions for a routine 3-step PCR

Step	Temperature	Time
Initial Denaturation	98°C	2 min
35 Cycles	98°C 60°C 72°C	10 seconds 30 seconds 15 – 30 seconds / kb
Final Extension	72°C	10 minutes
Hold	4°C	

2.2.6.2 Agarose gel electrophoresis

Gel electrophoresis was used to detect the presence of DNA. DNA bands were separated based on molecular weight via electrophoretic mobility. Firstly 1% (w/v) agarose gel was prepared by adding 0.5 g agarose to 50 ml 1 x TAE buffer (40 mM Tris, 20 mM, acetic acid, 1 mM EDTA, pH 8.3) was prepared for gel electrophoresis and 5 µl /100 ml RedSafe™ DNA dye was added into the molten agarose. The molten agarose was cast in a gel casting tray. This was allowed to cool at room temperature until solidified. The PCR samples were mixed with 5 x DNA loading buffer and the agarose gel was run at 100V for 30 min. DNA Ladders of 100 (bp) (NEB, #N3231S) or 1 kilobase (kb) (NEB, #N3232S) were loaded onto the gel lane for DNA length comparison. The PCR products were visualised under an illuminator Gel-Doc and cut out of the gel using a scalpel. This was placed into a 2 ml microcentrifuge tube and the PCR product was extracted from the gel. As per instructions of the QIAquick Gel Extraction Kit (50) QIAGEN's protocol. The eluted DNA was quantified in ng/µL using a Thermo Scientific NanoDrop™ 1000 Spectrophotometer. Then 400 ng of DNA and the same PCR primers were supplied to Micromon for DNA sequencing. Using FinchTV software to view the DNA sequence, PTEN loss was validated by the identification of insertions and deletions (INDELS) in the sequences from the PTEN KO clones.

2.3 Protein harvesting and BCA assay quantification

Protein lysates were extracted from the cultured cells using modified cell lysis radioimmunoprecipitation assay (RIPA) buffer (**Table 2.14)** added with phosphatase and protease inhibitors (**Table 2.15)**. On ice, media was aspirated off and cells were washed with ice-cold 1 x PBS and then lysed using RIPA buffer. Lysed cells were scraped with disposable scrapers (Sarstedt, # 83.1831), collected in 1.5 ml microcentrifuge tubes and spun at 15,000 rpm for 10-15 min by centrifugation at 4°C. Ensuring the cell pellet was undisturbed the protein supernatants were removed and pipetted into clean, labelled microcentrifuge tubes and stored in the minus 80°C freezer. Protein lysate concentrations were quantified with the Pierce™ BCA Protein Assay Kit (#23225) as per

manufacturer's instructions. Bovine serum albumin (BSA) was used as standards and absorbance was measured at 562 nm on the CLARIOstar (BMG, Labtech) or PHERAstar (BMG, Labtech) plate readers.

Table 2.14 Modified cell lysis RIPA Buffer ingredients

RIPA Buffer 0.5% (w/v) deoxycholate		
Chemicals	**Stock Chemical Conc.**	**Vol of Stock**
0.5% (w/v) Sodium Deoxycholate	Powder	2.5 g
150 mM NaCl	5 M NaCl	15 ml
1% NP40	100%	5 ml
50 mM Tris, pH 8.0	1 M	25 ml
0.1% SDS	10%	5 ml
10% Glycerol	100%	50 ml
5 mM EDTA	0.5 M	5 ml
20 mM NaF	0.5 M	20 ml
Contents all dissolved using Millipore H_2O		

Table 2.15 RIPA Buffer Protease and Phosphatase inhibitors

Inhibitors	Stock Concentration	Working concentration	Dilutions
Aprotinin	10 mg/ml	10 µg/ml	1:1000
Leupeptin	10 mg/ml	10 µg/ml	1:1000
Sodium Orthovanadate	100 mM	1 mM	1:100
PMSF	100 mM	1 mM	1:100

2.4 SDS-PAGE and immunoblotting

Sodium dodecyl sulphate-polyacrylamide gel electrophoresis (SDS-PAGE) was used to detect the presence and expression of proteins. Visible protein bands were separated based on molecular weight via electrophoretic mobility. Polyacrylamide gels with 1/1.5 mm thickness were cast for SDS-PAGE Protein lysates were prepared in 5 x sample loading buffer (**Table 2.16**) and denatured for 10 min at 96°C. Samples were resolved by SDS-PAGE on a 5% (w/v) stacking gel and 8-10% (v/v) resolving gel (**Table 2.16**). Protein samples (10-20 µg) were loaded onto the gels and separated in running buffer using a Mini–PROTEAN Tetra Cell electrophoresis (Bio-Rad) system. Precision Plus Protein™ Dual Color Standard markers (#1610374, Bio-Rad) were loaded onto the gel for molecular weight comparison. Samples were run at 80 V through the stacking gel until the dye front entered the separating gel, and then resolved at 120 V until the dye front reached the bottom of the separating gel.

Resolved proteins were wet transferred onto PVDF membrane (Merck-Millipore, #1PVH00010) in wet transfer buffer (25 mM Tris, 192 mM glycine, 10% ethanol (v/v), pH 8.3) for 1 h at 100 V at room

temperature. After transfer the PVDF membranes were blocked in BSA blocking solution for 1 h at room temperature. The membranes were then cut with a scalpel into strips based on the size of the target protein. The molecular weight (MW) ladder was used as a guide and each membrane strip was probed with the primary antibody in that size range (**Table 2.17)** diluted by 1:1000 in BSA blocking solution, and incubated at 4℃ overnight. Membranes were washed three times for 5 min with tris buffered saline with Tween 20 (TBS-T) (150 mM NaCl, 50 mM Tris, 0.05% Tween-20 (v/v), pH 7.6) and then probed with secondary anti-mouse (-Ms) or anti-rabbit (-Rb) antibody (**Table 2.17)**, diluted by 1:3000 in 5% milk TBS-T solution (**Table 2.18)** for 1 h at room temperature. Followed by three washes for 5 min with TBS-T and signal detection by enhanaced-chemiluminescence (ECL); Western Lighting (Perkin Elmer, #NEL105001EA) or Luminata Forte Western horse radish peroxidase (HRP) Substrate (Millipore, #WBLUF0500). Images were acquired with ChemiDoc Touch Imaging system (Bio-Rad, # 1708370).

Table 2.16 List of solutions for SDS-PAGE

Media	Components
Stacking Gel	5% (v/v) acrylamide /bis solution 25% (v/v) 0.5 M Tris pH 8.8 0.01% (v/v) SDS 0.01% (w/v) Ammonium Persulfate 0.08% (v/v) TEMED (161-0801, Bio-Rad)
Separating Gel	8% (v/v) 30% Acrylamide 25% (v/v) 1.5 M Tris pH 8.8 0.01% (v/v) SDS 0.01% (v/v) Ammonium Persulfate 0.08% (v/v) TEMED (161-0801, Bio-Rad)
5 x Sample Loading Buffer	9% (v/v) glycerol 0.03% Tris/HCL pH 6.8 2% (w/v) SDS 0.05% (v/v) β –mercapethanol 0.002% (w/v) bromophenol blue
Running Buffer	25 mM Tris, 192 mM glycine, 0.1% SDS (v/v), pH 8.3

Table 2.17 List of primary and secondary antibodies used in western blotting

Primary Antibody	Dilution	Species	Manufacturer	Catalogue #
p-EGFR (Y1068)	1:1000	Ms	Cell Signalling	#2236S
EGFR	1:1000	Rb	Cell Signalling	#4267S
p-mTOR (Ser2448)	1:1000	Rb	Cell Signalling	#5536P
mTOR	1:1000	Ms	Cell Signalling	#4517S
ERK1/2 Thr202/Tyr204	1:1000	Rb	Cell Signalling	#4370L
p44/42 MAPK (ERK1/2)	1:1000	Rb	Cell Signalling	#4695S
PTEN	1:1000	Rb	CST	#9188S
p-STAT3 (Y705)	1:1000	Rb	Cell Signalling	#9145S
STAT3	1:1000	Ms	Cell Signalling	#9139S
pS6 (Ser235/236)	1:1000	Rb	Cell Signalling	#2211
S6	1:1000	Ms	Cell Signalling	#2317
Cl. PARP (D214)	1:1000	Ms	Cell Signalling	#9546S
p-AKT (Ser473)	1:1000	Rb	Cell Signalling	#4058C
AKT Pan	1:1000	Rb	Cell Signalling	#4685s
α-tubulin	1:5000	Ms	Sigma	#T5168
β-actin	1:5000	Ms	MP Biomedicals	#691001
p-p130Cas (Y410)	1:1000	Rb	Cell Signalling	#4011S
p130 Cas	1:1000	Rb	Cell Signalling	#1338S
E-Cadherin	1:1000	Rb	CST	#3195S
Secondary Antibody	**Dilution**	**Species**	**Manufacturer**	**Catalogue #**
Goat anti-rabbit IgG (H + L)-HRP Conjugate	1:3000	Goat	Bio-Rad	#1706515
Goat anti-mouse IgG (H + L)-HRP Conjugate	1:3000	Goat	Bio-Rad	#1706516

Table 2.18 Western blotting blocking solutions and primary and secondary antibody preparation

	Ingredients and concentrations in molarity
TBS	150 mM NaCl, 50 mM Tris, pH 7.6
5% milk blocking solution	5% (w/v) skim milk powder in TBS-T
TBS-BSA blocking solution	50 g BSA, 4 ml 10% Sodium Azide, 1 x TBS, 4 ml phenol red, pH 7.4
Secondary antibody	1:3000 HRP conjugated anti-Rabbit/Mouse secondary antibody diluted in 5% milk solution
Primary antibody	1:1000 poly/monoclonal mouse/rabbit primary antibody diluted in BSA solution

2.5 Starvation and growth factor stimulation

2.5.1 EGF stimulation experiment and downstream signalling

These PTEN KO clones; E6-1 and E6-7 and WT MCF10A cells were seeded overnight in full DMEM/F12 media at a cell seeding density of 3.5 x 10^5 per 6 cm plate. Day 1 post seeding, the media was aspirated off and washed twice with 1 x PBS. Cells were then serum starved for 24 h with DMEM/F12 starvation media (DMEM/F12 cell media with 50 µl cholera toxin and 250 µl hydrocortisone, -EGF, -insulin, 0.4% Horse Serum). Following this, cells were treated with 10 ng/mL EGF and incubated for 0.5, 1, 2, 4, 6, 12 and 24 h. PBS was used as the vehicle control at 1 and 24 h. Cells were then lysed with RIPA buffer containing phosphatase and protease inhibitors and harvested for protein. Proteins were loaded (10 µg), separated by 10% SDS-PAGE, then transferred to PVDF membranes and immunoblotted with antibodies for total and phospho levels of key downstream signalling proteins.

2.5.2 Growth condition stimulation assay

WT and PTEN KO MCF10A cells were seeded at 0.4 x 10^6 in full media in 6cm plates. Day 1 post seeding cells were starved for 24 h with starvation DMEM/F12 media containing 0.4% HS and no EGF or insulin. Following the starvation period cells were treated with complete DMEM/F12 media for a range of time points and probed for 15 min, 30 min, 1 and 6 h. Cells were then lysed using RIPA lysis buffer and proteins harvested. PBS was used as the vehicle control. Proteins lysates were loaded (10 µg), separated by 10% SDS-PAGE, and transferred to PVDF membranes and immunoblotted for total and phospho levels of EGFR, STAT3, AKT, ERK1/2, P-p130cas and S6.

2.6 MEK1/2 and PI3K inhibitor experiments

2.6.1 Dose-response treatment with MEK inhibitor trametinib

The MEK inhibitor trametinib (MedChemExpress, #HY-10999) was dissolved and reconstituted in DMSO to obtain a stock concentration of 10 mM. In order to identify the optimal MEK inhibitor (MEKi) dose for the time-course experiments, a dose-response experiment was performed. In these dose-response experiments cell proliferation and cell signalling using MTS assays and immunoblotting respectively, were used as measures of drug response. Approx. 70% confluent cells were trypsinised and counted using a haemocytometer. WT MCF10A cells were seeded at 3000/well of a 96-well plate for the MTS assay. For the MTS assay day 1, 2 and 3 post seeding cells were treated acutely for 1 h with a range of drug concentrations; 1 nanomolar (nM), 5 nM, 10 nM, 50 nM, 100 nM, 500 nM, 1 micromolar (µM), 5 µM and 10 µM. A 1 h 1:1000 DMSO treatment was used as the vehicle control. After each 1 h MEK inhibitor treatment on each day MTS reagent was added to each well and incubated for 1 h at 37 °C. Absorbance readings were measured at 490 nm on the CLARIOstar (BMG, Labtech) or PHERAstar (BMG, Labtech) plate readers. For the immunoblotting experiments WT MCF10A cells were seeded at 1 x 10^6 /10 cm plate, SUM185PE were seeded at 2 x 10^6/10 cm plate and BT-549 cells were seeded at 0.5 x 10^6/10 cm plate. Day 1 post seeding cells were acutely treated for 1 h using the same range of trametinib concentrations given above and 1:1000 DMSO was used as the vehicle control. Drug treated cells were lysed and their proteins were harvested using RIPA lysis buffer. Equal amounts of protein lysates/lane were separated by 10% SDS-PAGE, transferred to PVDF membranes and immunoblotted for total and phospho levels of AKT and ERK protein.

2.6.2 Time-course treatment with MEK inhibitor trametinib

Following the trametinib dose determination experiment time-course treatments with this MEK inhibitor were performed in the WT and PTEN KO MCF10A cells, as well as the TNBC cell lines. Approx. 70% confluent cells were trypsinised and counted using a haemocytometer. WT and PTEN KO MCF10A cells were seeded at 1 x 10^6/10 cm plate or 0.35 x 10^6/6 cm plate. SUM185PE were seeded at 2 x 10^6/10 cm plate or 0.7 x 10^6/6 cm plate and BT-549 cells seeded at 0.5 x 10^6/10 cm plate or 1.9 x 10^5/6 cm plate. Day 1 post seeding the cells were treated with 1 or 5 nM trametinib for 1, 6, 12, 24, 48 h and DMSO vehicle control for 1 and 24 h. Drug treated cells were lysed and the proteins harvested using RIPA lysis buffer. Equal amounts of protein lysates/lane were separated by 8% SDS-PAGE, transferred to PVDF membranes and immunoblotted for total and phospho levels of EGFR, STAT3, AKT, ERK1/2 and S6 protein.

2.6.3 Dose-response treatment with PI3K inhibitor BYL719

The PI3Kα selective inhibitor alpelisib (BYL719) (Selleck Chemicals, #S2814-5mg) was dissolved and reconstituted in DMSO to obtain a stock concentration of 10 mM. A dose response experiment for BYL719 was performed in order to select the lowest dose of BYL719 that effectively inhibited AKT in both the WT MCF10A and TNBC cell lines SUM185PE and BT-549. Approx. 70% confluent cells were trypsinised and counted using a haemocytometer. WT and PTEN KO MCF10A cells were seeded at 1 x 10^6/10 cm plate or 0.35 x 10^6/6 cm plate. SUM185PE were seeded at 2 x 10^6/10 cm plate or 0.7 x 10^6/6 cm plate and BT-549 cells seeded at 0.5 x 10^6/10 cm plate or 1.9 x 10^5/6 cm plate. Day 1 post seeding cells were acutely treated for 1 h with of BYL719 at the following doses; 5 nM, 10 nM, 50 nM, 100 nM, 500 nM, 1 µM, 5 µM and 10 µM drug. A 1 h 1:1000 DMSO treatment was used as the vehicle control. Drug treated cells were lysed and their proteins were harvested using RIPA lysis buffer. Equal amounts of protein lysates/lane were separated by 10% SDS-PAGE, transferred to PVDF membranes and immunoblotted for total and phospho levels of AKT, ERK and S6 protein.

2.6.4 Time-course treatment with PI3K inhibitor BYL719

Following the BYL719 dose determination experiment time-course treatments with this PI3K inhibitor were performed. Approx. 70% confluent cells were trypsinised and counted using a haemocytometer. WT and PTEN KO MCF10A cells were seeded at 1 x 10^6/10 cm plate or 0.35 x 10^6/6 cm plate. SUM185PE seeded at 2 x 10^6/10 cm plate or 0.7 x 10^6/6 cm plate and BT-549 cells seeded at 0.5 x 10^6/10 cm plate or 1.9 x 10^5/6 cm plate. Day 1 post seeding the cells were treated with 5 µM BYL719 for 1, 6, 12, 24, 48 h and DMSO vehicle control for 1 and 24 h. Drug treated cells were lysed and proteins harvested using RIPA lysis buffer. Equal amounts of protein lysates/lane were separated by 8% SDS-PAGE, transferred to PVDF membranes and immunoblotted for total and phospho levels of EGFR, STAT3, AKT, ERK1/2 and S6 protein.

2.6.5 Combination treatment with dual PI3Kα and β selective inhibitors

Approx. 70% confluent cells were trypsinised and counted using a haemocytometer. Cells were seeded at 3000/well of a 96-well plate for MTS assay or at 0.5 x 10^6/6cm plate for immunoblotting. Day 1 post seeding MCF10A, PTEN KO clones E6-1 and E6-7 and TNBC cell lines; BT-549 (PTEN -/-) and MDA-MB-468 (PTEN -/-) were treated with 1 µM BYL719 (PI3Kα specific inhibitor) and 1 µM PI3Kβ specific inhibitors; AZD6482 (Selleck Chemicals, #S1462) or TGX221 (SYNkinase, #SYN-1089) alone and in combination for 1 and 24 h. Drug treated cells were lysed and proteins harvested using RIPA lysis buffer. Equal amounts of protein lysates/lane were separated by 8% SDS-PAGE, transferred to PVDF membranes and immunoblotted for total and phospho levels of EGFR, STAT3, AKT, ERK1/2 and S6.

2.7 Rescue experiment: Transient PTEN transfection by lipofection

Re-introducing PTEN back into the MCF10A PTEN KO clones using lipofectamine 3000 (Invitrogen, #L3000008) to carry out a transient reverse transfection with the plasmid vector PcDNA3.1 (Invitrogen, #V790-20). Firstly, pcDNA3.1 and pcDNA3.1 PTEN plasmids were transformed in DH5α cells followed by screening for positive colonies using resistance to ampicillin at a concentration of 100 µg/ml. The plasmid DNA was isolated and purified from the cells using QIAGEN Plasmid plus Maxi Kit (#12162, #12163, and #12165), and the Plasmid Buffer Set (#19046) as per manufacturer's instructions. The DNA was quantified in ng/µL using a Thermo Scientific NanoDrop™ 1000 Spectrophotometer. To validate that the plasmid DNA had been successfully extracted from the genomic DNA, the plasmid DNA was cut with restriction enzymes HINDII and EcoR1 and then run on a DNA gel and visualized. In order to optimise the transfection efficiency using the Lipofectamine 3000 reagent protocol a GFP tagged vector pEGFP-C2 (Addgene, #6083) was first used. The experiment was set up as per instructions of Invitrogen Lipofectamine 3000 reagent protocol (**Table 2.10**).

Following overnight transfection, the cells were visualized under the fluorescent microscope. Transfection efficiency was high with almost all cells being transfected with the GFP-vector based on the amounts of DNA and reagents used. For experimental set up cells were seeded at 3 x 10^6 per 10 cm plate and MCF10A parental cells were reverse transfected overnight for 24 h with an empty vector pcDNA3.1 and PTEN KO cells were reverse transfected with either pcDNA3.1 empty vector or pcDNA3.1 PTEN expressing vector. Day 1 post seeding the transfected cells were then trypsinised as usual and seeded at 3000 cells/well of 96-well plate for MTS assay experiment or 0.3 x 10^6 per 6 cm plate for immunoblotting experiments. After 24 h the transfected cells set up for the MTS cell viability assay were treated with 0.5/5 µM BYL719 or DMSO vehicle control for 24 or 48 h. On day 1 and 2 post-treatment MTS reagent was added to each well and incubated for 1 h at 37°C. Absorbance readings were measured at 490 nm on the CLARIOstar (BMG, Labtech) or PHERAstar (BMG, Labtech) plate readers. Cell viability is measured as a % over DMSO vehicle control for each cell line. After 24 h transfected cells for immunoblotting experiments were treated with 1 or 6 h of 5 uM BYL719 and DMSO was used as the vehicle control. Drug treated cells were lysed and their proteins were harvested using RIPA lysis buffer. Equal amounts of protein lysates/lane were separated by 8% SDS-PAGE, transferred to PVDF membranes and immunoblotted for total and phospho levels of EGFR, STAT3, AKT, ERK1/2 and S6.

2.8 Quantification and statistical analysis

Quantification by densitometry was performed using ImageLab (Bio-Rad). MS-Excel and GraphPad Prism 7.01 were used to graph cell viability and densitometry results. For normalization of the densitometry results both phospho and total protein levels were first normalised to their corresponding

loading control (β-actin or α-tubulin). Normalised phospho proteins were then normalised to normalised total protein levels. In experiments where different cell line's lysates were separated on different gels, a gel was run with each cell lines' untreated sample and the fold change compared to WT MCF10A levels was used to compare different samples on different gels. This correcting factor was used to get the relative protein expression levels to compare across gels and between different the cell lines. Using MS-Excel the paired two-tailed t-test was used and using GraphPad prism statistical significance was determined using multiple t-tests without correction for multiple comparisons. Each row was analysed individually, without assuming a consistent SD Statistical significance was considered at $P < 0.05$.

2.9 Calculation of drug synergy index

To evaluate if the selective PI3Kα and β isoform inhibitor combination, BYL719 and TGX221, respectively, had a synergistically inhibitory effect the Chou-Talalay's Combination Index, (CI score) was used (Chou 2010). The coefficient of drug interaction (CDI) is a simple model to test the synergism of a drug combination and is calculated as follows: CDI=$E_{12}/(E_1 \times E_2)$, where E_{12} is a normalised biological response (e.g. cell survival) measured following combination treatment of Drug A and Drug B by its control group, and E_1 and E_2 are the responses measured after single drug treatment, respectively. CDI < 1, = 1 or >1 indicates that the drugs are synergistic, additive or antagonistic, respectively. For instance, if cell survival is inhibited 60% by a combined drug treatment, and 30% and 20% inhibited by single drug treatment, respectively, then we have CDI = (1-0.6)/((1-0.3)×(1-0.2)) = 0.71, less than 1 thus implying that the combined treatment has a synergistic effect.

2.10 Construction of a PI3K-ERK MAPK crosstalk mathematical model

2.10.1 Model implementation

The PI3K-ERK crosstalk model was formulated using ordinary differential equations (ODEs). The model's schematic diagram containing all model reactions is given in (**Figure 4.17**). The ODEs were formulated using a combination of kinetic laws including Michaelis-Menten (MM) kinetics for catalytic reactions (e.g. phosphorylation and dephosphorylation), Hill kinetics (transcriptional activation/repression) and mass-action kinetics (association/dissociation) (Shin and Nguyen 2017). As a result, the model comprises of 33 ODEs and 69 kinetic parameters. The model ODEs, rate equations and the sets of best-fitted parameter values used for simulations are given in **(Tables 2.19, 2.20 and 2.21)**. The model was implemented and numerically simulated in MATLAB ® (The MathWorks. Inc. 2018b) using the variable-step and variable-order *ode15s* solver.

Table 2.19 Reactions and reaction rates of the PI3K-ERK crosstalk model

	Reaction	Reaction rates
v01	EGFR → pEGFR	kc01*EGF * EGFR / (Km01 + EGFR)
v02	pEGFR →EGFR	Vm02*pEGFR
v37	pEGFR → iEGFR	kc37*pEGFR*(1+alpha37*p-ERK/(Km37b+p-ERK))/(km37+pEGFR)
v38	iEGFR → EGFR	kc38 * iEGFR/ (km38 + iEGFR)
v03	PI3K → aPI3K	kc03 * pEGFR * PI3K / (Km03 + PI3K) / (1 + Ki03 * pS6K)
v04	aPI3K → PI3K	Vm04 * aPI3K
v05	GS → aGS	kc05 * pEGFR * GS / (Km05 + GS)
v06	aGS → GS	Vm06 * aGS
v07	GS → iGS	kc07 * p-ERK * GS / (Km07 + GS)
v08	iGS → GS	Vm08 * iGS
v09	dRas → tRas	kc09 * dRas * (aGS + aPI3K*(1 - PI3Ki / (ic_pi3k + PI3Ki))) / (Km09
v10	tRas → dRas	Vm10 * tRas
v11	Raf → aRaf	kc11 * tRas * Raf / (Km11 + Raf) / (1 + Ki11 * pSPRY)
v12	aRaf → Raf	Vm12a*(1 + kc12b * pp-AKT / (km12 + pp-AKT)) * aRaf
v13	∅ → PIP3	vs13a+vs13b*aPI3K*(1- PI3Ki/(ic_pi3k + PI3Ki))/(km13 + aPI3K)
v14	PIP3 → ∅	(vs13a + vs13b + kc14 * PTEN /(Km14 + PTEN))/5000 * PIP3
v15	PIP3 + mTORC2 ↔	(ka15 * mTORC2 * PIP3 - kd15 * amTORC2)c
v16	PIP3 + PDK1 ↔ mPDK1	(ka16 * PDK1 * PIP3 - kd16 * mPDK1)
v17	amTORC2 → pmTORC2	kc17 * amTORC2 * pp-AKT / (Km17 + amTORC2)
v18	pmTORC2 → amTORC2	kc18 * pmTORC2
v19	Akt → p-AKT	kc19 * mPDK1 * Akt / (Km19 + Akt)
v20	p-AKT → Akt	kc20 * p-AKT
v21	p-AKT → pp-AKT	kc21 * pmTORC2 * p-AKT / (Km21 + p-AKT)
v22	pp-AKT → p-AKT	Vm22 * pp-AKT
v23	mTORC1 → amTORC1	kc23 * mTORC1 * pp-AKT / (Km23 + mTORC1)
v24	amTORC1 → mTORC1	Vm24 * amTORC1
v25	S6K → pS6K	kc25*S6K*amTORC1/(Km25 + S6K)
v26	pS6K → S6K	Vm26*pS6K
v27	S6 → pS6	(kc27a*pS6K + kc27b * p-ERK) * S6 /(Km27 + S6)
v28	pS6 → S6	Vm28*pS6
v29	Mek → pMek	kc29 * aRaf * Mek / (Km29 + Mek)
v30	pMek → Mek	Vm30 * pMek
v31	Erk → p-ERK	kc31*Erk * pMek *(1 - MEKi / (ic_mek + MEKi)) / (Km31 + Mek)
v32	p-ERK → Erk	kc32 * p-ERK
v33	→ SPRY	vs33 + kc33 * p-ERK/(Km33 + p-ERK)
v34	SPRY →	(vs33 + kc33)/100 * SPRY
v35	SPRY → pSPRY	kc35 * SPRY / (Km35 + SPRY)
v36	pSPRY → SPRY	Vm36 * pSPRY

Table 2.20 Ordinary differential equations of the PI3K-ERK crosstalk model

Left-hand Sides	Right-hand Sides	Value
d[EGFR]/dt	-v01+v02+v38	0.12
d[pEGFR]/dt	v01-v02-v37	0.08
d[iEGFR]/dt	v37-v38	99.80
d[GS]/dt	-v05+v06-v07+v08	24.13
d[aGS]/dt	v05-v06	0.29
d[iGS]/dt	v07-v08	75.58
d[PI3K]/dt	-v03+v04	99.81
d[aPI3K]/dt	v03-v04	0.19
d[dRas]/dt	-v09+v10	100.00
d[tRas]/dt	v09-v10	0.00
d[PIP3]/dt	v13-v14-v15-v16	207.82
d[PDK1]/dt	-v16	93.46
d[mPDK1]/dt	v16	6.54
d[mTORC2]/dt	-v15	0.60
d[amTORC2]/dt	v15-v17+v18	99.40
d[pmTORC2]/dt	v17-v18	0.00
d[Akt]/dt	-v19+v20	97.58
d[p-AKT]/dt	v19-v20-v21+v22	2.42
d[pp-AKT]/dt	v21-v22	0.00
d[mTORC1]/dt	-v23+v24	100.00
d[amTORC1]/dt	v23-v24	0.00
d[S6K]/dt	-v25+v26	100.00
d[pS6K]/dt	+v25-v26	0.00
d[S6]/dt	-v27+v28	99.98
d[pS6]/dt	+v27-v28	0.02
d[Raf]/dt	-v11+v12	100.00
d[aRaf]/dt	+v11-v12	0.00
d[Mek]/dt	-v29+v30	99.99
d[pMek]/dt	+v29-v30	0.01
d[Erk]/dt	-v31+v32	74.60
d[p-ERK]/dt	+v31-v32	25.40
d[SPRY]/dt	+v33-v34-v35+v36	100.00
d[pSPRY]/dt	+v35-v36	1.13

Table 2.21 The best-fitted parameter sets used for simulations

Parameter	Value	Unit
kc01	73.961	min^{-1}
Km01	211.836	nM
Vm02	0.023	min^{-1}
kc37	26.062	min^{-1}
km37	5.236	nM
kc38	0.420	min^{-1}
km38	0.865	nM
kc03	0.726	min^{-1}
Km03	40.926	nM
Vm04	0.215	min^{-1}
kc05	414.000	min^{-1}
Km05	297.167	nM
Vm06	8.531	min^{-1}
kc07	0.005	min^{-1}
Km07	0.025	nM
Vm08	0.002	min^{-1}
kc09	2.109	min^{-1}
Km09	414.954	nM
Vm10	5597.576	min^{-1}
kc11	35.075	min^{-1}
Km11	0.188	nM
Ki11	0.664	nM
Vm12a	0.553	min^{-1}
kc12b	127.350	min^{-1}
km12	648.634	nM
vs13a	2.944	nM min^{-1}
vs13b	1088.930	nM min^{-1}
km13	4.775	nM
kc14	90.365	min^{-1}
Km14	0.015	nM
ka15	0.007	nM^{-1} min^{-1}
kd15	0.009	min^{-1}
ka16	0.067	nM^{-1} min^{-1}
kd16	198.609	min^{-1}
kc17	668.344	min^{-1}
Km17	0.157	nM
kc18	0.349	min^{-1}
kc19	1.746	min^{-1}

Km19	24.889	nM
kc20	3.758	min^{-1}
kc21	0.005	min^{-1}
Km21	0.067	nM
Vm22	301.301	min^{-1}
kc23	0.136	min^{-1}
Km23	0.273	nM
Vm24	479.733	min^{-1}
kc25	54.075	min^{-1}
Km25	0.312	nM
Vm26	5.129	min^{-1}
kc27a	1.754	min^{-1}
kc27b	0.197	min^{-1}
Km27	17.498	nM
Vm28	209.411	min^{-1}
kc29	501.187	min^{-1}
Km29	0.511	nM
Vm30	96.383	min^{-1}
kc31	1006.932	min^{-1}
Km31	0.948	nM
kc32	0.196	min^{-1}
vs33	2535.129	nM min^{-1}
kc33	0.003	min^{-1}
Km33	0.003	nM
kc35	94.624	min^{-1}
Km35	0.077	nM
Vm36	83.946	min^{-1}
Ki03	5.224	nM
alpha37	1.648	-
Km37b	794.328	nM
kc33	0.003	min^{-1}

2.10.2 Model fitting (calibration)

The adequacy of a mathematical model is generally justified by its ability to recapitulate known experimental data, which is ensured through a process known as model fitting or calibration where unmeasured model parameters are numerically estimated so that model simulations fit the data. Parameter estimation was done by minimizing the following 'objective function' that quantifies the discrepancy between simulated values and corresponding experimental measurements:

$$J(\boldsymbol{p}) = \sum_{j=1}^{M} \sum_{i=1}^{N} \left(\frac{y_{j,i}^{D} - y_j(t_i, \boldsymbol{p})}{\sigma_{j,i}} \right)^2$$

where M is the number of the given experimental data sets used for fitting and N is the number of time points within each experimental data set. $y_j(t_i, \boldsymbol{p})$ represents the numerical solution for the model state variable y_j evaluated at time t_i and parameter set $\boldsymbol{p}$; while $y_{j,i}^{D}$ is the mean value of the corresponding data point at t_i with the associated error variance $\sigma_{j,i}$.

A Genetic Algorithm (GA) was used to optimise the objective function (Man, Tang et al. 1996, Shin, Kim et al. 2014, Reali, Priami et al. 2017). This was done by using the Global Optimisation Toolbox and the function *ga* in MATLAB. Selection rules select the individual solutions with the best fitted values (called 'elite solutions') from the current population. The elite count was set to 5% of the population size. Crossover rules combine two parents to generate offspring for the next generation. The crossover faction was set at 0.8. Mutation rules apply random changes to individual parents to generate the population of the next generation. For the mutation rule, we generated a random number from a Gaussian distribution with mean 0 and standard deviation σ_k, which was applied to the individuals of the current generation. The standard deviation function (σ_k) is given by the recursive formula as follows:

$$\sigma_k = \sigma_{k-1} \left(1 - \frac{k}{G} \right),$$

where k is the k^{th} generation, G is the number of the generation, and $\sigma_0 = 1$.

Chapter 3: Establishment and characterisation of the isogenic MCF10A PTEN KO cells

3.1 Generate MCF10A PTEN KO clones using CRISPR/Cas9 gene editing

PTEN KO clones were generated by knocking out PTEN using the powerful and highly site-specific genome editing technology of CRISPR/Cas9. The previously mentioned PTEN deletion studies (Vitolo, Weiss et al. 2009, Pires, Hopkins et al. 2013) utilised small interfering RNA (siRNA) to delete PTEN in MCF10A cells. However, this RNA interference approach, which includes both siRNA and shRNA has several limitations. For instance, it doesn't completely shut off a gene nor is it a permanent manipulation, thus causing transient knockdown phenotypes that only reduce, not eliminate gene function. In contrast, the highly specific gene editing tool of CRISPR enables complete and permanent loss of gene expression leading to robust gene knockout phenotypes (Doudna and Charpentier 2014, Kirchner and Schneider 2015, Lu, Qi et al. 2015, Wen, Yuan et al. 2016).

Frequently the effects of PTEN loss have also been performed in tumour cell lines which naturally harbour numerous oncogenic mutations, which makes it challenging to identify which effects were due to PTEN loss alone. Therefore, in order to overcome these limitations and elucidate the direct causal effects in cell signalling, tumorigenesis and altered drug responsiveness conferred by PTEN loss, PTEN was knocked out using the powerful gene editing tool CRISPR/Cas9 in the immortalized human mammary epithelial cell line MCF10A. MCF10A cells were obtained from a patient with benign fibrocystic disease and thus are representative of non-tumourigenic breast cells (Soule, Maloney et al. 1990). PTEN knock out with CRISPR/Cas9 was followed by fluorescence-activated cell sorting (FACs) of positive cells into single cell colonies, thus producing isogenic clones that only differ from parental cells by the status of PTEN. This reductionist approach generates a model in which only PTEN is perturbed so we can examine the direct effects of PTEN loss on drug response and network changes.

First discovered in the *E. coli* genome in 1987 (Ishino, Shinagawa et al. 1987) it wasn't until 2005 that CRISPR was found to be part of an adaptive immune system in bacteria. This observation was made when researchers found that the majority of the intervening sequences between the identical repeats were derived from invading phage and plasmid genomes (Mojica, Diez-Villasenor et al. 2005). The CRISPR process has now been modified for genome engineering and consists of two components: a single "guide" RNA (sgRNA) and a non-specific CRISPR-associated endonuclease (Cas9) (**Figure 3.1**). SgRNA are short synthetic RNA composed of a "scaffold" sequence necessary for Cas9-binding and ~20 nucleotide "targeting" sequence which is tailored by the user to target a specific site for gene editing. Thus, CRISPR/Cas9 is a highly flexible methodology, which by changing the nucleotide sequence of the targeting sequence, the artificial Cas9 system can essentially target any DNA sequence for cleavage. Cas9 is an endonuclease which cleaves the target DNA if sufficient homology exists resulting in double stranded DNA breaks which leads to the efficient, but highly error-prone repair mechanism known as non-homologous end joining (NHEJ) (**Figure 3.1**). This NHEJ is used for deletion of a gene as it generates small nucleotide insertions or deletions (InDels) in the target DNA sequence

leading to in-frame mutations, or more often, frameshift mutations, causing premature stop codons and nonsense mediated protein arrest (Rodriguez-Rodriguez, Ramirez-Solis et al. 2019). The polypeptide being created could be truncated or abnormally long. Ideally the end result is to obtain a loss of function mutation in the target sequence. The approach of inserting an activating mutation e.g. PIK3CA via CRISPR/Cas9 is technically more challenging than knocking out a gene as it utilises the DNA repair pathway known as Homology Directed Repair (HDR) which has far higher fidelity, but is less efficient than NHEJ. In addition to the endonuclease Cas9 and the sgRNA to target the gene sequence of interest, the template DNA containing the desired edit and the additional homologous sequence immediately upstream and downstream of the target must be included. The aim is for the edit to be inserted into the gene sequence of interest generating the desired mutation.

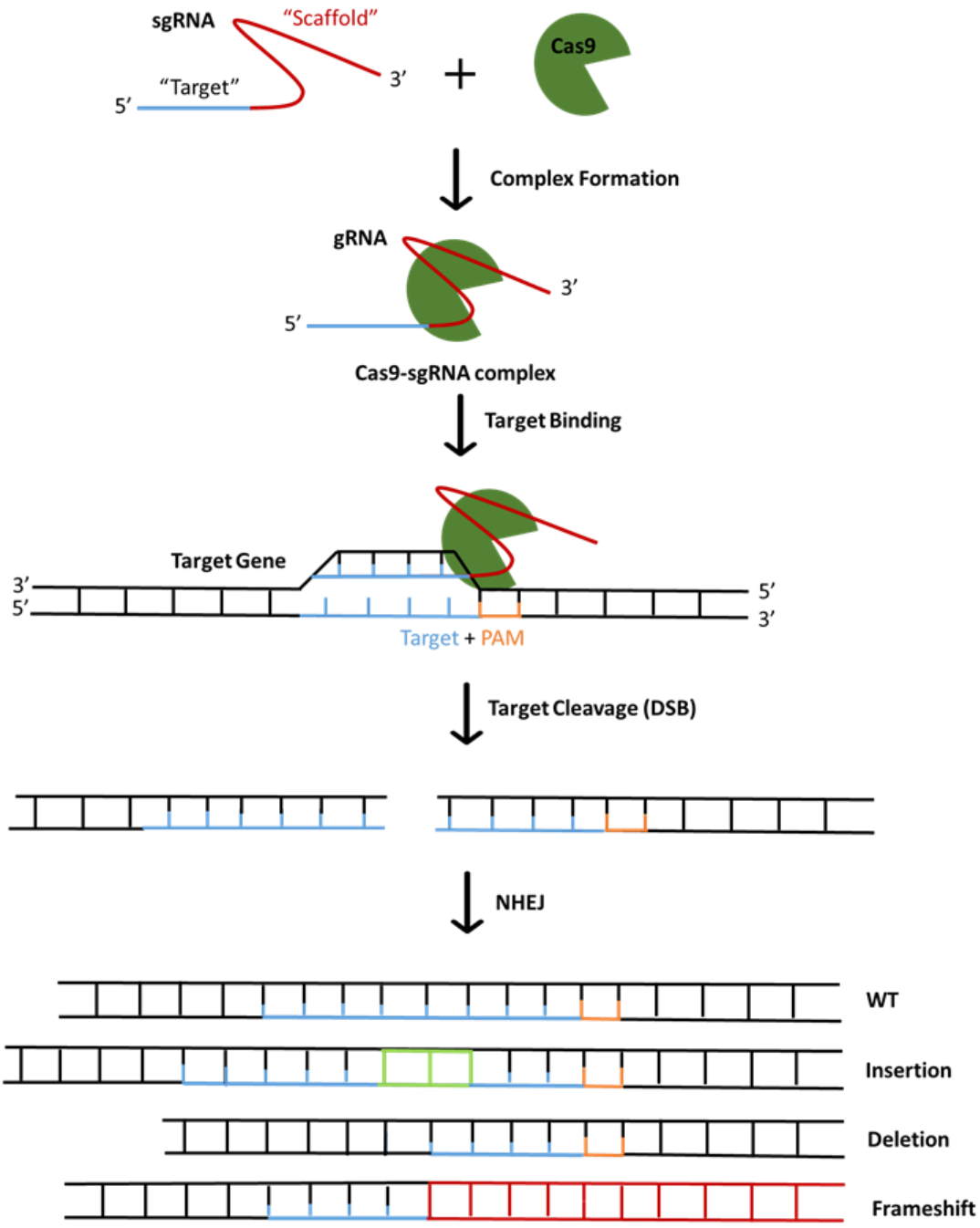

Figure 3.1 The steps involved in CRISPR/Cas9-mediated gene deletion via NHEJ repair pathway. The Clustered Regularly Interspaced Short Palindromic Repeat (CRISPR) process consists of two components: a short "guide" RNA (sgRNA) and a non-specific CRISPR-associated endonuclease (Cas9). SgRNA are short synthetic RNA composed of a "scaffold" sequence necessary for Cas9-binding and ~20 nucleotide "targeting" sequence which is tailored to target a specific site for gene editing. The target sequence needs to be unique in the genome and the site needs to be immediately adjacent to a Protospacer Adjacent Motif (PAM). After formation of the Cas9-sgRNA complex Cas9 cleaves the target sequence, provided sufficient homology exists, resulting in DNA double strand breaks (DSB) which leads to the efficient, but highly error-prone repair mechanism known as non-homologous end joining (NHEJ). NHEJ generates small nucleotide insertions or deletions (InDels) at the DSB site which result in amino acid deletions, insertions, or frameshift mutations leading to premature stop codons and nonsense mediated protein arrest. Inspired by https://www.addgene.org/crispr/guide/.

Since its discovery, CRISPR/Cas9 gene editing technology has revolutionized molecular genetics and offers immense therapeutic potential for the treatment of human diseases. CRISPR has gained popularity over other gene editing systems due to its simplicity, efficiency, versatility and low cost (Rodriguez-Rodriguez, Ramirez-Solis et al. 2019). However, this gene editing technique also has drawbacks, one major one is the risk of off-target alterations, where the Cas9 complex cuts at an undesirable site, and thus edits the wrong target gene which may lead to genomic instability and disrupt the functionality of otherwise normal genes (Zhang, Tee et al. 2015). Although the targeting specificity of Cas9 is thought to be tightly regulated by the nucleotide "targeting" sequence of the sgRNA and the presence of the protospacer adjacent motif (PAM) next to the target sequence in the genome, possible off-target activity could still occur in DNA sequences with even 3-5 bp mismatches as the system allows cleavage at genomic locations which are only partially complementary to the sgRNA (Fu, Foden et al. 2013).

Recently, two independent studies examining the editing accuracy of the CRISPR/Cas9 system were published. One study which characterised on-target and reputed off-target alleles, concluded that there was no unexpected off-target activity in mouse embryos (Iyer, Boroviak et al. 2018). Another study utilising long-read sequencing and long-range PCR genotyping showed that CRISPR/Cas9-induced DNA breaks frequently resulted in extensive on-target genomic deletions over many kbs in size which may have pathogenic consequences (Kosicki, Tomberg et al. 2018). The potential for off-target effects when using CRISPR/Cas9 emphasizes the importance for experimentally validating any gene editing process as was conducted in our research. Further issues with CRISPR/Cas9 in the context of cancer gene function in amplified regions came to light in 2016 (Aguirre, Meyers et al. 2016). The authors found that when the locus targeted by CRISPR/Cas9 is subject to copy-number gains, CRISPR/Cas9 elicits a gene-independent anti-proliferative cell response, thus confounding the interpretation of the results. This highlights the importance of taking into consideration target gene copy number and function when using CRISPR technology. Given the discussed limitations, further research is required to address the current challenges associated with CRISPR/Cas9-based gene editing.

The first step in the CRISPR/Cas9 methodology to knockout PTEN was to design sgRNA vectors to target PTEN. To achieve this the PTEN gene was searched on Ensemble and AceView to view the different isoforms and mRNA transcripts both predicted and observed. The most commonly found isoform **(NM_000314, isoform 1)** was chosen as the target of interest (**Figure 3.2**). Using the gene editing web tool CHOPCHOP (http://chopchop.cbu.uib.no) (Labun, Montague et al. 2016) sgRNA constructs were designed to target exon 4 and exon 6 of PTEN gene (**Figure 3.3**). Exon 1 was not chosen for targeting as it is absent from some of the PTEN isoforms. Exons 2 and 3 had no specific target sites for sgRNA. Exons 4 and 6 were selected as they were common to most of the isoforms and had specific sites for sgRNA targeting. Exon 4 is common to all isoforms and has a specific sgRNA target site (orange) (**Figure 3.3**). This exon 4 sgRNA site has one off-target hit on the gene called Lingo. However, due to the mismatches that exist it is unlikely to be a problem. Exon 6 had a highly specific sgRNA target site which is near the splice site (green) (**Figure 3.3**). Disruption at this site is predicted to cause a frame-shift mutation and subsequent gene deletion.

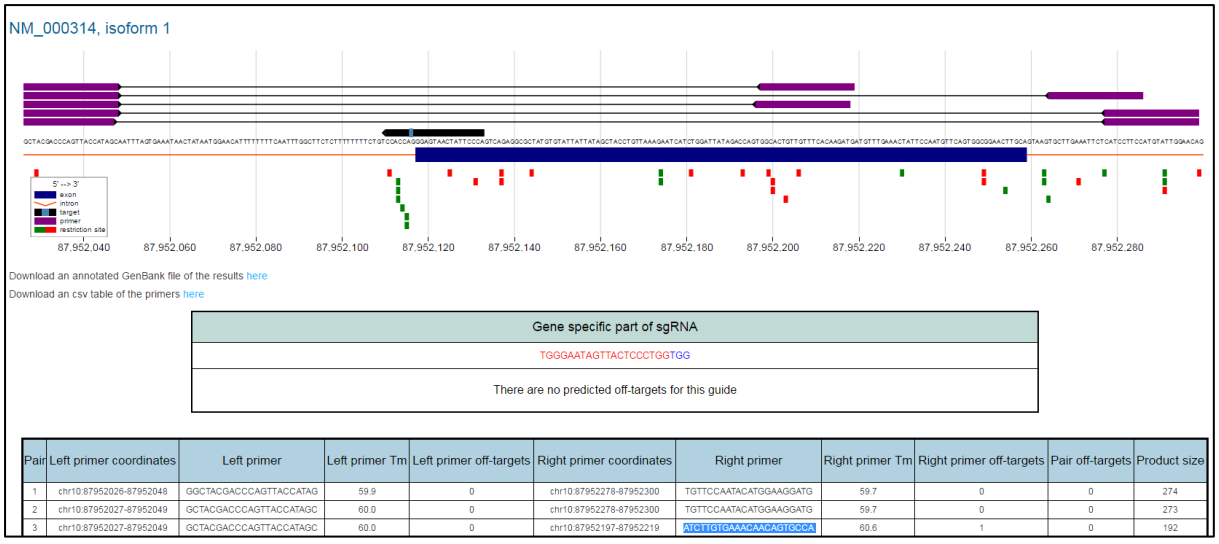

Pair	Left primer coordinates	Left primer	Left primer Tm	Left primer off-targets	Right primer coordinates	Right primer	Right primer Tm	Right primer off-targets	Pair off-targets	Product size
1	chr10:87952026-87952048	GGCTACGACCCAGTTACCATAG	59.9	0	chr10:87952278-87952300	TGTTCCAATACATGGAAGGATG	59.7	0	0	274
2	chr10:87952027-87952049	GCTACGACCCAGTTACCATAGC	60.0	0	chr10:87952278-87952300	TGTTCCAATACATGGAAGGATG	59.7	0	0	273
3	chr10:87952027-87952049	GCTACGACCCAGTTACCATAGC	60.0	0	chr10:87952197-87952219	ATCTTGTGAAACAACAGTGCCA	60.6	1	0	192

Figure 3.2 Construction of sgRNA targeting exon 6 of the PTEN isoform (NM_000314) using the gene editing web tool CHOPCHOP (http://chopchop.cbu.uib.no.) NM_000314, isoform 1 was chosen as the gene editing target as it is the most common PTEN isoform. The diagram shows the different left and right PCR primers which can amplify the target sequence (purple) and the sgRNA target site (black) and exon 6 of PTEN (navy blue).

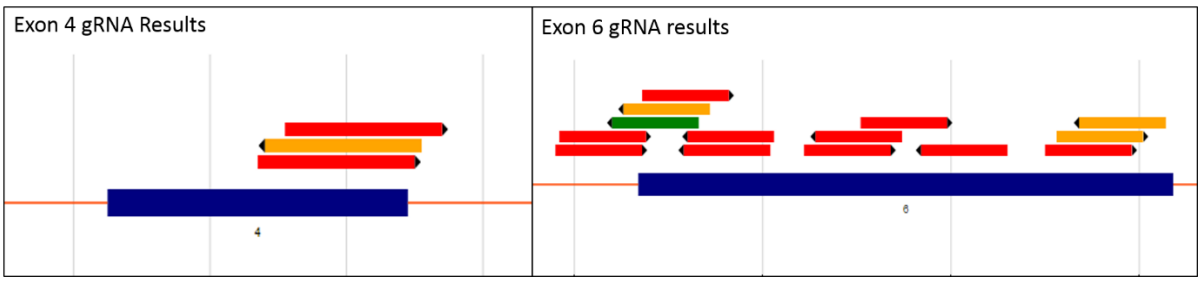

Figure 3.3 PTEN Exon 4 and Exon 6 sgRNA construction results showing the targeting sites on Exon 4 and Exon 6 of PTEN. The above target site results were obtained using the gene-editing web tool CHOPCHOP **(http://chopchop.cbu.uib.no)**. The site which is green indicate a highly selective site, orange is fairly specific and red is non-specific. The orange sgRNA target site has an off target hit on the gene called Lingo. However, due to the mismatches that exist it is unlikely to be a problem.

Cloning and annealing of sgRNA into plasmid vector, was followed by DNA purification and transformation of sgRNA vector into *E. coli* cells. Screening for positive colonies was then carried out using resistance to ampicillin (100 µg/ml). DNA was extracted from the cells using mini-prep and quantified using the NanoDrop. The DNA construct samples were sequenced using the vector primers to ensure the sgRNA was correctly inserted into the vector. After this transfection of exon 4 and exon 6 sgRNA constructs into MCF10A cells was carried out using transient lipofection, followed by cell sorting using FACS to select only transfected cell populations using Blue Fluorescent Protein (BFP). Single cells were sorted into each well of a 96-well plate and one 96-well plate was used per sgRNA construct (**Figure 3.4**). Over the next three months PTEN KO clones were maintained and expanded. This resulted in the generation of 22 isogenic somatic PTEN KO cell lines, E4-1 to -13 and E6-1 to -8. The names E6 and E4 reflects the PTEN exon that was targeted for deletion in that clone i.e. Exon 6 and Exon 4, respectively.

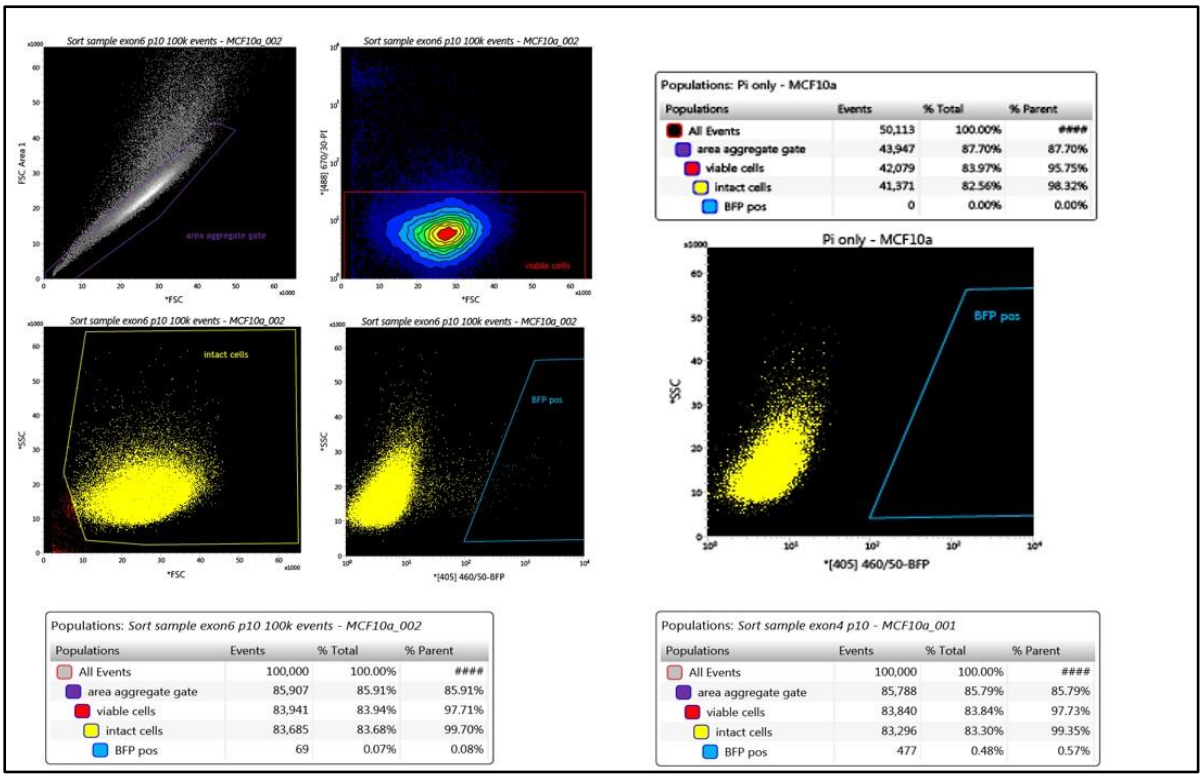

Figure 3.4 Cell sorting of heterogeneous MCF10A cells using FACS to select only cell populations which had transfected positively for the sgRNA constructs targeting Exon 4 or Exon 6 of the PTEN gene. Only positively transfected MCF10A cells with the CRISPR vector pU6-(BbsI) CBh-Cas9-T2A-BFP containing the sgRNA constructs (sgRNA targeting either Exon 4 or Exon 6 of PTEN) to KO PTEN would fluoresce blue as the vector contained BFP. The heterogeneous population of cells was sorted one cell at a time based upon the specific light scattering and fluorescent characteristics of each cell. Each cell was gated for aggregation, viability and intactness i.e. only viable and intact cells were included. Single cells with BFP (0.07% obtained from Exon 6 BFP construct and 0.48% from Exon 4-BFP construct were sorted into wells of a 96-well plate. Fluorescence-activated cell sorting (FACS), single guide RNA (sgRNA) Blue Florescent Protein (BFP), and Knockout (KO).

3.1.1 PTEN KO validation using DNA Sanger sequencing and immunoblotting

To validate the PTEN gene, knockout PCR primers designed to amplify the PTEN sequence were used on the genomic DNA extracted from the control and potential knockout cell lines E6-1 and E6-7. These PCR products were then run on an agarose gel and purified before being quantified by Thermo Scientific NanoDrop™ 1000 Spectrophotometer. The samples were then analysed by Sanger sequencing at the Monash Micromon DNA sequencing facility. The DNA sequencing results of the PTEN KO clones indicate a total knockout of PTEN. The sequence results for the PTEN KO E6-7 clone shows a single cytosine base insertion and the E6-1 clone shows single cytosine base insertion and a double guanine (GG) base deletion (**Figure 3.5**). The presence of these confirmed insertions and deletions (INDELs) suggests frameshift mutations, leading to loss of function and PTEN deletion. To determine if these INDEL mutations led to PTEN deletion at the protein level and a complete loss of function, immunoblotting by probing with PTEN antibody directed against the C-terminal epitope of PTEN was conducted. The results validate PTEN loss as the blots confirmed the absence of PTEN protein in the clones (**Figure 3.6**).

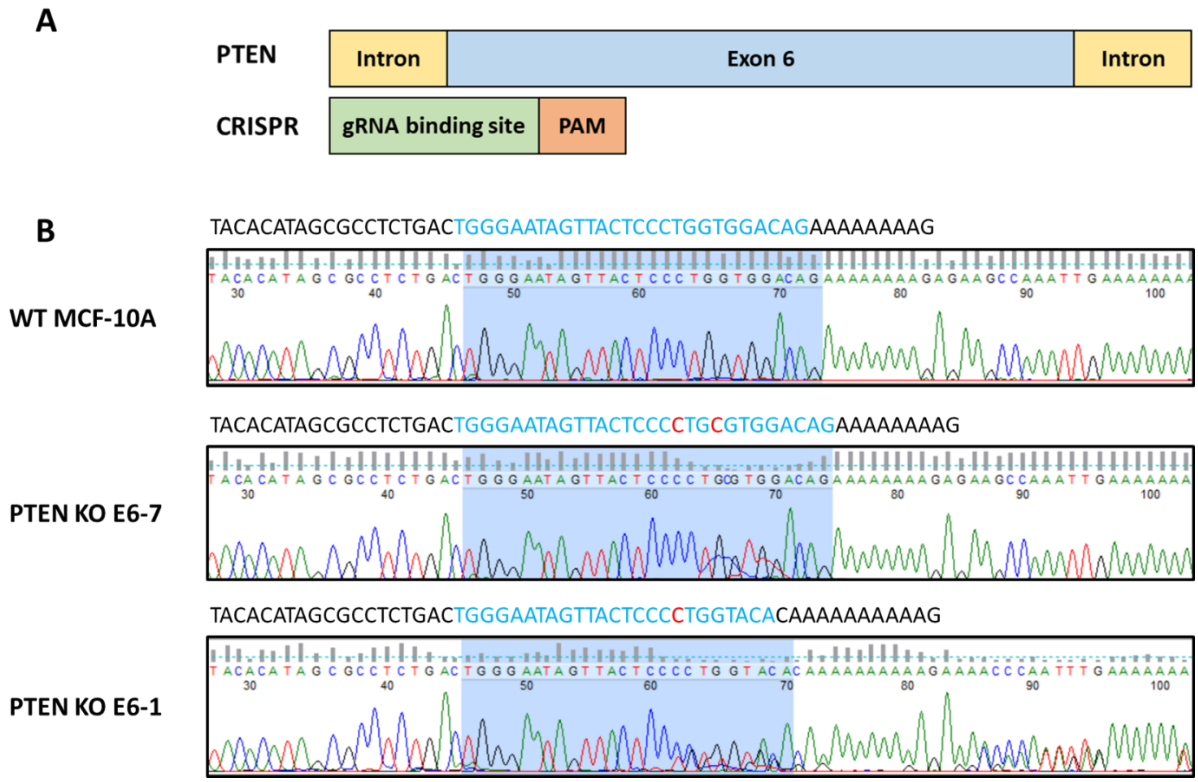

Figure 3.5 DNA sequencing of the WT and PTEN KO MCF10A clones shows base insertions and deletions (INDELs) in the PTEN KO clones validating PTEN loss. (A) Schematic of CRISPR/Cas9 encoding sgRNA targeting exon 6 of PTEN. **(B)** Sanger sequencing results of the CRISPR/Cas9 target site show insertion and deletions of single cytosine nucleotides (red bases) in both PTEN KO clones; E6-1 and E6-7. Highlighted section and blue nucleotides show the CRISPR/Cas9 target sequence.

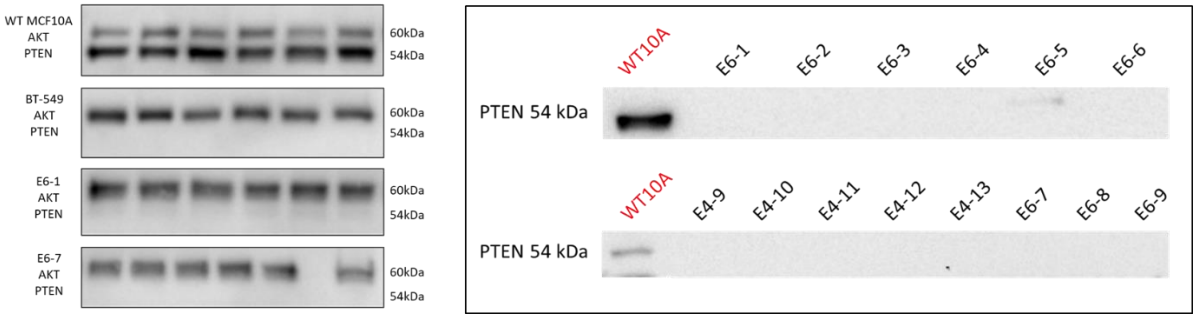

Figure 3.6 Immunoblotting with anti-PTEN antibody to validate PTEN KO in the MCF10A clones E6-1 and E6-7. In brief, WT MCF10A, PTEN KO MCF10A clones (E6-1 to E6-8 and E4-1 to E4-12 not all shown) and TNBC BT-549 cells (PTEN -/-) were lysed and proteins harvested using RIPA lysis buffer. Proteins were separated by 8% SDS-PAGE, transferred to PVDF membranes and immunoblotted with a PTEN specific antibody which recognises the C-terminal epitope of PTEN.

3.2 Characterisation of the PI3K and MAPK signalling pathways in the MCF10A PTEN KO clones

To characterise the activation status of the PI3K and MAPK pathways following PTEN loss, the phospho and total levels of key downstream signalling targets, namely EGFR, STAT3, AKT, ERK and S6, were examined by immunoblot analysis in WT and PTEN KO cells. The levels of these signalling proteins and the activation status of the PI3K and MAPK pathways were also examined in the TNBC cell lines; BT-549, SUM185PE and MDA-MB-468 cells. Both BT-549 and MDA-MB-468 cells harbour a PTEN deletion and SUM185PE cells have a PIK3CA activating mutation (Lehmann, Bauer et al. 2011). Thus, these TNBC cell lines were chosen in order to further elucidate the role these genetic disruptions might play.

As previously mentioned following AKT recruitment to the plasma membrane by binding to PIP3, the product of PI3K, PDK1 phosphorylates Thr308 in its kinase domain. However, to achieve full AKT activity a second phosphorylation at Ser473 by mTORC2 is required (Bellacosa, Chan et al. 1998, Sarbassov, Guertin et al. 2005). Hence, in this work, we immunoblotted for this phospho site. Importantly, the immunoblot results showed significantly higher basal p-AKT (Ser473) expression levels in the MCF10A PTEN KO clones compared to WT MCF10A (**Figure 3.7A-B**). This result is consistent with the fact that PTEN is a key negative regulator of PI3K signalling and thus, its deletion would lead to amplified PI3K signalling. However, despite the significantly higher p-AKT expression levels following PTEN loss in the PTEN KO clones the activated AKT level is still higher in the MDA-MB-468 cells and significantly higher in TNBC BT-549 cells (**Figure 3.7A-B**).

The PIK3CA-mutant SUM185PE cells had high total AKT expression levels; thus, when p-AKT was normalised to the high total AKT levels this cell lines overall proportion of activated AKT was very low. In fact, they had the lowest levels of p-AKT and these were significantly lower compared to p-AKT levels in BT-549 and the PTEN KO clones, but not WT MCF10A cells (**Figure 3.7A-B**). This was an unexpected finding considering the activating *PIK3CA* mutation in these cells which would be expected to increase catalytic activity of the PI3K p110α isoform and thus PI3K-AKT signalling. Low AKT activity as well as low S6 activity has previously been observed in SUM185PE cells by other studies (Lehmann, Bauer et al. 2014). This poor association between *PIK3CA* mutation status and AKT Ser473 phosphorylation level, as well as other markers of PI3K pathway activity (AKT, GSK3, mTOR, or p70S6K) has also been previously reported in both human tumours and breast cancer cell lines (Stemke-Hale, Gonzalez-Angulo et al. 2008). In this study the researchers examined over 40 breast cancer cell lines and found that in *PIK3CA*-mutant cell lines AKT Ser473 phosphorylation was not significantly different compared to cell lines with WT PTEN or PIK3CA (Stemke-Hale, Gonzalez-Angulo et al. 2008). In contrast, *PTEN*-mutant cell lines had significantly higher p-AKT levels than *PIK3CA*-mutant cells. Thus, although there is a clear association between PTEN loss and PI3K pathway

activation as shown by Gonzalez-Angulo et al. and in this work by the elevated levels of AKT Ser473 phosphorylation in the PTEN KO clones, there seems to be a poor association between *PIK3CA* mutation (or mutation subtype) and PI3K pathway activation.

However, despite the reported poor associations between *PIK3CA* mutation status and AKT Ser473 phosphorylation level, another possible reason for this discrepancy in PI3K activity and Ser473 phosphorylation observed in the SUM185PE cells, is that this phospho site, although often used as a proxy for AKT activity, is not necessarily always the best indicator of AKT activity. Indeed, there have been publications showing increased AKT activity and substrate phosphorylation with only Thr308 active site phosphorylation and no changes in Ser473 (Jacinto, Facchinetti et al. 2006, Vincent, Elder et al. 2011). Despite defective Ser473 phosphorylation in mTORC2 disrupted cells AKT retained a substantial amount of enzymatic activity suggesting that singly phosphorylated (Thr308) AKT is an active, but weaker enzyme (Jacinto, Facchinetti et al. 2006). Taken together this suggests that, in addition to blotting for AKT Ser473 phosphorylation, future work, particularly in the SUM185PE cells should focus on blotting for downstream AKT substrates such as glycogen synthase kinase-3 (GSK3) and FOXO-family transcription factors, as well as the AKT Thr308 phosphorylation site.

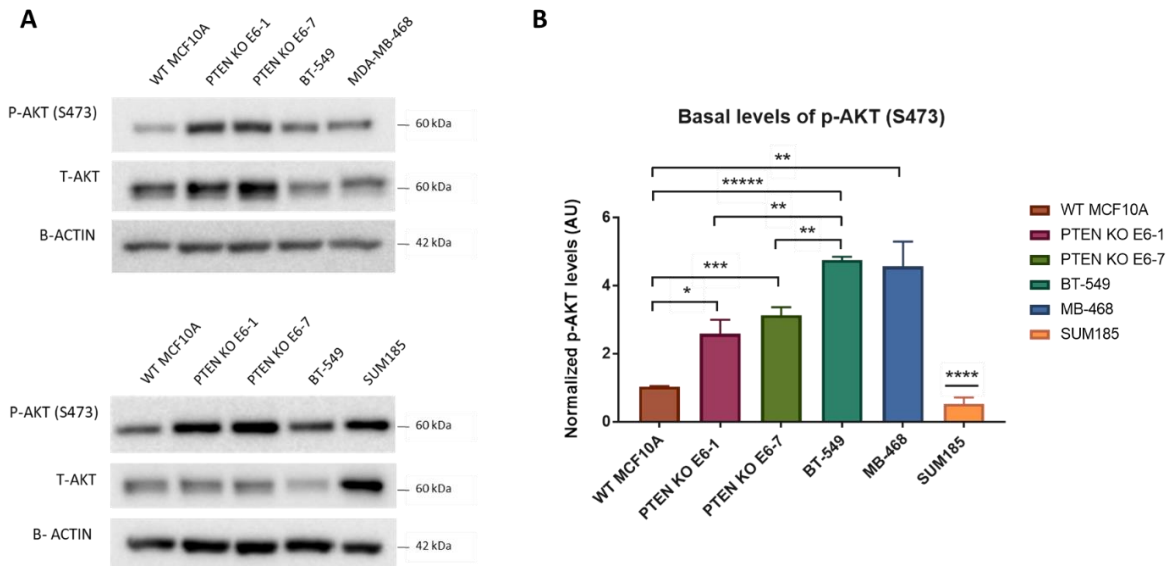

Figure 3.7 Characterisation of basal AKT expression levels. (**A**) Representative western blots of total and phospho AKT protein expression levels in WT MCF10A and PTEN KO cells (E6-1, E6-7) and TNBC cells; BT-549 (PTEN-/-), MDA-MB-468 (PTEN-/-) (top blot) and SUM185PE (PIK3CAmut) (bottom blot). Proteins were loaded (10 µg), separated by 10% SDS-PAGE, then transferred to PVDF membranes, cut and immunoblotted with antibodies for total and phospho AKT and β-actin loading control. (**B**) Quantified levels of relative p-AKT (Ser473). Protein levels were quantified by densitometry and the data (both total and phospho protein) normalised to their corresponding β-actin loading control (an example shown here) and then normalised to total levels to obtain relative phospho levels. Data is represented as the mean values ± standard error of the mean of six independent biological replicates. Paired two-tailed t–test was used and statistical significance was considered at $P < 0.05$. * = $P < 0.05$, ** = $P < 0.01$, *** = $P < 0.001$, **** = $P < 0.0001$, ***** = $P < 0.00001$. AU (arbitrary units).

Interestingly when immunoblotting for STAT3 both total and tyrosine 705 site (Tyr705) phosphorylated STAT3 levels were significantly elevated in the MCF10A PTEN KO clones compared to WT MCF10A (**Figure 3.8A-B**). STAT3 is a known oncogenic transcription factor and strongly associated with driving tumour development, angiogenesis, migration, invasion and chemoresistance by regulating the expression of its downstream target genes involved in cell survival, proliferation, cell cycle progression, anti-apoptosis, immunosuppression, stem cell self-renewal and differentiation (Huynh, Chand et al. 2019). STAT3 through its phospho-tyrosine recognition SH2 domain, is recruited from the cytosol to associate with activated receptors and then transcriptionally activated by receptor associated Janus-kinases (JAK) and Src (Heinrich, Behrmann et al. 1998), as well as other kinases phosphorylating its tyrosine site (Tyr705) on its C-terminal or its serine 727 site (Ser727) (Qin, Yan et al. 2019). Phosphorylated STAT3 then dimerizes and translocates into the nucleus, where it binds to specific promoter sequences and regulates the expression of target genes involved in cell growth and survival, such as cyclin D1, and c-MYC (Ihle 1996, Pellegrini and Dusanter-Fourt 1997).

SUM185PE cells had undetectable phosphorylated STAT3 (Tyr705) levels (**Figure 3.10A-B**) and BT-549 cells expressed similar levels of activated STAT3 as the PTEN KO clones (**Figure 3.8A-B**). In contrast MDA-MB-468 cells expressed lower levels of phosphorylated STAT3 (Tyr705) compared to the PTEN KO clones and BT-549 cells, and these were similar to WT MCF10A levels. These findings of low STAT3 activity in MDA-MB-468 cells are inconsistent with the reports in the literature. Firstly, TNBC cell lines characteristically display constitutive phosphorylation of STAT3, and the viability of these cells is inhibited by STAT3 inhibitors (Walker, Xiang et al. 2014). Indeed, both BT-549 and MDA-MB-468 cells have constitutive activation of STAT3. In addition, MDA-MB-468 cell are considered to possess relatively high levels of constitutively Tyr705-phosphorylated STAT3 and are shown to be dependent on STAT3 for growth (Garcia, Bowman et al. 2001). Known STAT3 inhibitors such as Stattic and Eriocalyxin B are reported to inhibit the growth of MDA-MB-468 cells and this was greater than that of the MDA-MB-453 cells which have no dectable levels of STAT3 Tyr705 phosphorylatION (Yu, He et al. 2015). Furthermore, they demostrated that constitutive STAT3 DNA-binding activity in MDA-MB-468 cells was specifically blocked by selective inhibitors of Src or JAK (Yu, He et al. 2015), the known upstream activators of STAT3 (Heinrich, Behrmann et al. 1998).

A more recent study also showed that MDA-MB-468 cells were more susceptible to growth inhibiton by the alkylating agent Bendamustine than MDA-MB-453 cells and that these effects were in part related to Bendamustine's inhibitory effect on the SH2 domain of STAT3.This study reported that Bendamustine suppressed the function of cellular STAT3 as a transcriptional activator in MDA-MB-468 cells and this STAT3 inhibition stopped the growth of cancer cells by binding to DNA and interfering with its replication. Together these studies provide strong evidence for elevated STAT3 activity in the MDA-MB-468 cells which is inconsistent with our findings of low STAT3 Tyr705

phosphorylation levels in this cell line. Although unclear as to the cause of this inconsistent finding, future experiments should further investigate this discrepancy.

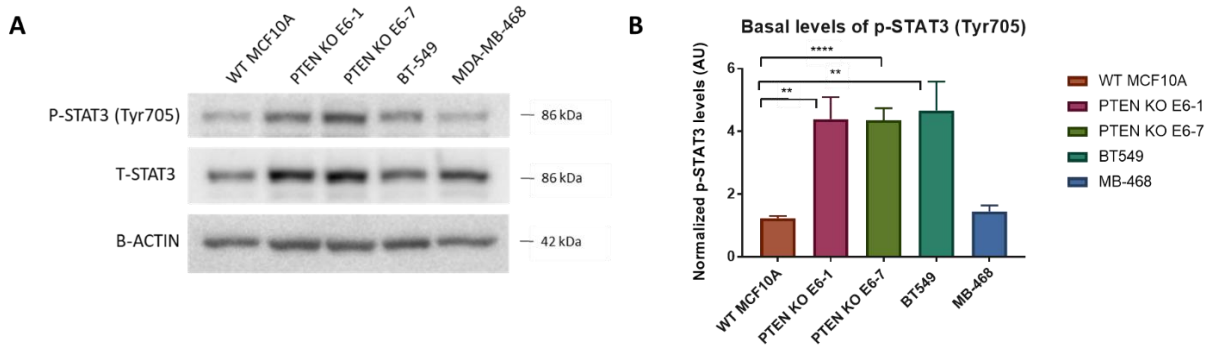

Figure 3.8 Characterisation of basal STAT3 expression levels. (**A**) Representative western blots of total and phospho STAT3 protein expression levels in WT MCF10A and PTEN KO cells (E6-1, E6-7) and TNBC cells; BT-549 (PTEN-/-) and MDA-MB-468 (PTEN-/-). (**B**) Quantified levels of relative p-STAT3 (Tyr705). Proteins were loaded (10 µg), separated by 10% SDS-PAGE, then transferred to PVDF membranes, cut and immunoblotted with antibodies for total and phospho STAT3 and β-actin loading control. Protein levels were quantified by densitometry and the data (both total and phospho protein) normalised to their corresponding β-actin loading control (an example shown here) and then normalised to total levels to obtain relative phospho levels. Data is represented as the mean values ± standard error of the mean of six independent biological replicates. Paired two-tailed *t*–test was used and statistical significance was considered at $P < 0.05$. * = $P < 0.05$, ** = $P < 0.01$, *** = $P < 0.001$, **** = $P < 0.0001$, ***** = $P < 0.00001$. AU (arbitrary units).

PTEN loss failed to significantly affect the MAPK-ERK pathway as expression levels of total and phosphorylated ERK1/2 (Thr202/Tyr204) appear to be relatively unchanged in these PTEN KO clones when compared to the WT MCF10A cells (**Figure 3.9A-B and Figure 3.10A-B**). In addition, WT MCF10A cells express higher levels of the smaller ERK2 isoform (42 kDa) than ERK1 (44 kDa), phosphorylated ERK2 (Tyr204) being the predominant active form and this appears unchanged in the PTEN KO cells (**Figure 3.9A and Figure 3.10A-B**) further suggesting ERK signalling was unperturbed following PTEN loss. Moreover, the upstream RTK EGFR and canonical mediator of MAPK signalling also appeared to be relatively unchanged in the PTEN KO clones as phospho tyrosine (Y1068) and total EGFR expression levels are similar to WT MCF10A cells (**Figure 3.10A-B)**. EGFR phosphorylation on Y1068 and Y1086 can activate both the MAPK and PI3K pathways as their phosphorylation creates sites for GRB2 binding (Batzer, Rotin et al. 1994) leading to MAPK/ERK signalling, and a binding site for GAB1 that recruits the PI3K p85 subunit triggering AKT activation (Rodrigues, Falasca et al. 2000).

Interestingly, total and phospho (Thr202) levels of the larger ERK1 isoform (44 kDa) is more highly expressed in the TNBC cell lines compared to the WT and PTEN KO MCF10A cells (**Figure 3.9A**), however relative expression levels of phosphorylated ERK2 were significantly lower in all the TNBC cell lines; BT-549, MDA-MB-468 and SUM185PE compared to the WT MCF10As, but not the PTEN KO clones (**Figure 3.9A-B**). MDA-MB-468 cells had the lowest levels of ERK1/2 phosphorylation and this was significantly lower than both BT-549 and SUM185PE cells $P < 0.05$ (**Figure 3.9B**). This is interesting considering the known EGFR over-expression and elevated activity in the MDA-MB-468 cells (Filmus, Pollak et al. 1985) which is also recapitulated here by high total and phospho EGFR (Y1068) expression (**Figure 3.10B**).

In contrast, SUM185PE cells express low levels of total EGFR and phosphorylated EGFR at site Y1068 was undetected (**Figure 3.10A)**, despite this ERK activity was significantly higher in this cell line than in MDA-MB-468 cells (**Figure 3.9B**). Therefore, suggesting that activation of ERK is not due to EGFR activity. Numerous alterations in SUM185PE cells could be leading to the activation of ERK in the absence of EGFR activity. For instance, it is known that this cell line has fibroblast growth factor receptor 3 (FGFR3) gene amplification (Guest, Kratche et al. 2016). Using genome-scale shRNA growth and viability screens Guest et al. determined that this amplified gene played a functional role in driving cell growth and viability in this cell line (Guest, Kratche et al. 2016). Thus, FGFR acts as an activated driver oncogene and could be leading to elevated activation of the MAPK/ERK sinalling cascade. Indeed, upon ligand binding FGFR activation adaptors such as FGFR substrate 2 (FRS2) associate with the receptor to trigger downstream signalling of the MAPK (Tiong, Mah et al. 2013) and PI3K pathways (Chell, Balmanno et al. 2013).

However, it must also be noted that there are many other phospho sites on EGFR which are important for its activity. There are six known autophosphorylation sites in the C-terminal tail of EGFR, these are tyrosines 992, 1045, 1068, 1086, 1148, and 1173 (Abe, Kuroda et al. 2006). Phosphorylation of these sites act as docking sites for intracellular signalling proteins containing Src homology 2 (SH2) or phosphotyrosine binding (PTB) domains leading to the activation of specific downstream signal transduction pathways (Shoelson 1997). Therefore, it cannot be ruled out that other phospho sites are not playing a role in ERK1/2 activation. It is unclear which other phospho sites are activated due to being highly cell line specfic and thus, expression of many sites were not detected by immunoblotting. This apparent disconnect between upstream activators and their downstream targets highlights the complexities of signalling pathways. For instance, many more signalling proteins than investigated here are involved in these pathways. In addition, the pathways activation status, topology and crosstalk is context dependent and cell line specific, thus this would account for the large variation seen here between the cell lines.

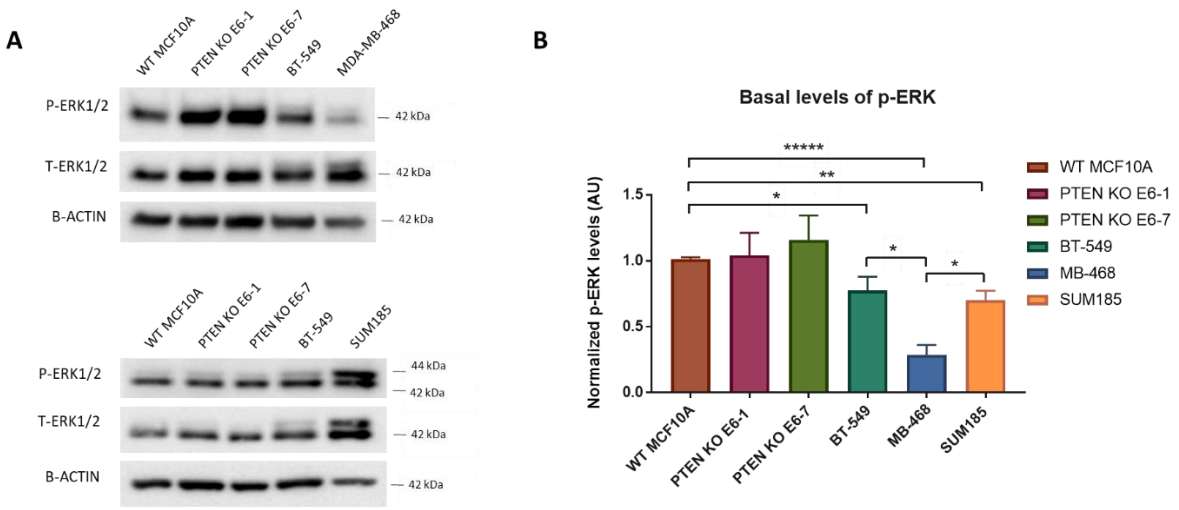

Figure 3.9 Characterisation of basal ERK expression levels. (**A**) Representative western blots of total and phospho ERK1/2 protein expression levels in WT MCF10A and PTEN KO cells (E6-1, E6-7) and TNBC cells; BT-549 (PTEN-/-), MDA-MB-468 (PTEN-/-) (top blot) and SUM185PE (PIK3CAmut) (bottom blot). (**B**) Quantified levels of relative p-ERK (Thr202/Tyr204). Proteins were loaded (10 µg), separated by 10% SDS-PAGE, then transferred to PVDF membranes, cut and immunoblotted with antibodies for total and phospho ERK and β-actin loading control. Protein levels were quantified by densitometry and the data (both total and phospho protein) normalised to their corresponding β-actin loading control (an example shown here) and then normalised to total levels to obtain relative phospho levels. Data is represented as the mean values ± standard error of the mean of six independent biological replicates. Paired two-tailed *t*–test was used and statistical significance was considered at $P < 0.05$. * = $P < 0.05$, ** = $P < 0.01$, *** = $P < 0.001$, **** = $P < 0.0001$, ***** = $P < 0.00001$. AU (arbitrary units).

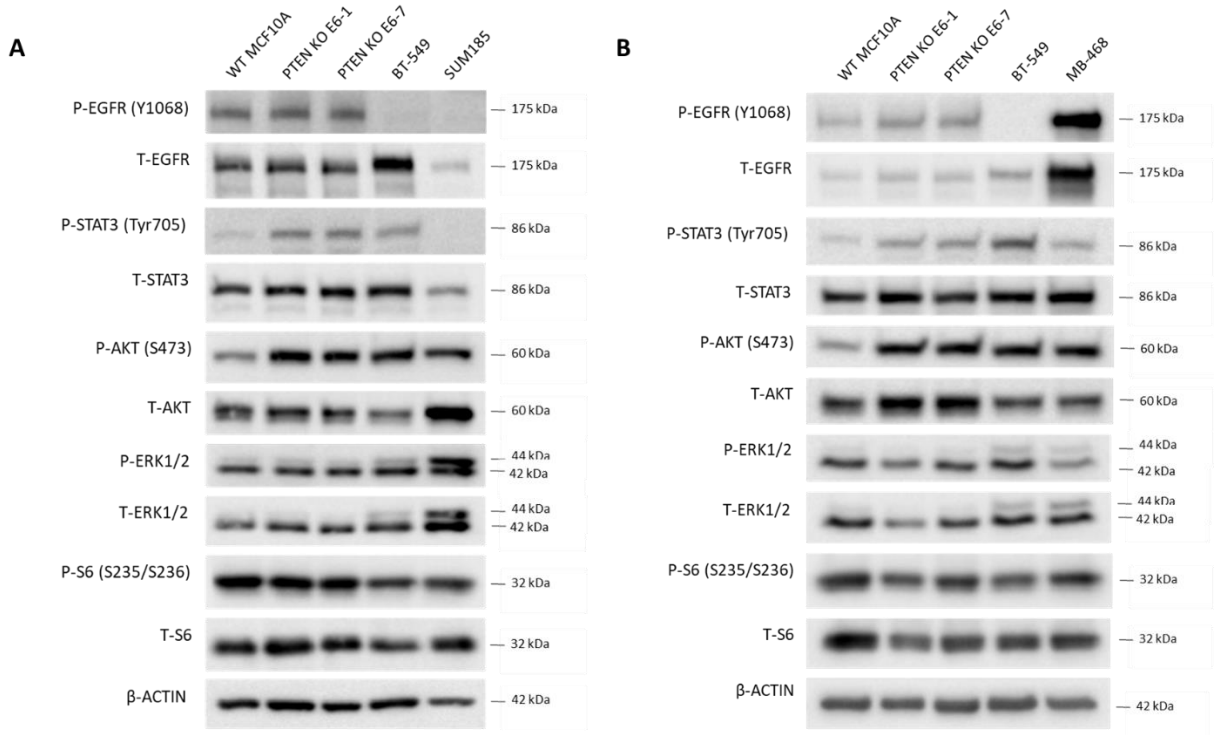

Figure 3.10 Characterisation of basal EGFR, STAT3, AKT, ERK and S6 expression levels. Representative western blots (**A-B**) showing the basal protein expression levels of total and phospho EGFR, STAT3, AKT, S6 and ERK1/2 in WT and PTEN KO MCF10As; (E6-1 and E6-7) and TNBC cells; BT-549 (PTEN-/-), and SUM185PE (*PIK3CA*mut) (**A**) or MDA-MB-468 (**B**). Proteins were loaded (10 µg), separated by 10% SDS-PAGE, then transferred to PVDF membranes, cut and immunoblotted with antibodies for total and phospho proteins and β-actin loading control (representative examples shown here).

Although, phosphorylated AKT was significantly elevated in the PTEN KO clones indicative of upregulated PI3K-AKT-mTOR pathway activity, the level of phosphorylated ribosomal protein S6 (Ser235/236), a downstream target of the AKT pathway and marker of mTORC1 activity, appeared to be expressed similary regardless of PTEN status (**Figure 3.10**). Considering the upregulated AKT Ser473 phosphorylation it was unexpected for the downstream marker of PI3K signalling to not increase as well. Ribosomal protein S6 is highly conserved from yeast to higher eukaryotes. S6 has five phosphorylation sites on its serine residues (Ser235, Ser236, Ser240, Ser244, and Ser247) in the region close to the carboxyl terminus (Krieg, Hofsteenge et al. 1988). The serine residues, Ser235 and Ser236 in S6 are directly phosphorylated by S6K which is regulated by mTORC1 signalling in a nutrient-dependent manner (Ruvinsky and Meyuhas 2006). It is well known that mTORC1 signalling contributes to cell growth by controlling translation through its ability to directly phosphorylate the translation regulators, S6K and eIF4E-binding protein (4E-BP) (Hay and Sonenberg 2004). AKT and S6K are well-known substrates of mTORC2 and mTORC1, respectively (Jacinto and Lorberg 2008). Thus this disconnect between AKT activity and S6 activation, which is downstream of AKT may be explained by the fact that S6 is a direct marker of S6K activity and an indirect marker mTORC1, whereas activated

AKT by mTORC2 on Ser473 site, subsequently activates not only mTORC1, but also a plethora of other substrates, including important substrates such as FOXO transcription factors and GSK3β (Manning and Cantley 2007). Hence, AKT phosphorylation doesn't only reflect mTORC1 signalling, but also other pathways such as FOXO signalling, and thus it is possible for S6 activity to fail to reflect enhanced AKT signalling.

To further analyse the effect of PTEN loss on the signalling response of MAPK and PI3K pathways, growth factor stimulation experiments with EGF were performed in the isogenic MCF10A cell lines. Firstly, cells were serum starved for 24 h with starvation DMEM/F12 media containing 0.4% horse serum (HS) and lacking EGF and insulin. Following the starvation period, cells were stimulated by time-course treatment with EGF, the signalling pathways were assessed by immunoblotting, probing the membrane with antibodies targeted against the phospho and total levels of key downstream signalling targets; AKT (**Figure 3.11**), S6 (**Figure 3.12**) and ERK1/2 (**Figure 3.13**), which as previously discussed, are key markers of PI3K and MAPK pathway activation. Consistent with the previous results showing elevated phospho AKT levels in the MCF10A PTEN KO clones indicating upregulated PI3K activation, in the EGF stimulation experiments at the 0 h time-point (basal levels) phosphorylated AKT and S6 levels were higher in the MCF10A PTEN KO clones, and significantly so in E6-7 compared to parental WT MCF10A cells (**Figure 3.11 and Figure 3.12**). In support of the previous immunoblot data, these findings suggest that PI3K pathway signalling was upregulated in PTEN-KO cells which is expected given these cells have lost PTEN and with it the negative regulation of the PI3K pathway.

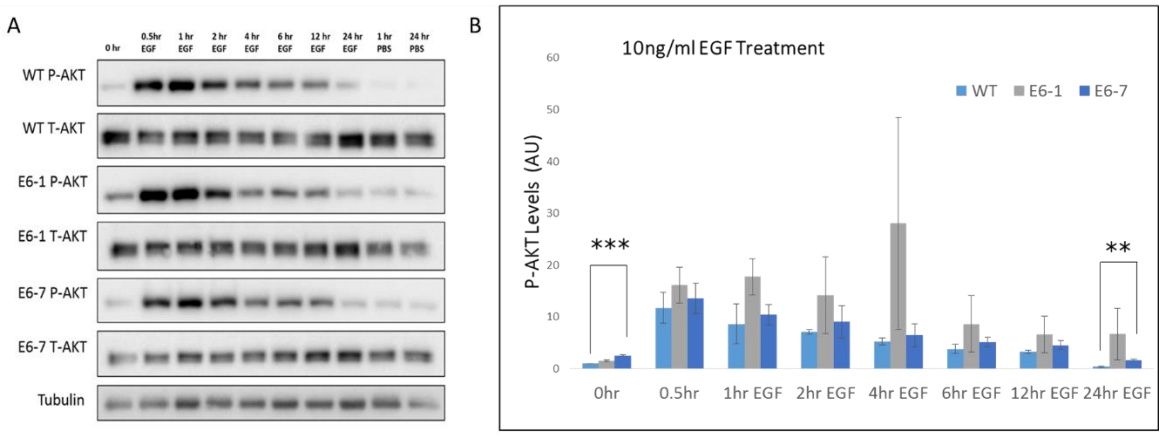

Figure 3.11 Examination of AKT levels following EGF stimulation. (**A**) Representative western blots showing protein expression levels of total and phospho AKT in WT MCF10A and MCF10A PTEN KO clones; E6-1 and E6-7 following stimulation with EGF. In brief, cells were serum starved for 24 h with DMEM/F12 starvation media (-EGF, -Insulin, 0.4% HS). Following this, cells were treated with 10 ng/mL EGF and incubated for 0.5, 1, 2, 4, 6, 8, 12 and 24 h, then lysed using RIPA lysis buffer and proteins harvested. 1:1000 PBS was used as the vehicle control. Proteins were loaded (10 µg), separated by 10% SDS-PAGE, then transferred to PVDF membranes and immunoblotted with antibodies for total and phospho AKT and tubulin loading control. Graph (**B**) showing quantified levels of relative p-AKT. Protein levels were quantified by densitometry and the data (both total and phospho protein) was normalised to their corresponding α-tubulin loading control (an example shown here) and then normalised to total levels to obtain relative phospho levels. Data is represented as the mean values ± standard error of the mean of three independent biological replicates. Paired two-tailed *t*–test was used and statistical significance was considered at $P < 0.05$. *** = $P < 0.0005$, **= $P < 0.01$. AU (arbitrary units).

However, there were no significant differences in either p-AKT or p-S6 in the PTEN KO cells compared to WT MCF10A cells in response to EGF stimulation over the time-course except with higher p-AKT levels after 24 h EGF treatment in both PTEN KO clones, but this was only significantly higher in the E6-7 clone (**Figure 3.11 and Figure 3.12**). This finding suggests the PTEN KO cells seem to maintain p-AKT levels for longer following EGF stimulation. A slower 'off-rate' makes sense since PIP3 levels would presumably be maintained following the loss of PTEN. This is an interesting observation and suggests that not only is there higher AKT signalling in the PTEN loss cells, but also that EGF-induced activation of the PI3K pathway is sustained for a longer period of time. Another explanation for the observed phenomenon is that after 24 h EGF treatment homeostasis has been reached and thus, AKT activity reflects basal p-AKT levels. In contrast to the differences in AKT signalling, but in support of the previous findings, there was no significant difference in ERK signalling in PTEN KO clones compared to MCF10A WT cells (**Figure 3.13**). In all cells, regardless of PTEN status, AKT (**Figure 3.11**) and ERK (**Figure 3.13**) phosphorylation peaks after 0.5 h EGF stimulation and then over the time-course reduces back to basal levels. This suggests that PTEN loss did not change the dynamic response pattern of MAPK or PI3K signalling to EGF stimulation, but supports the previous finding that the basal levels of AKT activity are higher in the KO clones.

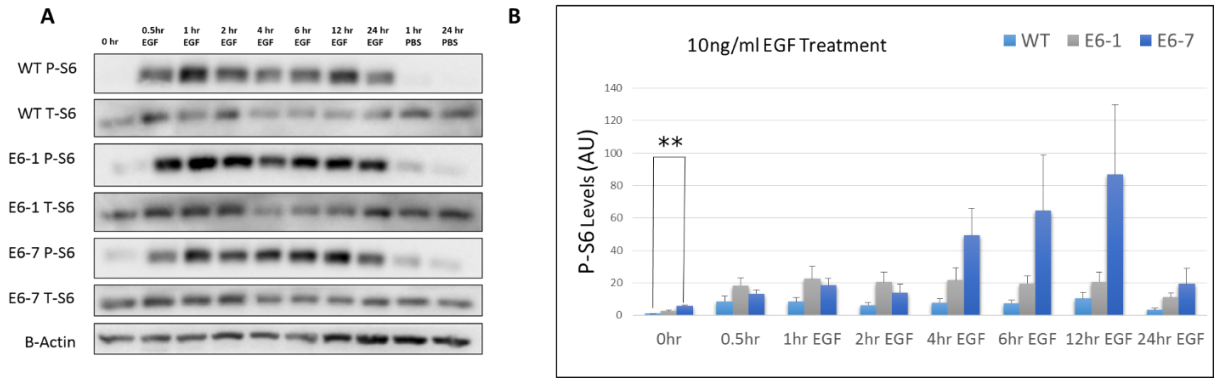

Figure 3.12 Examination of S6 levels following EGF stimulation. (**A**) Representative western blots showing protein expression levels of total and phospho S6 (Ser235/236) in WT MCF10A and MCF10A PTEN KO clones; E6-1 and E6-7 following stimulation with EGF. In brief, cells were serum starved for 24 h with DMEM/F12 starvation media (-EGF, -Insulin, 0.4% HS). Following this, cells were treated with 10 ng/mL EGF and incubated for 0.5, 1, 2, 4, 6, 8, 12 and 24 h. 1:1000 PBS was used as the vehicle control. (**B**) Quantified levels of relative p-S6. Protein levels were quantified by densitometry and the data (both total and phospho protein) was normalised to their corresponding β-actin loading control (an example shown here) and then normalised to total levels to obtain relative phospho levels. Data is represented as the mean values ± standard error of the mean of three independent biological replicates. Paired two-tailed *t*–test was used and statistical significance was considered at $P < 0.05$. AU (arbitrary units).

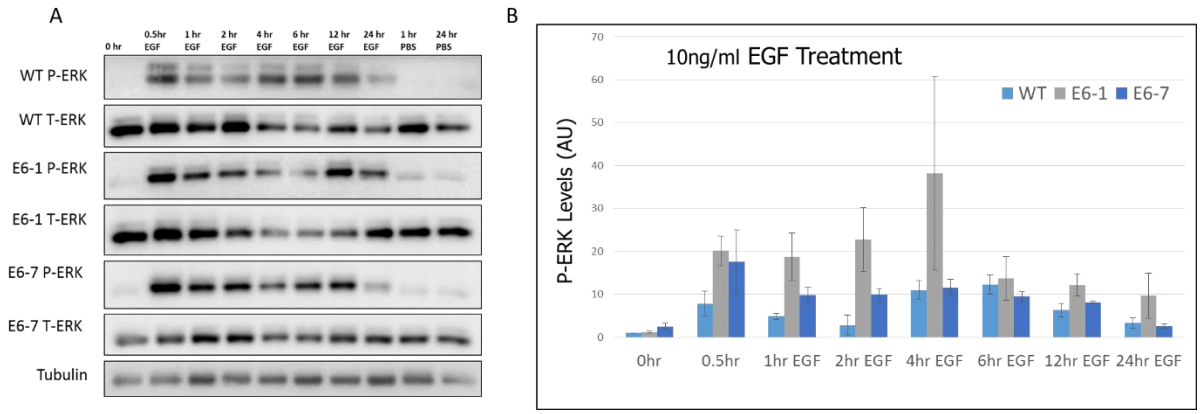

Figure 3.13 Examination of ERK levels following EGF stimulation. (**A**) Representative western blots showing protein expression levels of total and phospho ERK1/2 (Thr202/Tyr204) in WT MCF10A and MCF10A PTEN KO clones; E6-1 and E6-7 following stimulation with EGF. In brief, cells were serum starved for 24 h with DMEM/F12 starvation media (-EGF, -Insulin, 0.4% HS). Following this, cells were treated with 10 ng/mL EGF and incubated for 0.5, 1, 2, 4, 6, 8, 12 and 24 h. 1:1000 PBS was used as the vehicle control. (**B**) Quantified levels of relative p-ERK. Protein levels were quantified by densitometry and the data (both total and phospho protein) was normalised to their corresponding α-tubulin loading control (an example shown here) and then normalised to total levels to obtain relative phospho levels. Data is represented as the mean values ± standard error of the mean of three independent biological replicates. Paired two-tailed *t*–test was used and statistical significance was considered at $P < 0.05$. AU (arbitrary units).

In order to identify the EGF concentration equivalent to the growing condition (GC) parameter in the model, a growth condition time-course experiment was conducted in the WT MCF10A cells and the PTEN KO clone E6-1. Using our model phosphorylated ERK and AKT were simulated by gradually increasing EGF concentrations and then compared to the response time profiles of phospho ERK and

AKT measured in the growing condition. Then by calculating the difference between responses to EGF and growth condition, the EGF concentration that causes the minimal difference was defined as the growth condition parameter for the model. In addition, this GC time course data can be used as independent validation data for the model.

Firstly, cells were serum starved for 24 h with starvation DMEM/F12 media containing 0.4% HS and lacking EGF and insulin. Following the starvation period, cells were stimulated using complete DMEM/F12 media supplemented with all additives as per **Table 2.2** in Chapter 2 and probed for 15 min, 30 min, 1 and 6 h, followed by immunoblot analysis of total and phospho EGFR, ERK1/2, S6, AKT and STAT3. The results revealed that despite PTEN loss, both PTEN KO clone E6-1 and WT MCF10A cells responded similarly to growth factor stimulation over time with regard to activity levels of these signalling proteins (**Figure 3.14**). Despite similar dynamic responses which supports the previous findings, higher levels of p-AKT, p-S6 and p-STAT3 were observed in the cells with PTEN KO. Interestingly, treatment with starvation media appears to further enhance the activation of STAT3 as its levels were highest after 24 h of starvation (**Figure 3.14**), however, this was only observed in the PTEN KO cells. In contrast the highest levels of STAT3 phosphorylation (Tyr705) in WT MCF10A was observed after 15 min stimulation with complete media. This result suggests that lack of growth factors and cell starvation enhances STAT3 activation in the absence of PTEN.

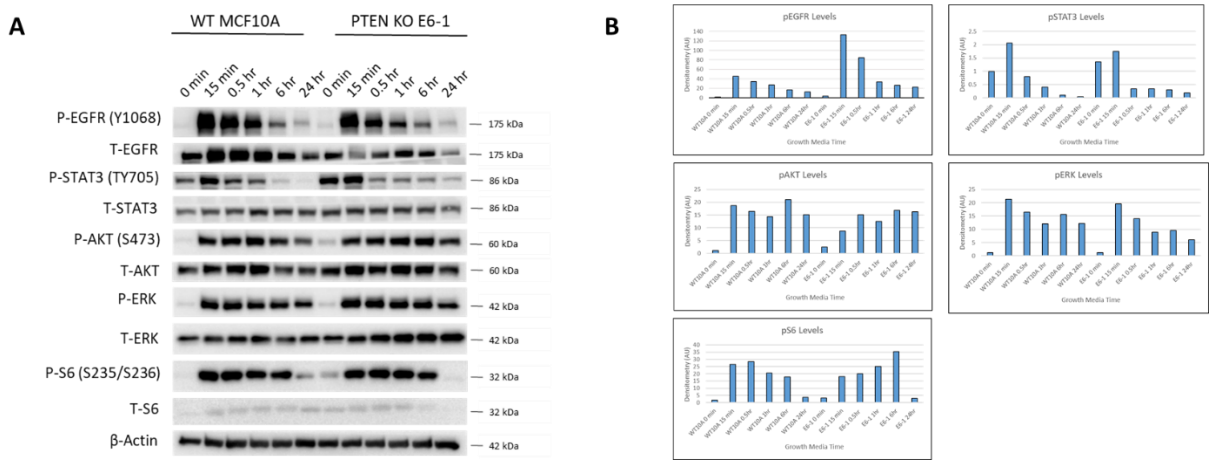

Figure 3.14 DMEM/F12 media time-course experiment to identify the EGF concentration equivalent to the growing condition parameter in the model. Representative western blots (**A**) and graphs (**B**) following starvation for 24 h showing the protein expression levels of total and phospho EGFR (Y1068), STAT3 (Tyr705), AKT (Ser473), S6 (Ser235/236) and ERK1/2 (Thr202/Tyr204) in WT and PTEN KO MCF10A cells; E6-1 and E6-7 in response to time-course treatment with complete DMEM/F12 media containing all additives (**Table 2.2**). Cells were incubated for 24 h with starvation DMEM/F12 media (0.4% HS and no EGF or insulin). Following this, cells were treated with complete DMEM/F12 media for 15 min, 30 min, 1 and 6 h. PBS was used as the vehicle control. Protein levels were quantified by densitometry and the data normalised to β-actin loading control (an example shown here) and then to total levels to obtain relative phosho protein levels. AU (arbitrary units).

In summary, following successful PTEN KO as validated by both DNA sequencing showing INDELs and loss of PTEN expression by immunoblot analysis, MAPK and PI3K signalling characterisation of these PTEN KO cells compared to WT MCF10A was carried out. The results confirmed that PTEN loss led to increased PI3K signalling as demonstrated by the elevated AKT Ser473 phosphorylation in these cells. EGF stimulation experiments were then performed in these cells to investigate whether PTEN loss influenced the MAPK and PI3K signalling response to growth factor stimulation. The results showed that the PTEN KO clones behaved similarly to WT MCF10A cells in response to EGF stimulation since phosphorylated levels of AKT, ERK and S6 were relatively unchanged between them suggesting PTEN loss failed to alter the dynamic response. Consistent with these findings, a growth condition stimulation experiment, which was conducted for the model, also revealed a similar dynamic signalling response to time-course treatment with full serum media (EGF and insulin) between WT MCF10A and the tested PTEN KO clone E6-1. The next step was to characterise the MAPK and PI3K signalling response to MEK and PI3K inhibition in both WT and PTEN loss MCF10A cells in order to determine whether PTEN loss influences this drug-induced response, which is our second aim.

3.3 Characterisation of the dynamic network changes in response to MEK inhibition

Many studies investigating network signalling solely focus on one pathway in isolation at single points in time. In doing so, the research fails to reflect and incorporate the complex interconnectivity of pathways and the network crosstalk of cells. This static approach lacks the valuable dynamic changes that occur in the pathway over time which greatly limits our understanding of the network behaviour as a whole. Understanding the dynamic circuitry of signal transduction networks that regulate functions such as cell proliferation and survival are key to understanding tumourigenesis and cancer cell behaviour including drug resistance (Kolch, Halasz et al. 2015). Therefore, in order to investigate how PTEN loss influences the signalling response to PI3K and MEK inhibition (Aim 2) the dynamic MAPK-PI3K network-level changes in the PTEN KO and WT MCF10A cells were examined in response to time-course treatment with a MEK inhibitor and later a PI3K inhibitor. In addition, if any altered drug responsiveness due to PTEN loss was found we wanted to determine if this was driven by PI3K-MAPK pathway crosstalk.

3.3.1 MEK inhibitor dose-response experiment

Trametinib (GSK1120212/JTP-74057) is an adenosine triphosphate (ATP)-noncompetitive and selective allosteric inhibitor of MEK1/2 (Gilmartin, Bleam et al. 2011). In order to identify the optimal MEK inhibitor (MEKi) dose to use for the time-course experiments, dose-response experiments were first performed. In these dose-response experiments WT MCF10A cell proliferation (**Figure 3.15**) and cell signalling (**Figure 3.16**) using MTS assays and immunoblotting respectively, were used as measures of drug response. Cells were treated acutely for 1 h over a range of trametinib concentrations.

The immunoblotting results demonstrated that 5 nM of MEKi was sufficient to inhibit ERK1/2 activity (**Figure 3.16**). Higher doses of trametinib starting at ~ 500 nM inhibited AKT (Ser473) phosphorylation and this was completely suppressed after treatment with 10 µM MEKi (**Figure 3.16**). This is likely due to the positive feedback loop of PI3K-RAS which would result in decreased ERK levels thus reducing AKT activity.

In the MTS assay a growth inhibitory effect was only observed after 48 and 72 h of MEKi treatment as within the first 24 h the cells failed to undergo sufficient proliferation as observed by the low cell count in the untreated condition and the DMSO vehicle control on day 1 (**Figure 3.15**). In addition, cell growth inhibition was not observed until doses of 50 nM MEKi or higher were used. This finding which is in contrast to the 5 nM dose needed to supress ERK activity shows the lack of correlation between trametinib's IC50 value ~ 50 nM and inhibition of ERK signalling. A drug's IC50 value is the concentration of the drug that is required for 50% inhibition of growth *in vitro*. However, this disconnect between signalling and proliferation has been previously shown. A study investigating the relationship between pathway usage and sensitivity to trametinib also observed that inhibition of ERK signalling as measured by phosphorylation of ERK was observed at much lower drug concentrations than the dose needed to affect proliferation (Leung, E.Y., et al, 2014). A dose of 5 nM was used since we wanted to investigate the signalling changes and to test the dynamic response to MEK inhibition in both the WT MCF10A and PTEN KO clones, as well as the TNBC cell lines SUM185PE and BT-549.

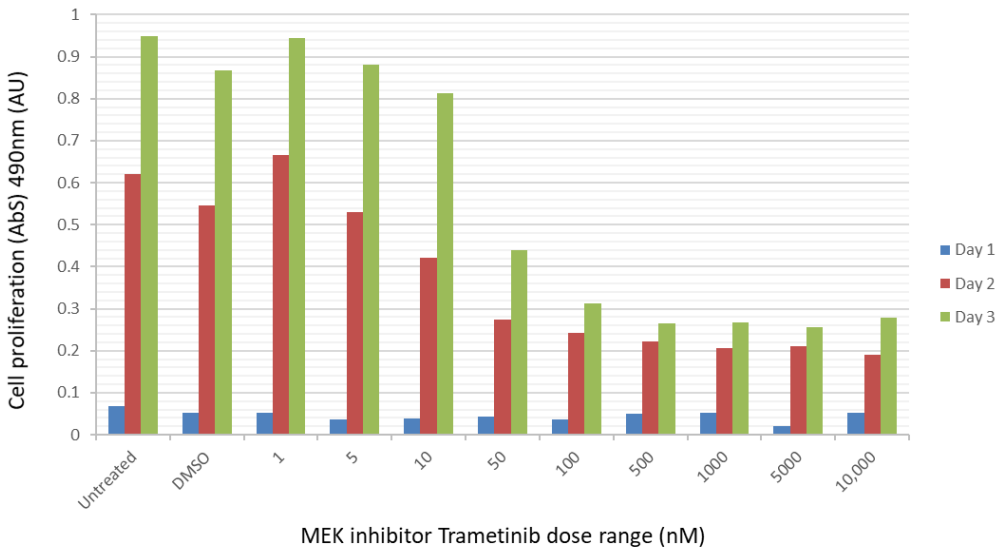

Figure 3.15 MCF10A cell proliferation after 24, 48 and 72 h of MEKi trametinib treatment using MTS assay. Cells were seeded at a density of 3000 cells per well of a 96-well plate and there were five technical replicates per treatment condition. Day 1 post-seeding cells were treated acutely treated with trametinib for 1 h at 1 nM, 5 nM, 10 nM, 50 nM, 100 nM, 1 µM, 5 µM and 10 µM concentrations for 24, 48 and 72 h. 1:1000 DMSO was used as the vehicle control. Following drug treatment 10 µl of MTS reagent was added to each well and cells were incubated for 1 h at 37℃. Absorbance readings were measured at 490 nm on a plate reader. MEKi (MEK inhibitor), Arbitrary units (AU).

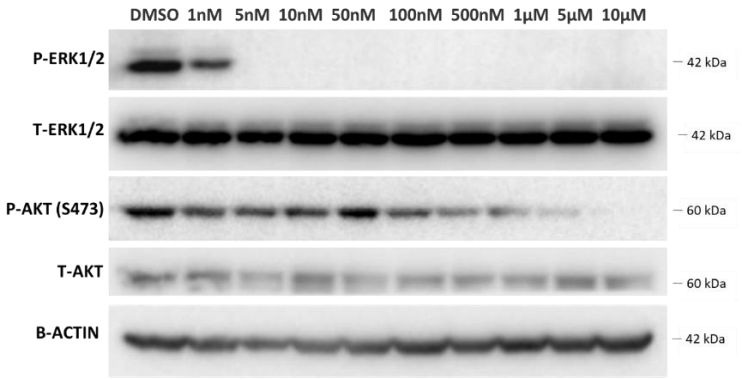

Figure 3.16 Dose-response effect of MEK inhibitor trametinib treatment on AKT and ERK1/2 levels. MCF10A cells were acutely treated with trametinib for 1 h at 1 nM, 5 nM, 10 nM, 50 nM, 100 nM, 1 µM, 5 µM and 10 µM concentrations. 1:1000 DMSO was used as the vehicle control. Cells were lysed and proteins harvested using RIPA lysis buffer. Proteins were loaded (10 µg), separated by 10% SDS-PAGE, transferred to PVDF membranes and immunoblotted with antibodies for total and phospho ERK and AKT.

3.3.2 PI3K and MAPK signalling in response to time-course treatment with MEK1/2 inhibitor

In the MEKi time-course experiment cells were treated with 5 nM trametinib for 0.5, 1, 6, 12, and 24 h and DMSO vehicle control for 1 and 24 h. In brief, drug treated cells were lysed and the proteins harvested using RIPA lysis buffer. Proteins were normalised to equal loading and separated by 8% SDS-PAGE, transferred to PVDF membranes and immunoblotted for total and phospho levels of EGFR, STAT3, AKT, ERK1/2 and S6. The MEKi time-course experiment allowed investigation of the dynamic changes in the PI3K and MAPK signalling pathways over time in WT MCF10A compared to MCF10A PTEN KO clones and the TNBC cell lines BT-549 and SUM185PE.

The MEKi time-course data showed no significant drug-induced differences between WT MCF10A and PTEN KO cells as there was no significant change in EGFR, STAT3 (data not shown), ERK, S6 or AKT activity between them, following MEK inhibition (**Figure 3.17**, **Figure 3.18**, and **Figure 3.19**). The time-course results of phosphorylated ERK activity show that in response to 0.5 h MEK inhibition all the cell lines, except SUM185PE cells, showed reduced p-ERK levels and maximum suppression of ERK activity was reached at either 1 or 2 h following MEK inhibition (**Figure 3.17**). A reduction in p-ERK is observed only after 1 h of drug exposure in SUM185PE cells. In all the cell lines tested, phosphorylated ERK remained inhibited at the later time points indicating that the drug maintains its effectiveness for at least 24 h, which was the longest duration of exposure tested, and that the cells were unable to circumvent this blockade.

The TNBC SUM185PE cells were the least sensitive to trametinib as shown by the lower decrease in p-ERK levels at all time-points in response to MEK inhibition compared to all other cells (**Figure 3.17**). This was followed by BT-549 cells as they showed higher levels of ERK activity over the duration of the treatment compared to the WT MCF10A and PTEN KO clones. Basal levels of total and phospho

ERK appear relatively unchanged when PTEN is lost as WT MCF10A and PTEN KO clones show similar levels of basal ERK expression which is consistent with our previous data. Moreover, in response to drug treatment the WT and PTEN KO MCF10A cells show a similar level of responsiveness to MEK inhibition as evidenced by similar levels of p-ERK following treatment (**Figure 3.17**). This finding indicates that PTEN loss does not appear to alter ERK signalling in response to trametinib. In addition, the PI3K pathway seems unaffected by MEK inhibition as both p-AKT and p-S6 levels remain relatively unchanged during the entire duration of drug treatment (**Figure 3.18 and Figure 3.19**). Taken together, these findings suggest that loss of PTEN and the resulting upregulation of PI3K/AKT signalling did not significantly disrupt PI3K-ERK crosstalk, at least not in response to MEK inhibition using 5 nM trametinib.

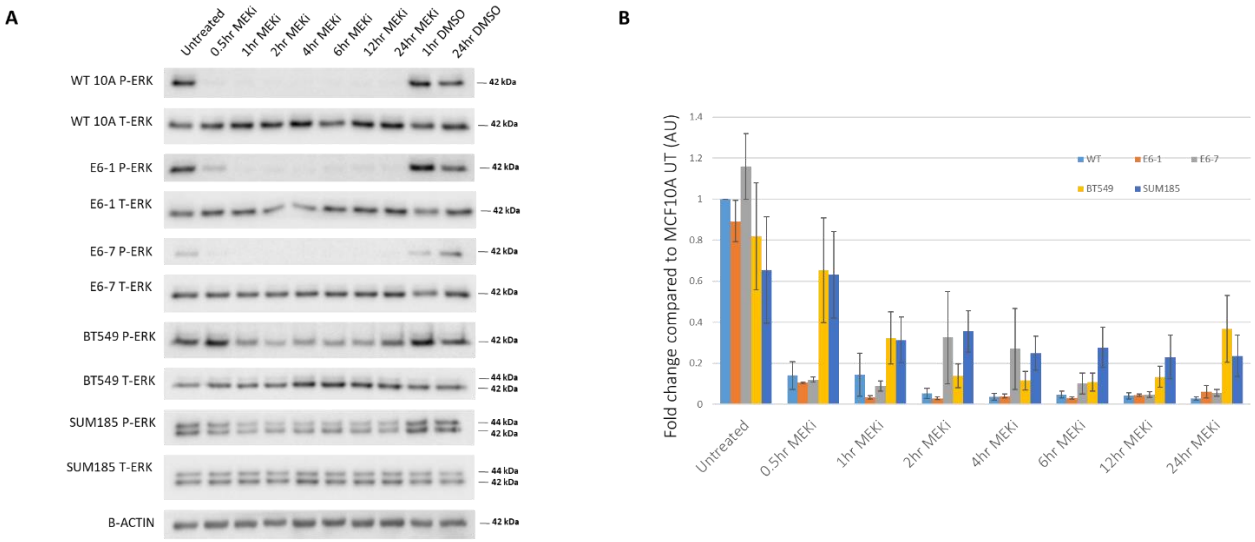

Figure 3.17 ERK protein expression levels in response to MEKi time-course treatment. Representative western blots (**A**) showing protein expression levels of total and phospho ERK in WT and PTEN KO MCF10As; (E6-1 and E6-7) and TNBC cells; BT-549 (PTEN-/-) and SUM185PE (*PIK3CA*mut) in response to MEK inhibition with 5 nM trametinib for 0, 1, 2, 4, 6, 12 and 24 h. Time-course graph (**B**) showing quantified p-ERK (Thr202/Tyr204) levels following MEK inhibition. Protein levels were quantified by densitometry and the data (both total and phospho protein) was normalised to their corresponding β-actin loading control (a representative blot shown here) and then normalised to total levels to obtain relative phospho levels. Relative p-ERK/ERK levels were then normalised to their untreated protein levels (untreated=1) and this was normalised to the untreated WT MCF10A protein levels. Thus, the results shown represent the fold change compared to untreated WT MCF10A cells. Data is represented as the mean values ± standard error of the mean of three independent biological replicates. Paired two-tailed *t*–test was used and statistical significance was considered at $P < 0.05$. AU (arbitrary units).

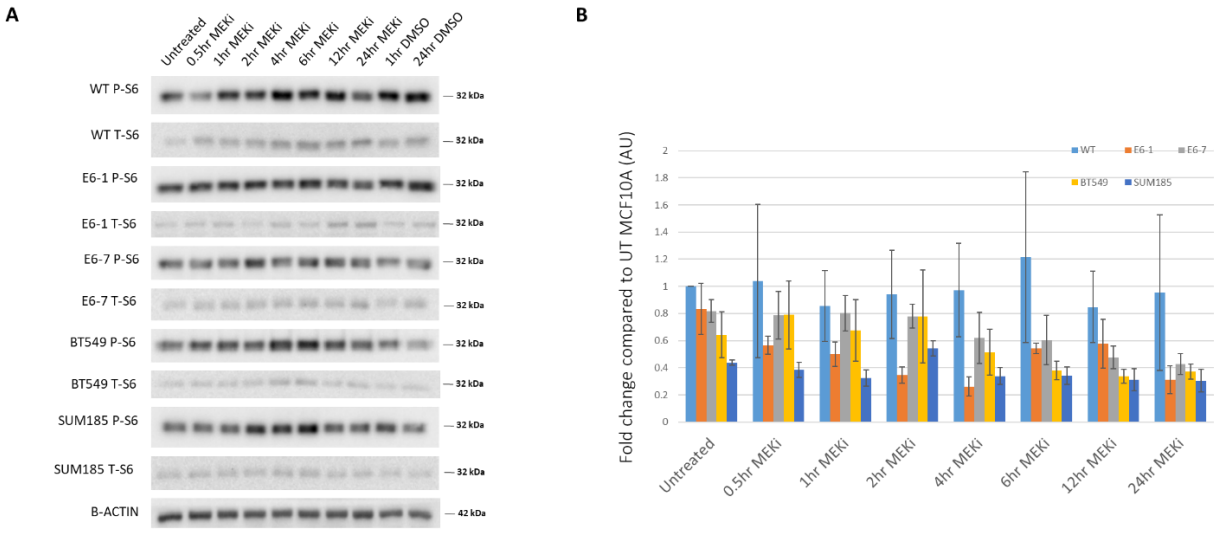

Figure 3.18 S6 protein expression levels in response to MEKi time-course treatment. Representative western blots (**A**) showing protein expression levels of total and phospho S6 in WT and PTEN KO MCF10As; (E6-1 and E6-7) and TNBC cells; BT-549 (PTEN-/-) and SUM185PE (*PIK3CA* mut) in response to MEK inhibition with 5 nM trametinib for 0, 1, 2, 4, 6, 12 and 24 h. Time-course graph (**B**) showing quantified p-S6 (S235/236) levels following MEK inhibition. Protein levels were quantified by densitometry and the data (both total and phospho protein) was normalised to their corresponding β-actin loading control (a representative blot shown here) and then normalised to total levels to obtain relative phospho levels. Relative p-S6/S6 levels were then normalised to their untreated protein levels (untreated=1) and this was normalised to the untreated WT MCF10A protein levels. Thus, the results shown represent the fold change compared to untreated WT MCF10A cells. Data is represented as the mean values ± standard error of the mean of three independent biological replicates. Paired two-tailed *t*–test was used and statistical significance was considered at $P < 0.05$. AU (arbitrary units).

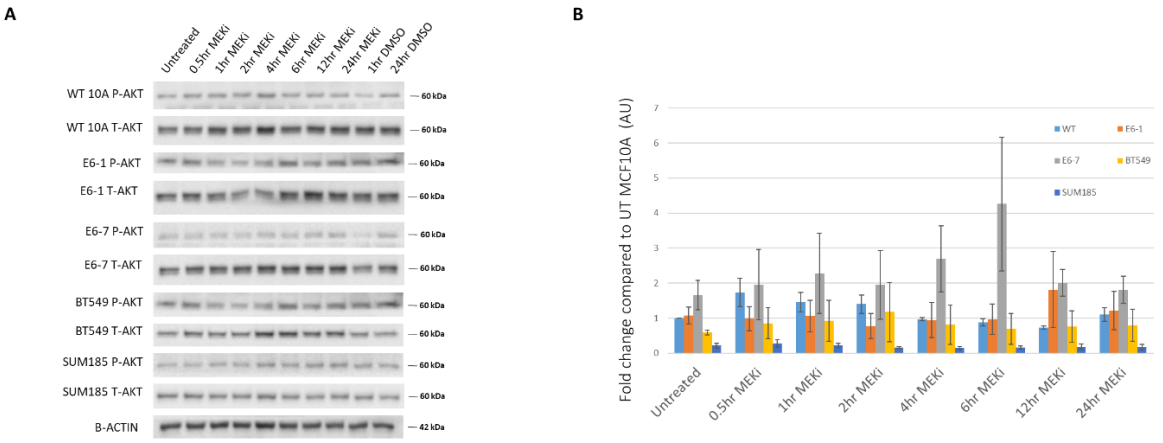

Figure 3.19 AKT protein expression levels in response to MEKi time-course treatment. Representative western blots (**A**) showing protein expression levels of total and phospho AKT in WT and PTEN KO MCF10As; (E6-1 and E6-7) and TNBC cells; BT-549 (PTEN-/-) and SUM185PE (*PIK3CA*mut) in response to MEK inhibition with 5 nM trametinib for 0, 1, 2, 4, 6, 12 and 24 h. Time-course graph (**B**) showing quantified p-AKT (S473) levels following MEK inhibition. Protein levels were quantified by densitometry and the data (both total and phospho protein) was normalised to their corresponding β-actin loading control (a representative blot shown here) and then normalised to total levels to obtain relative phospho levels. Relative p-AKT/AKT levels were then normalised to their untreated protein levels (untreated=1) and this was normalised to the untreated WT MCF10A protein levels. Thus, the results shown represent the fold change compared to untreated WT MCF10A cells. Data is represented as the mean values ± standard error of the mean of three independent biological replicates. Paired two-tailed *t*–test was used and statistical significance was considered at $P < 0.05$. AU (arbitrary units).

3.4 Characterisation of the network changes in response to PI3K inhibition

3.4.1 PI3K inhibitor BYL719 dose-response experiment

Alpelisib (**BYL719**), is a potent PI3K inhibitor selective for p110α subunit (Furet, Guagnano et al. 2013) currently undergoing Phase III clinical trials with the ER antagonist fulvestrant for the treatment of men and postmenopausal women with advanced HR+/HER2– breast cancer (Andre, Ciruelos et al. 2019, Yang, Nie et al. 2019). Firstly, a dose-response experiment was performed in order to select the lowest dose of BYL719 that effectively inhibited AKT in both the WT MCF10A and TNBC cell lines SUM185PE and BT-549. Cells were acutely treated for 1 h with increasing doses of BYL719 and proteins were harvested and immunoblotted for total and phospho AKT, ERK and S6 protein levels.

Since AKT is the downstream target of PI3K and an established downstream output of PI3K signalling, phosphorylated AKT (Ser473) levels served as a direct indicator of drug response and readout of PI3K inhibitor target engagement. The dose-response data shows AKT phosphorylation was suppressed in a dose-dependent manner by BYL719 treatment in all cell lines (**Figure 3.20**). This is most clear for MCF10A cells starting at dose 10 nM and in the TNBC cell lines the dose-dependent reduction in p-AKT levels is clear after a dose of 100 μM. Similarly, activity of the downstream target S6 was also inhibited in a dose-dependent manner and importantly this seems to reflect p-AKT levels, thus indicating that downstream PI3K signalling was adequately suppressed (**Figure 3.21**).

As expected, the dose response results showed that PIK3CA mutant SUM185PE cells were the most sensitive to selective PI3Kα isoform inhibition (**Figure 3.20**). In this cell line, p-AKT appeared completely inhibited with 100 nM of BYL719. This high level of sensitivity of the SUM185PE cells to BYL is an expected finding and supports reports in the literature which show that cell lines and tumours expressing oncogenic PIK3CA mutations require PI3Kα for proliferation and survival rendering PIK3CA mutant cells highly vulnerable to PI3Kα inhibition (Zhao and Vogt 2008, Fritsch, Huang et al. 2014). WT MCF10A cells were the next most sensitive and immunoblot analysis showed that treatment with 100 nM of BYL caused a marked reduction in phospho AKT levels, this was further decreased by 500 nM BYL and 1 µM of the drug caused near complete inhibition of AKT Ser473 phosphorylation. BT-549 cells were the least responsive to PI3Kα inhibition, this finding is supported by other studies which show this cell line to have low sensitivity to BYL. For instance, McDonald et al. found that the IC50 for BT-549 cells to BYL719 was over 10 µM (O'Brien, McDonald et al. 2014). At a dose of 5 µM BYL719 phospho AKT levels were significantly inhibited in MCF10A cells, as well as in the less sensitive BT-549 cells (**Figure 3.20**). Based on these data, 5 µM of BYL719 was chosen for follow-up experiments as lower doses of the drug were unable to reduce p-AKT levels in BT-549 by more than 50%.

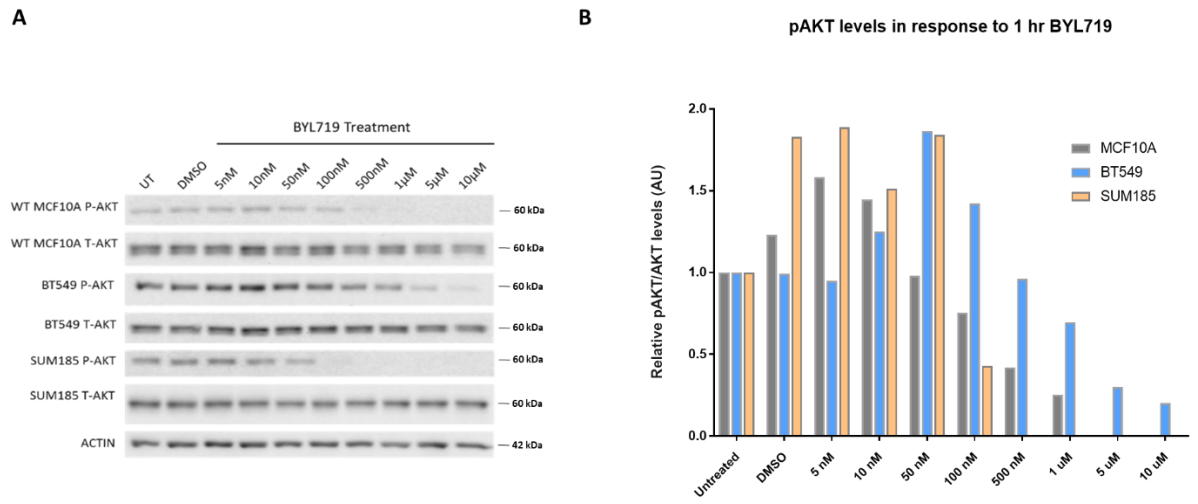

Figure 3.20 Relative AKT protein levels after 1 h PI3Ki dose-response treatment. (**A**) Representative western blots showing expression levels of total and phospho AKT in WT MCF10A and TNBC cells; BT-549 (*PTEN*-/-) and SUM185PE (*PIK3CA* mut) in response to 1 h BYL719 treatment at the following doses of 5 nM, 10 nM, 50 nM, 100 nM, 500 nM, 1 µM, 5 µM and 10 µM drug or 1:1000 DMSO vehicle control. (**B**) Quantified p-AKT (S473) levels in response to BYL719 treatment. Protein levels were quantified by densitometry and the data (both total and phospho protein) was normalised to their corresponding β-actin loading control (a representative blot shown here) and then to total levels to obtain relative phospho levels. Relative p-AKT/AKT levels was then normalised relative to untreated=1. AU (arbitrary units).

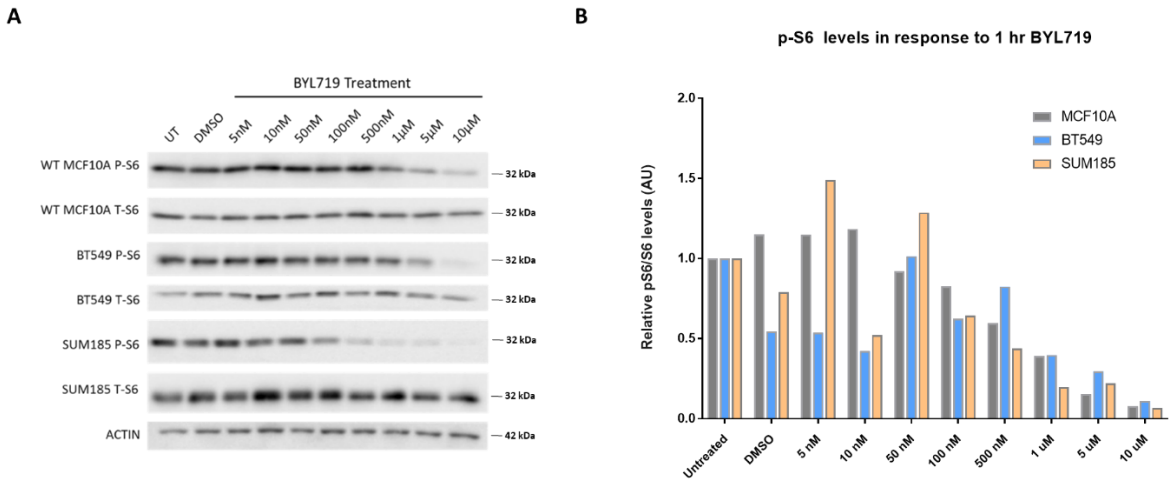

Figure 3.21 Relative S6 protein levels after 1 h PI3Ki dose-response treatment. (**A**) Representative western blots showing expression levels of total and phospho S6 in WT MCF10A and TNBC cells; BT-549 (*PTEN*-/-) and SUM185PE (*PIK3CA* mut) in response to 1 h BYL719 treatment at the following doses of 5 nM, 10 nM, 50 nM, 100 nM, 500 nM, 1 µM, 5 µM and 10 µM drug or 1:1000 DMSO vehicle control. (**B**) Quantified p-S6 (S235/236) levels in response to BYL719 treatment. Protein levels were quantified by densitometry and the data (both total and phospho protein) was normalised to their corresponding β-actin loading control (a representative blot shown here) and then to total levels to obtain relative phospho levels. Relative p-S6/S6 levels was then normalised relative to untreated=1. AU (arbitrary units).

Interestingly, ERK signalling was also impacted in a dose-dependent manner to treatment with higher doses of BYL719 in WT MCF10A cells, but this was not observed in the TNBC cell lines (**Figure 3.22**). In contrast, ERK activity appears to show a trend towards an increase with increasing dose in the TNBC cell lines, this is particularly evident in the highly sensitive SUM185PE cells. This increase is most clear up to a dose of 50 nM BYL719. This observed ERK upregulation in response to p-AKT suppression suggests activity of some form of PI3K-ERK pathway crosstalk. It is an interesting finding which would indicate a possible mechanism of adaptive resistance, yet SUM185PE cells are well established as highly sensitive to PI3Kα inhibition. In the future our model will be used to analyse such intriguing findings and provide new insights into the mechanistic links driving them.

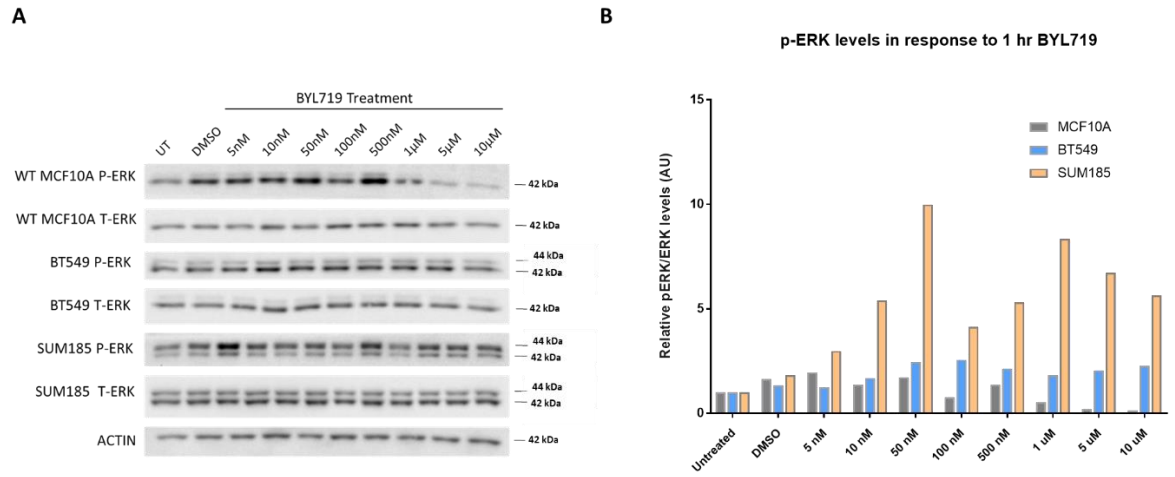

Figure 3.22 Relative ERK protein levels after 1 h PI3Ki dose-response treatment. Representative western blot (**A**) showing expression levels of total and phospho ERK in WT MCF10A and TNBC cells; BT-549 (*PTEN*-/-) and SUM185PE (*PIK3CA* mut) in response to 1 h BYL719 treatment at the following doses of 5 nM, 10 nM, 50 nM, 100 nM, 500 nM, 1 µM, 5 µM and 10 µM drug or 1:1000 DMSO vehicle control. (**B**) Quantified p-ERK (Thr202/Tyr204) levels in response to BYL719 treatment. Protein levels were quantified by densitometry and the data (both total and phospho protein) was normalised to their corresponding β-actin loading control (a representative blot shown here) and then to total levels to obtain relative phospho levels. Relative p-ERK/ERK levels was then normalised relative to untreated=1. AU (arbitrary units).

3.4.2 PI3K and MAPK signalling in response to time-course treatment with BYL719

The time-course treatment experiment with BYL719 allowed the investigation of the dynamic responses of the PI3K and MAPK signalling pathways over time to PI3K inhibition in WT MCF10A compared to MCF10A PTEN KO clones and TNBC cell lines BT-549 and SUM185PE. In support of the previous findings, the BYL719 time-course treatment results reflect the previous cell line sensitivity findings observed following the dose-response experiment, as SUM185PE cells were the most sensitive to BYL719 treatment followed by WT MCF10A and the BT-549 cells were the least responsive to PI3K inhibition (**Figure 3.23A-B**). The novel finding here was that using AKT phosphorylation as a read out of drug response, the WT MCF10A cells were more sensitive than the MCF10A PTEN KO cells suggesting that PTEN loss could possibly be driving reduced responsiveness to PI3K inhibition. The differences at certain time-points are significant when compared to WT MCF10A cells. AKT Ser473 phosphorylation levels were significantly inhibited in MCF10A cells compared to the PTEN KO clones E6-1 and E6-7 at 1, 6 and 12 h BYL719 treatment and compared to BT-549 cells at 24 h of drug treatment. AKT Ser473 phosphorylation levels in SUM185PE cells were significantly lower than WT MCF10A at 6 and 12 h of exposure to drug treatment.

The drug response results show that higher basal levels of phosphorylated AKT expression in the untreated cells predict a weaker response to the PI3K inhibitor as indicated by the lower reduction in p-

AKT levels following BYL719 treatment. Thus, is the level of drug sensitivity observed simply a reflection of the level of basal AKT expression levels? Indeed, to address this question it was later shown that when the PTEN KO cells are normalised to their basal levels of p-AKT there is no significant difference in AKT activity when compared to WT MCF10A cells following PI3K inhibition (**Figure S6.1**, **Figure S6.2).** Thus, suggesting that enhanced PI3K signalling as a result of PTEN loss resulted in less sensitivity to PI3K inhibition as higher doses of BYL are required to achieve the same level of p-AKT inhibition.

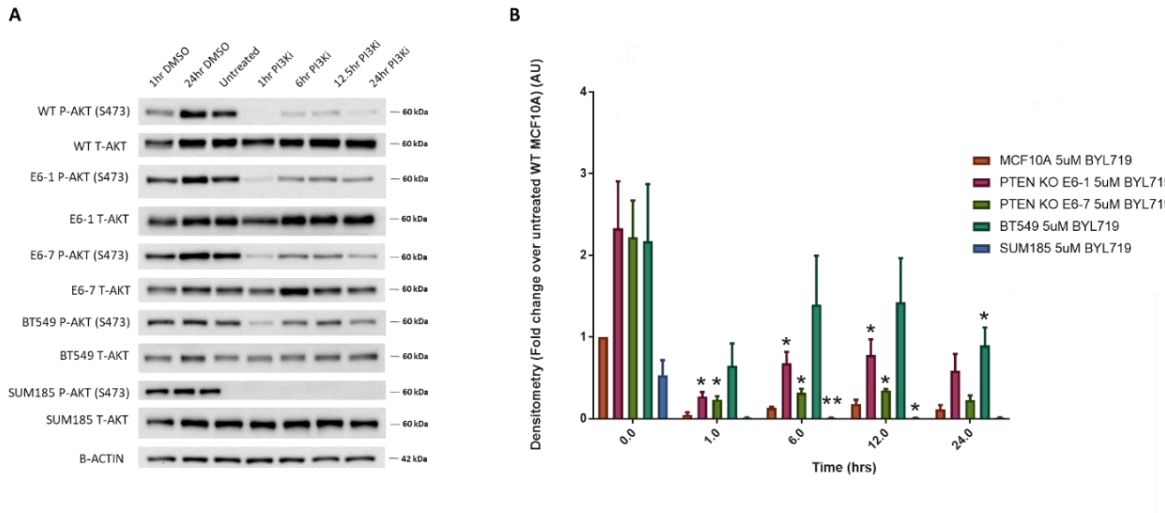

Figure 3.23 Relative AKT levels in response to BYL719 time-course treatment. (**A**) Representative western blots showing protein expression levels of total and phospho AKT in WT and PTEN KO MCF10As; (E6-1 and E6-7) and TNBC cells; BT-549 (PTEN-/-) and SUM185PE (*PIK3CA* mut) in response to 1 hr DMSO vehicle control or 5 µM BYL719 treatment for 0, 1, 6, 12 and 24 h. (**B**) Time-course graph of quantified p-AKT (S473) levels. Protein levels were quantified by densitometry and the data (both total and phospho protein) was normalised to their corresponding β-actin loading control (a representative blot shown here) and then normalised to total levels to obtain relative phospho levels. Relative p-AKT/AKT levels were then normalised to their untreated protein levels (untreated=1) and this was normalised to the untreated WT MCF10A protein levels. Thus, the results shown represent the fold change compared to WT MCF10A untreated condition. Data is represented as the mean values ± standard error of the mean of three independent biological replicates. Paired two-tailed *t*–test was used and statistical significance was considered at $P < 0.05$. ** = $P < 0.005$, * = $P < 0.05$. AU (arbitrary units).

Interestingly, phosphorylated ERK levels appear to be transiently inhibited after 1 h treatment with 5 µM BYL719 in the WT MCF10A cells, rebounding after 6 h of drug treatment (**Figure 3.24**). This transient ERK inhibition following PI3K inhibition was less clear in the TNBC cell lines, but also appears to occur in the PTEN KO cells based on the immunoblot results, with ERK activity decreasing after 1 h and bouncing back again at the 6 h time point (**Figure 3.24A**). In contrast, the graphs of the quantified p-ERK levels across the three replicates don't re-capitulate this clearly (**Figure 3.24B**). At the later time points of 12 and 24 h BYL719 treatment, p-ERK levels remain relatively unchanged as shown by both the representative blot and graph (**Figure 3.24A-B**).

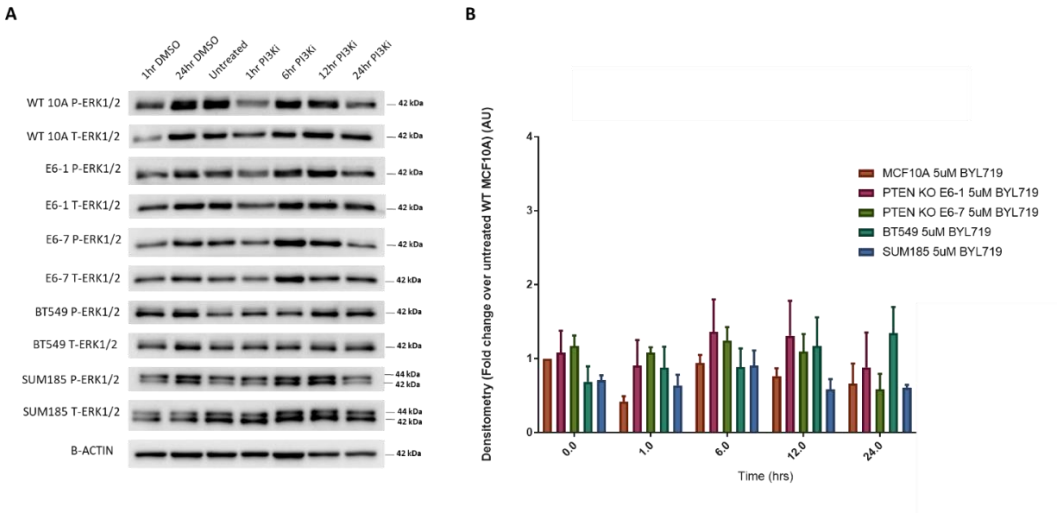

Figure 3.24 Relative ERK1/2 levels in response to BYL719 time-course treatment. Representative western blots (**A**) showing protein expression levels of total and phospho ERK in WT MCF10As, PTEN KO clones (E6-1 and E6-7) and TNBC cells; BT-549 (PTEN-/-) and SUM185PE (*PIK3CA*-mut) in response to 5 µM BYL719 treatment for 0, 1, 6, 12 and 24 h. (**B**) Time-course graph of quantified p-ERK (Thr202/Tyr204) levels. Protein levels were quantified by densitometry and the data (both total and phospho protein) was normalised to their corresponding β-actin loading control (a representative blot shown here) and then normalised to total levels to obtain relative phospho levels. Relative p-ERK/ERK levels were then normalised to their untreated protein levels (untreated=1) and this was normalised to the untreated WT MCF10A protein levels. Thus, the results shown represent the fold change compared to WT MCF10A untreated condition. Data is represented as the mean values ± standard error of the mean of three independent biological replicates. Paired two-tailed *t*–test was used and statistical significance was considered at $P < 0.05$. AU (arbitrary units).

Examining the response of phosphorylated S6 following BYL719 treatment, we found that its levels decreased after 1 h of drug treatment in all the tested cell lines. However, reduction in S6 phosphorylation was greatest in the most sensitive SUM185PE cells, followed by WT MCF10A and then the PTEN KO clones and lowest in the least sensitive BT-549 cells (**Figure 3.25A-B**). In the SUM185PE cells S6 activity is significantly inhibited after 1 h BYL and is further reduced to almost undetectable levels after 6 h PI3K inhibition, with levels remaining suppressed at later time points. Indeed, at 12 and 24 h following BYL719 treatment, the level of p-S6 is significantly lower in the SUM185PE cells compared to WT MCF10A cells. In contrast, in all the other cell lines the largest suppression of S6 was observed after 1 h of PI3K inhibition and after 6 h of drug exposure S6 begins to increase its activity with the highest levels in the drug treated cells seen following 24 h BYL treatment (**Figure 3.25A-B**). This is consistent with the pattern of AKT activity following BYL treatment in these cell lines as the largest reduction in AKT activity is seen after 1 h PI3K inhibition and begins to bounce back at the 6 h time point (**Figure 3.23A-B**). However, one observable difference between the response of AKT activity compared to S6 activity, is that phospho AKT levels appears to be highest at the 6 and 12 h time points after BYL treatment and after 24 h of drug exposure the level is in fact reduced slightly, however this was not significant (**Figure 3.23A-B**).

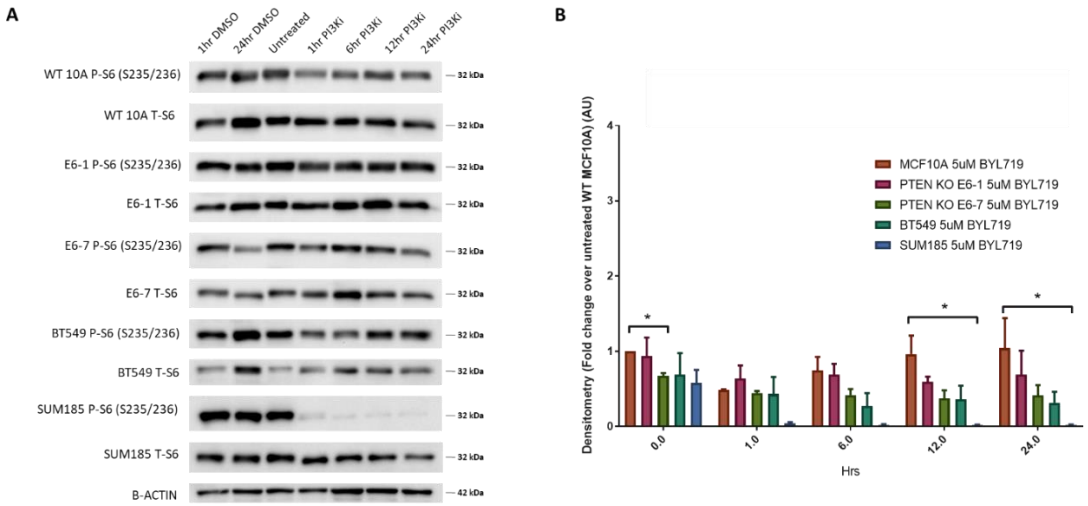

Figure 3.25 Relative S6 levels in response to BYL719 time-course treatment. Representative western blot (**A**) showing protein expression levels of total and phospho S6 in WT MCF10As, PTEN KO clones (E6-1 and E6-7) and TNBC cells; BT-549 (PTEN-/-) and SUM185PE (*PIK3CA*-mut) in response to 5 µM BYL719 treatment for 0, 1, 6, 12 and 24 h. (**B**) Time-course graph of quantified p-S6 (S235/236) levels. Protein levels were quantified by densitometry and the results shown represent the fold change compared to untreated WT MCF10A levels. Protein levels were quantified by densitometry and the data (both total and phospho protein) was normalised to their corresponding β-actin loading control (a representative blot shown here) and then normalised to total levels to obtain relative phospho levels. Relative p-S6/S6 levels were then normalised to their untreated protein levels (untreated=1) and this was normalised to the untreated WT MCF10A protein levels. Thus, the results shown represent the fold change compared to WT MCF10A untreated condition. Data is represented as the mean values ± standard error of the mean of three independent biological replicates. Paired two-tailed *t*–test was used and statistical significance was considered at $P < 0.05$. * = $P < 0.05$. AU (arbitrary units).

In summary, the results show BYL719 maintained downstream PI3K signalling suppression over the 24 h duration in all cell lines, as in 24 h treated cells both p-AKT and downstream p-S6 levels remained significantly lower compared to the untreated condition (**Figure 3.25A-B**). Consistent with PIK3CA mutant cell lines being highly sensitive to PI3Kα inhibition, the SUM185PE cells were highly sensitive to BYL719 treatment, and BT-549 cells were the least responsive which has been shown by other researchers (O'Brien, McDonald et al. 2014). Importantly, the key finding from the PI3Ki time-course data was that the PTEN KO clones were less sensitive to PI3Kα inhibition with BYL compared to the WT MCF10A cells suggesting that PTEN loss is driving this reduced responsiveness to BYL. In order to validate that this was a direct effect of PTEN loss in these cells a rescue experiment was performed by re-introducing PTEN back into the PTEN KO clones using a transient transfection experiment. In addition, the observation of phospho ERK rebound in the WT and possibly the PTEN KO MCF10A cells in response to PI3K inhibition is of interest and will be further investigated. Together these findings are discussed in the following Chapter.

Chapter 4: Investigating how PTEN loss influences the signalling response to MAPK and PI3K inhibition

4.1 PTEN loss drives reduced responsiveness to BYL719 treatment

4.1.1 PTEN re-expression re-sensitizes MCF10A PTEN KOs to PI3K inhibition

In order to evaluate the role of PTEN in modulating the growth inhibitory actions of BYL719, PTEN was transiently re-introduced back into the PTEN KO clones. Briefly, MCF10A parental cells were reverse transfected overnight for 24 h with an empty vector pcDNA3.1 and MCF10A PTEN KO cells were transfected with either pcDNA3.1 empty vector or pcDNA3.1 PTEN expressing vector using the p3000 lipofectamine protocol. PTEN transfection was successful as immunoblotting with PTEN antibody directed against the C-terminal epitope of PTEN showed PTEN re-expression in the previously PTEN-null clones (**Figure 4.1**).

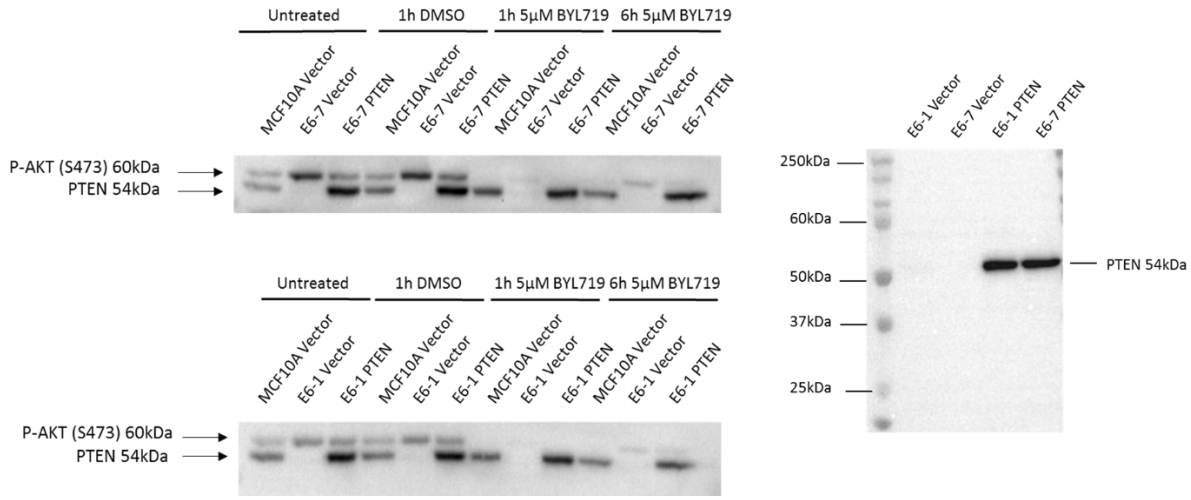

Figure 4.1 Validation of PTEN re-expression in the MCF10A PTEN KO clones E6-1 and E6-7. MCF10A parental cells were reverse transfected overnight for 24 h with an empty vector pcDNA3.1 and MCF10A PTEN KO cells were transfected with either pcDNA3.1 empty vector or pcDNA3.1 PTEN expressing vector using the p3000 lipofectamine protocol. Equal amounts of protein lysates/lane were separated by 8% SDS-PAGE, transferred to PVDF membranes and probed with a PTEN specific antibody which recognises the C-terminal epitope of PTEN. These are representative blots from three independent biological replicates, n=3.

Next, we compared the viability of the above cell lines in response to increasing doses of BYL719 treatment using an MTS cell viability assay. Not unexpectedly, the degree of cell viability lost was dependent on the dose of the drug as the higher dose of 5 µM BYL719 decreased cell viability further than the lower dose in all cells i.e. it was a dose-dependent effect (**Figure 4.2**) The results showed that for cells transfected with the empty vector MCF10A PTEN KO clones are more resistant to 0.5 µM BYL719 compared to the WT PTEN cells, evident by the increased cell viability at 48 h following the treatment, although due to variance between biological replicates this was not statistically significant. This is in accordance with our previous data. However, for PTEN KO clones where PTEN has been re-expressed, cell viability was reduced to levels comparable to that in the MCF10A WT cells (**Figure 4.3**), thus suggesting that loss of PTEN was indeed driving the reduced sensitivity to PI3K inhibition and allowing the cells to be more resistant to BYL719.

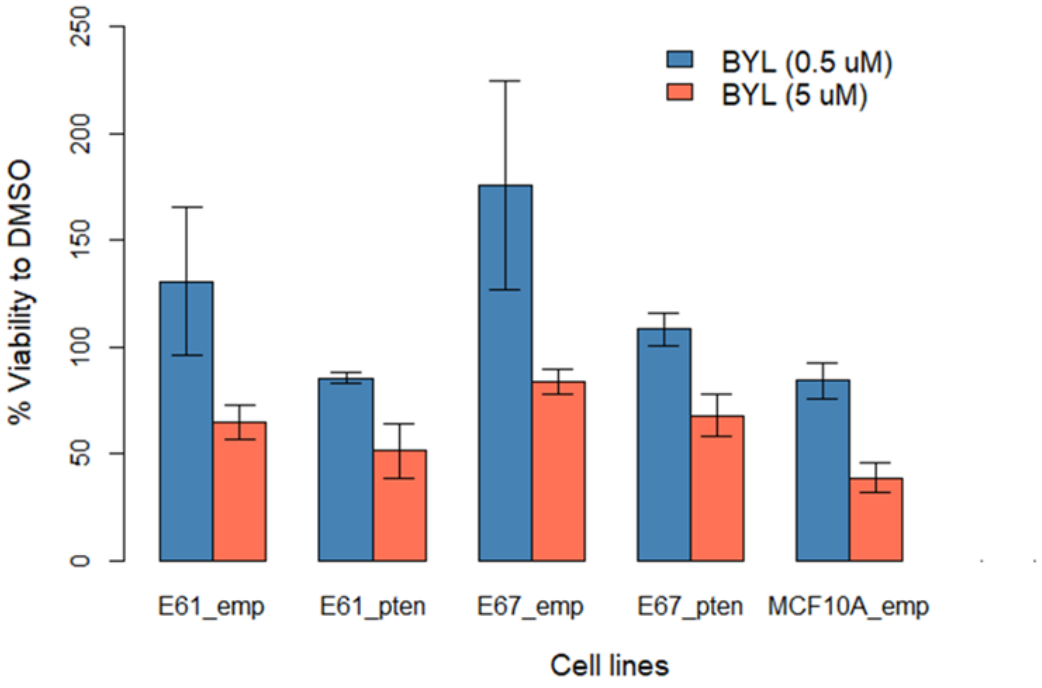

Figure 4.2 Dose comparison graph of cell viability after 48 h PI3K inhibition in WT, PTEN loss and PTEN re-expressing cells. MTS cell viability results in WT MCF10As, PTEN KO clones (E6-1 and E6-7) and re-expressing PTEN clones after 48h of 0.5 µM (Blue) and 5 µM BYL719 (Red) treatment. Absorbance readings were measured at 490 nm on the PHERAstar (BMG, Labtech) plate reader. Cell viability is measured as a percentage over DMSO vehicle control for each cell line. Data is represented as the mean values ± standard error of the mean of three independent biological replicates. Paired two-tailed *t*–test was used and statistical significance was considered at $P < 0.05$. AU (arbitrary units).

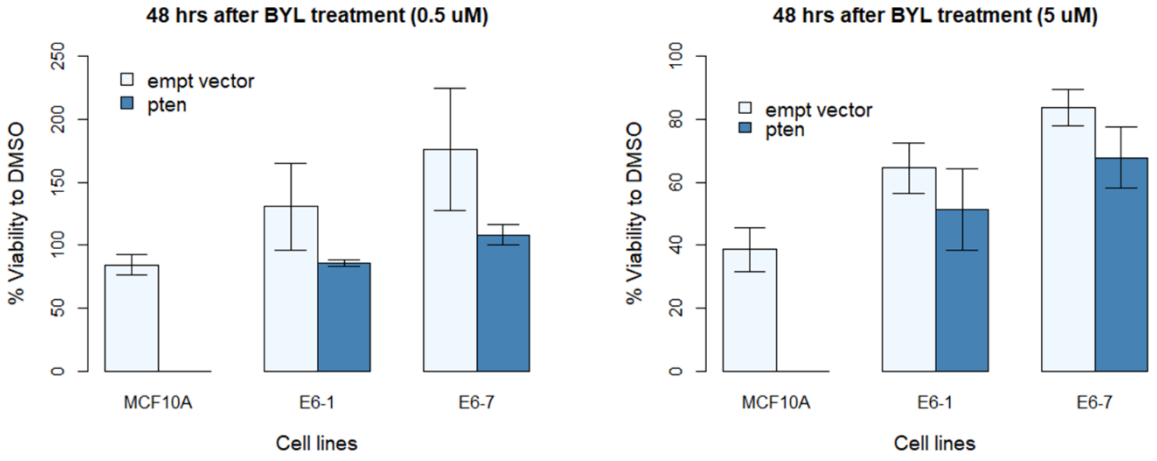

Figure 4.3 Cell viability after 48 h of PI3K inhibition in WT, PTEN loss and PTEN re-expressing cells. Graphs show MTS cell viability in WT MCF10As, PTEN KO clones (E6-1 and E6-7) and re-expressing PTEN clones after 48 h of 0.5 µM (left graph) and 5 µM BYL719 (right graph). MTS assay absorbance readings were measured at 490 nm on the PHERAstar (BMG, Labtech) plate reader. Cell viability is measured as a percentage over DMSO vehicle control for each cell line. Data is represented as the mean values ± standard error of the mean of three independent biological replicates. Paired two-tailed *t*–test was used and statistical significance was considered at $P < 0.05$. AU (arbitrary units).

4.1.2 PI3K and MAPK pathway activity following PTEN reintroduction

Next the cell signalling changes following PTEN reintroduction were examined by immunoblotting for the total and phosho levels of key signalling proteins from both PI3K and MAPK pathways, including EGFR, STAT3, AKT, ERK1/2 and S6 in the WT MCF10A and PTEN KO clones E6-7 (**Figure 4.4A**) and E6-1 (**Figure 4.4B**). Consistent with our earlier findings, p-AKT levels seem to be strongly upregulated in untreated and DMSO treated KO cells compared to the WT cells, and importantly this was reduced by the reintroduced PTEN, indicating the transient transfection was effective (**Figure 4.5A-B and Figure 4.6 A-B).** The levels appear to be reduced to a level in between that of WT and KO cells. Since it was a transient transfection it is possible that as PTEN levels slowly decrease, the levels of p-AKT start to increase back to KO cell levels and hence at 48 h post transfection the levels of PTEN are in between both WT and KO cells.

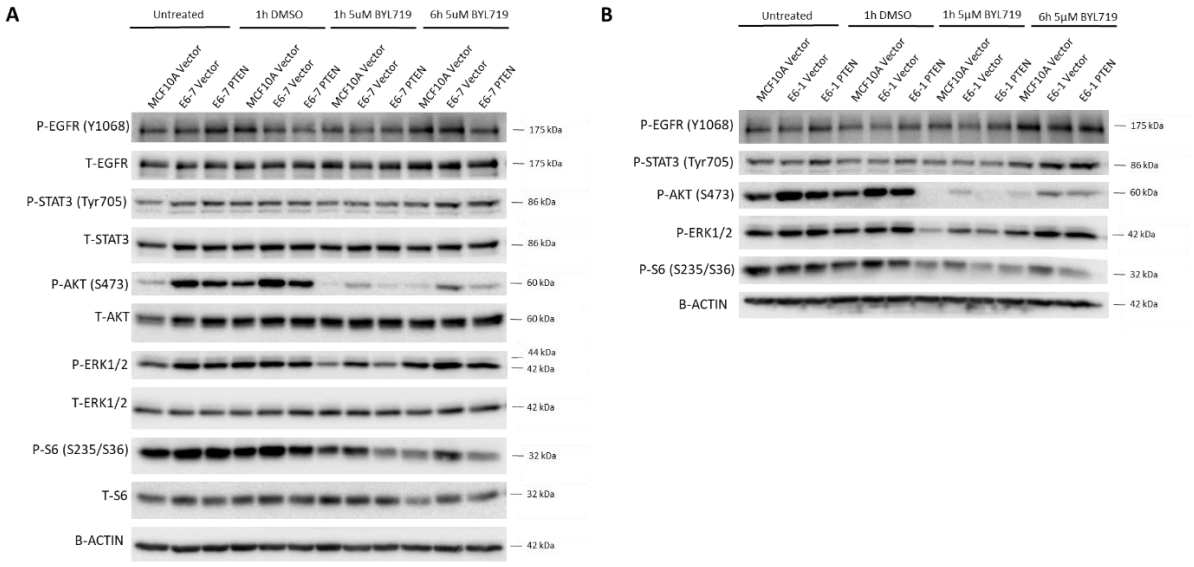

Figure 4.4 PI3K and MAPK signalling after 48 h of PI3K inhibition in WT, PTEN loss and PTEN re-expressing cells. Representative western blots showing protein expression levels of total and phospho EGFR, STAT3, AKT, ERK, S6 and β-actin, following transfection in WT MCF10As, PTEN KO clones; E6-7 (**A**) and E6-1 (**B**) and re-expressing PTEN clones in response to 5 μM BYL719 treatment for 1 and 6 h. These blots are representative of three independent biological replicates.

In response to 1 h PI3K inhibition with BYL all cells showed a significant suppression of PI3K signalling as shown by decreased AKT Ser473 phosphorylation. An interesting observation was that p-AKT expression increased after 6 h following BYL treatment in all cells, but appears most pronounced in the E6-7 PTEN KO clone (**Figure 4.5A-B and Figure 4.6A-B**). This response was consistent with my previous findings following time-course PI3Ki treatment (**Figure 3.23**) and suggests that already after 6 h some adaptive mechanism is in place allowing reactivation of AKT activity. Importantly, re-introducing PTEN back into the E6-7 PTEN KO clone increased the sensitivity to BYL719 as seen by the lower level of p-AKT in the PTEN re-expressing cells compared to the PTEN KO clones after 1 h PI3K inhibition and this difference in AKT activity was even more pronounced after 6 h of drug treatment (**Figure 4.5A-B and Figure 4.6A-B**). In support with previous findings using p-AKT as a read out of target inhibition, the WT MCF10A cells appear to be the most sensitive to BYL treatment followed by the PTEN re-expressing cells and last the PTEN KOs (**Figure 4.5A-B**). However, this finding was not observed in the E6-1 PTEN KO clone as both PTEN re-expressing cells and PTEN KO cells showed a similar level of AKT phosphorylation after 1 and 6 h of drug treatment and neither were as sensitive as the WT cells (**Figure 4.6A-B**).

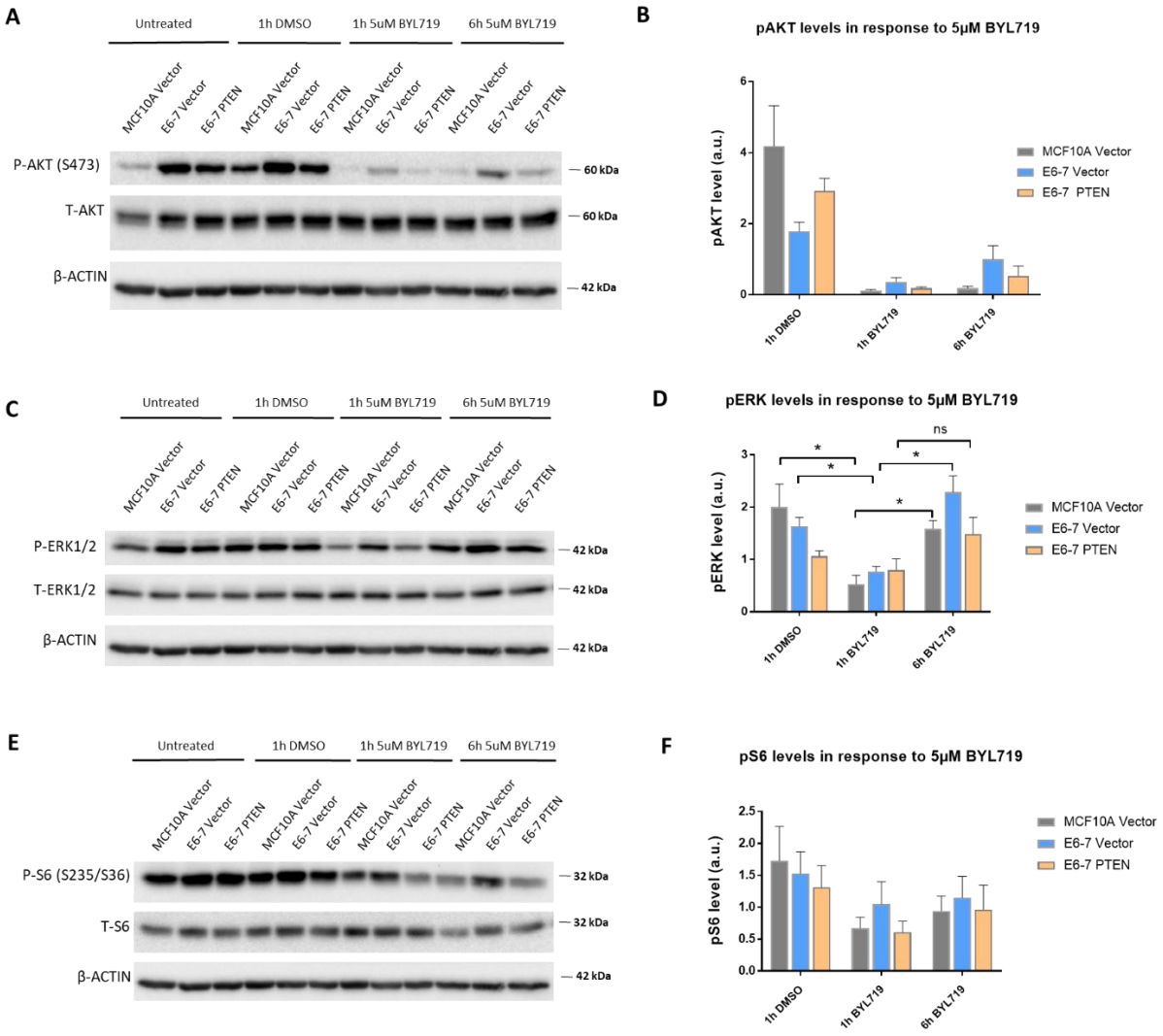

Figure 4.5 The influence of PTEN on PI3K and MAPK signalling in response to 48 h PI3K inhibition in WT MCF10A cells, E6-7 PTEN KO cells, and in PTEN re-expressing E6-7 cells. Representative western blots of the total and phospho protein expression levels of AKT (**A**) ERK1/2 (**C**) and S6 levels (**E**) in WT MCF10A cells (MCF10A Vector), E6-7 PTEN KO cells (E6-7 Vector) and PTEN re-expressing E6-7 cells (E6-7 PTEN) in response to 5 μM BYL719 treatment for 1 and 6 h. Graphs showing relative p-AKT (**B**) p-ERK (**D**) and p-S6 (**F**) levels. Briefly, WT MCF10A cells were reverse transfected overnight for 24 h with an empty vector pcDNA3.1 (Vector) and MCF10A PTEN KO cells were transfected with either pcDNA3.1 empty vector or pcDNA3.1 PTEN expressing vector (PTEN) using the p3000 lipofectamine protocol. After 24 h transfected cells were treated with 1 or 6 h of 5 μM BYL719 and DMSO was used as the vehicle control. Drug treated cells were lysed and their proteins were harvested using RIPA lysis buffer. Equal amounts of protein lysates/lane were separated by 8% SDS-PAGE, transferred to PVDF membranes and immunoblotted. Protein levels were quantified by densitometry and the data (both total and phospho protein) was normalised to their corresponding β-actin loading control (representative blots shown here) and then normalised to total levels to obtain relative phospho levels. Data is represented as the mean values ± standard error of the mean of three independent biological replicates. Paired two-tailed *t*–test was used and statistical significance was considered at $P < 0.05$. * = $P < 0.05$, ** = P <0.01. AU (arbitrary units).

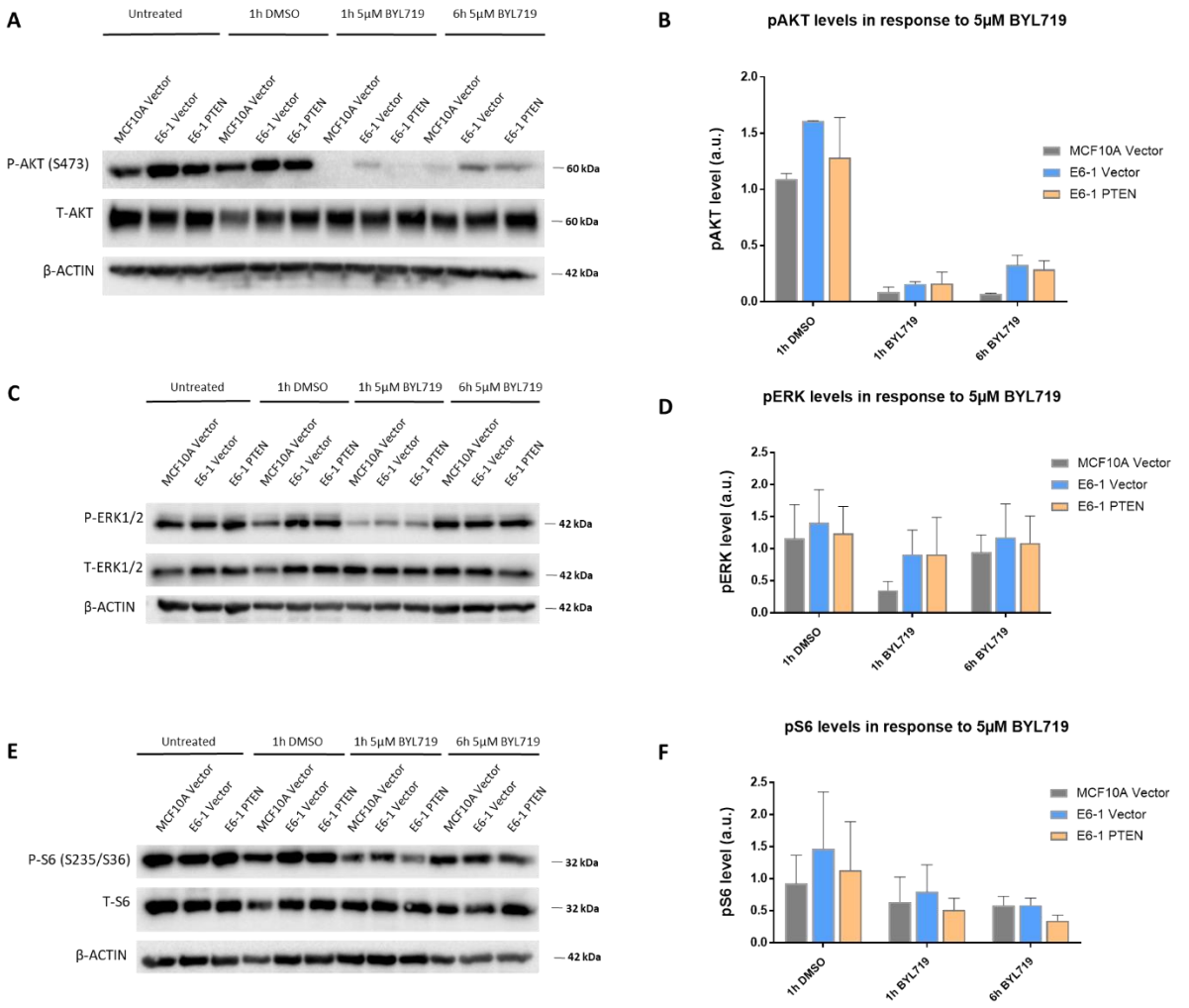

Figure 4.6 The influence of PTEN on PI3K and MAPK signalling in response to 48 h PI3K inhibition in WT MCF10A cells, E6-1 PTEN KO cells, and in PTEN re-expressing E6-1 cells. Representative western blots of the total and phospho protein expression levels of AKT (**A**) ERK1/2 (**C**) and S6 levels (**E**) in WT MCF10A cells (MCF10A Vector), E6-1 PTEN KO cells (E6-1 Vector) and PTEN re-expressing E6-1 cells (E6-1 PTEN) in response to 5 μM BYL719 treatment for 1 and 6 h. Graphs showing relative p-AKT (**B**) p-ERK (**D**) and p-S6 (**F**) levels. Briefly, WT MCF10A cells were reverse transfected overnight for 24 h with an empty vector pcDNA3.1 (Vector) and MCF10A PTEN KO cells were transfected with either pcDNA3.1 empty vector or pcDNA3.1 PTEN expressing vector (PTEN) using the p3000 lipofectamine protocol. After 24 h transfected cells were treated with 1 or 6 h of 5 μM BYL719 and DMSO was used as the vehicle control. Drug treated cells were lysed and their proteins were harvested using RIPA lysis buffer. Equal amounts of protein lysates/lane were separated by 8% SDS-PAGE, transferred to PVDF membranes and immunoblotted. Protein levels were quantified by densitometry and the data (both total and phospho protein) was normalised to their corresponding β-actin loading control (representative blots shown here) and then normalised to total levels to obtain relative phospho levels. Data is represented as the mean values ± standard error of the mean of three independent biological replicates. Paired two-tailed *t*–test was used and statistical significance was considered at $P < 0.05$. * = $P < 0.05$, ** = $P < 0.01$. AU (arbitrary units).

In the MCF10A WT and E6-7 PTEN KO cells transfected with the empty vector, phosphorylated ERK was significantly decreased after 1 h of BYL719 treatment, but then significantly bounced back at 6 h. This p-ERK bounce back had been observed previously following the BYL time-course treatment and appeared most pronounced in the WT MCF10A cells (**Figure 3.24A-B**). Here ERK activity rebound was not significant in the PTEN re-expressing cells, but these cells do show a similar trend (**Figure 4.5C-D and Figure 4.6C-D**).

This rebound in p-ERK levels, thus appears to be independent of PTEN status. Consistent with our previous data that ERK signalling is not affected by PTEN loss, basal levels of p-ERK appear to be similar in all cells and re-expression of PTEN doesn't seem to affect p-ERK, again suggesting that PTEN loss does not crosstalk to MAPK signalling in this cell line. In contrast, this rebound in ERK was not clear in the E6-1 PTEN KO cells and the immunoblot analysis results show that ERK activity only bounced back in the WT cells (**Figure 4.6C-D**). The differential results seen in E6-1 compared to E6-7 may be explained if residual PTEN expression is returned somehow in the E6-1 clone. To rule this out another long ECL exposure following immunoblotting for PTEN was carried out. The blots showed both cell lines had no PTEN expression and thus this cannot explain the differences observed between the PTEN KO clones.

The graphs discussed above show the relative levels of phospho protein and suggest a possible stronger ERK-AKT crosstalk in the PTEN KO E6-7, but not E6-1 since only PI3K inhibitor-induced p-ERK rebound appears to occur in the former, but not the latter. In order to further investigate these conflicting findings between the PTEN KO clones and to see if the results might be better explained by the differential basal levels of p-ERK, p-AKT and p-S6 between WT and the PTEN KO clones, the data was normalised to basal levels for each cell line i.e. the level in the untreated condition. The results showed that when the phospho protein levels were normalised to untreated levels it was evident that there was no significant change in the magnitude of p-ERK or p-AKT reduction following BYL treatment between WT and PTEN KO MCF10A cells and the PTEN re-expressing cells, nor was there any difference in the level of p-ERK bounce back (**Figure S6.1, Figure S6.2**). Thus, the differences observed between the WT and PTEN KO cells appears to be due to the higher levels of p-AKT and p-ERK in the cells leading to higher levels in response to BYL treatment. Moreover, when the data was normalised to basal levels, all cells showed a significant decrease in ERK activity, which was not seen before in E6-7 cells using the previous normalization method as shown in the previous graphs. Yet still the p-ERK bounce back only occurred in the blot with E6-7 and WT MCF10A cells.

These differential findings between blots suggest they are caused by variations between gels. Thus, in order to rule that out as the source of the observed variation and obtain more definitive results the drug treatment experiment was repeated and all the samples were run on the same gel eliminating any gel to gel variation. In addition, non-transfected cells were used for this experiment to ensure this was not

only occurring in the transfection experiment and as before, the levels of p-ERK were normalised to each cell's untreated condition (**Figure 4.7A-B**). The findings show that treatment with 5 µM BYL for 1 h significantly decreased p-ERK levels and at 6 h they bounced back. This ERK reactivation was significant in WT MCF10A and the PTEN KO clone E6-1, and not significant, in the E6-7 cells. Together these findings suggest that ERK rebound is indeed occurring in all cells, both PTEN loss and WT indicating that it is in fact a PTEN independent effect. This transient inhibition in p-ERK levels following PI3K inhibition has been reported previously (Will, Qin et al. 2014). Will et al. revealed that PI3K inhibition, but not AKT inhibition, leads to the rapid, but transient inhibition of the RAS-ERK signalling axis in HER2+ breast cancer cell. They found that although inhibition of RAS-ERK signalling was transient, rebounding a few hours after drug administration. Despite being transient, it is suggested to be critical for the enhanced and rapid induction of apoptosis caused by PI3K over AKT inhibitors. The authors posited that inhibiting PI3K causes the rapid inhibition of both AKT-mTOR and RAS-ERK signalling, whereas AKT inhibitors suppress only the former and, in fact, activate the latter.

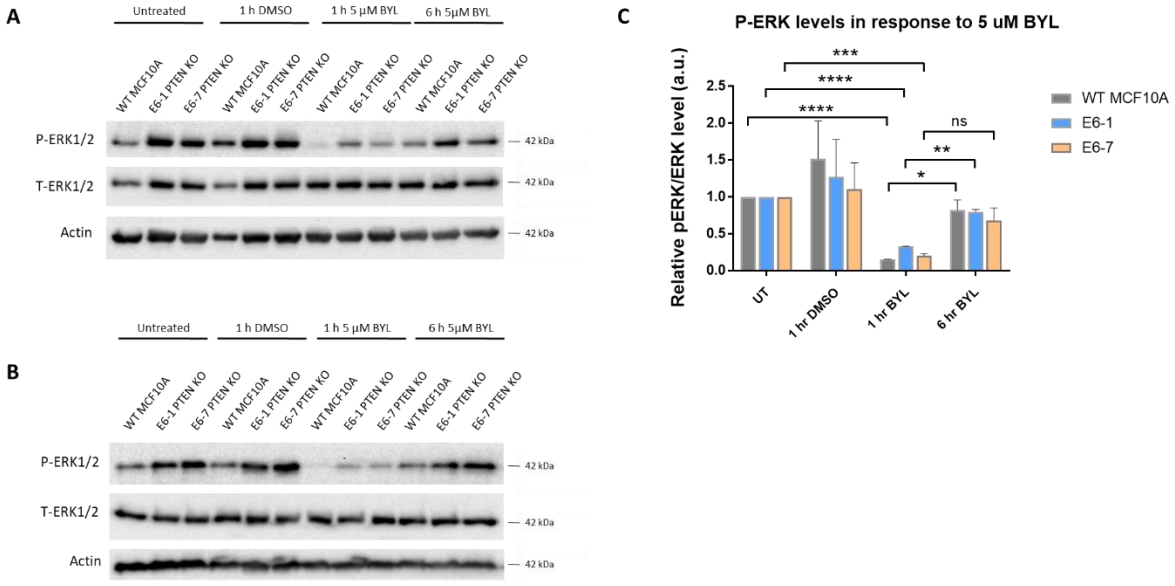

Figure 4.7 PI3K inhibition results in ERK reactivation in a PTEN independent manner. (**A-B**) Representative western blots of the total and phospho protein expression levels of ERK1/2 in WT MCF10A and PTEN KO clone (**A**) E6-7 and (**B**) E6-1 in response to 5 µM BYL719 treatment for 1 and 6 h. (**C**) Quantified p-ERK levels normalised by untreated protein levels and quantified by densitometry. Data is represented as the mean values ± standard error of the mean of two independent biological replicates. Paired two-tailed *t*–test was used and statistical significance was considered at $P < 0.05$. * = $P < 0.05$, ** = $P < 0.01$, *** = $P < 0.001$. AU (arbitrary units).

As observed previously in the time-course treatment and again here there were no significant differences observed in p-S6 (S235/236) levels between WT, PTEN KO and PTEN re-expressing cells. In all cells, p-S6 levels decrease in response to 1 h BYL719 and remain inhibited after 6 h of treatment as levels are lower than the DMSO vehicle control (**Figure 4.5E-F and Figure 4.6E-F**). Thus consistently PTEN loss alone did not appear to influence S6 activity in response to PI3K inhibition. Nor were there higher levels observed in the PTEN KO clones compared to the WT cells. As was previously discussed this could be explained by the fact that AKT phosphorylation doesn't only reflect mTORC1 signalling, but also other signalling pathways such as FOXO and GSK3β (Manning and Cantley 2007), and thus it is impossible for S6 activity, a marker of mTORC1 activity to fail to reflect enhanced AKT signalling.

In summary, these data show reintroduction of PTEN in the KO cells reduces the level of p-AKT and re-sensitizes the cells to BYL719 at the signalling level, suggesting that PTEN loss in the KO cells drives the reduced responsiveness to PI3K inhibition. This was further supported by the cell viability results which demonstrated that re-expression of PTEN reduced cell viability in response to BYL719 treatment compared to the KO cells.

4.1.3 Investigate if altered drug responsiveness due to PTEN loss is driven by PI3K-MAPK pathway crosstalk

In order to investigate PI3K-MAPK pathway crosstalk, we examined changes in signalling proteins of the MAPK pathway in the PTEN KO clones compared to WT MCF10As following PI3K inhibition and vice versa, i.e. changes in protein levels of the PI3K pathway components following MEK inhibition. The data so far indicated that PTEN loss did not enhance pathway crosstalk in this cell line. PTEN loss did not seem to alter responsiveness to MEK inhibition as the PTEN KO clones displayed a similar ERK signalling response following MEKi treatment as observed in the WT MCF10A cells, thus suggesting both WT and PTEN loss cells had a similar level of senstivity to MEKi trametinib.

Although the PTEN re-expression experiment confirmed PTEN loss was driving the reduced sensitivity to PI3K inhibition observed in the PTEN KO cells compared to WT MCF10A cells. It was not shown that this altered drug sensitvity was due to a change in crosstalk between the PI3K and MAPK pathways induced by PTEN loss. Indeed, we observed PI3K-ERK crosstalk in response to PI3K inhibition as the PI3K inhibitor BYL719 induced transient suppression of ERK suggesting the presence of a positive link from PI3K signalling to ERK. However, this transient inhibition of ERK activity signalling, rebounding after 6 hours following drug treatment was observed irrespective of PTEN status as it occurred in both WT and PTEN KO MCF10A cells. Taken together, these finding thus suggest that this crosstalk was not modulated by PTEN loss. Interestingly, when MEK was inhibited suppression of PI3K signalling was not observed, thus suggests that this PI3K-ERK crosstalk is unidirectional. Additional crosstalk between these pathways possibly further downstream cannot be ruled out only a

handful of proteins were examined, but from signalling proteins exmained the PI3K-ERK crosstalk was the only example observed.

4.2 Investigate if reduced drug responsiveness to BYL719 treatment in the PTEN KO clones is caused by p110β isoform driven PI3K signalling.

Phosphoinositide 3-kinases (PI3Ks) are a ubiquitous family of signal transducing enzymes which are comprised of 3 classes. Of relevance here, are the class 1 PI3Ks, which are subdivided into four members (p110α, p110β, p110γ and p110δ) can be activated by a range of receptors, both RTKs and GPCRs on the cell surface to produce PIP3 which triggers downstream PI3K signalling cascades promoting cell growth, proliferation, survival and migration (Vanhaesebroeck, Stephens et al. 2012). The class IA PI3Ks (PIK3Cα, PIK3Cβ, PIK3Cδ) exist as heterodimeric proteins made up of a regulatory p85 subunit (derived from three genes, p85a, p85b and p55) bound to one of three p110 catalytic subunits (p110α, p110β or p110δ encoded by PIK3CA, PIK3CB and PIK3CD, respectively).

Earlier studies focused on the use of selective mTOR and AKT inhibitors. However, PI3K signals downstream through other targets in addition to these. Furthermore, AKT and mTOR inhibitors all relieve feedback inhibition of receptor tyrosine kinases, only PI3K inhibitors suppress rather than reactivate PI3K. PI3K inhibition may therefore be more a more effective therapy than downstream inhibitors of this pathway. In support of this, recent preclinical work showing that PI3K inhibitors have more potent anti-tumour activity than AKT inhibitors (Ebi, Costa et al. 2013, Will, Qin et al. 2014). Although numerous pan-PI3K inhibitors have been designed to target the PI3K enzyme with some success, early results with inhibitors of pan-class 1 PI3K were also disappointing however (Martini, Ciraolo et al. 2013). An increasingly evident limitation of the use and development of this class of therapies is a less favourable toxicity profile from both PI3K inhibition and off-target toxicity due to lack of drug selectivity, and of course network adaptation to the inhibition of the pathway.

Isoform specific PI3K inhibitors have now been developed which, unlike pan-PI3K inhibitors which target all class 1A isoforms, selectively target the each PI3Kα, β or δ isoforms. These isoform-selective PI3K inhibitors have limited toxicity in preclinical models and early clinical trials and thus may be more beneficial due to this reduced toxicity to normal tissues even at high doses (Juric et al., 2012). However, the use of single PI3K isoform selective inhibitors is also limited due to the differential regulation of the PI3K isoforms, as other isoforms can compensate to re-activate the PI3K pathway. To overcome this, dual PI3K isoform inhibition is a potentially effective therapeutic approach. Prior preclinical studies have demonstrated that combined targeting of both p110β and p110α isoforms of PI3K can be synergistic and improve the anti-tumour effects compared to single-isoform inhibition (Edgar, Wallin et al. 2010, Schwartz, Wongvipat et al. 2015). While p110α plays a dominant role in RTK signalling, p110β is a major effector for GPCRs and has important kinase-independent functions as well (Thorpe,

Yuzugullu et al. 2015).The literature shows that in many cancer cells and tumours with PI3Kα mutations or RTK driven PI3K signalling, the PI3Kα isoform is the dominant one, whereas in tumours or cancer cells with loss or inactivation of PTEN, PI3K signalling is predominantly driven by the p110β isoform of PI3K (Torbett et al., 2008, Wee et al., 2008, Ni et al., 2012). Hence selective targeting of the PI3Kβ could be an effective therapy for select types of PTEN deficient cancers.

Based on these findings, and recent findings by Zhang et al. (Zhang et al., 2017) which showed that CRKL is involved in regulating this p110β-dependent PI3K activity in PTEN-null cancer cells, we thus sought to investigate whether the reduction in sensitivity of the PTEN KO cells to BYL719 treatment observed in the last Aim was caused by this mechanism of preferential activation and signalling of the PI3K p110β isoform in the absence of PTEN (**Figure 4.8**). This was tested by treating the MCF10A WT and PTEN KO cells with the PI3Kβ-isoform selective inhibitors TGX221 and AZD6482 alone and in combination with the selective PI3Kα-isoform inhibitor BYL719. AZD6482 has an IC50 of 10 nM in cell-free assays and targets the kinase activity of the β isoform more potently than p110α, δ and γ isoforms. It is observed to be 8, 87 and 109 times more selective for PI3Kβ than PI3Kδ, PI3Kα and PI3Kγ respectively. TGX-221 is more potent and more selective than AZD6482 with an IC50 of 5 nM in cell-free assays, and is 1000 times more selective for PI3Kβ than PI3Kα. By using two different PI3Kβ-isoform selective inhibitors we could ensure that PI3Kβ inhibition response observed was consistent between them both and thus validate our findings. In addition, the above drug treatment experiment was also performed in the TNBC cell lines BT-549 and MDA-MB-468. These cell lines were selected based on their PTEN-null status, as both harbour PTEN homo-deletion with no PTEN protein expression (Meric-Bernstam, Akcakanat et al. 2012). Western blot analysis was performed to evaluate the PI3K and MAPK pathway signalling changes in response to these PI3K isoform selective inhibitors used alone and in combination and MTS assay was used to determine the drug sensitivity.

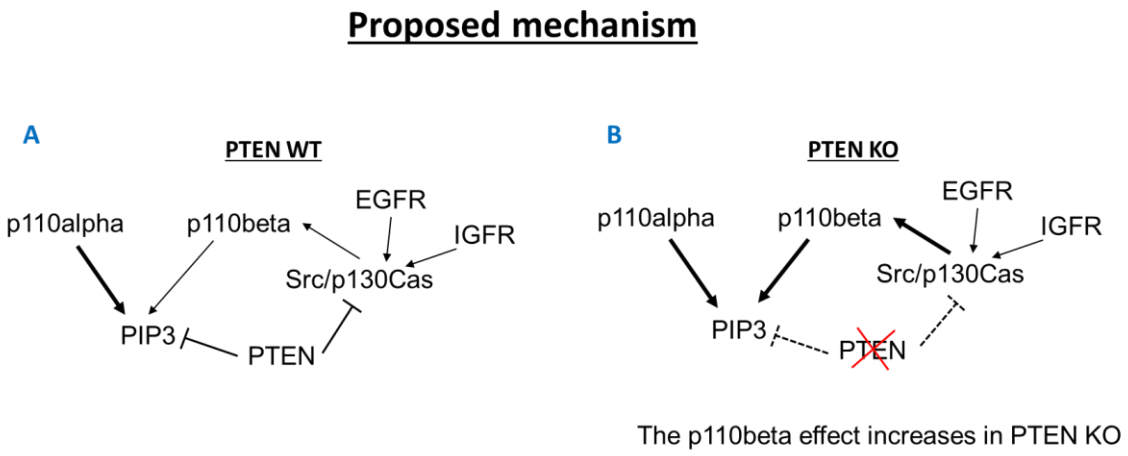

Figure 4.8 Proposed mechanism for how PTEN loss in MCF10A cells causes increased PI3K p110β driven signalling. (**A**) In cells with WT PTEN, both PIP3 and Src/p130Cas complex are negatively regulated by PTEN and thus, signalling via the PI3Kp110β isoform is supressed (thinner black arrows). The PI3Kp110α isoform is the dominant isoform in these cells so signalling occurs predominantly through the α isoform activating PIP3 (thick black arrow). (**B**) In cells with PTEN loss the negative regulation on PIP3 signalling and the PI3Kp110β isoform via Src/p130Cas complex is removed (dashed lines) and PIP3 signalling now occurs through both PI3K α and β isoforms (thick black arrows).

4.2.1 PI3K and MAPK signalling in response to selective PI3Kα inhibition alone and in combination with PI3Kβ inhibitors: TGX or AZD

4.2.1.1 Reduced AKT activity in response to single and dual PI3Kα/β inhibition

As shown previously from my drug treatment experiments and viability assays, the PTEN KO cell lines were less responsive to single-agent BYL719 treatment compared to WT MCF10A cells. Based on the findings in the literature that PTEN loss drives a preferential dependence on the P13Kβ isoform, it was hypothesized that the reduced responsiveness to BYL by the PTEN KO clones may be due to this PTEN loss-induced P13Kβ dependence. If this were true then it was expected the PTEN KO clones would be more responsive to PI3K p110β inhibition (TGX221 or AZD). However, this was not observed as we found that single treatment with TGX or AZD in the PTEN KO clones failed to result in an improved response to PI3Kβ inhibition (**Figure 4.9A-C**). In fact, on the contrary, the PTEN KO clones showed a similar response to selective PI3Kβ inhibition as WT MCF10A at both 1 and 24 h treatment (**Figure 4.9C**). AKT activity was significantly inhibited after 1 h of TGX treatment in the E6-1 clone compared to untreated cells, but this was lost after 24 h of PI3Kβ inhibition and no significant AKT inhibition was found in the WT MCF10A cells or the PTEN KO clone E6-7 (**Figure 4.12A**).

However, high variation between replicates means some AKT inhibition by TGX cannot be ruled out. Importantly though, in both WT and PTEN KO MCF10A cells, PI3Kβ inhibition failed to suppress p-AKT (S473) to the same degree as the PI3Kα inhibitor BYL719 at both the 1 and 24 h time points demonstrating that the PTEN KO cells are still more sensitive to PI3Kα inhibition (**Figure 4.9C**). In addition, the levels of AKT phosphorylation were significantly lower in response to BYL compared to

TGX at 24 h of treatment in both PTEN KO cells and after 1 h treatment in the E6-1 cells (**Figure 4.12A)**. Taken together, these results indicate that AKT activity is still primarily driven by PI3Kα signalling in these cells. Thus, suggesting that in these cells PTEN loss alone doesn't switch the P13K signalling dependency from the PI3Kα to PI3Kβ isoform, but instead the PTEN KO clones retained the p110α isoform dependency of the parental cells. These findings are supported by a previous study which showed that phosphorylation of AKT in parental MCF10As depends on p110α- but not β- or δ- activity, and even after PTEN deletion with siRNA, the cells maintain their dependency on the α isoform of PI3K for AKT activation (Juvin, Malek et al. 2013). However, it is important to note that in this paper the phosphorylation of AKT is via EGF stimulation whereas in my experiment no such stimulation was used. Importantly though, these findings were also observed basally without EGF stimulation.

In contrast to the MCF10A cells higher sensitivity to BYL than TGX, the TNBC cell lines BT-549 and MDA-MB-468 showed less response to selective PI3Kα compared to PI3Kβ inhibition (**Figure 4.9C**). The results show that in both TNBC cell lines, TGX-mediated PI3Kβ inhibition was more effective at inhibiting p-AKT than PI3Kα inhibition with BYL719 after 1 and 24 h of treatment (**Figure 4.9C**) and was significant in the MDA-MB-468 cells after 1 h TGX treatment compared to 1 h of treatment with BYL (**Figure 4.13A**). Although p-AKT inhibition by TGX was not significant compared to BYL after 1 h in the BT-549 cells, the trend suggests a similar response as observed in the MDA-MB-468 cells. Additionally, when comparing between cell lines, MDA-MB-468 cells were the least sensitive to PI3Kα inhibition, evident by a significantly higher level of p-AKT compared to E6-1 after 1 h BYL treatment, WT MCF10A at 24 h BYL treatment, and E6-7 at both 1 and 24 h BYL treatment (**Figure 4.9C**).

The higher sensitivity of the TNBC cells to PI3Kβ inhibition is consistent with previous findings in the literature which demonstrate that PTEN deficient cancer cells depend more heavily on the PI3Kβ isoform to drive PI3K signalling (Edgar, Wallin et al. 2010, Schwartz, Wongvipat et al. 2015, Zhang, Gao et al. 2017). However, after 24 h of treatment this increased responsiveness is reduced as inhibition of p-AKT by TGX is only slightly higher compared to BYL719 treatment in the TNBC cells (**Figure 4.9C and Figure 4.13A**). These findings suggest that despite the dominance of the beta isoform in PTEN-deficient tumour cells, in both of the tested TNBC cell lines the alpha isoform still plays a significant role in activating AKT.

Importantly, the combined treatment of BYL and TGX after both 1 and 24 h (**Figure 4.9A-C**) was highly synergistic as it was more effective than either drug used alone in all cell lines regardless of PTEN status suggesting a PTEN independent effect on p-AKT response. Dual PI3Kα/β inhibitor treatment inhibited p-AKT levels significantly more than either 1 h BYL or TGX treatment in both PTEN KO clones; E6-1 and E6-7, but not WT MCF10A cells (**Figure 4.12A**). Furthermore, p-AKT levels were still significantly decreased following 24 h dual treatment compared to either inhibitor used alone in the PTEN KO clone E6-1. However, this finding was not observed in the WT MCF10A or E6-

7 cells (**Figure 4.12A**). Similarly, dual PI3Kα/β inhibition was synergistic in the TNBC cell lines at 1 h as p-AKT levels were significantly decreased compared to each inhibitor used alone (**Figure 4.13A**). AKT phosphorylation remained significantly suppressed in MDA-MB-468 cells, following 24 h dual PI3Kα/β inhibition compared to 24 h BYL, but not compared to 24 h TGX treatment.

The effectiveness of the combination in the WT and PTEN KO cells is likely explained by the incomplete suppression of PI3K signalling when only the alpha or beta PI3K isoform is inhibited, allowing rebound of PIP3 levels due to the uninhibited PI3K isoform triggering some re-activation of AKT and hence downstream S6 activity. Dual PI3Kα/β inhibition abolishes the rebound of p-AKT caused by the uninhibited isoform and thus is highly synergistic. Indeed, Costa et al. (Costa, Ebi et al. 2015) showed that in cancers driven by PI3Kα isoform despite the initial efficacy of PI3Kα inhibition, PI3K suppression was invariably diminished by rapid re-accumulation of PIP3 which they showed was produced by the p110β isoform reactivating PI3K. Therefore, suggesting that p110β or p110α inhibition on its own incompletely blocks AKT/mTORC1 signalling. In support of this they show that concomitant inhibition of both p110β and p110α isoform with BYL719 and a PI3Kβ inhibitor prevented the PIP3 rebound and induced greater anti-tumour efficacy in *HER2*-amplified and *PIK3CA* mutant cancers.

In summary, this combined PI3Kα/β inhibition may be an effective treatment strategy regardless of PTEN status since this dual treatment was synergistic in both WT PTEN and PTEN-null cells. Taken together, this suggests PTEN loss did not influence this synergy to dual PI3Kα/β inhibition and its loss alone failed to drive a switch to PI3Kβ dominant signalling in the PTEN KO MCF10A cells. Indeed, the TNBC cell lines have a plethora of other genetic disruptions which could be involved in influencing this preferential PI3Kβ activation when PTEN is lost. In conclusion, PTEN loss is not the sole driver of this preferential PI3Kβ activation, thus highlighting other factors may be at play, at least in this cell line.

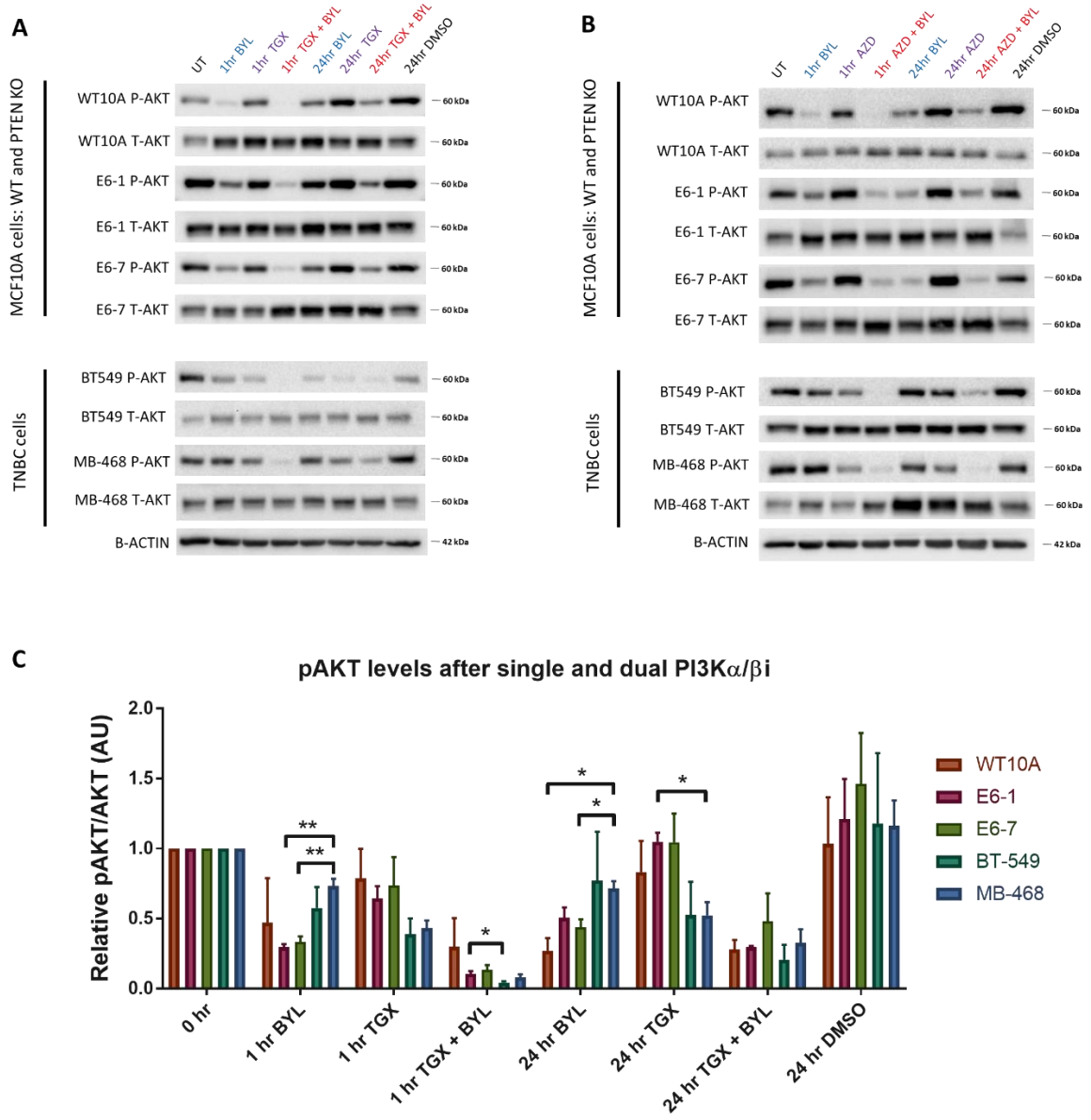

Figure 4.9 Reduced AKT expression levels following single or dual PI3Kα/β inhibition. Representative western blots (**A**-**B**) and graph (**C**) of relative p-AKT after single and dual PI3K α/β inhibition. Protein expression levels of total and phospho AKT (S473) in WT MCF10As, PTEN KO clones (E6-1 and E6-7) and TNBC cells; BT-549 (PTEN-/-) and MDA-MB-468 cells (PTEN-/-) in response to (**A**) 1 µM BYL719 and 1 µM TGX221 or 1 µM BYL719 and (**B**) 1 µM AZD6482 treatment alone and in combination for 1 and 24 h. (**C**) Quantified p-AKT levels in response to 1 or 24 h treatment with 1 µM BYL719 (PI3Kα selective inhibitor) or 1 µM TGX221 (PI3Kβ selective inhibitor) or dual PI3Kα/β inhibition (1 µM each). 1:1000 DMSO was sued as the vehicle control. Protein levels were quantified by densitometry and the data (both total and phospho protein) was normalised to their corresponding β-actin loading control (representative blots shown here) and then to total levels to obtain relative phospho levels. Relative p-AKT/AKT levels were then normalised relative to untreated=1. Data is represented as the mean values ± standard error of the mean of three independent biological replicates. Paired two-tailed *t*–test was used and statistical significance was considered at $P < 0.05$. * = $P < 0.05$, ** = $P < 0.01$. AU (arbitrary units).

4.2.1.2 S6 expression in response to single and dual PI3Kα/β inhibition

In all the tested cell lines, combined inhibition of PI3Kα and PI3Kβ not only further decreased the p-AKT levels, but also caused a marked decrease of p-S6 activity after 1 h of drug exposure compared to single treatment with either inhibitor (**Figure 4.10A-C**). In addition, this p-S6 inhibition following 1 h dual treatment was significant compared to untreated condition, in all cells, except the PTEN KO clone E6-7 (**Figure 4.13B and Figure 4.12B**). Furthermore, p-S6 was also significantly inhibited in BT-549 cells following 1 h dual treatment compared to single treatment of TGX or BYL, but not in the MDA-MB-468 cells (**Figure 4.13B**). After 24 h dual treatment S6 activity remained significantly suppressed compared to 24 h DMSO control in the BT-549 cells, but this was not observed in the MDA-MB-468 cells (**Figure 4.13B**). Similarly, in the WT MCF10A and PTEN KO cells the p-S6 levels remained inhibited in all drug treatment conditions, but this could not be attributed to the PI3K inhibition as strangely p-S6 levels also appeared inhibited in the DMSO control condition and this inhibition was at a similar level compared to both dual single BYL/TGX treatment. This makes it hard to interpret the 24 h data for S6 signalling (**Figure 4.10C**). Since this PI3Kα and β inhibition in combination appeared synergistic in reducing S6 activity in both the TNBC cell lines and PTEN KO clones as well as the WT MCF10A cells it appears PTEN loss did not influence the response of S6 to this combination treatment. Significant inhibition of S6 phosphorylation following 1 h dual treatment correlated with the most pronounced inhibition of AKT activity as this was also observed after 1 h dual treatment. Taken together these findings suggest that S6 activity is maximally suppressed when p-AKT levels are reduced below a certain threshold which considering S6 activity is downstream of AKT activity this would make sense. In support of this, p-S6 was not significantly inhibited in any cell line in response to 1 h single treatment with either inhibitor (BYL or TGX) suggesting the AKT activity, which was higher here than following combination treatment, was not sufficiently reduced for S6 activity to also be suppressed. Similar to the p-AKT results this is likely explained by the incomplete suppression of PI3K signalling when only the alpha or beta PI3K isoform is inhibited allowing PIP3 levels to rebound due to the uninhibited PI3K isoform triggering some activation of AKT and hence downstream S6 activity.

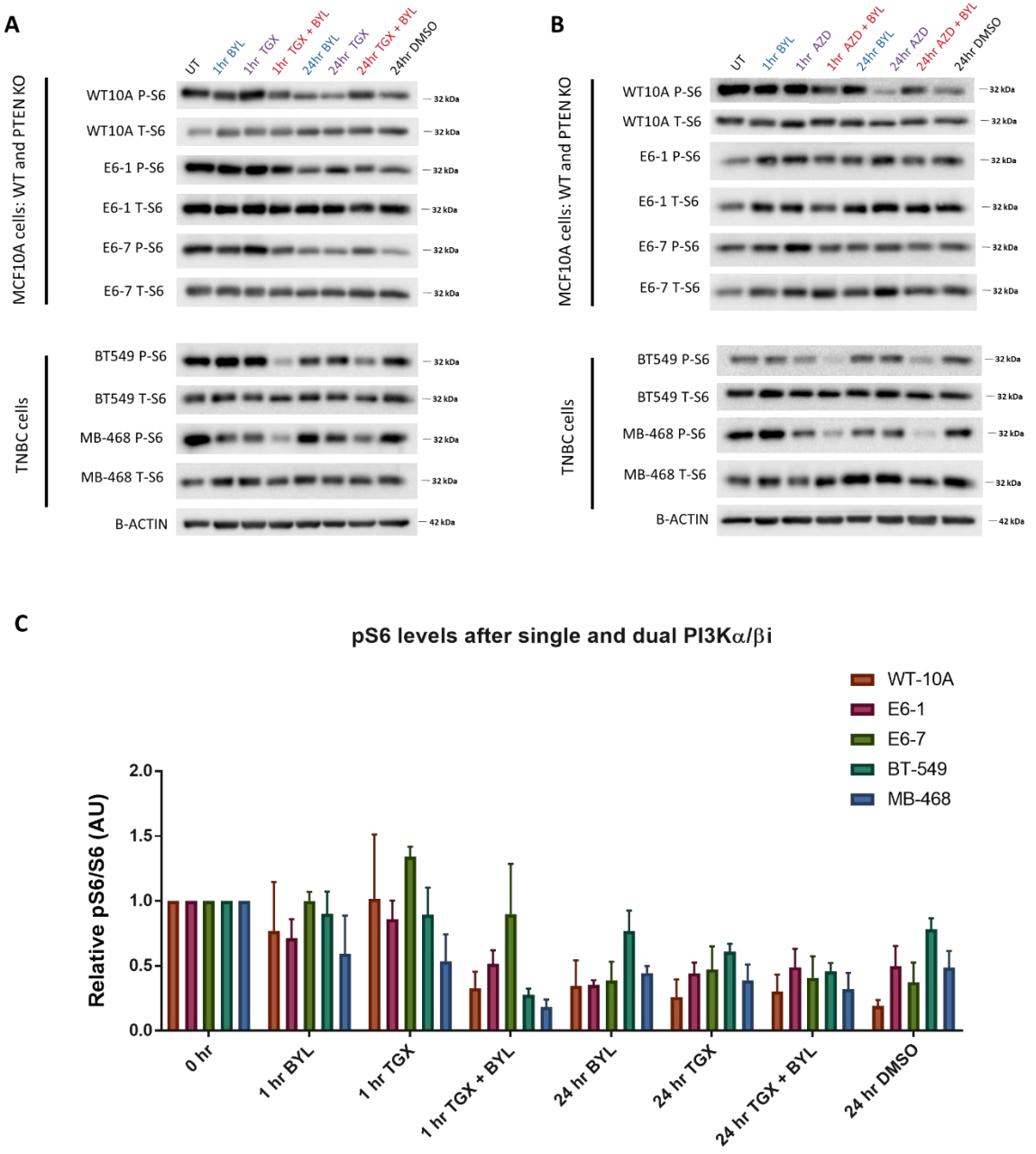

Figure 4.10 S6 expression levels following single and dual PI3Kα/β inhibition. Representative western blots (**A-B**) and graph (**C**) of relative p-S6 after single and dual PI3K α/β inhibition. Protein expression levels of total and phospho S6 (S235/S236) in WT MCF10As, PTEN KO clones (E6-1 and E6-7) and TNBC cells; BT-549 (PTEN-/-) and MDA-MB-468 cells (PTEN-/-) in response to (**A**) 1 µM BYL719 and 1 µM TGX221 or (**B**) 1 µM BYL719 and 1 µM AZD6482 treatment alone and in combination for 1 and 24 h. (**C**) Quantified p-S6 levels in response to 1 or 24 h treatment with 1 µM BYL719 or TGX221 or dual PI3Kα/β inhibition (1 µM each). 1:1000 DMSO was used as the vehicle control. Protein levels were quantified by densitometry and the data (both total and phospho protein) was normalised to their corresponding β-actin loading control (representative blots shown here) and then to total levels to obtain relative phospho levels. Relative p-S6/S6 levels were then normalised relative to untreated=1. Data is represented as the mean values ± standard error of the mean of three independent biological replicates. Paired two-tailed *t*–test was used and statistical significance was considered at $P < 0.05$. * = $P < 0.05$. AU (arbitrary units).

4.2.1.3 **ERK activity was suppressed in response to single and dual PI3Kα/β inhibition**

Consistent with the previous results which showed PI3Kβ inhibition alone caused no changes in AKT and S6 levels, ERK levels remain unchanged following 1 and 24 h single TGX or AZD treatment in the WT MCF10A cells and PTEN KO clones (**Figure 4.11A, B and C**). We found that following 1 h treatment with BYL p-ERK was inhibited, but only in the WT MCF10A and not the PTEN KO clones. Interestingly, ERK activity was also significantly inhibited following 1 h dual PI3Kα/β inhibition in the WT MCF10A cells and this was significantly lower than the E6-1 PTEN KO clone and close to significance compared to the E6-7 clone (P = 0.06) (**Figure 4.11C**). In the MDA-MB-468 cells we found that p-ERK was significantly inhibited after 1 h PI3K inhibition regardless of the inhibitor or whether drugs were given alone or in combination as both single BYL and TGX, as well combined BYL-TGX treatment at 1 h resulted in decreased ERK activity (**Figure 4.13C).** Furthermore, this p-ERK level after 1 h TGX treatment was significantly lower compared to BT-549 cells and the PTEN KO clone E6-7 (**Figure 4.11C)**.

However, BT-549 cells showed no p-ERK suppression following PI3Kα and β inhibition, alone or in combination suggesting this was a cell-line dependent effect (**Figure 4.13C)**. Moreover, the fact the MCF10A cells also showed ERK suppression following PI3K inhibition suggests that this was also independent of PTEN status. Indeed, previously 1 h BYL treatment reduced ERK activity in both WT and PTEN KO cells. The discrepancy found here can be due to the lower dose of 1 μM used in these experiments as previously 5 μM BYL was used. Thus, suggesting that in order for ERK activity to be maximally suppressed following PI3K inhibition in both WT and PTEN KO cells, AKT activity needs to be maximally inhibited. The PTEN KO cells are less sensitive to BYL and hence required the higher dose to robustly elicit p-ERK inhibition. In support of this 1 h dual PI3Kα/β inhibition caused the most pronounced decrease in ERK signalling in most cell lines compared to the other treatments at this time point and this correlated with the lowest p-AKT levels previously observed. This p-ERK inhibition following 1 h dual PI3Kα/β inhibition was significant in MCF10A and MDA-MB-468 cells and close to significant in both PTEN KO clones; E6-1 and E6-7 with P values of 0.06 and 0.07, respectively compared to untreated cells (**Figure 4.12C and Figure 4.13C**). Furthermore, longer PI3K inhibition following 24 h BYL or dual TGX-BYL treatment also appeared to reduce ERK activity. Indeed, ERK activity further decreased in the E6-1 clone after 24 h dual treatment and this was significant compared to 1 h dual treatment (**Figure 4.12C**), despite this, p-ERK inhibition was not significant in the case of the E6-7 clone. However, this does not explain why BT-549 cells had no observed reduction in ERK activity as these cells also showed decreased p-AKT levels following dual treatment suggesting that the degree of ERK suppression following PI3K inhibition is also cell line dependent.

Taken together these data show that in response to PI3K inhibition, p-ERK is also decreased in some of the cell lines and this occurs indiscriminately of PTEN status. In summary, combined TGX-BYL

treatment had a more additive effect than single treatment on ERK activity, but PTEN loss did not influence this nor did it influence the response of p-ERK to PI3Kα and β inhibition, alone or in combination.

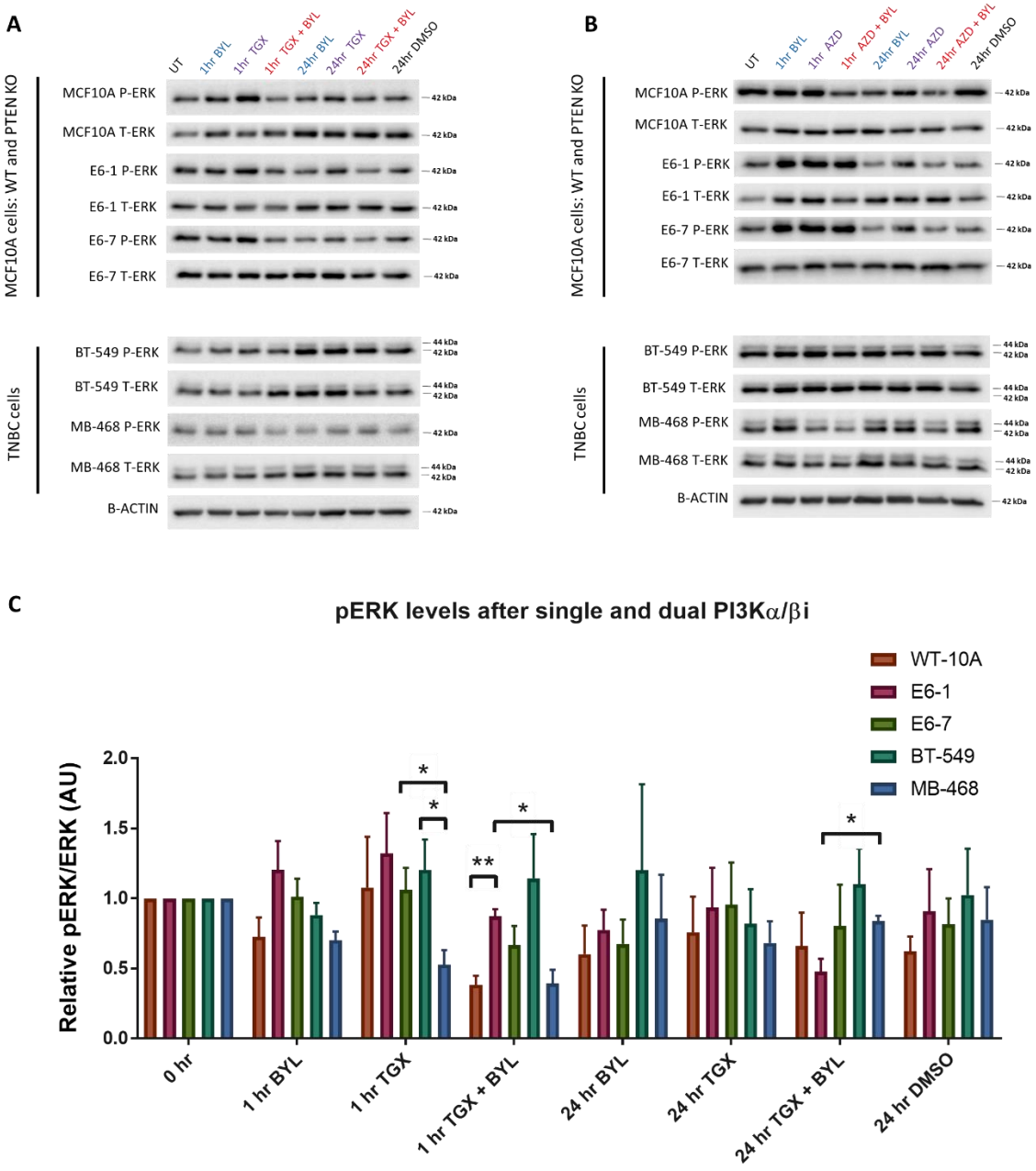

Figure 4.11 Comparison of ERK expression levels following single and dual PI3Kα/β inhibition in WT MCF10A cells, PTEN KO clones (E6-1 and E6-7) and TNBC cells. Representative western blots (**A**-**B**) and graph (**C**) of relative p-ERK after single and dual PI3K α/β inhibition. Protein expression levels of total and phospho ERK (Thr202/Tyr204) in WT MCF10As, PTEN KO clones (E6-1 and E6-7) and TNBC cells; BT-549 (PTEN-/-) and MDA-MB-468 cells (PTEN-/-) in response to (**A**) 1 μM BYL719 and 1 μM TGX221 or (**B**) 1 μM BYL719 and 1 μM AZD6482 treatment alone and in combination for 1 and 24 h. Graph **(C)** of relative p-ERK levels in response to 1 or 24 hr treatment with 1 μM BYL719 or TGX221 or dual PI3Kα/β inhibition (1 μM each). 1:1000 DMSO was used as the vehicle control. Protein levels were quantified by densitometry and the data (both total and phospho protein) was normalised to their corresponding β-actin loading control (representative blots shown here) and then to total levels to obtain relative phospho levels. Relative p-ERK/ERK levels were then normalised relative to untreated=1. Data is represented as the mean values ± standard error of the mean of three independent biological replicates. Paired two-tailed *t*–test was used and statistical significance was considered at $P < 0.05$. * = $P < 0.05$ ** = $P < 0.01$, *** = $P < 0.001$. AU (arbitrary units).

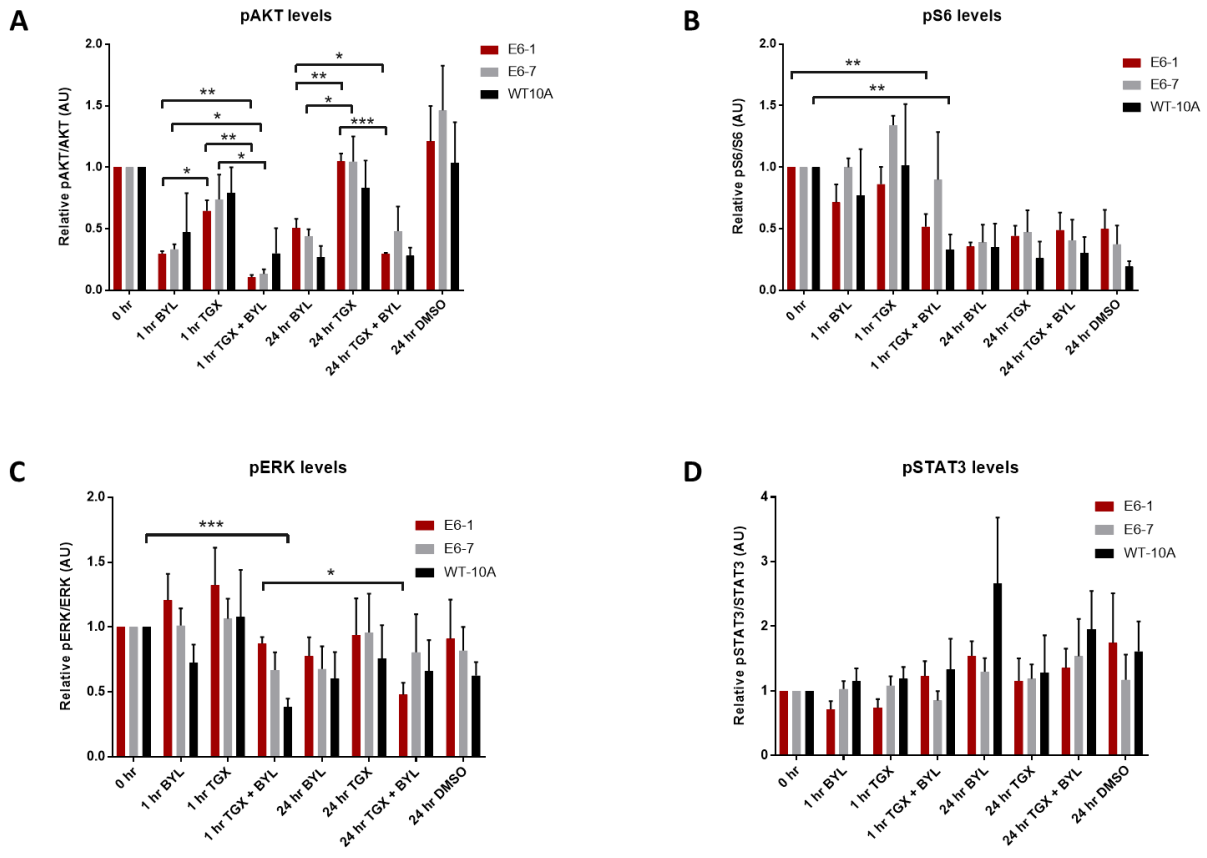

Figure 4.12 Protein expression levels of AKT, S6, ERK and STAT3 following single and dual PI3Kα/β inhibition in WT and PTEN loss MCF10A cells. Graphs of relative (**A**) p-AKT, (**B**) p-S6, (**C**) p-ERK and (**D**) p-STAT3 levels after single and dual PI3K α/β inhibition. Protein levels in MCF10A WT and PTEN KO clones (E6-1 and E6-7) in response to 1 µM BYL719 and 1 µM TGX221 treatment alone and in combination for 1 and 24 h. 1:1000 DMSO was used as the vehicle control. Protein levels were quantified by densitometry and the data (both total and phospho protein) was normalised to their corresponding β-actin loading control (representative blots shown here) and then to total levels to obtain relative phospho levels. Relative protein levels were then normalised relative to untreated=1. Data is represented as the mean values ± standard error of the mean of three independent biological replicates. Paired two-tailed *t*–test was used and statistical significance was considered at $P < 0.05$. Comparisons made between treatment conditions. * = $P < 0.05$ ** = $P < 0.01$, *** = $P < 0.001$. AU (arbitrary units).

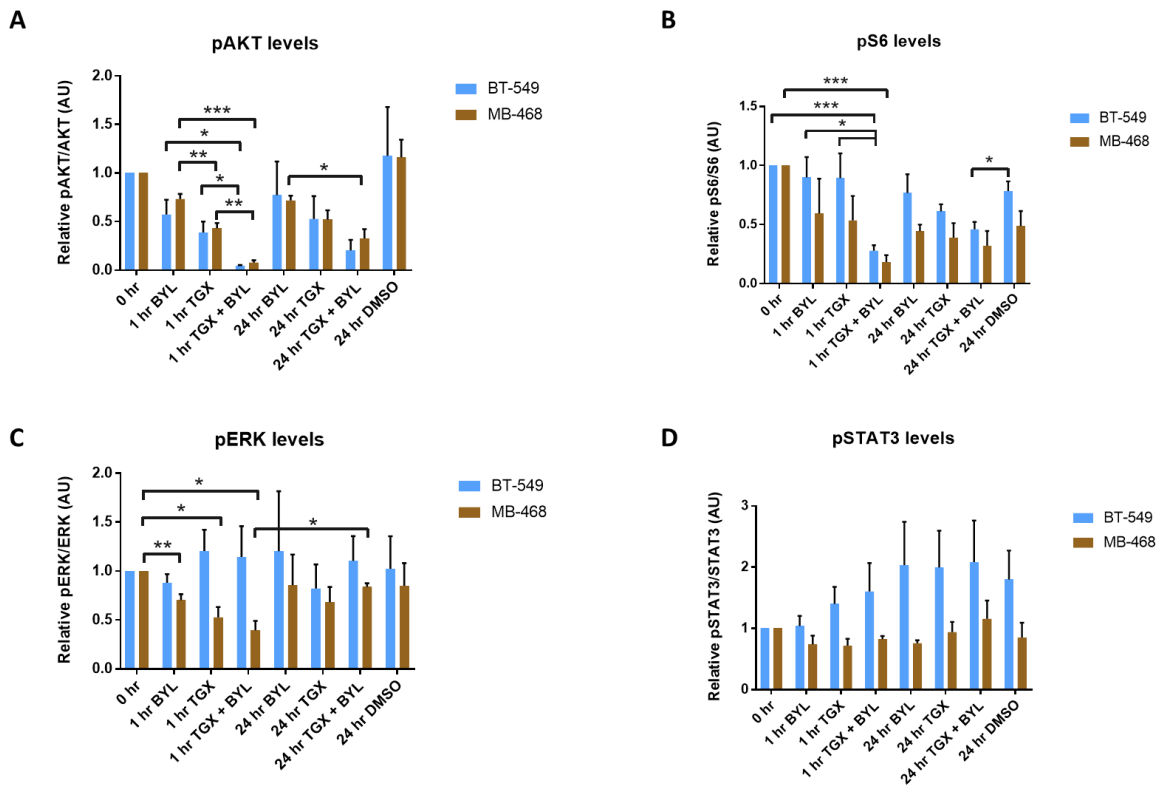

Figure 4.13 Protein expression levels of AKT, S6, ERK and STAT3 following single and dual PI3Kα/β inhibition in TNBC. Graphs of relative (**A**) p-AKT, (**B**) p-S6, (**C**) p-ERK and (**D**) p-STAT3 levels after single and dual PI3K α/β inhibition. Protein levels in TNBC cells; BT-549 (PTEN-/-) and MDA-MB-468 cells (PTEN-/-) in response to 1 μM BYL719 and 1 μM TGX221 treatment alone and in combination for 1 and 24 h. 1:1000 DMSO was used as the vehicle control. Protein levels were quantified by densitometry and the data (both total and phospho protein) was normalised to their corresponding β-actin loading control (representative blots shown here) and then to total levels to obtain relative phospho levels. Relative protein levels were then normalised relative to untreated=1. Data is represented as the mean values ± standard error of the mean of three independent biological replicates. Paired two-tailed *t*–test was used and statistical significance was considered at $P < 0.05$. Comparisons made between treatment conditions. * = $P < 0.05$ ** = $P < 0.01$, *** = $P < 0.001$. AU (arbitrary units).

4.2.2 Cell viability following single or dual PI3Kα and PI3Kβ inhibition

At the signalling level there appeared to be no significant difference in response to PI3Kβ inhibition alone or in combination with PI3Kα inhibition in the PTEN KO clones compared to the WT MCF10A cells, suggesting that the KO cells were still more dependent on the PI3Kα. However, we then sought to determine if the PTEN KO clones proved more sensitive following PI3Kα inhibition using cell viability as a measure of drug efficacy. Cell viability was examined using MTS assay, set up as per page 50 in Chapter 2. Briefly, day 1 post cell seeding in 96-well plate, cells were treated with 1 μM BYL719 or 1 μM TGX221 alone and in combination for 24 or 48 h. Inhibition effects on cell viability are depicted as a percentage relative DMSO treated cells.

4.2.2.1 **PTEN KO results in reduced sensitivity to BYL, but not TGX**

In response to single BYL treatment for 24 h in WT MCF10A cells there is a marked reduction in viable cells compared to DMSO (**Figure 4.15A**) and this is further decreased after 48 h of treatment (**Figure 4.15B**). In contrast, in the PTEN KO clones 24 h BYL treatment alone, only caused a significant decrease in the viability of the E6-7 cells, and this response was lost after 48 h of treatment (**Figure 4.15E-F**). Moreover, at both 24 and 48 h, E6-1 cells showed no response to single BYL treatment (**Figure 4.15C-D**) and at 48 h PI3K inhibition this was significantly higher than WT MCF10A cells (**Figure 4.14B**). These results support my previous biochemical findings which show PTEN-loss cells have reduced drug responsiveness to BYL as observed by both increased viability and AKT activity in the PTEN KO cells.

Similarly, in the TNBC cell lines, the MTS assay results show that single treatment with BYL for both 24 and 48 h seems to have no effect in the BT-549 and MDA-MB-468 cells as viability remained unchanged compared to the DMSO control condition (**Figure 4.15G-J**). In addition, BT-549 cell viability following 24 h BYL treatment was significantly higher compared to WT MCF10A cells and trending towards significance in the MDA-MB-468 cells (**Figure 4.14A**). This reduced response to BYL treatment supports the knowledge that these cell lines are not as dependent on the PI3Kα isoform for growth. This lack of TNBC cell response to BYL is consistent with previous immunoblot data which showed both TNBC cell lines had a lower reduction in p-AKT levels in response to 1 h BYL treatment compared to the WT and PTEN KO MCF10A cells. Indeed, AKT activity was significantly higher in the MDA-MB-468 cells compared to the WT MCF10A cells following 24 h BYL treatment (**Figure 4.10**).

Taken together this data further supports the knowledge that these TNBC cells are more dependent on the PI3Kβ isoform for growth and survival. Consistent with this, MDA-MB-468 cells displayed a significant reduction in cell viability after 24 h TGX treatment (**Figure 4.15I**) and this was significantly lower than WT MCF10A (**Figure 4.14A**). This is consistent with the immunoblot data which showed a significant reduction in AKT activity at both 1 and 24 h of TGX treatment in MDA-MB-468 cells (**Figure 4.10**). However, this reduction in viability was lost after 48 h TGX exposure (**Figure 4.15J**) and there was only a slight non-significant reduction in BT-549 cell viability cells at 24 h and no change observed after 48 h PI3Kβ inhibition (**Figure 4.15G-H**).

4.2.2.2 **PTEN loss alone does not activate preferential PI3Kβ signalling**

In contrast to the TNBC cell lines, both the WT and PTEN loss MCF10A cells appear to be non-responsive to single TGX221 treatment as no loss in cell viability is observed following either 24 or 48 of PI3Kβ inhibition. Together these findings correlate with the unchanged p-AKT levels observed in the immunoblots following PI3Kβ inhibition with TGX221 treatment in both the WT and PTEN loss

MCF10A cells. Thus, the key finding here is that PTEN loss alone is insufficient to cause a switch to PI3Kβ dominant signalling and other interacting molecules are involved, at least in these cells.

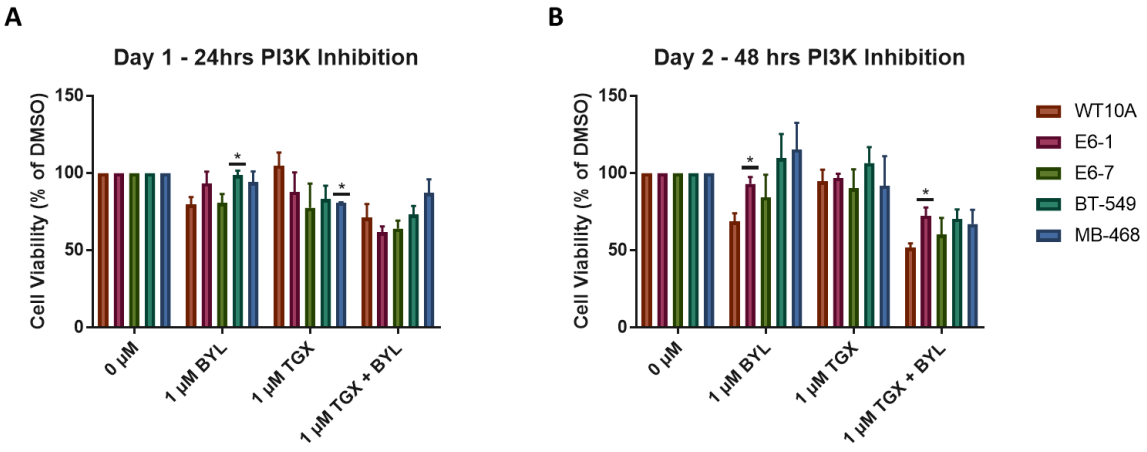

Figure 4.14 Comparing cell viability after single and dual PI3Kα/β inhibition for 24 (A) and 48 h (B) in WT and PTEN loss cells. Graph of MTS cell viability results in WT MCF10As, PTEN KO clones (E6-1 and E6-7) TNBC cell lines; BT-549 (PTEN-/-) and MDA-MB-468 (PTEN-/-) after treatment with 1 µM BYL719 or 1 µM TGX221 alone and in combination for (**A**) 24 or (**B**) 48 h. Absorbance readings were measured at 490 nm on a plate reader. Cell viability is measured as a % over DMSO vehicle control for each cell line. Data is represented as the mean values ± standard error of the mean of three independent biological replicates. Paired two-tailed *t*–test was used and statistical significance was considered at $P < 0.05$ compared to WT MCF10A cells. * = $P < 0.05$

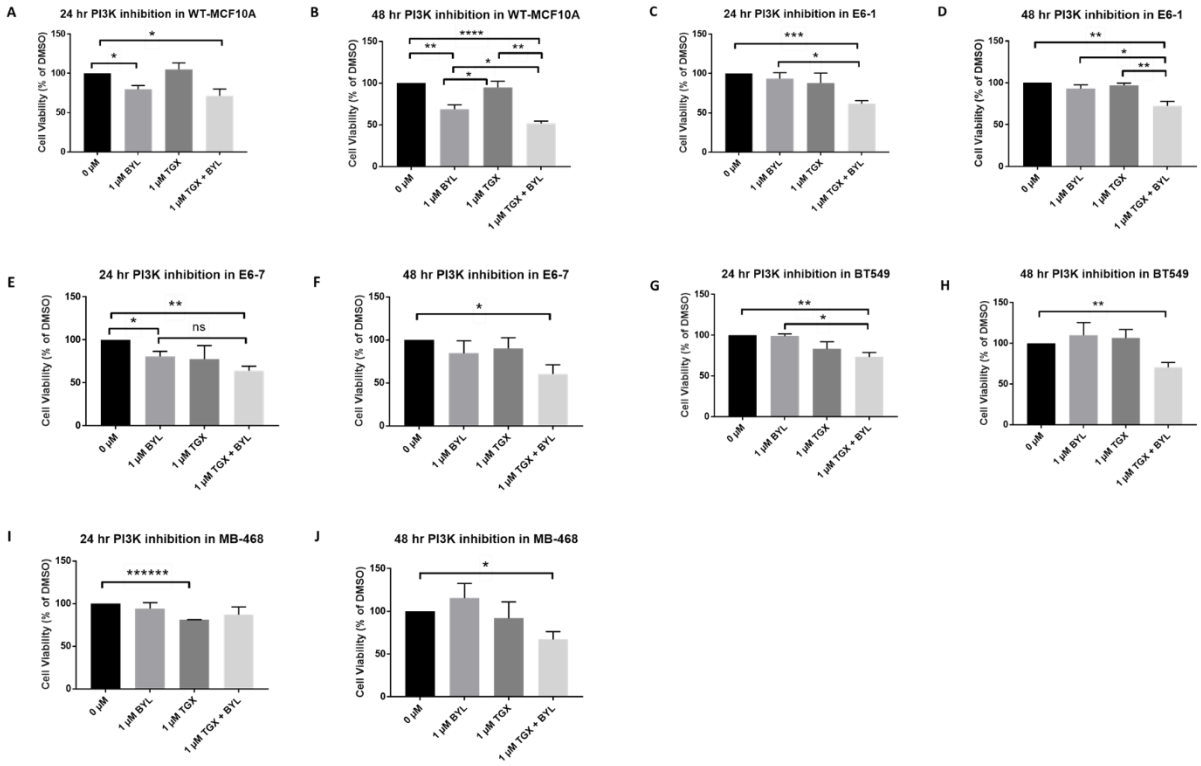

Figure 4.15 Comparing cell viability after single or dual PI3Kα/β inhibition within WT and PTEN loss cells. Graph of MTS cell viability results in WT MCF10As (**A-B**), PTEN KO clones; (E6-1 (**C-D**) and E6-7 (**E-F**)) and TNBC cell lines; BT-549 (PTEN-/-) (**G-H**) and MDA-MB-468 (PTEN-/-) (**I-J**) after treatment with 1 µM BYL719 or 1 µM TGX221 alone and in combination for 24 or 48 h. Absorbance readings were measured at 490 nm on a plate reader. Cell viability is measured as a % over DMSO vehicle control for each cell line. Data is represented as the mean values ± standard error of the mean of three independent biological replicates. Paired two-tailed *t*–test was used and statistical significance was considered AT $P < 0.05$. * = $P < 0.05$ ** = $P < 0.01$, *** = $P < 0.001$, **** = $P < 0.0001$, ****** = $P < 0.000001$.

4.2.2.3 Dual p110α/β inhibition was the most effective treatment regardless of PTEN status

The MTS assay results indicated that the largest decrease in AKT phosphorylation following dual p110α/β inhibition correlates with the greatest reduction in cell viability for 24 h and 48 h in all the cells, indiscriminately of PTEN status (**Figure 4.15**). Indeed, dual PI3Kα/β inhibition resulted in a significant reduction in cell survival compared to DMSO control after both 24 h and 48 h in all cells, with the exception of MDA-MB-468 cells at 24 h of treatment (**Figure 4.15A-J**). After 24 h treatment both WT and PTEN KO MCF10As had a similar level of cell viability following dual PI3Kα/β inhibition. Thus, regardless of PTEN status and PI3K isoform dependence combined PI3Kα/β inhibition was highly effective. After 48 h the WT MCF10A cells were the most sensitive to dual PI3Kα/β inhibition with almost a 50% loss of cell viability, which was a decrease of 20% compared to 24 h treatment (71% to 51% respectively) (**Figure 4.15A**). E6-1 cells had an increase in the number of viable cells after 48 h dual PI3Kα/β inhibition compared to the 24 h drug exposure and this was significantly higher compared to WT MCF10A cells. (**Figure 4.15D**). This was not observed for the E6-7 cells, but the error bar is large and the data would need to be confirmed with additional replicates.

4.2.3 PTEN loss results in unsustained PI3K pathway inhibition

The efficacy of the combination treatment with PI3Kα/β inhibition increased after 48 h in the WT MCF10A cells compared to DMSO control, but in the PTEN loss cells maximal efficacy of PI3K pathway inhibition is achieved in the first 24 h of treatment and either unchanged or reduced after 48 h in E6-7 and E6-1 cells respectively (**Figure 4.15A-F**). Moreover, in support of this sensitivity to BYL after 48 h treatment is increased in the WT MCF10A cells. In contrast, sensitivity to BYL is lost after 48 h of drug exposure in both the PTEN KO clones. Taken together these findings suggest that PTEN loss results in unsustained PI3K pathway inhibition as efficacy is reduced or lost following longer exposures of dual PI3Kα/β or single BYL treatment, respectively. Sustained and durable inhibition of the PI3K pathway is likely harder to achieve as a result of PTEN loss leading to upregulated PI3K signalling and constitutively active AKT, which over time leads to signalling reactivation. Failure to cause durable suppression of PI3K signalling in the absence of PTEN may explain why the PTEN KO cells show reduced sensitivity to not only single PI3Kα suppression, but also possibly dual PI3Kα/β inhibition. In support of this, as mentioned earlier, both TNBC PTEN-null cell lines lost sensivity to single PI3Kβ inhibition following 48 h of TGX exposure, and although like the PTEN KO clones dual treatment retained efficacy this was not significantly changed for BT-549 cells from 24 h to 48 h.

4.2.4 Combined PI3Kα/β inhibition was synergistic in all cells

Although, the viability data indicated that co-targeting both PI3Kα and β appeared to be synergistic we wanted to confirm this BYL-TGX drug combination was synergistic as opposed to an additive effect i.e. the inhibition on cell survival was greater than the sum of the two drugs given alone. To confirm drug synergy the Chou-Talalay's Combination Index (CI score) was used (Chou 2010) as described on page 52 in Chapter 2. The results showed that indeed co-targeting both PI3Kα & β isoforms by combined PI3Kα/β inhibition was synergistic (**Table 4.1**). After 24 h of treatment the dual PI3Kα/β inhibition was synergistic in all cell lines, except the PTEN KO clone E6-7 and the TNBC cell line MDA-MB-468 which had a CI score of 1 indicating an additive effect (**Table 4.1**). However, it appears that in the case of these cell lines a longer duration of treatment was needed to achieve synergism as after 48 h of treatment the BYL-TGX drug combination was synergistic in all cell lines (**Table 4.1**). The highest synergy was observed in the TNBC cell lines as either drug (TGX/BYL) alone had either no effect or a very slight in inhibitory effect after 48 h, in BT-549 and MDA-MB-468 cells, respectively.

Table 4.1 Talalay's Combination Index to determine the synergism of dual BYL + TGX inhibition

Cell lines	**WT MCF10A**		**PTEN KO E6-1**		**PTEN KO E6-7**		**MDA-MB-468**		**BT-549**	
Dual inhibition	24 h	48 h	24 h	48 h	24 h	48 h	24 h	48 h	24 h	48 h
CDI Index	0.88	0.79	0.75	0.80	1.0	0.79	1.1	0.73	0.89	0.70
Synergistic	yes	yes	yes	yes	no	yes	no	yes	yes	yes
Additive					yes		yes			

As expected considering the dominance of the PI3Kβ isoform in these PTEN deficient TNBC cells lines; BT-549 and MDA-MB-468, these cells had almost no loss in cell survival after 24 h of PI3Kα inhibition with BYL719, with a loss of 1 and 5% viable cells in MDA-MB-468 and BT-549 cells, respectively and no loss in cell survival after 48 h. In contrast, both BT-549 and MDA-MB-468 cells were moderately responsive to PI3Kβ inhibition with TGX221 after 24 h of treatment, with a loss of 17 and 19% viability, respectively. Despite this initial, albeit moderate response, after 48 h this was lost in BT-549 cells which showed no loss of viability compared to DMSO control and an 8% decrease in cell survival in the MDA-MB-468 cells. Thus, suggesting over the longer duration of drug exposure the cells adapt to the stress of the drug and continue to grow despite its presence. Importantly though the dual treatment was effective in reducing cell viability after 24 h by an average of 13 and 27% in MDA-MB-468 and BT-549 cells, respectively and after 48 hours of treatment this increased to approx. 30% loss of cell viability in both TNBC cell lines.

4.2.5 Summary of single or dual PI3Kα/β inhibition results

Taken together, the immunoblotting and MTS results show that, independent of PTEN status, co-targeting both PI3Kα and β isoforms by combined PI3Kα/β inhibition was synergistic. The observed synergy of dual PI3Kα/β inhibition is consistent with studies in the literature which have demonstrated that combined targeting of both p110β and p110α isoforms of PI3K was synergistic and improved the anti-tumour effects compared to single-isoform inhibition (Edgar, Wallin et al. 2010, Schwartz, Wongvipat et al. 2015). In both WT and PTEN KO MCF10A cells dual PI3Kα/β inhibition was a highly synergistic combination resulting in the greatest reduction in cell viability and PI3K signalling. Similarly, in the TNBC cell lines the TGX-BYL combination treatment is also more effective than single treatment with either PI3Kα or β inhibitor. A key finding was that despite PTEN loss in the MCF10A cells the PTEN KO clones show no change in sensitivity to PI3Kβ inhibition compared to the WT cells, therefore suggesting that PTEN loss alone is unable switch the dependence from the parental PI3Kα dominant isoform to the PI3Kβ isoform in driving PI3K signalling. Although there are some changes in the PTEN loss cells compared to WT MCF10A cells, for instance ERK activity was significantly reduced after 1 h dual treatment, but not in the PTEN KO clones, and the reduced sensitivity to BYL, they still closely resemble the parental cells in many aspects. The phenotype of the PTEN KO clones appear to be somewhere in between that of a normal mammary epithelial cell and a cancerous one and not fully transformed.

In conclusion, these data show that despite PTEN loss in the MCF10A cells the PTEN KO cells behave similarly in response to the p110α/β inhibition suggesting that PTEN loss in these cells does not cause a switch to the PI3Kβ as a dominant isoform in driving PI3K signalling as p-AKT levels were minimally suppressed in both the PTEN KO clones and WT MCF10A cells following TGX treatment at both 1 and 24 h. Thus, it would appear that preferential activation of PI3Kβ isoform was not the mechanism responsible for the reduced sensitivity to BYL719 observed in the PTEN KO clones compared to the WT MFCT10A cells.

4.3 Computational model-based analysis of network rewiring and response to drug treatment

The experimental studies above and others in the literature (Nguyen and Kholodenko 2016, Shin, Muller et al. 2018) have revealed the complexity related to targeted drug-induced network rewiring, which are strongly dynamic and context-specific. This phenomenon reflects, in part, the presence of complex pathway crosstalk, intertwined positive and negative feedback loops, and post-translational modifications that together make signalling networks highly plastic and highly nonlinear. In-depth understanding of drug-induced network remodelling therefore requires an ability to quantitatively describe drug-affected signalling-transcriptional networks and their dynamic behaviours over time, which extends beyond experimental approaches alone. To this end, systems-based approaches that

integrate mathematical network modelling with experimental work are useful for systematic interrogation of feedback and crosstalk disruption, dynamic drug response and ultimately drug-mediated network rewiring (Kolch, Halasz et al. 2015, Nguyen and Kholodenko 2015, Fabian, Taylor et al. 2016, Nguyen 2016, Shin and Nguyen 2016, Claas, Atta et al. 2018). Mathematical models offer useful abstractions and powerful quantitative frameworks that enable us to validate our intuitive understanding, and gain new insights into these complex processes through formal analysis and predictive simulations (Romano, Nguyen et al. 2014, Byrne, Monsefi et al. 2016, Shin and Nguyen 2016, Varusai and Nguyen 2018).

In collaboration with Dr Sungyoung Shin, a mathematical modeller in the Nguyen laboratory, we have utilised the experimental data generated in this thesis to construct a new mathematical model of the PI3K-ERK MAPK signalling crosstalk network, which integrates major known feedback loops and interactions between the two pathways. Our primary goal was to utilise this integrative and quantitative model to interrogate the emergent properties of this network, including complex dynamic response to targeted drugs and the effect of PTEN loss on the network as a whole. Such analysis would be challenging if using experimental approaches alone. Model development and analysis followed an iterative research paradigm central to systems biology approaches that typically involve multiple steps as visually illustrated in (**Figure 4.16**).

The first step in modelling is to construct a network scheme based on known knowledge in the literature. Selection of which components are included depends on the scope of the model, which is defined according to the specific aim of the modelling process, often underlined by one or more biological questions. As such, the model may encompass a single pathway or multiple pathways linked together. The second step is to describe the network model using a mathematical formulation. Model building using ODEs is one of the most common and suitable methods for describing, analyzing and simulating dynamic signalling networks (Shin and Nguyen 2017, Shin, Muller et al. 2018). The rate equations of an ODEs-based model are usually formulated at an elementary reaction level based on mass-action kinetics or more abstract levels using reduced forms of alternative kinetic laws. For example, under the conditions of fast complex formation between a substrate and its enzyme and if the substrate abundance greatly exceeds that of the enzyme, the quasi-steady state assumption (QSSA) could be made which reduces the rate of an enzyme-catalyzed reaction to a form of Michaelis-Menten (MM) kinetics, where the rate is expressed as a function of the substrate. The third step is to calibrate the mathematical model and estimate kinetic parameter values of the model using time-course and dose-response data, which enhances the model's predictive power. There are usually two ways to get the parameter values. If previously measured, one can obtain the values directly from the literature. If not, one needs to train/calibrate the model against available experimental data/observations to estimate the remaining

unknown parameters. Quantitative time-course and/or dose-response data are often most useful for the training of dynamic models, although data for this purpose is not restricted to these types.

In the modelling process, steps 1 to 3 are the most critical and time-consuming processes. Once the model is fully calibrated and validated using independent data, in the fourth step we can carry out many different simulations such as *in silico* knock-down/-out experiments, sensitivity analyses to identify the functional roles of key regulatory mechanisms, and *in silico* perturbation analyses. Through these simulation analyses, we can generate experimentally testable hypotheses, which is step five. As a last step, the proposed new hypotheses are tested and validated *in vivo* and *in vitro*.

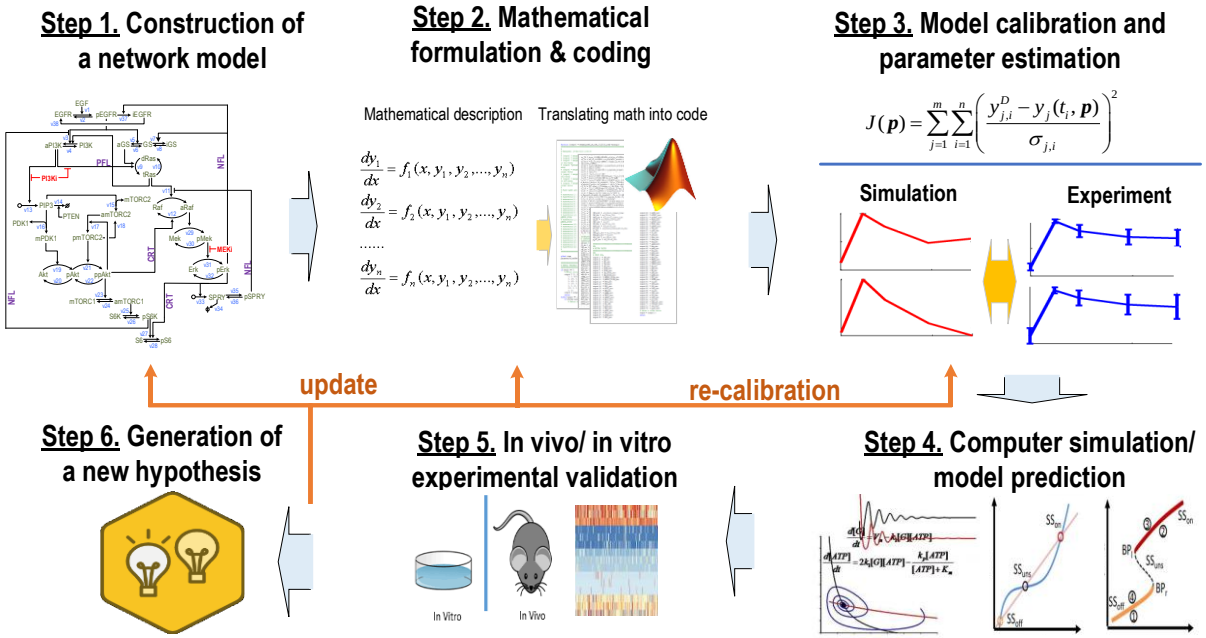

Figure 4.16 A general multi-step workflow of a mathematical modelling process. This schematic diagram visually illustrates the key steps 1-6 involved in the process of building a mathematical model.

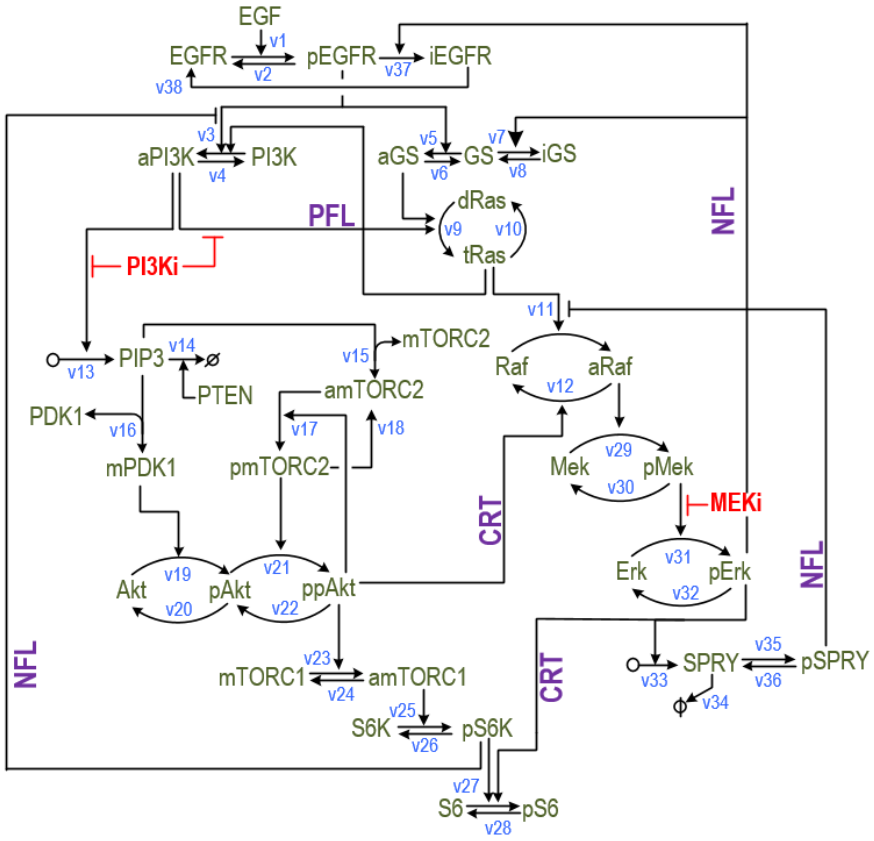

Figure 4.17 Schematic diagram of PI3K-ERK MAPK crosstalk network. pEGFR: phosphorylated, active EGFR; iEGFR: phosphorylated (by pERK), inactive EGFR; aPI3K: active PI3K; GS: complex of Grb2 and SOS; aGS: active form of Grb2 and SOS complex; dRas: Ras-GDP; tRas: Ras-GTP; aRaf: active Raf; pMEK: phosphorylated, active MEK; pErk: phosphorylated, active Erk; amTORC2: PIP2-bound mTORC2; pmTORC2: phosphorylated, active mTORC2; pAkt: phosphorylated Akt; ppAkt: double phosphorylated Akt; amTORC1: active mTORC1; pS6K: phosphorylated S6K; pS6: phosphorylated S6; pSPRY: phosphorylated SPRY; NFL: negative feedback loop; PFL: positive feedback loop; CRT: crosstalk; PI3Ki: PI3K inhibitor; MEKi: MEK inhibitor.

4.3.1 Construction of a new PI3K-ERK MAPK crosstalk mathematical model

The model ODEs, rate equations and the sets of best-fitted parameter values used for simulations are given in **Tables 2.19-2.20** in Chapter 2 Materials and Methods. The model was implemented and numerically simulated in MATLAB ® (The MathWorks. Inc. 2018b) using the variable-step and variable-order *ode15s* solver.

Key model assumptions

Below, we describe the mechanistic biological observations and regulatory mechanisms that underlie the key model assumptions built into the model.

Negative feedback loops involving EGFR.

As indicated in (**Figure 4.17**), EGFR is assumed to exist in three inter-convertible molecular states: unmodified, phosphorylated (activated) and inhibited (iEGFR); transition between these states are regulated by the relevant enzyme regulators. Upon EGF binding, EGFR undergoes rapid phosphorylation, internalization and ubiquitination by ubiquitin ligase. In our model, we included ERK phosphorylation and inhibition of EGFR as a negative feedback loop (reaction v37). Note that for simplicity, we avoid modelling of EGFR synthesis and degradation processes, and instead assume that EGFR molecules targeted for degradation are locked in a dynamic pool of ubiquitinated EGFR.

Negative feedback loop mediated by S6K. PI3K has been known to be activated in response to growth factor stimulation and oncogenic activation of RTKs or activation of GPCRs as well as oncogenes such as RAS (Hemmings and Restuccia 2012). Upon activation, PI3K is recruited to the membrane, where the p110 catalytic subunit of PI3K then generates PIP3 by catalysing the phosphorylation of PIP2, subsequently activating multiple downstream signalling pathways (Janku, Yap et al. 2018). The lipid phosphatase PTEN, a tumour suppressor counteracts PI3K activity by converting PIP3 back to PIP2 (Janku, Yap et al. 2018). For simplicity, we modelled PI3K as activated by EGFR (as a representative RTK) and RAS (Reaction 3 and 4), and then transferred the upstream signal downstream through PDK1-AKT-mTORC1 pathways (reaction 16, 19, 21, 23). Activated mTORC1 phosphorylates S6K, which suppresses PI3K activation through the phosphorylation of IRS (Zhang, Gao et al. 2008), which forms a negative feedback loop.

Positive feedback loops mediated by PI3K and RAS. The EGFR activated GRB2-SOS complex catalyses the exchange of GDP for GTP, which activates RAS (Wee and Wang 2017). The active RAS-GTP binds to and activates p110α/p85. On the other hands, the activated PI3K produces PIP3, which binds to GAB1, forming a complex mGAB1. mGAB1 activates RAS through suppression of SHP2 (Yart, Laffargue et al. 2001, Will, Qin et al. 2014). These two regulatory mechanisms form a positive feedback loop under EGFR stimulation (reaction 3 and 9).

Coupled negative feedback loop through ERK. ERK is phosphorylated by the RAS-RAF-MEK. The active ERK feeds back to the pathway activation at several levels (Kolch, Calder et al. 2005). SOS is one of the target molecules where ERK interfere with RAS activation through SOS phosphorylation, forming a negative feedback loop (Shin, Rath et al. 2009) (reaction 7). Another group of relatively well-characterised transcriptionally induced inhibitors of ERK1/2 signalling are the sprouty (SPRY) proteins, which bind to two intracellular components of the RAS pathway and inhibit RAS pathway signal transduction (reaction 11) (Casci, Vinos et al. 1999, Yusoff, Lao et al. 2002, Rubin, Litvak et al. 2003).

To derive the best fitted parameter set, we carried out repeated Genetic Algorithm (GA) runs with a population size of 500 and the generation number set to 100. In this computation, we also changed the mutation and crossover rates and even the population size to escape from being trapped in local minima. After multiple repetitions of the GA process where the best fitted set obtained from a previous repeat was used as the starting point of the next repeat, we arrived at the final best fitted set as the objective function was not further reduced, and the fitted parameter values no longer change. The best-fitted parameter set is displayed in (**Table 2.20**), which was subsequently used for the simulations.

To fit our model, we utilised a range of time-course datasets measuring the response of key network nodes including phosphorylated EGFR, AKT, S6 and ERK, to various doses of EGF stimulation, as well as dose-response dataset measuring p-ERK response to increasing EGF stimulation. The model fitting results are displayed in (**Figure 4.18**), where model simulations using the best-fitted parameter set obtained from the GA-based optimisation (described above) show good agreement with the experimental data.

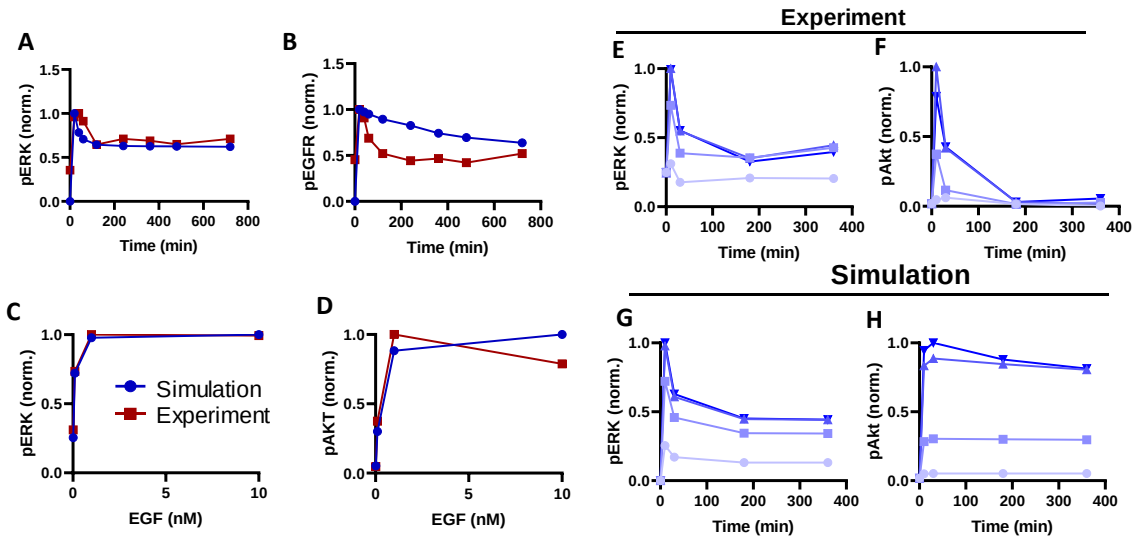

Figure 4.18 Model fitting results. Comparison of simulated (red lines, showing the best-fitting model) and experimentally observed (blue lines) time-courses. (**A-B**) The time courses of p-ERK and p-EGFR in response to EGF stimulation (20ng/mL) for 12 hours, which were reproduced from the previous experimental data (Golan-Lavi, Giacomelli et al. 2017). (**C-D**) The dose-response of p-ERK and p-AKT to EGF stimulation (at 10 min after EGF stimulation), which were reproduced from the previous experimental data (Bouhaddou, Barrette et al. 2018). (Fritsche-Guenther, Witzel et al.) The time course of p-ERK and p-AKT in response to EGF stimulation for multiple doses, which were reproduced from the previous experimental data (Bouhaddou, Barrette et al. 2018). All experiments were performed using MCF10A breast cells. (**G-H**) simulated values of p-ERK and p-AKT.

4.3.2 Model-based simulations of drug response

Using the quantitatively calibrated model, we first simulated the time profiles of p-ERK and p-AKT to different dosages of the PI3K inhibitor BYL719 (BYL). Model simulation shows that BYL decreased p-ERK at earlier time point in a dose dependent manner (**Figure 4.19A**); however, p-ERK started to rebound after 1 hour of the inhibitor treatment. Like p-ERK, the level of p-AKT was sharply decreased by BYL in a dose dependent manner, but, unlike ERK, AKT did not display any rebound pattern (**Figure 4.19B**). These model simulations agree with our experimental finding that BYL179 induces a reactivation of p-ERK in MCF10A cells (**Figure 3.25**).

Next, we carried out another simulation by treating cells with different dosages of the MEK inhibitor trametinib. In response to trametinib treatment, p-ERK was rapidly and significantly suppressed as expected (**Figure 4.20A**). Interestingly, p-AKT was not significantly affected by trametinib. The p-AKT level was even slightly increased at higher doses of MEK inhibitor (**Figure 4.20B**). This simulation result is qualitatively agreed with our experimental data where 5 nM trametinib significantly suppressed p-ERK (**Figure 3.17**), but did not inhibit p-AKT (**Figure 3.19**) in MCF10A cells. Taken together, these *in silico* simulations support experimental observations that PI3K inhibitor (BYL719) strongly regulates both PI3K and ERK pathways, while MEK inhibitors effectively regulates the MAPK-ERK pathway, but not the PI3K pathway.

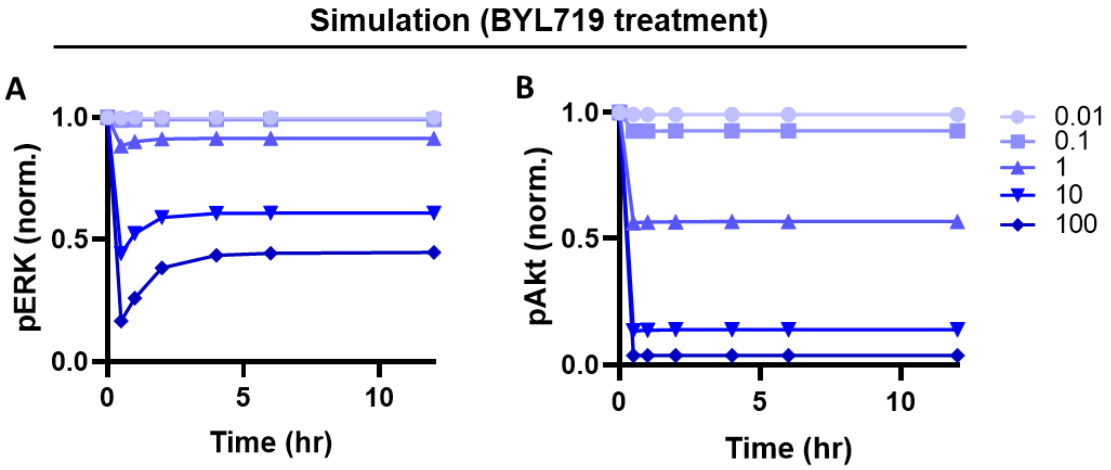

Figure 4.19 Simulated time-dependent response of phosphorylated ERK and AKT to BYL719. (**A**) Time profiles of p-ERK in response to BYL719 treatment. Different colour indicates different BYL179 concentrations. (**B**) Time profile of p-AKT in response to BYL719.

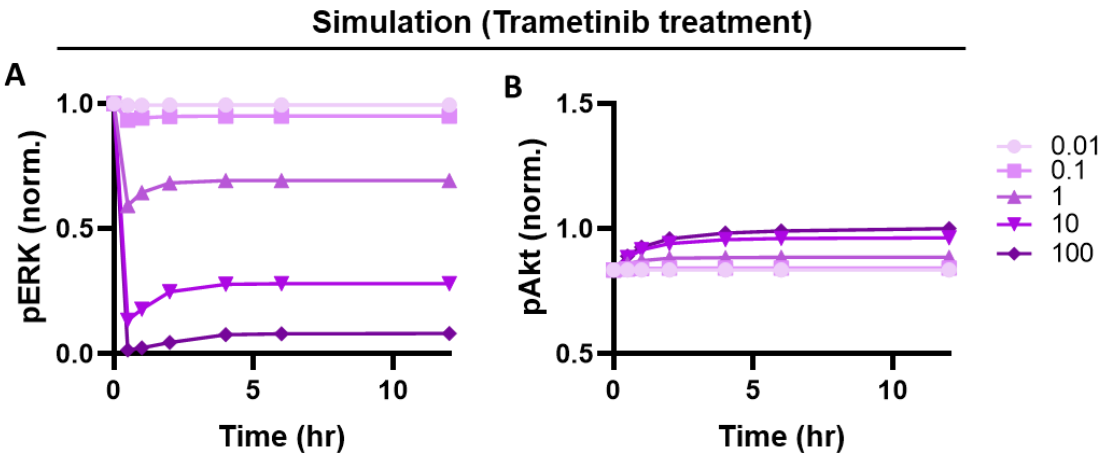

Figure 4.20 Simulated time-dependent response of phosphorylated of ERK and AKT to trametinib. (**A**) Time profiles of p-ERK in response to trametinib treatment. Different colour indicates different trametinib concentrations. (**B**) Time profile of p-AKT in response to trametinib.

4.3.3 Model-based simulations of the effect of PTEN loss

Our calibrated model has been specifically designed for WT MCF10A cells. Using this model, we performed further simulation analyses to examine the effect of PTEN depletion on drug response and network behaviours. First, we asked what effect does PTEN loss inflict on the time-course response of p-AKT/p-ERK to MEK or PI3K inhibition in the simulation. Second, how likely is the time-dependent rebound activation of p-AKT/p-ERK upon MEK or PI3K inhibition in the WT MCF10A cells, and if there is rebound activation, how does PTEN loss influence this?

To address these questions, we simulated the profile of p-ERK and p-AKT for 12 hours in response to BYL719 in the PTEN WT and PTEN KO contexts. BYL generated a clear rebound pattern of p-ERK in both PTEN WT and KO conditions, but there was no significant difference between them (**Figure 4.21A**). In contrast to p-ERK, the basal level of p-AKT level was dramatically increased in the PTEN KO cells while p-AKT was suppressed by the BYL719 treatment in both PTEN WT and KO cells (**Figure 4.21B**). These model predictions were validated by our experimental data where the 5 µM BYL719 treatment generated a clear rebound of p-ERK in both WT and PTEN KO MCF10A cells (**Figure 4.21C-D, Figure 3.24, and Figures 4.5 and 4.6C-D)** and the basal level of p-AKT was highly elevated in the PTEN KO cells (**Figure 3.24**).

Next, we simulated the profile of p-ERK and p-AKT for 12 hours in response to trametinib under control conditions and when PTEN is knocked out. The basal p-ERK level did not change much in the PTEN KO condition, and following MEKi treatment it was dramatically decreased in both WT and PTEN KO conditions (**Figure 4.22A**). Overall there was no significant differences in the effect of trametinib on p-ERK between WT and PTEN KO conditions, which is consistent with the experimental data where both

WT MCF10A and PTEN KO cells displayed significant trametinib-induced suppression of p-ERK (**Figure 4.22C, Figure 3.17**).

The basal level of p-AKT was elevated in the PTEN KO condition, however, AKT phosphorylation was not suppressed by MEKi treatment in either PTEN WT or KO settings (**Figure 4.22B**). This model prediction was consistent with the experimental data, although there is some variation in the measurement due to the heterogeneity between cells (**Figure 4.22D and Figure 3.19**). Together, our simulation results suggest that PTEN does not have a significant effect on the dynamic profiles of p-ERK and p-AKT in response to trametinib, although it increases basal level of p-AKT.

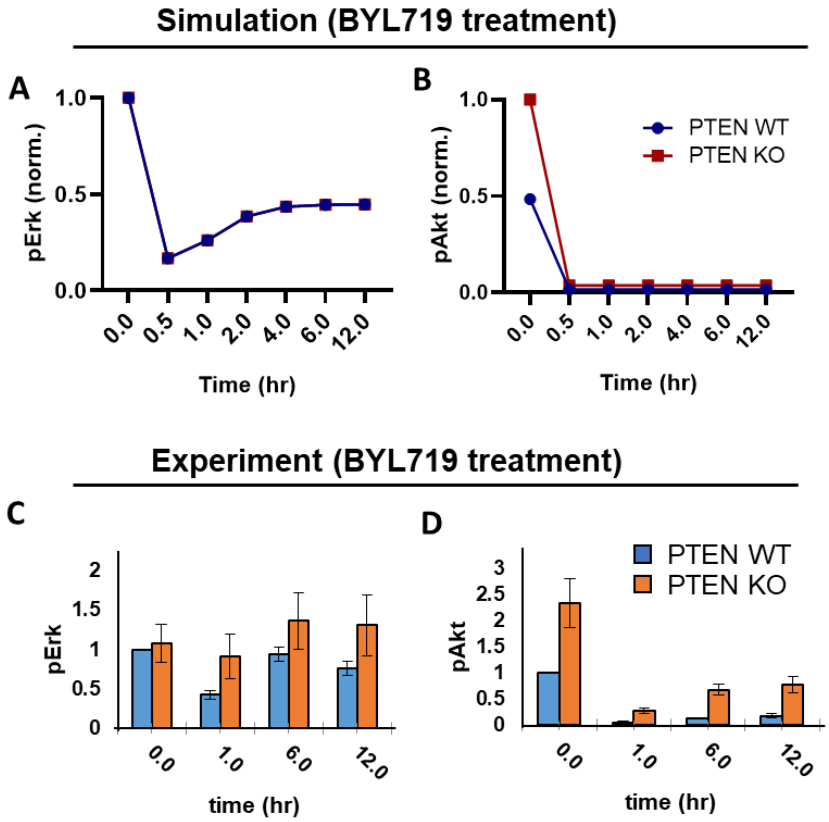

Figure 4.21 Effect of PTEN knockout on the dynamic response of p-ERK and p-AKT to 5 µM BYL. (**A**-**B**) Time profiles of p-ERK to BYL treatment. Blue line indicates the WT PTEN and the red line indicated PTEN KO condition. Experimental data (**C**-**D**) of p-ERK and p-AKT in PTEN WT and KO cells, which was captured from **(Figure 3.25 and 3.24)**. Data is represented as the mean values ± standard error of the mean of three independent biological replicates.

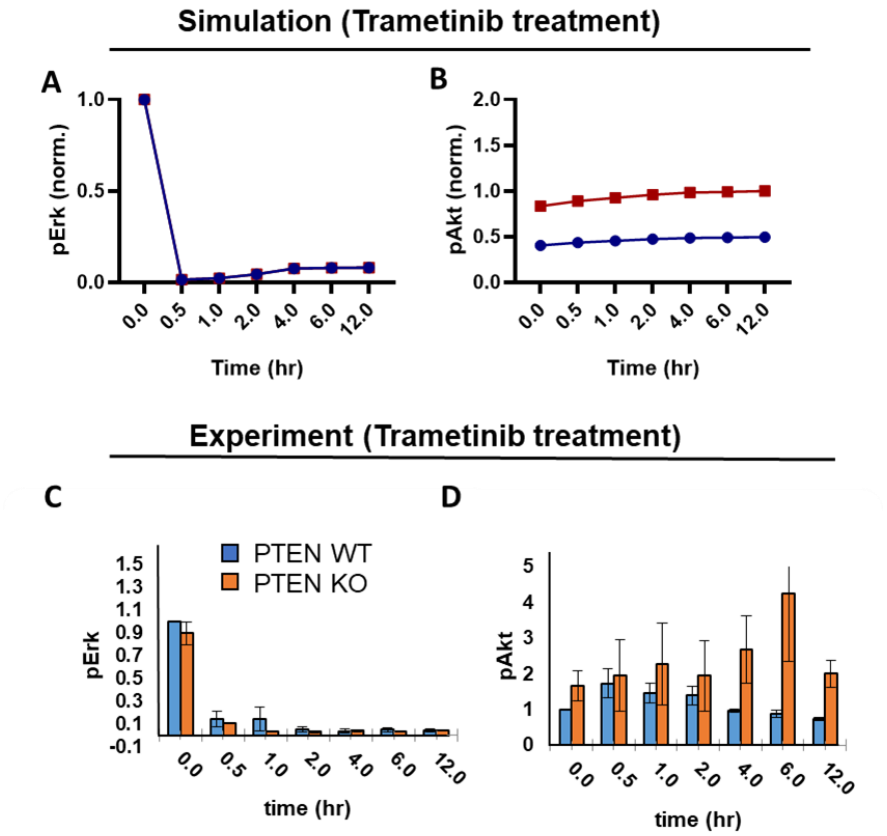

Figure 4.22 PTEN knockout effect on response time-profiles of p-ERK and p-AKT to 5 nM trametinib. (**A**-**B**) Time profiles of p-ERK to trametinib treatment. Blue line indicates the WT PTEN and the red line indicates the PTEN KO. (**C**-**D**) Experimental data of p-ERK and p-AKT in PTEN WT and KO cells, which was captured from **(Figure 3.17 and 3.19)**. Data is represented as the mean values ± standard error of the mean of three independent biological replicates.

Chapter 5: General Discussion & Future Directions

5.1 Discussion of the main thesis findings

The tumour suppressor PTEN is a major negative regulator of the PI3K pathway and after the p53 tumour suppressor, PTEN is the most frequently disrupted gene in human cancers. PTEN inactivation is associated with tumourigenesis in multiple human cancers, including breast cancer. Complete loss of PTEN protein or reduced expression levels occurs in many tumour types, but is frequently observed in breast cancer, in particular TNBC (Marty, Maire et al. 2008). Approximately 30% of breast cancer have loss of PTEN expression (Stemke-Hale, Gonzalez-Angulo et al. 2008) and PTEN loss is commonly associated with poor prognosis (Depowski, Rosenthal et al. 2001, Nagata, Lan et al. 2004).

Using CRISPR/Cas9 technology PTEN was successfully deleted in the non-tumourigenic mammary epithelial cell line MCF10A to generate a MCF10A PTEN KO model. MCF10A cells are a diploid, and genetically stable cell line which were derived from a benign breast tissue of a female patient who had fibrocystic disease (Soule, Maloney et al. 1990). Therefore, this PTEN KO model provided a clean background of minimal mutations to determine the role of PTEN loss in mediating adaptive resistance to PI3K and MEK inhibitors and decipher how PTEN deletion might influence the dynamic response to these drugs. As was discussed in the review by Chavez et al. (Chavez, Garimella et al. 2010), based on complementary DNA (cDNA) expression array analysis, non-transformed cells lines such as MCF10A cells cluster closely with TNBC cell lines and thus can be considered non-transformed counterparts of TNBC (Kao, Salari et al. 2009). Additionally, MCF10A cells with added mutations such as PTEN loss begin to model TNBC, since these cells do not express ER, PR, nor do they have HER2 receptor amplification. Upregulation of the PI3K-AKT-mTOR pathway was demonstrated by the significantly higher level of AKT activation in the MCF10A PTEN KO cells, which was an expected result considering the de-repression of the PI3K/AKT pathway induced by the loss of PTEN, a potent negative regulator of the PI3K pathway.

5.1.1 PTEN loss as a single event does not drive preferential PI3Kβ activation

As previously mentioned in many cancer cells and tumours with PI3Kα mutations or RTK-driven PI3K signalling, PI3Kα is the dominant isoform; whereas tumours or cancer cells which have loss (or inactivation) of PTEN are predominantly driven by the p110β isoform (Torbett, Luna-Moran et al. 2008, Wee, Wiederschain et al. 2008). In normal cells, both PI3Kα and PI3Kβ contribute to the effects of the pathway on metabolism and growth (Foukas, Claret et al. 2006, Jia, Liu et al. 2008) and both are ubiquitously expressed. This may be the basis for the lower toxicity of isoform selective inhibitors as combined PI3Kα/β inhibition is likely to cause greater 'on-target' toxicity. Hence, PI3Kβ selective targeting could be an effective therapy for PTEN-deficient cancers including a subset of TNBC. In fact, a number of PI3Kβ inhibitors GSK2636771, SAR260301 and AZD8186 have progressed to clinical trials for the treatment of PTEN-null tumours (Barlaam, Cosulich et al. 2015, Hancox, Cosulich et al.

2015, Bedard, Davies et al. 2018). Despite this, multiple mechanisms of feedback mediated re-activation of PI3K signalling leading to resistance to PI3Kβ inhibition have emerged (Ebi, Costa et al. 2013, Schwartz, Wongvipat et al. 2015). These mechanisms include RTK activation (EGFR, IGFR and IR) and activation of ERK or PI3Kα signalling, which are discussed in depth in our review paper in Appendix 1. All of these kinases and pathways have the potential to limit drug efficacy, hence identifying combination strategies that increase or sustain pathway inhibition will be necessary for optimal and lasting therapeutic effect.

While it has been known that in PTEN-deficient cancer cells, PI3K signalling is driven by PI3Kβ, the mechanism linking loss of PTEN with p110β activation remains poorly understood. One hypothesis is that under normal growth conditions p110β is constitutively active, but PTEN molecules specifically counteract this by associating with the p110β/p85 complex (Chagpar, Links et al. 2010). Therefore, upon loss of PTEN, its control on basal activity of p110β is also lost triggering constitutively activated downstream PI3K signalling. In support of this, it has been shown that PTEN associates with this p110β/p85 complex and this enhances PTEN phosphatase activity (Rabinovsky, Pochanard et al. 2009). However, it still remains to be determined whether loss of PTEN interaction with p110β/p85 complex solely explains why PTEN-null tumours are highly p110β isoform dependent. A possible mechanism linking PTEN loss with preferential p110β activation was only recently illuminated. In 2017 Zhang et al. reported a role for the adaptor protein CRKL in associating with and regulating p110β-dependent PI3K activity in PTEN-null cancer cells (Zhang et al., 2017). Mechanistically, loss of PTEN activates Src, which in turn tyrosine phosphorylates the scaffolding protein p130Cas and phosphorylated p130Cas provides a platform for recruitment of CRKL that preferentially binds to p110β over p110α (Zhang et al., 2017). Thus, a PTEN/Src/p130Cas axis activates CRKL/p110β in PTEN-null cancer cells **(Figure 5.1)**. In support of this notion, the authors showed that Src inhibition co-operates with PI3K or p110β inhibition to suppress the growth of PTEN-null breast and prostate tumour cells (Zhang et al., 2017). However, the findings here should be validated in larger cancer-cell panels and it still remains to be proven whether p110β dependency in PTEN loss cells can be explained solely by loss of PTEN interaction with p110β/p85 complex. In addition, further animal testing of these combinations is needed to confirm their synergistic effects in an *in vivo* setting.

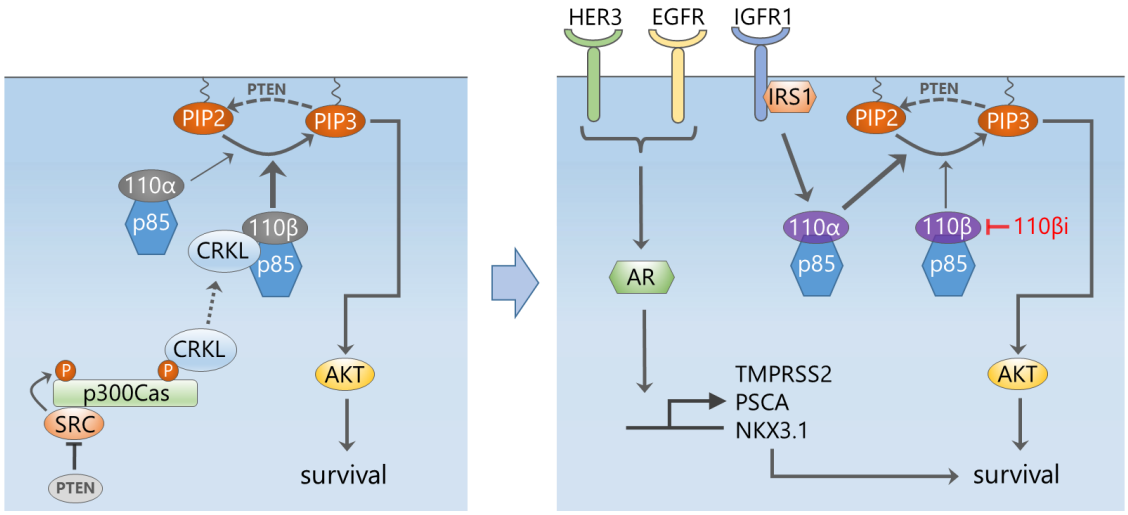

Figure 5.1 CRKL mediates p110β-dependent PI3K signalling in PTEN loss cells. A PTEN/Src/p130Cas signalling axis activates CRKL/p110β in PTEN-deficient tumour cells, providing a link between PTEN loss and activation of p110β in these cells (Zhang et al., 2017). Specific PI3Kβ inhibition causes feedback upregulation of IRS1 and IGF1R which then activates the PI3Kα isoform and results in a rebound of PI3K signalling following transient suppression. The androgen receptor (AR) downstream of several RTKs also provides another escape mechanism for continued survival following PI3K inhibition.

Chapter 3 results show that the PTEN KO clones displayed reduced responsiveness to PI3Kα inhibition with BYL719 as evident not only by higher levels of p-AKT following BYL treatment, but also by the higher cell viability compared to WT MCF10A cells. Moreover, it was demonstrated that PTEN loss was driving this reduced responsiveness as transient re-expression of PTEN in these PTEN KO cell lines restored their sensitivity which was comparable to the wild-type MCF10A cells as confirmed by a similar reduction in cell viability following BYL treatment. Based on the knowledge that in PTEN-deficient cancer cells PI3K signalling is predominantly driven by PI3Kβ isoform (Torbett, Luna-Moran et al. 2008, Wee, Wiederschain et al. 2008, Ni, Liu et al. 2012), it was then hypothesized that this reduced sensitivity to PI3Kα inhibition in the PTEN KO clones was due to preferential p110β activation.

To test this hypothesis treatment with the selective PI3Kβ selective inhibitor TGX221/AZD6482 was carried out alone and in combination with PI3Kα inhibition using BYL719. If PTEN loss in these had induced a switch to PI3Kβ as the dominant isoform then it was anticipated that these cells would show increased sensitivity comparable to the PI3Kβ dominant MDA-MB-468 and BT-549 PTEN-null cells, however, this was not the case and it seemed that the PTEN KO clones retained the p110α isoform dependency of the parental MCF10A cells. Despite PTEN loss, the PTEN KO clones showed very little response to p110β inhibitor TGX when used alone. Together, these findings indicate that PTEN loss alone in these cells does not cause a switch to the PI3Kβ as a dominant isoform in driving PI3K signalling and thus PI3Kβ-dependent signalling was not the mechanism responsible for the reduced sensitivity to BYL719 treatment observed in the PTEN KO clones when compared to the WT MCF10A cells.

Together these findings demonstrate that PTEN loss alone was not sufficient to cause a selective p110β activation in the PTEN KO cells. Since the PTEN-null TNBC cells have multiple additional genetic alterations other than PTEN deletion, the response to PI3Kβ inhibition in these cells are potentially shaped not just by PTEN loss alone, but is likely contributed by the intricate interplay between other interactors of the PI3K pathway and other cell signalling pathways which are perturbed in these cells. Importantly, studies that claim PTEN loss is a driving factor in the drug response observed should confirm this finding by reintroducing PTEN into PTEN-null cells and see if PTEN re-expression switches the dependence towards the PI3Kα isoform. In addition to PTEN homo deletion (Meric-Bernstam, Akcakanat et al. 2012), both TNBC cell lines MDA-MB-468 and BT-549 have a plethora of other mutations. The Catalogue of Somatic Mutations in Cancer (COSMIC) database shows that both MDA-MB-468 and BT-549 cell lines cluster together based on similar gene expression profiles. COSMIC - Cell Lines Project reported 426 mutations in BT-549 cells and the Copy Number Variation (CNV) data found no genes with a gain in copy number, but there were 389 genes with copy number loss (https://cansar.icr.ac.uk/cansar/cell-lines/BT-549/mutations/). In MDA-MB-468 cells, a staggering 1039 mutations were reported in COSMIC - Cell Lines Project and analysing CNV data these cells had 132 genes with a gain in copy number and 409 genes with copy number loss (https://cansar.icr.ac.uk/cansar/cell-lines/MDA-MB-468/). These mutations, included numerous mutations in the TP53 gene (COSMIC database) which has also been studied by Nagel et al. (Hollestelle, Nagel et al. 2010) and mutant retinoblastoma protein 1 (RB1) in both MDA-MB-468 and BT-549 cells. In addition, MDA-MB-468 cells also have amplified EGFR expression (Filmus, Pollak et al. 1985) which was also clearly evident from our immunoblot results (**Figure 3.10B)**.

Of possible interest here is the missense mutation in PIK3C2B found to be present in the MDA-MB-468 cells (COSMIC database). Could this mutant PIK3C2B be involved in mediating this cell lines sensitivity to PI3Kβ inhibition? PI3K-C2β is a member of the Class II PI3K (PI3KC2) subfamily, which in mammals includes two other members PI3K-C2α and PI3Kly-C2γ (Jean and Kiger 2014). The class II PI3Ks, like the well-established Class I PI3Ks, were previously thought to generate both PIP3 and PIP2, albeit to a lesser extent. However, this was incorrect and now it is quite well accepted that class II PI3Ks do not result in the synthesis of PIP3 (Jean and Kiger 2014). Although, Class II PI3Ks can potentially generate PIP2, (Zhou, Wulfkuhle et al. 2007), the monophosphate PIP is the main *in vitro* product (Falasca and Maffucci 2012). In support of this, siRNA knockdown of class II PI3Ks has confirmed the lack of involvement of these enzymes in generating PIP2 (Malek, Kielkowska et al. 2017). This means that although both Class I and Class II PI3K generate different lipid products, together they can change the pool of PIP products altering the downstream signalling. Thus, a mutant Class II PI3K could lead to increased PIP and PIP2 levels which as precursors of PIP2 and PIP3 respectively could therefore indirectly increase the amount of PIP3 molecule generation. Indeed, both PI3KC2α and β are involved in growth factor receptor responses, and in activation of Rho GTPases in cell contraction and

migration (Falasca and Maffucci 2012). Thus, could this PI3K-C2β mutation in the MDA-MB-468 cells be also be playing a role in mediating sensitivity to PI3Kβ inhibition by co-regulating the monophosphate PIP pool?

Although class II PI3Ks have received less research attention to date there is growing evidence that they play important roles in cancer development, including PI3K-C2β in breast cancer (Chikh, Ferro et al. 2016). Not only did Ferro et al. find PI3K-C2β to be overexpressed in several human breast cancer cell lines and breast cancer specimens, but their data indicated that PI3K-C2β regulates breast cancer cell growth. Moreover, PI3K-C2β expression in breast tissues correlated with the proliferative status of the tumour (Chikh, Ferro et al. 2016). In addition, downregulation of PI3KC2β inhibited breast cancer cell invasion *in vitro* and breast cancer metastasis formation *in vivo*. Taken together, this study and others establishes PI3K-C2β as driver of breast cancer progression and in metastasis development (Chikh, Ferro et al. 2016), thus a mutant PI3KC2β could potentially be leading to dysregulated PI3K signalling including upregulation of the PI3Kβ isoform. Of course, this would needed to be further investigated and is only speculative at this stage. In addition, the functional effects of this PI3KC2β mutation would need to be determined. But if the functional effects of this PI3KC2β mutation could possibly explain the switch of dependence from the dominant parental PI3Kα isoform to the PI3Kβ isoform in PTEN loss TNBC cells then this should be investigated by introducing this mutation using CRISPR/Cas9 HDR into the MCF10A PTEN KO cells to observe whether this mutation along with PTEN loss was sufficient to induce the switch.

Our findings that PTEN KO cells were insensitive to PI3Kβ inhibition indicates that multiple factors work together to determine the dependency on PI3Kβ in the absence of PTEN and other mechanisms can activate this PI3Kβ isoform. Consistent with the insensitivity of our PTEN KO cells to PI3Kβ inhibition, a study investigating the anti-tumour effects of AZD8186 alone and in combination with docetaxel showed that a number of PTEN-null TNBC and prostate cancer lines were insensitive to the PI3Kβ inhibitor AZD8186 (Hancox, Cosulich et al. 2015). Understanding which pathways cause the PTEN-null cells to become more or less dependent on PI3Kβ will inform both patient selection and combination therapies to maximize the benefit of these agents. Candidate pathways include IGFR, EGFR, alternate PI3K pathway signalling, and the presence of RAS and RAF mutations (Chandarlapaty, Sawai et al. 2011, Serra, Scaltriti et al. 2011).

Although in contrast to the PI3Kα isoform which is frequently mutated (Vanhaesebroeck, Stephens et al. 2012), PI3Kβ mutations are a rare event (Pazarentzos, Giannikopoulos et al. 2015, Nakanishi, Walter et al. 2016), therefore elevated PI3Kβ activation remains dependent on other proteins and genetic disruptions such as PTEN loss. PI3Kβ is unique as it is the only Class 1 PI3K isoform which can be activated by both GPCR and RTKs (Ciraolo, Iezzi et al. 2008, Jia, Liu et al. 2008). GPCR regulating thrombin and platelet aggregation have been shown to activate PI3Kβ (Nylander, Kull et al. 2012) as

well as GPCR–mediated signals via RAS-related C3 botulinum toxin substrate 1, also known as RAC1 and cell division cycle 42 (CDC42) from the RHO subfamily of small GTPases (Fritsch, de Krijger et al. 2013). Furthermore, cells with mutant RAC were shown to be dependent on PI3Kβ for survival (Kawazu, Ueno et al. 2013). Although RAS protein is known to be direct activators of p110α, p110γ, and p110δ Class I PI3Ks, interacting via a RAS-binding domain (RBD), in contrast to these isoforms RAS is unable to interact with p110β (Fritsch, de Krijger et al. 2013). This is consistent with a study which failed to detect any activation of p110β by RAS following a systematic analysis of RAS effector proteins in co-transfected cells (Rodriguez-Viciana, Sabatier et al. 2004). These findings were surprising considering the apparently similar level of relatedness between the RBDs across the four isoforms. Together these findings show how distinct isoforms of class 1 PI3K are deferentially regulated.

Our findings show that PTEN loss as a single event did not cause preferential PI3Kβ activation, thus suggesting PTEN does not act alone to elicit a switch from the parental PI3Kα isoform to the PI3Kβ isoform, at least in this MCF10A cell line, and indicates that other proteins are likely involved in this process. This finding agrees with a previous study which showed that phosphorylation of AKT in parental MCF10As depends on p110α- but not β- or δ- activity, and this was surprising as mRNA-seq data revealed that MCF10A cells in fact have higher expression levels of p110β than the p110α isoform, with lowest levels of p110δ (p110β>>α>δ) (Juvin, Malek et al. 2013). Critically, the authors found that even after targeted PTEN KD with siRNA, the cells maintain their dependency on the parental PI3Kα isoform for AKT activation in either basal or EGF-stimulated AKT phosphorylation.

These findings, as well as ours, which show loss of PTEN did not change the dominant role of PI3K to the p110β isoform, strongly suggests that there is no hard-wired molecular context that mean loss of PTEN will always lead to PI3Kβ becoming functionally dominant. This suggests that the reason(s) why PI3Kβ is more dominant in MDA-MB 468 cells is, at best only weakly linked to their PTEN status. Instead multiple factors and other proteins likely work together in a context dependent manner to influence the dependency on PI3Kβ in the absence of PTEN. For instance, the small GTPases RAC1 and CDC42 could possibly interact with PTEN through the p85 regulatory subunit and influence PI3Kβ dependency. Indeed, an emerging pattern is co-regulation of specific PI3Ks and phosphatases through shared interactions with adaptor proteins, namely the regulatory subunit p85. Although first identified as a p110 regulatory subunit, p85 has since been shown to also bind to PTEN. PTEN association with p85 involves the unphosphorylated form of PTEN and also includes the p110β isoform of PI3K (Rabinovsky, Pochanard et al. 2009, Chagpar, Links et al. 2010). In this way, p85 reversibly regulates the conversion of PIP2 to PIP3. Gaining insights into why PTEN loss alone failed to switch the PI3K signalling PI3Kβ isoform will broaden our understanding of the drivers behind PI3K isoform dependency and hence the application of isoform selective PI3K inhibitors.

5.1.2 Co-targeting PI3Kα and β was synergistic independent of PTEN status

Our results show that independent of PTEN status, co-targeting both PI3Kα and β isoforms by combined PI3Kα/β inhibition was synergistic. The observed synergy of dual PI3Kα/β inhibition is consistent with studies in the literature which have demonstrated that combined targeting of both p110β and p110α isoforms of PI3K was synergistic and improved the anti-tumour effects compared to single-isoform inhibition. Schwartz et al. (Schwartz, Wongvipat et al. 2015) showed that PI3Kβ inhibition by AZD8186 only transiently suppressed PI3K signalling in PTEN-deficient breast (and prostate) cancer cells, with rapid rebound of PI3K/AKT signalling observed just 2 h after drug treatment. Interestingly, it was found that the rebound depended on activation of the PI3Kα isoform, which was caused by feedback upregulation of its activators IRS1 and IGF1R. Combination of AZD8186 with a PI3Kα isoform inhibitor (BYL719) or IGF1R/IR inhibitor (OSI-906) both significantly attenuated this AKT rebound and efficiently suppressed cancer cell growth (Schwartz, Wongvipat et al. 2015). In the same vein, the work by Costa and colleagues showed that PI3Kα inhibition by BYL719 initially abrogated PI3K signalling, but within 24 h induced a rebound increase in PI3K activation (indicated by the phosphoinositide PIP3 level) in HER2+ or PIK3CA-mutant luminal breast cancer cells (Costa, Ebi et al. 2015). Further analysis revealed that the elevated PIP3 was due to increased recruitment of the PI3Kβ isoform to HER3. As in (Schwartz, Wongvipat et al. 2015), co-inhibition of both PI3Kα and β significantly enhanced breast cancer cell death and induced tumour regression *in vivo* (Costa, Ebi et al. 2015). These reciprocal feedback regulation among the PI3K isoforms highlight another intricate layer of the feedback circuitry controlling the PI3K signalling pathway. Systems-level understanding of complex feedback mechanisms and isoform-specific PI3K signalling will be important in identifying tumours susceptible to individual isoform inhibition, and informing appropriate combination therapy.

5.1.3 Transient p-ERK suppression induced by PI3K inhibition

Our data showed that MEK inhibition with trametinib did not affect PI3K-AKT signalling in either the WT or PTEN KO MCF10A clones, and there was no change in response to trametinib as a result of PTEN loss. In contrast, PI3K inhibition suppressed ERK signalling after 1 h of treatment, but only transiently with ERK activity rebounding at 6 h. Taken together, it therefore appears that in this context and in these cells, the PI3K-ERK crosstalk was unidirectional as perturbation of PI3K pathway affected ERK signalling, but the reverse was not the case, i.e. when MEK was inhibited suppression of PI3K signalling was not observed implying unidirectional crosstalk.

This transient suppression of ERK by PI3K inhibition was reported by Qin et al. (Will, Qin et al. 2014), but in the context of HER2+ breast cancer cells and indicates the existence of a PI3K-RAS feedback loop upstream of ERK. In these HER2+ breast cancer cells Qin et al. showed that inhibition of PI3K, but not AKT, leads to the rapid, but transient inhibition of wild-type RAS-ERK signalling axis in HER2+ breast cancer cells; This inhibition, though transient, rebounding a few hours after drug

administration, was critical for the enhanced cell death caused by PI3K over AKT inhibitors. The authors posited that inhibiting PI3K causes the rapid inhibition of both AKT-mTOR and RAS-ERK signalling, whereas AKT inhibitors suppress only the former and, in fact, activate the latter via AKT/mTOR-dependent feedback mechanisms (Carracedo, Ma et al. 2008, Chandarlapaty, Sawai et al. 2011, Serra, Scaltriti et al. 2011). They proposed that in this model selective PI3K inhibition inhibits RAS directly, but also relieves feedback inhibition of receptors that would ultimately lead to RAS activation, but because the former occurs more rapidly than the latter initially a decline is observed followed by a subsequent rebound in ERK activity. Thus, the clue to understanding the complexity of RAS/ERK signalling regulation by PI3K and the apparent paradox was in the transience of this phenomenon.

Qin et al. also showed another selective class-I PI3K inhibitor, GDC-0941, also caused rapid inhibition of ERK signalling in the TNBC cell line MDA-MB-468 (Will, Qin et al. 2014). The researchers also found that PI3Ki-induced p-ERK inhibition occurred with all the different PI3K class-I isoform-selective inhibitors as long as they were targeting the isoform driving the cells e.g. PI3Kβ in MDA-MB-468 cells, thus suggesting the transient p-ERK inhibition was non-specific for a particular Class-I isoform. This was consistent with our results which showed ERK activity was suppressed in MDA-MB-468 cells following inhibition of the dominant PI3Kβ isoform (**Figure 4.13A-C**) and suppressed in the WT MCF10A cells, and PTEN KO cells, but to a lesser extent, following 1 h PI3Kα inhibition. Indeed, addition it was observed that ERK activity was most significantly inhibited after 1 h combined BYL-TGX treatment. Thus, suggesting that though the dominant isoform is the driver of PI3K signalling the non-dominant PI3K isoform is still playing a role in generating PIP3 and activating downstream signalling.

In order to determine whether inhibition of the PI3K pathway had a similar effect when PTEN is present the authors utilised an MDA-MB-468 cell line engineered to express wild-type PTEN when induced with doxycycline (Will, Qin et al. 2014). The results showed that PTEN protein expression reduced AKT phosphorylation and led to decreased phosphorylation of ERK, MEK, and CRAF. These findings suggest that inhibition of PI3K reduces ERK signalling by reducing PIP3, and since selective mTOR or AKT inhibition does not inhibit ERK, this must be occurring via an AKT/mTOR independent pathway (Will, Qin et al. 2014). Next the authors assessed how common this phenomenon of transient ERK inhibition was by treating a panel of tumour cell lines with the pan-PI3K inhibitor BAY 80-6946 and found that the majority of them (16/23) showed suppression of ERK phosphorylation including those with PI3K mutation, HER amplification, or PTEN or inositol polyphosphate-4-phosphatase type II B (INPP4B) deficiency. PI3K inhibitors were shown to inhibit AKT signalling in all cells, but they observed that inhibition of RAS-ERK signalling only occurred in cells not harbouring a mutant allele of RAS suggesting that it may be due to direct inhibition of wild-type RAS activity. Indeed, to confirm

that mutant RAS signals independently of PI3K, the authors induced mutant RAS expression in a model with wild-type RAS and found that both mutant RAS-GTP levels and downstream RAF-MEK-ERK activation were unaffected by the PI3K inhibitor. Together, these data suggest PI3K regulates wild-type, but not mutant RAS (Will, Qin et al. 2014). Importantly, MCF10As and the TNBC cell lines BT-549 and MDA-MB-468 all displayed a decrease in ERK phosphorylation after PI3K inhibition and all of these cells harbour wild-type RAS alleles (Eckert, Repasky et al. 2004). Qin et al. postulated that the reason why this phenomenon is under reported and why inhibition of ERK signalling has not, for the most part, been recognized as a prominent feature of PI3K inhibitors is two-fold (Will, Qin et al. 2014). First, many if not all inhibitors used in the past have other targets, including, prominently, mTOR inhibition, which would be expected to blunt or remove the observed p-ERK inhibition. Second, the effect is rapid and transient thus obscured by relief of feedback and other adaptations over time.

Around a similar time, another group reported PI3Ki-induced down-regulation of ERK phosphorylation (Ebi, Costa et al. 2013). Early clinical trial reports have found that PI3K inhibition sometimes led to suppression of MEK/ERK signalling (King, Mattaliano et al. 1997). Several studies have in fact shown that inhibition of PI3K signalling by AKT and mTOR inhibitors actually triggered activation of the MEK/ERK signalling in many cancer types and such feedback activation may impair sensitivity to PI3K pathway inhibitors (Carracedo, Ma et al. 2008, Faber, Li et al. 2009, Chandarlapaty, Sawai et al. 2011, Serra, Scaltriti et al. 2011).These findings demonstrate the differential effect that targeting different nodes in the PI3K pathway can elicit, as these studies all used AKT and mTOR inhibitors, thus highlighting the importance of targeting the node that leads to least unwanted feedback inhibition in the PI3K pathway.

Our findings together with the findings in the studies mentioned above, reveal the importance of understanding the signalling changes in response to pathway inhibition, even the pathway adaptions which are transient. A better understanding of drug-induced network adaptations, such as the PI3Ki-induced transient p-ERK inhibition observed here, will be important in guiding effective treatment strategies by limiting adaptive bypass mechanisms. Indeed, Qin et al. (Will, Qin et al. 2014) revealed that combined MEK and AKT inhibition induced cell death, and in murine models of $HER2^{+}$ cancer, either intermittent PI3K inhibition or combined MEK-AKT inhibition had potent anti-tumour activity, including tumour regression. These findings, in particular the *in vivo* data, suggest that periodic target inhibition is sufficient for effective anti-tumour activity rather than continuous inhibition which is currently the treatment strategy that dominates the development of these drugs in the clinic. They suggested that transient PI3K inhibition was more effective because of the limited relief of feedback and reactivation of upstream signalling due to the shorter inhibition time of the target. Thus, pulsatile schedules of inhibitors of key reactivated RTKs and administering them in combinations at high doses could be a promising alternative treatment strategy. This approach may allow more effective PI3K

pathway inhibition without excessive toxicity or chronic feedback reactivation of receptors, both of which frequently occur with continuous target inhibition.

5.1.4 PTEN negatively regulates STAT3

Unexpectedly and interestingly following our characterisation experiments, we found increased expression and Tyr705 phosphorylation of STAT3 in the MCF10A PTEN KO clones, which were significantly higher compared to parental MCF10A cells. Phosphorylation of STAT on the Tyr705 site is important for cell migration, invasion and anchorage-independent growth (Vultur, Cao et al. 2004). Our findings that loss of PTEN increases STAT3 activity suggest that in normal mammary epithelial cells PTEN loss contributes to the transformation of these cells, not only by upregulated PI3K signalling, but also by STAT3 activation. Furthermore, under normal physiological conditions PTEN may act to negatively regulate STAT3 in breast cells.

STAT3 is a member of the STAT family of transcription factors which is comprised of 6 other members; STAT1, STAT2, STAT4, STAT5a, STAT5b, and STAT6, all sharing high similarity in structure and function (Bousoik and Montazeri Aliabadi 2018). In 1994, STAT3 was initially discovered to bind to DNA in response to interleukin-6 (IL-6) and EGF (Zhong, Wen et al. 1994). Since then STAT3 has become one of the most investigated oncogenic transcription factors (Bromberg, Wrzeszczynska et al. 1999, Ling and Arlinghaus 2005, Yu, Lee et al. 2014). STAT3 is significantly linked with driving tumour development, angiogenesis, migration, invasion and chemoresistance by regulating the expression of its downstream target genes involved in functions such as cell survival, proliferation, cell cycle progression, anti-apoptosis, immunosuppression, stem cell self-renewal and differentiation (Huynh, Chand et al. 2019). Moreover, the JAK/STAT3 signalling pathway is a driver of cell proliferation and has been shown to be necessary for the growth of stem-like cancer cells in various tumours, including breast cancer (Marotta, Almendro et al. 2011).

STAT3 is persistently tyrosine phosphorylated and constitutively activated in clinical samples from a wide range of cancer types, including breast, lung and prostrate as well as in melanoma, leukemia, and lymphoma, further indicating that STAT3 activity plays a critical role in cell survival and growth (Yu and Jove 2004). A study in 2017 using omics approaches to characterise a large, panel of breast cancer cell lines which are commonly employed in research including 18 TNBC cell lines, found increased phosphorylation of STAT3 (Tyr705) across most cell lines regardless of breast cancer subtype (Smith, Mellor et al. 2017) indicating the high frequency of STAT3 activation in breast cancer cells. Importantly, a study last year showed that STAT3 is overexpressed and constitutively activated in TNBC cells and contributes to TNBC initiation, progression, metastasis, resistance to chemotherapy, and to poor survival outcomes (Sirkisoon, Carpenter et al. 2018). The study found that p-STAT3 (Tyr705), glioma oncogene homolog (GLI1), and truncated GLI1 are co-overexpressed in the majority of triple-negative breast carcinomas (64%) and HER2-enriched (68%) breast carcinomas, and in lymph node metastases

(65%). Gene enrichment analysis of 710 breast tumours showed that STAT3 activation and GLI1/tGLI1 activation signatures are co-enriched in TNBC and HER2-enriched breast cancer, but not in luminal subtypes of breast cancers (Sirkisoon, Carpenter et al. 2018). Moreover, recent evidence from both preclinical and clinical studies has demonstrated that STAT3 plays a critical role in TNBC and STAT3 inhibitors have shown some efficacy in inhibiting TNBC tumour growth and metastasis (Huynh, Etemadi et al. 2017, Qin, Yan et al. 2019). Together these studies emphasise the importance of STAT3 in breast cancer, in particular in TNBC.

Importantly, a study in using a side population of the MCF7 breast cancer cells line enriched in cancer stem-like cells identified PTEN as a as a negative regulator of both STAT3 and mTOR signalling (Zhou, Wulfkuhle et al. 2007). In this MCF7 model for cancer stem-like cells PTEN KD by shRNA increased mTOR, p-mTOR (S2448), STAT3, and phosphorylated STAT3 (S727) expression. mTOR signalling was shown to positively regulate the STAT3 pathway in this model. Through the use of pathway specific inhibitors, selected gene knockdown, and an *in vivo* tumourigenicity assay the authors found the existence of a PTEN/mTOR/STAT3 pro-survival signalling pathway which was required for cancer stem-like cell viability and maintenance. Although, further validation of cancer stem cells isolated from patient specimens is needed in future studies this study clearly supports a role for PTEN as a negative regulator of STAT3 in breast cancer cells.

In addition, to the above study in breast cancer which showed PTEN negatively regulated STAT3, regulatory links between STAT3 and PTEN has been observed in other cancer types, such as a type of brain cancer know as glioblastoma (Moon, Kim et al. 2013) and in other diseases such as human papillomavirus (Sun and Steinberg 2002) and possibly diabetes mellitus (Weng, Zhao et al. 2019). In a 2002 study PTEN was shown to negatively regulate STAT3 activation, but this was in HPV-infected papilloma cells PTEN (Sun and Steinberg 2002). Immunodepletion of PTEN in papilloma extracts using PTEN antibodies resulted in decreased phosphorylated STAT3 (Tyr705) phosphatase activity. The authors showed that PTEN mediated STAT3 (Tyr705) dephosphorylation *in vitro*, and PTEN overexpression in HeLa cells led to a robust decrease in activated STAT3. The authors posited that in these HPV-infected papilloma cells induction of PTEN and reduction of p-STAT3 (Tyr705) might function as part of a host defence mechanism or a virus-directed strategy to alter normal epithelial differentiation programming (Sun and Steinberg 2002).

Kim et al. (Moon, Kim et al. 2013) identified STAT3 and AKT signalling pathways as downstream targets of PTEN since ectopic expression of PTEN in a glioblastoma cell line disrupted p-AKT (Ser473) and pSTAT3 (Tyr705) expression, the same phospho sites examined in this thesis. In addition, PTEN expression suppressed the glioblastoma stem cell (GSC) population and furthermore, inhibited cell proliferation and induced senescence, reducing tumourigenicity both *in vitro* and *in vivo*. This study provides a mechanism by which PTEN modulates cell proliferation, senescence and maintenance of the

GSC population and this is mechanistic link was mediated by PTEN perturbation of AKT and STAT3 signals. Therefore, demonstrating a role for PTEN in regulating STAT3 activity.

Paradoxically, in view of the reported oncogenic function of STAT3, and in contrast to the study by Kim et al. another group identified an unexpected PTEN-regulated STAT3 tumour suppressive function in astrocytes (de la Iglesia, Konopka et al. 2008). However, they showed that in fact depending on the mutational status of the tumour, STAT3 plays distinct roles in cell transformation, acting as either a pro-oncogene or tumour-suppressor. Using gene knockout studies, they showed that in the PTEN pathway STAT3 suppresses malignant transformation of astrocytes which is a key step in the development of glioblastoma. STAT3 KO promoted astrocyte proliferation and invasiveness, and upon PTEN KD strongly enhanced tumourigenesis. PTEN KD and consequent AKT activation inhibited FOXO-dependent transcription of leukemia inhibitory factor receptor β (LIFRβ) which led to suppression of LIFRβ–STAT3 signalling pathway in astrocytes as LIFRβ is a FOXO target gene. Thus, PTEN deficiency led to STAT3 inactivation and malignant transformation. In striking contrast, STAT3 also had a pro-oncogenic role when the oncoprotein EGFR type III variant (EGFRvIII) was present in the tumour (de la Iglesia, Konopka et al. 2008). EGFRvIII is a common mutant isoform of EGFR in glioblastomas and results in constitutively active EGFR form (Moscatello, Montgomery et al. 1996) which induces malignancy of glial cells (Bachoo, Maher et al. 2002). In this study, Konopka et al. found STAT3 associated with EGFRvIII in the nucleus and in doing so induced glial transformation. RT–PCR assays showed that EGFRvIII expression in astrocytes stimulated inducible NO synthase (de la Iglesia, Konopka et al. 2008). Although this data was not shown by the authors. In addition, STAT3 knockout led to a significant reduction in the number of EGFRvIII-expressing astrocytes. Together these findings highlight the complexity of STAT3's function and show that STAT3 acts in a context-specific manner, playing opposing roles in cell transformation depending on the genetic background of the tumour and subsequent oncogenic environment.

This year another paper found a link between STAT3 and PTEN again in a different context, this time in β-cell dysfunction and apoptosis (Weng, Zhao et al. 2019). In diabetes mellitus insulin-producing β-cells are destroyed, but the molecular mechanisms underlying this are complex and poorly defined. Weng et al. showed that STAT3 was involved in the negative regulation of PTEN-AKT signalling pathway associated with β-cell dysfunction and apoptosis (Weng, Zhao et al. 2019). STAT3 activation intensely and specifically inhibited β-cells under hyperglycaemic conditions and STAT3 loss by KO in mouse β-cells, sensitized mice to three low doses of streptozotocin-stimulation. STAT3 deficiency induced an increase in PTEN which repressed AKT activity promoting apoptotic signalling, and finally inducing β-cell apoptosis. PTEN inhibitor treatment completely rescued defective secretion of insulin and β-cells apoptosis in these STAT3-null islets. Thus, in this study STAT3 was again acting as a negative regulator of PTEN.

Together the above studies link PTEN loss and STAT3 upregulation in a range of different diseases, including brain cancer and breast cancer. Considering the widespread role of PTEN as a negative regulator of STAT3, suggests this relationship is important in many disease contexts. Thus, it is clear that further investigation into how PTEN loss in the setting of breast cancer may be leading to the observed upregulation of p-STAT3 in our PTEN KO model needs to be carried out. Furthermore, future work here should determine the functional role STAT3 is playing in the PTEN KO clones. Is it acting as an oncogene and in addition to the elevated PI3K signalling in the KO cells, further assisting in driving cell survival and growth through the JAK/STAT pathway? Additionally, is STAT3 playing a role in the reduced responsiveness to PI3K inhibition? These are all valid questions that require further research and functional studies to address.

5.1.5 Conclusion and future directions

It is becoming increasingly evident that a form of acquired drug resistance known as 'adaptive resistance' is a common cause of treatment failure and patient relapse in many cancers. Therefore, studying these underlying mechanisms of cancer drug resistance is key to identifying new drug targets, and assisting with the discovery of predictive and synergistic drug combinations to improve therapeutic outcomes. To address the complexities of drug response and signalling crosstalk, our research combined experimental investigations in the lab with mathematical modelling. This integrative systems-based approach has emerged as a powerful method to capture network dynamics, allowing a quantitative understanding of the complex drug-induced network re-wiring.

In this work we focused on investigating how loss of the tumour suppressor PTEN influences PI3K-ERK signalling and the response to PI3K and MEK inhibition. We achieved this by generating genetically modified MCF10A cells in which only PTEN was perturbed. Our findings showed that loss of PTEN led to increased PI3K signalling as shown by upregulation of phosphorylated AKT. Importantly, we found that PTEN loss resulted in reduced responsiveness to the selective PI3Kα isoform inhibitor BYL719 as demonstrated by reduced target inhibition and by increased cell viability compared to the WT MCF10A cells. Importantly, it was demonstrated that PTEN loss was driving this decreased sensitivity to PI3K inhibition as reintroduction of PTEN by transfection into the PTEN KO clones re-sensitized the cells to BYL719 treatment.

Interestingly, the known oncogene STAT3 was also elevated in the PTEN KO cells, suggesting it may play a role in this reduced responsiveness to PI3K inhibition by further amplifying the pro-survival signalling. In response to PI3K inhibition ERK was transiently suppressed, but reactivated after 6 h of BYL treatment and this was observed irrespective of PTEN status, suggesting this is a PTEN-independent phenomenon. Thus, we have demonstrated that inhibition of the PI3K pathway perturbed the MAPK/ERK signalling, but targeting the MAPK pathway with MEK inhibition did not perturb the

PI3K signalling pathway. Together, this data highlights the complexity of crosstalk between the two pathways and shows that this crosstalk is not always bidirectional, i.e. perturbation of PI3K pathway affected ERK signalling, but the reverse was not the case, implying unidirectional crosstalk.

Furthermore, it was found that PTEN loss as a single event was insufficient for cells to switch to the PI3Kβ as the dominant isoform in driving PI3K signalling. Instead, the cells harbouring PTEN loss following KO retained the PI3Kα isoform dominance of the parental MCF10A cells. Finally, we found that dual PI3Kα and β inhibition was highly synergistic in suppressing PI3K activity and reducing cell viability compared to single treatment with either isoform-selective inhibitor in both the WT and PTEN KO cells, as well as the TNBC cell lines, suggesting PTEN loss alone did not influence this synergistic response. In conclusion, the work in this thesis provides novel-systems level insights into the crosstalk between PI3K and ERK signalling, and demonstrates how common genetic alterations in cancer such as PTEN loss might influence such crosstalk to modulate the response to kinase inhibitors targeting these pathways. The mathematical model generated in this work further provides a quantitative framework for future investigations of adaptive drug responses and combination therapies related to PI3K-ERK signalling. The developed quantitative model could be, in the future, exploited to make predictions on novel effective drug combinations with kinase inhibitors. Thus, together these findings provide a potential platform for optimising treatment strategies for breast cancer patients, in particular the aggressive subtype TNBC.

Future investigations should utilise the tools of mass spectrometry and RNA-seq to capture a more global network understanding into the changes resulting from PTEN loss and untangle the possible changes to kinase inhibition as a result. In addition, future work should perform more functional assays e.g. cell proliferation assays, soft agar migration assays, invasion assays etc. to further elucidate the effect of PTEN loss at the functional level in response to pathway inhibitors. In addition, *In vivo* studies should be conducted to confirm any *in vitro* findings. Due to time constraints not all the experimental findings were examined by the model we generated. Notably, a network-level explanation for the higher levels of activated STAT3 upon PTEN KO was not investigated by the model. Thus, future versions of the model should incorporate STAT3 signalling and also the insulin receptor as this is the key upstream receptor of the PI3K signalling pathway.

Supplementary Figures

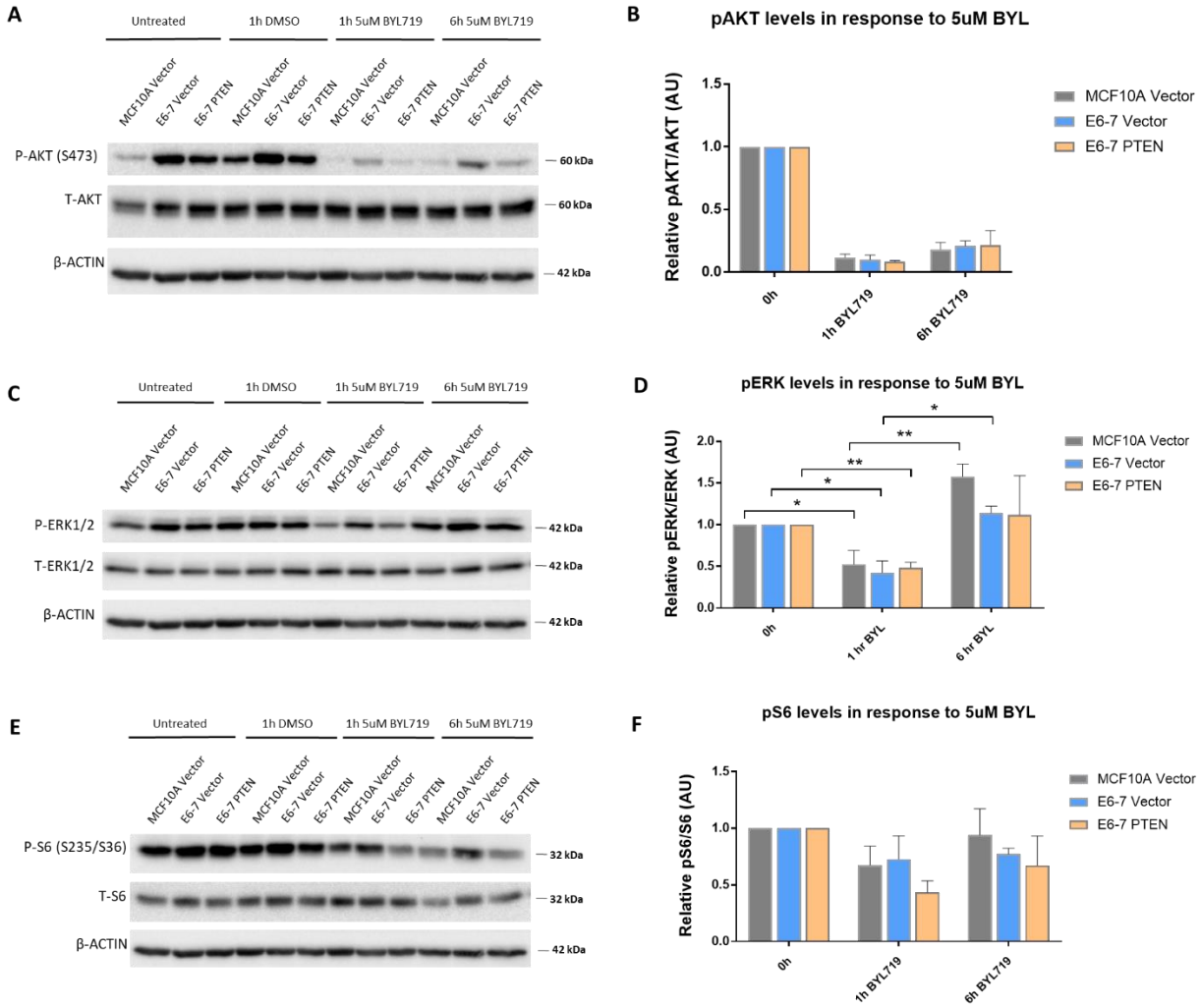

Figure S6.1 The influence of PTEN on PI3K and MAPK signalling in response to 48 h PI3K inhibition in WT MCF10A cells, E6-7 PTEN KO cells, and in transient PTEN re-expressing E6-7 cells. Representative western blots following 24 h transfection with either PTEN or empty vector of the total and phospho protein expression levels of AKT (**A**) ERK1/2 (**C**) and S6 levels (**E**) in WT MCF10As, E6-7 PTEN KO clone in response to 5 µM BYL719 treatment for 1 and 6 h. Graphs showing relative p-AKT (**B**) p-ERK (**D**) and p-S6 **(F**) levels. Protein levels were quantified by densitometry and the data (both total and phospho protein) was normalised to their corresponding β-actin loading control (representative blots shown here) and then to total levels to obtain relative phospho levels. Relative protein levels were then normalised relative to untreated=1. Data is represented as the mean values ± standard error of the mean of three independent biological replicates. Paired two-tailed *t*–test was used and statistical significance was considered at $P < 0.05$. * = $P < 0.05$, ** = $P < 0.01$. AU (arbitrary units).

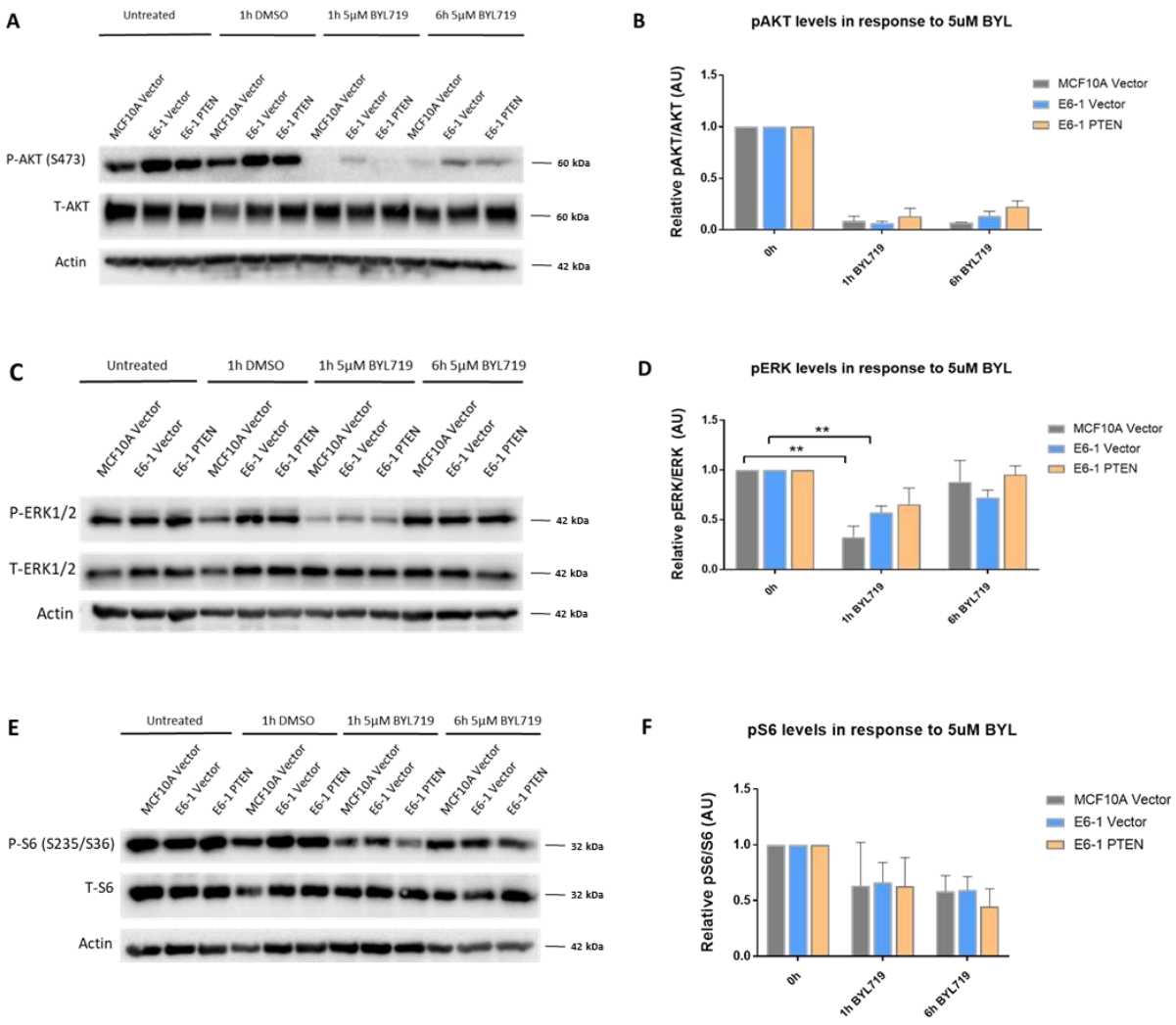

Figure S6.2 The influence of PTEN on PI3K and MAPK signalling in response to 48 h PI3K inhibition in WT MCF10A cells, E6-1 PTEN KO cells, and in transient PTEN re-expressing E6-1 cells. Representative western blots following 24 h transfection with either PTEN or empty vector of the total and phospho protein expression levels of AKT (**A**) ERK1/2 (**C**) and S6 levels (**E**) in WT MCF10As, E6-1 PTEN KO clone in response to 5 μM BYL719 treatment for 1 and 6 h. Graphs showing relative p-AKT (**B**) p-ERK (**D**) and p-S6 **(F**) levels. Protein levels were quantified by densitometry and the data (both total and phospho protein) was normalised to their corresponding β-actin loading control (representative blots shown here) and then to total levels to obtain relative phospho levels. Relative protein levels were then normalised relative to untreated=1. Data is represented as the mean values ± standard error of the mean of three independent biological replicates. Paired two-tailed *t*–test was used and statistical significance was considered at $P < 0.05$. * = $P < 0.05$, ** = $P < 0.01$. AU (arbitrary units).

References

Abe, M., Y. Kuroda, M. Hirose, Y. Watanabe, M. Nakano and T. Handa (2006). "Inhibition of autophosphorylation of epidermal growth factor receptor by small peptides in vitro." Br J Pharmacol **147**(4): 402-411.

Abramson, V. G., M. Cooper Lloyd, T. Ballinger, M. E. Sanders, L. Du, D. Lai, Z. Su, I. Mayer, M. Levy, D. R. LaFrance, C. L. Vnencak-Jones, Y. Shyr, K. B. Dahlman, W. Pao and C. L. Arteaga (2014). "Characterization of breast cancers with PI3K mutations in an academic practice setting using SNaPshot profiling." Breast Cancer Res Treat **145**(2): 389-399.

Adjei, A. A., R. B. Cohen, W. Franklin, C. Morris, D. Wilson, J. R. Molina, L. J. Hanson, L. Gore, L. Chow, S. Leong, L. Maloney, G. Gordon, H. Simmons, A. Marlow, K. Litwiler, S. Brown, G. Poch, K. Kane, J. Haney and S. G. Eckhardt (2008). "Phase I pharmacokinetic and pharmacodynamic study of the oral, small-molecule mitogen-activated protein kinase kinase 1/2 inhibitor AZD6244 (ARRY-142886) in patients with advanced cancers." J Clin Oncol **26**(13): 2139-2146.

Al-Khouri, A. M., Y. Ma, S. H. Togo, S. Williams and T. Mustelin (2005). "Cooperative phosphorylation of the tumor suppressor phosphatase and tensin homologue (PTEN) by casein kinases and glycogen synthase kinase 3beta." J Biol Chem **280**(42): 35195-35202.

Amirikia, K. C., P. Mills, J. Bush and L. A. Newman (2011). "Higher population-based incidence rates of triple-negative breast cancer among young African-American women : Implications for breast cancer screening recommendations." Cancer **117**(12): 2747-2753.

Anders, C. K. and L. A. Carey (2009). "Biology, metastatic patterns, and treatment of patients with triple-negative breast cancer." Clin Breast Cancer **9 Suppl 2**: S73-81.

Andre, F., E. Ciruelos, G. Rubovszky, M. Campone, S. Loibl, H. S. Rugo, H. Iwata, P. Conte, I. A. Mayer, B. Kaufman, T. Yamashita, Y. S. Lu, K. Inoue, M. Takahashi, Z. Papai, A. S. Longin, D. Mills, C. Wilke, S. Hirawat, D. Juric and S.-S. Group (2019). "Alpelisib for PIK3CA-Mutated, Hormone Receptor-Positive Advanced Breast Cancer." N Engl J Med **380**(20): 1929-1940.

Bachman, K. E., P. Argani, Y. Samuels, N. Silliman, J. Ptak, S. Szabo, H. Konishi, B. Karakas, B. G. Blair, C. Lin, B. A. Peters, V. E. Velculescu and B. H. Park (2004). "The PIK3CA gene is mutated with high frequency in human breast cancers." Cancer Biol Ther **3**(8): 772-775.

Bachoo, R. M., E. A. Maher, K. L. Ligon, N. E. Sharpless, S. S. Chan, M. J. You, Y. Tang, J. DeFrances, E. Stover, R. Weissleder, D. H. Rowitch, D. N. Louis and R. A. DePinho (2002). "Epidermal growth factor receptor and Ink4a/Arf: convergent mechanisms governing terminal differentiation and transformation along the neural stem cell to astrocyte axis." Cancer Cell **1**(3): 269-277.

Barlaam, B., S. Cosulich, S. Degorce, M. Fitzek, S. Green, U. Hancox, C. Lambert-van der Brempt, J.-J. Lohmann, M. Maudet, R. Morgentin, M.-J. Pasquet, A. Péru, P. Plé, T. Saleh, M. Vautier, M. Walker, L. Ward and N. Warin (2015). "Discovery of (R)-8-(1-(3,5-Difluorophenylamino)ethyl)-N,N-dimethyl-2-morpholino-4-oxo-4H-chromene-6-carboxamide (AZD8186): A Potent and Selective Inhibitor of PI3Kβ and PI3Kδ for the Treatment of PTEN-Deficient Cancers." Journal of Medicinal Chemistry **58**(2): 943-962.

Batzer, A. G., D. Rotin, J. M. Urena, E. Y. Skolnik and J. Schlessinger (1994). "Hierarchy of binding sites for Grb2 and Shc on the epidermal growth factor receptor." Mol Cell Biol **14**(8): 5192-5201.

Bedard, P. L., M. A. Davies, S. Kopetz, D. Juric, G. I. Shapiro, J. J. Luke, A. Spreafico, B. Wu, C. Castell, C. Gomez, S. Cartot-Cotton, F. Mazuir, M. Dubar, S. Micallef, B. Demers and K. T. Flaherty (2018). "First-in-human trial of the PI3Kbeta-selective inhibitor SAR260301 in patients with advanced solid tumors." Cancer **124**(2): 315-324.

Beg, S., A. K. Siraj, S. Prabhakaran, Z. Jehan, D. Ajarim, F. Al-Dayel, A. Tulbah and K. S. Al-Kuraya (2015). "Loss of PTEN expression is associated with aggressive behavior and poor prognosis in Middle Eastern triple-negative breast cancer." Breast Cancer Res Treat **151**(3): 541-553.

Bellacosa, A., T. O. Chan, N. N. Ahmed, K. Datta, S. Malstrom, D. Stokoe, F. McCormick, J. Feng and P. Tsichlis (1998). "Akt activation by growth factors is a multiple-step process: the role of the PH domain." Oncogene **17**(3): 313-325.

Bouhaddou, M., A. M. Barrette, A. D. Stern, R. J. Koch, M. S. DiStefano, E. A. Riesel, L. C. Santos, A. L. Tan, A. E. Mertz and M. R. Birtwistle (2018). "A mechanistic pan-cancer pathway model informed by multi-omics data interprets stochastic cell fate responses to drugs and mitogens." PLoS Comput Biol **14**(3): e1005985.

Bousoik, E. and H. Montazeri Aliabadi (2018). ""Do We Know Jack" About JAK? A Closer Look at JAK/STAT Signaling Pathway." Front Oncol **8**: 287.

Brenton, J. D., S. A. Aparicio and C. Caldas (2001). "Molecular profiling of breast cancer: portraits but not physiognomy." Breast Cancer Res **3**(2): 77-80.

Britschgi, A., R. Andraos, H. Brinkhaus, I. Klebba, V. Romanet, U. Muller, M. Murakami, T. Radimerski and M. Bentires-Alj (2012). "JAK2/STAT5 inhibition circumvents resistance to PI3K/mTOR blockade: a rationale for cotargeting these pathways in metastatic breast cancer." Cancer Cell **22**(6): 796-811.

Bromberg, J. F., M. H. Wrzeszczynska, G. Devgan, Y. Zhao, R. G. Pestell, C. Albanese and J. E. Darnell, Jr. (1999). "Stat3 as an oncogene." Cell **98**(3): 295-303.

Brunet, A., A. Bonni, M. J. Zigmond, M. Z. Lin, P. Juo, L. S. Hu, M. J. Anderson, K. C. Arden, J. Blenis and M. E. Greenberg (1999). "Akt promotes cell survival by phosphorylating and inhibiting a Forkhead transcription factor." Cell **96**(6): 857-868.

Byrne, K. M., N. Monsefi, J. C. Dawson, A. Degasperi, J. C. Bukowski-Wills, N. Volinsky, M. Dobrzynski, M. R. Birtwistle, M. A. Tsyganov, A. Kiyatkin, K. Kida, A. J. Finch, N. O. Carragher, W. Kolch, L. K. Nguyen, A. von Kriegsheim and B. N. Kholodenko (2016). "Bistability in the Rac1, PAK, and RhoA Signaling Network Drives Actin Cytoskeleton Dynamics and Cell Motility Switches." Cell Syst **2**(1): 38-48.

Cancer Genome Atlas, N. (2012). "Comprehensive molecular portraits of human breast tumours." Nature **490**(7418): 61-70.

Carey, L. A., C. M. Perou, C. A. Livasy, L. G. Dressler, D. Cowan, K. Conway, G. Karaca, M. A. Troester, C. K. Tse, S. Edmiston, S. L. Deming, J. Geradts, M. C. Cheang, T. O. Nielsen, P. G. Moorman, H. S. Earp and R. C. Millikan (2006). "Race, breast cancer subtypes, and survival in the Carolina Breast Cancer Study." JAMA **295**(21): 2492-2502.

Carracedo, A., L. Ma, J. Teruya-Feldstein, F. Rojo, L. Salmena, A. Alimonti, A. Egia, A. T. Sasaki, G. Thomas, S. C. Kozma, A. Papa, C. Nardella, L. C. Cantley, J. Baselga and P. P. Pandolfi (2008). "Inhibition of mTORC1 leads to MAPK pathway activation through a PI3K-dependent feedback loop in human cancer." J Clin Invest **118**(9): 3065-3074.

Casci, T., J. Vinos and M. Freeman (1999). "Sprouty, an intracellular inhibitor of Ras signaling." Cell **96**(5): 655-665.

Chagpar, R. B., P. H. Links, M. C. Pastor, L. A. Furber, A. D. Hawrysh, M. D. Chamberlain and D. H. Anderson (2010). "Direct positive regulation of PTEN by the p85 subunit of phosphatidylinositol 3-kinase." Proc Natl Acad Sci U S A **107**(12): 5471-5476.

Chakrabarty, A., B. N. Rexer, S. E. Wang, R. S. Cook, J. A. Engelman and C. L. Arteaga (2010). "H1047R phosphatidylinositol 3-kinase mutant enhances HER2-mediated transformation by heregulin production and activation of HER3." Oncogene **29**(37): 5193-5203.

Chakrabarty, A., V. Sanchez, M. G. Kuba, C. Rinehart and C. L. Arteaga (2012). "Feedback upregulation of HER3 (ErbB3) expression and activity attenuates antitumor effect of PI3K inhibitors." Proc Natl Acad Sci U S A **109**(8): 2718-2723.

Chalhoub, N. and S. J. Baker (2009). "PTEN and the PI3-kinase pathway in cancer." Annu Rev Pathol **4**: 127-150.

Chandarlapaty, S., A. Sawai, M. Scaltriti, V. Rodrik-Outmezguine, O. Grbovic-Huezo, V. Serra, P. K. Majumder, J. Baselga and N. Rosen (2011). "AKT inhibition relieves feedback suppression of receptor tyrosine kinase expression and activity." Cancer Cell **19**(1): 58-71.

Chavez, K. J., S. V. Garimella and S. Lipkowitz (2010). "Triple negative breast cancer cell lines: one tool in the search for better treatment of triple negative breast cancer." Breast Dis **32**(1-2): 35-48.

Chell, V., K. Balmanno, A. S. Little, M. Wilson, S. Andrews, L. Blockley, M. Hampson, P. R. Gavine and S. J. Cook (2013). "Tumour cell responses to new fibroblast growth factor receptor tyrosine kinase inhibitors and identification of a gatekeeper mutation in FGFR3 as a mechanism of acquired resistance." Oncogene **32**(25): 3059-3070.

Cheng, H., P. Liu, C. Ohlson, E. Xu, L. Symonds, A. Isabella, W. J. Muller, N. U. Lin, I. E. Krop, T. M. Roberts, E. P. Winer, C. L. Arteaga and J. J. Zhao (2016). "PIK3CA(H1047R)- and Her2-initiated mammary tumors escape PI3K dependency by compensatory activation of MEK-ERK signaling." Oncogene **35**(23): 2961-2970.

Chikh, A., R. Ferro, J. J. Abbott, R. Pineiro, R. Buus, M. Iezzi, F. Ricci, D. Bergamaschi, P. Ostano, G. Chiorino, R. Lattanzio, M. Broggini, M. Piantelli, T. Maffucci and M. Falasca (2016). "Class II phosphoinositide 3-kinase C2beta regulates a novel signaling pathway involved in breast cancer progression." Oncotarget **7**(14): 18325-18345.

Chou, T. C. (2010). "Drug combination studies and their synergy quantification using the Chou-Talalay method." Cancer Res **70**(2): 440-446.

Chu, V. T., T. Weber, B. Wefers, W. Wurst, S. Sander, K. Rajewsky and R. Kuhn (2015). "Increasing the efficiency of homology-directed repair for CRISPR-Cas9-induced precise gene editing in mammalian cells." Nat Biotechnol **33**(5): 543-548.

Cintra, J. R., M. T. Teixeira, R. W. Diniz, H. Goncalves Junior, T. M. Florentino, G. F. Freitas, L. R. Oliveira, M. T. Neves, T. Pereira and M. R. Guerra (2012). "Immunohistochemical profile and clinical-pathological variables in breast cancer." Rev Assoc Med Bras (1992) **58**(2): 178-187.

Ciraolo, E., M. Iezzi, R. Marone, S. Marengo, C. Curcio, C. Costa, O. Azzolino, C. Gonella, C. Rubinetto, H. Wu, W. Dastru, E. L. Martin, L. Silengo, F. Altruda, E. Turco, L. Lanzetti, P. Musiani, T. Ruckle, C. Rommel, J. M. Backer, G. Forni, M. P. Wymann and E. Hirsch (2008). "Phosphoinositide 3-kinase p110beta activity: key role in metabolism and mammary gland cancer but not development." Sci Signal **1**(36): ra3.

Ciuffreda, L., C. Di Sanza, U. Cesta Incani, A. Eramo, M. Desideri, F. Biagioni, D. Passeri, I. Falcone, G. Sette, P. Bergamo, A. Anichini, K. Sabapathy, J. A. McCubrey, M. R. Ricciardi, A. Tafuri, G. Blandino, A. Orlandi, R. De Maria, F. Cognetti, D. Del Bufalo and M. Milella (2012). "The mitogen-activated protein kinase (MAPK) cascade controls phosphatase and tensin homolog (PTEN) expression through multiple mechanisms." J Mol Med (Berl) **90**(6): 667-679.

Claas, A. M., L. Atta, S. Gordonov, A. S. Meyer and D. A. Lauffenburger (2018). "Systems Modeling Identifies Divergent Receptor Tyrosine Kinase Reprogramming to MAPK Pathway Inhibition." Cell Mol Bioeng **11**(6): 451-469.

Corkery, B., J. Crown, M. Clynes and N. O'Donovan (2009). "Epidermal growth factor receptor as a potential therapeutic target in triple-negative breast cancer." Ann Oncol **20**(5): 862-867.

Cossu-Rocca, P., S. Orru, M. R. Muroni, F. Sanges, G. Sotgiu, S. Ena, G. Pira, L. Murgia, A. Manca, M. G. Uras, M. G. Sarobba, S. Urru and M. R. De Miglio (2015). "Analysis of PIK3CA Mutations and Activation Pathways in Triple Negative Breast Cancer." PLoS One **10**(11): e0141763.

Costa, C., H. Ebi, M. Martini, S. A. Beausoleil, A. C. Faber, C. T. Jakubik, A. Huang, Y. Wang, M. Nishtala, B. Hall, K. Rikova, J. Zhao, E. Hirsch, C. H. Benes and J. A. Engelman (2015). "Measurement of PIP3 levels reveals an unexpected role for p110beta in early adaptive responses to p110alpha-specific inhibitors in luminal breast cancer." Cancer Cell **27**(1): 97-108.

Crown, J., J. O'Shaughnessy and G. Gullo (2012). "Emerging targeted therapies in triple-negative breast cancer." Ann Oncol **23 Suppl 6**: vi56-65.

Csermely, P., V. Agoston and S. Pongor (2005). "The efficiency of multi-target drugs: the network approach might help drug design." Trends Pharmacol Sci **26**(4): 178-182.

Davies, H., G. R. Bignell, C. Cox, P. Stephens, S. Edkins, S. Clegg, J. Teague, H. Woffendin, M. J. Garnett, W. Bottomley, N. Davis, E. Dicks, R. Ewing, Y. Floyd, K. Gray, S. Hall, R. Hawes, J.

Hughes, V. Kosmidou, A. Menzies, C. Mould, A. Parker, C. Stevens, S. Watt, S. Hooper, R. Wilson, H. Jayatilake, B. A. Gusterson, C. Cooper, J. Shipley, D. Hargrave, K. Pritchard-Jones, N. Maitland, G. Chenevix-Trench, G. J. Riggins, D. D. Bigner, G. Palmieri, A. Cossu, A. Flanagan, A. Nicholson, J. W. Ho, S. Y. Leung, S. T. Yuen, B. L. Weber, H. F. Seigler, T. L. Darrow, H. Paterson, R. Marais, C. J. Marshall, R. Wooster, M. R. Stratton and P. A. Futreal (2002). "Mutations of the BRAF gene in human cancer." Nature **417**(6892): 949-954.

de la Iglesia, N., G. Konopka, S. V. Puram, J. A. Chan, R. M. Bachoo, M. J. You, D. E. Levy, R. A. Depinho and A. Bonni (2008). "Identification of a PTEN-regulated STAT3 brain tumor suppressor pathway." Genes Dev **22**(4): 449-462.

Dent, R., M. Trudeau, K. I. Pritchard, W. M. Hanna, H. K. Kahn, C. A. Sawka, L. A. Lickley, E. Rawlinson, P. Sun and S. A. Narod (2007). "Triple-negative breast cancer: clinical features and patterns of recurrence." Clin Cancer Res **13**(15 Pt 1): 4429-4434.

Depowski, P. L., S. I. Rosenthal and J. S. Ross (2001). "Loss of expression of the PTEN gene protein product is associated with poor outcome in breast cancer." Mod Pathol **14**(7): 672-676.

Dogruluk, T., Y. H. Tsang, M. Espitia, F. Chen, T. Chen, Z. Chong, V. Appadurai, A. Dogruluk, A. K. Eterovic, P. E. Bonnen, C. J. Creighton, K. Chen, G. B. Mills and K. L. Scott (2015). "Identification of Variant-Specific Functions of PIK3CA by Rapid Phenotyping of Rare Mutations." Cancer Res **75**(24): 5341-5354.

Doudna, J. A. and E. Charpentier (2014). "Genome editing. The new frontier of genome engineering with CRISPR-Cas9." Science **346**(6213): 1258096.

Duncan, J. S., M. C. Whittle, K. Nakamura, A. N. Abell, A. A. Midland, J. S. Zawistowski, N. L. Johnson, D. A. Granger, N. V. Jordan, D. B. Darr, J. Usary, P. F. Kuan, D. M. Smalley, B. Major, X. He, K. A. Hoadley, B. Zhou, N. E. Sharpless, C. M. Perou, W. Y. Kim, S. M. Gomez, X. Chen, J. Jin, S. V. Frye, H. S. Earp, L. M. Graves and G. L. Johnson (2012). "Dynamic reprogramming of the kinome in response to targeted MEK inhibition in triple-negative breast cancer." Cell **149**(2): 307-321.

Ebbesen, S. H., M. Scaltriti, C. U. Bialucha, N. Morse, E. R. Kastenhuber, H. Y. Wen, L. E. Dow, J. Baselga and S. W. Lowe (2016). "Pten loss promotes MAPK pathway dependency in HER2/neu breast carcinomas." Proc Natl Acad Sci U S A **113**(11): 3030-3035.

Ebi, H., R. B. Corcoran, A. Singh, Z. Chen, Y. Song, E. Lifshits, D. P. Ryan, J. A. Meyerhardt, C. Benes, J. Settleman, K. K. Wong, L. C. Cantley and J. A. Engelman (2011). "Receptor tyrosine kinases exert dominant control over PI3K signaling in human KRAS mutant colorectal cancers." J Clin Invest **121**(11): 4311-4321.

Ebi, H., C. Costa, A. C. Faber, M. Nishtala, H. Kotani, D. Juric, P. Della Pelle, Y. Song, S. Yano, M. Mino-Kenudson, C. H. Benes and J. A. Engelman (2013). "PI3K regulates MEK/ERK signaling in breast cancer via the Rac-GEF, P-Rex1." Proc Natl Acad Sci U S A **110**(52): 21124-21129.

Eckert, L. B., G. A. Repasky, A. S. Ulku, A. McFall, H. Zhou, C. I. Sartor and C. J. Der (2004). "Involvement of Ras activation in human breast cancer cell signaling, invasion, and anoikis." Cancer Res **64**(13): 4585-4592.

Edgar, K. A., J. J. Wallin, M. Berry, L. B. Lee, W. W. Prior, D. Sampath, L. S. Friedman and M. Belvin (2010). "Isoform-specific phosphoinositide 3-kinase inhibitors exert distinct effects in solid tumors." Cancer Res **70**(3): 1164-1172.

Engelman, J. A. (2009). "Targeting PI3K signalling in cancer: opportunities, challenges and limitations." Nat Rev Cancer **9**(8): 550-562.

Eroglu, Z. and A. Ribas (2016). "Combination therapy with BRAF and MEK inhibitors for melanoma: latest evidence and place in therapy." Ther Adv Med Oncol **8**(1): 48-56.

Faber, A. C., D. Li, Y. Song, M. C. Liang, B. Y. Yeap, R. T. Bronson, E. Lifshits, Z. Chen, S. M. Maira, C. Garcia-Echeverria, K. K. Wong and J. A. Engelman (2009). "Differential induction of apoptosis in HER2 and EGFR addicted cancers following PI3K inhibition." Proc Natl Acad Sci U S A **106**(46): 19503-19508.

Fabian, Z., C. T. Taylor and L. K. Nguyen (2016). "Understanding complexity in the HIF signaling pathway using systems biology and mathematical modeling." J Mol Med (Berl) **94**(4): 377-390.

Falasca, M. and T. Maffucci (2012). "Regulation and cellular functions of class II phosphoinositide 3-kinases." Biochem J **443**(3): 587-601.

Faratian, D., A. Goltsov, G. Lebedeva, A. Sorokin, S. Moodie, P. Mullen, C. Kay, I. H. Um, S. Langdon, I. Goryanin and D. J. Harrison (2009). "Systems biology reveals new strategies for personalizing cancer medicine and confirms the role of PTEN in resistance to trastuzumab." Cancer Res **69**(16): 6713-6720.

Feala, J. D., J. Cortes, P. M. Duxbury, C. Piermarocchi, A. D. McCulloch and G. Paternostro (2010). "Systems approaches and algorithms for discovery of combinatorial therapies." Wiley Interdiscip Rev Syst Biol Med **2**(2): 181-193.

Fey, D., M. Halasz, D. Dreidax, S. P. Kennedy, J. F. Hastings, N. Rauch, A. G. Munoz, R. Pilkington, M. Fischer, F. Westermann, W. Kolch, B. N. Kholodenko and D. R. Croucher (2015). "Signaling pathway models as biomarkers: Patient-specific simulations of JNK activity predict the survival of neuroblastoma patients." Science Signaling **8**(408).

Filmus, J., M. N. Pollak, R. Cailleau and R. N. Buick (1985). "MDA-468, a human breast cancer cell line with a high number of epidermal growth factor (EGF) receptors, has an amplified EGF receptor gene and is growth inhibited by EGF." Biochem Biophys Res Commun **128**(2): 898-905.

Fitzgerald, J. B., B. Schoeberl, U. B. Nielsen and P. K. Sorger (2006). "Systems biology and combination therapy in the quest for clinical efficacy." Nat Chem Biol **2**(9): 458-466.

Forbes, S. A., D. Beare, P. Gunasekaran, K. Leung, N. Bindal, H. Boutselakis, M. Ding, S. Bamford, C. Cole, S. Ward, C. Y. Kok, M. Jia, T. De, J. W. Teague, M. R. Stratton, U. McDermott and P. J. Campbell (2015). "COSMIC: exploring the world's knowledge of somatic mutations in human cancer." Nucleic Acids Res **43**(Database issue): D805-811.

Foukas, L. C., M. Claret, W. Pearce, K. Okkenhaug, S. Meek, E. Peskett, S. Sancho, A. J. Smith, D. J. Withers and B. Vanhaesebroeck (2006). "Critical role for the p110alpha phosphoinositide-3-OH kinase in growth and metabolic regulation." Nature **441**(7091): 366-370.

Fritsch, C., A. Huang, C. Chatenay-Rivauday, C. Schnell, A. Reddy, M. Liu, A. Kauffmann, D. Guthy, D. Erdmann, A. De Pover, P. Furet, H. Gao, S. Ferretti, Y. Wang, J. Trappe, S. M. Brachmann, S. M. Maira, C. Wilson, M. Boehm, C. Garcia-Echeverria, P. Chene, M. Wiesmann, R. Cozens, J. Lehar, R. Schlegel, G. Caravatti, F. Hofmann and W. R. Sellers (2014). "Characterization of the novel and specific PI3Kalpha inhibitor NVP-BYL719 and development of the patient stratification strategy for clinical trials." Mol Cancer Ther **13**(5): 1117-1129.

Fritsch, R., I. de Krijger, K. Fritsch, R. George, B. Reason, M. S. Kumar, M. Diefenbacher, G. Stamp and J. Downward (2013). "RAS and RHO families of GTPases directly regulate distinct phosphoinositide 3-kinase isoforms." Cell **153**(5): 1050-1063.

Fritsche-Guenther, R., F. Witzel, A. Sieber, R. Herr, N. Schmidt, S. Braun, T. Brummer, C. Sers and N. Bluthgen (2011). "Strong negative feedback from Erk to Raf confers robustness to MAPK signalling." Mol Syst Biol **7**: 489.

Furet, P., V. Guagnano, R. A. Fairhurst, P. Imbach-Weese, I. Bruce, M. Knapp, C. Fritsch, F. Blasco, J. Blanz, R. Aichholz, J. Hamon, D. Fabbro and G. Caravatti (2013). "Discovery of NVP-BYL719 a potent and selective phosphatidylinositol-3 kinase alpha inhibitor selected for clinical evaluation." Bioorg Med Chem Lett **23**(13): 3741-3748.

Gajulapalli, V. N. R., V. L. Malisetty, S. K. Chitta and B. Manavathi (2016). "Oestrogen receptor negativity in breast cancer: a cause or consequence?" Biosci Rep **36**(6).

Garcia, R., T. L. Bowman, G. Niu, H. Yu, S. Minton, C. A. Muro-Cacho, C. E. Cox, R. Falcone, R. Fairclough, S. Parsons, A. Laudano, A. Gazit, A. Levitzki, A. Kraker and R. Jove (2001). "Constitutive activation of Stat3 by the Src and JAK tyrosine kinases participates in growth regulation of human breast carcinoma cells." Oncogene **20**(20): 2499-2513.

Garrett, J. T., C. R. Sutton, M. G. Kuba, R. S. Cook and C. L. Arteaga (2013). "Dual blockade of HER2 in HER2-overexpressing tumor cells does not completely eliminate HER3 function." Clin Cancer Res **19**(3): 610-619.

Garrett, J. T., C. R. Sutton, R. Kurupi, C. U. Bialucha, S. A. Ettenberg, S. D. Collins, Q. Sheng, J. Wallweber, L. Defazio-Eli and C. L. Arteaga (2013). "Combination of antibody that inhibits ligand-independent HER3 dimerization and a p110alpha inhibitor potently blocks PI3K signaling and growth of HER2+ breast cancers." Cancer Res **73**(19): 6013-6023.

Gazinska, P., A. Grigoriadis, J. P. Brown, R. R. Millis, A. Mera, C. E. Gillett, L. H. Holmberg, A. N. Tutt and S. E. Pinder (2013). "Comparison of basal-like triple-negative breast cancer defined by morphology, immunohistochemistry and transcriptional profiles." Mod Pathol **26**(7): 955-966.

Gbelcova, H., P. Bakes, P. Priscakova, V. Sisovsky, I. Hojsikova, L. Straka, M. Konecny, J. Markus, C. W. D'Acunto, T. Ruml, D. Bohmer, L. Danihel and V. Repiska (2015). "PTEN sequence analysis in endometrial hyperplasia and endometrial carcinoma in Slovak women." Anal Cell Pathol (Amst) **2015**: 746856.

Gilmartin, A. G., M. R. Bleam, A. Groy, K. G. Moss, E. A. Minthorn, S. G. Kulkarni, C. M. Rominger, S. Erskine, K. E. Fisher, J. Yang, F. Zappacosta, R. Annan, D. Sutton and S. G. Laquerre (2011). "GSK1120212 (JTP-74057) is an inhibitor of MEK activity and activation with favorable pharmacokinetic properties for sustained in vivo pathway inhibition." Clin Cancer Res **17**(5): 989-1000.

Giltnane, J. M. and J. M. Balko (2014). "Rationale for targeting the Ras/MAPK pathway in triple-negative breast cancer." Discov Med **17**(95): 275-283.

Golan-Lavi, R., C. Giacomelli, G. Fuks, A. Zeisel, J. Sonntag, S. Sinha, W. Kostler, S. Wiemann, U. Korf, Y. Yarden and E. Domany (2017). "Coordinated Pulses of mRNA and of Protein Translation or Degradation Produce EGF-Induced Protein Bursts." Cell Rep **18**(13): 3129-3142.

Gorre, M. E., M. Mohammed, K. Ellwood, N. Hsu, R. Paquette, P. N. Rao and C. L. Sawyers (2001). "Clinical resistance to STI-571 cancer therapy caused by BCR-ABL gene mutation or amplification." Science **293**(5531): 876-880.

Guan, K. L., C. Figueroa, T. R. Brtva, T. Zhu, J. Taylor, T. D. Barber and A. B. Vojtek (2000). "Negative regulation of the serine/threonine kinase B-Raf by Akt." J Biol Chem **275**(35): 27354-27359.

Guest, S. T., Z. R. Kratche, J. C. Irish, R. C. Wilson, R. Haddad, J. W. Gray, E. Garrett-Mayer and S. P. Ethier (2016). "Functional oncogene signatures guide rationally designed combination therapies to synergistically induce breast cancer cell death." Oncotarget **7**(24): 36138-36153.

Haffty, B. G., Q. Yang, M. Reiss, T. Kearney, S. A. Higgins, J. Weidhaas, L. Harris, W. Hait and D. Toppmeyer (2006). "Locoregional relapse and distant metastasis in conservatively managed triple negative early-stage breast cancer." J Clin Oncol **24**(36): 5652-5657.

Hanahan, D. and R. A. Weinberg (2011). "Hallmarks of cancer: the next generation." Cell **144**(5): 646-674.

Hancox, U., S. Cosulich, L. Hanson, C. Trigwell, C. Lenaghan, R. Ellston, H. Dry, C. Crafter, B. Barlaam, M. Fitzek, P. D. Smith, D. Ogilvie, C. D'Cruz, L. Castriotta, S. R. Wedge, L. Ward, S. Powell, M. Lawson, B. R. Davies, E. A. Harrington, E. Foster, M. Cumberbatch, S. Green and S. T. Barry (2015). "Inhibition of PI3Kbeta signaling with AZD8186 inhibits growth of PTEN-deficient breast and prostate tumors alone and in combination with docetaxel." Mol Cancer Ther **14**(1): 48-58.

Haruta, T., T. Uno, J. Kawahara, A. Takano, K. Egawa, P. M. Sharma, J. M. Olefsky and M. Kobayashi (2000). "A rapamycin-sensitive pathway down-regulates insulin signaling via phosphorylation and proteasomal degradation of insulin receptor substrate-1." Mol Endocrinol **14**(6): 783-794.

Hay, N. and N. Sonenberg (2004). "Upstream and downstream of mTOR." Genes Dev **18**(16): 1926-1945.

Heinrich, P. C., I. Behrmann, G. Muller-Newen, F. Schaper and L. Graeve (1998). "Interleukin-6-type cytokine signalling through the gp130/Jak/STAT pathway." Biochem J **334 (Pt 2)**: 297-314.

Hemmings, B. A. and D. F. Restuccia (2012). "PI3K-PKB/Akt pathway." Cold Spring Harb Perspect Biol **4**(9): a011189.

Hennessy, B. T., A. M. Gonzalez-Angulo, K. Stemke-Hale, M. Z. Gilcrease, S. Krishnamurthy, J. S. Lee, J. Fridlyand, A. Sahin, R. Agarwal, C. Joy, W. Liu, D. Stivers, K. Baggerly, M. Carey, A.

Lluch, C. Monteagudo, X. He, V. Weigman, C. Fan, J. Palazzo, G. N. Hortobagyi, L. K. Nolden, N. J. Wang, V. Valero, J. W. Gray, C. M. Perou and G. B. Mills (2009). "Characterization of a naturally occurring breast cancer subset enriched in epithelial-to-mesenchymal transition and stem cell characteristics." Cancer Res **69**(10): 4116-4124.

Hoadley, K. A., V. J. Weigman, C. Fan, L. R. Sawyer, X. He, M. A. Troester, C. I. Sartor, T. Rieger-House, P. S. Bernard, L. A. Carey and C. M. Perou (2007). "EGFR associated expression profiles vary with breast tumor subtype." BMC Genomics **8**: 258.

Hoeflich, K. P., C. O'Brien, Z. Boyd, G. Cavet, S. Guerrero, K. Jung, T. Januario, H. Savage, E. Punnoose, T. Truong, W. Zhou, L. Berry, L. Murray, L. Amler, M. Belvin, L. S. Friedman and M. R. Lackner (2009). "In vivo antitumor activity of MEK and phosphatidylinositol 3-kinase inhibitors in basal-like breast cancer models." Clin Cancer Res **15**(14): 4649-4664.

Hollestelle, A., J. H. Nagel, M. Smid, S. Lam, F. Elstrodt, M. Wasielewski, S. S. Ng, P. J. French, J. K. Peeters, M. J. Rozendaal, M. Riaz, D. G. Koopman, T. L. Ten Hagen, B. H. de Leeuw, E. C. Zwarthoff, A. Teunisse, P. J. van der Spek, J. G. Klijn, W. N. Dinjens, S. P. Ethier, H. Clevers, A. G. Jochemsen, M. A. den Bakker, J. A. Foekens, J. W. Martens and M. Schutte (2010). "Distinct gene mutation profiles among luminal-type and basal-type breast cancer cell lines." Breast Cancer Res Treat **121**(1): 53-64.

Holohan, C., S. Van Schaeybroeck, D. B. Longley and P. G. Johnston (2013). "Cancer drug resistance: an evolving paradigm." Nat Rev Cancer **13**(10): 714-726.

Housman, G., S. Byler, S. Heerboth, K. Lapinska, M. Longacre, N. Snyder and S. Sarkar (2014). "Drug resistance in cancer: an overview." Cancers (Basel) **6**(3): 1769-1792.

Huynh, J., A. Chand, D. Gough and M. Ernst (2019). "Therapeutically exploiting STAT3 activity in cancer - using tissue repair as a road map." Nat Rev Cancer **19**(2): 82-96.

Huynh, J., N. Etemadi, F. Hollande, M. Ernst and M. Buchert (2017). "The JAK/STAT3 axis: A comprehensive drug target for solid malignancies." Semin Cancer Biol **45**: 13-22.

Ihle, J. N. (1996). "STATs: signal transducers and activators of transcription." Cell **84**(3): 331-334.

Ishino, Y., H. Shinagawa, K. Makino, M. Amemura and A. Nakata (1987). "Nucleotide sequence of the iap gene, responsible for alkaline phosphatase isozyme conversion in Escherichia coli, and identification of the gene product." J Bacteriol **169**(12): 5429-5433.

Jacinto, E., V. Facchinetti, D. Liu, N. Soto, S. Wei, S. Y. Jung, Q. Huang, J. Qin and B. Su (2006). "SIN1/MIP1 maintains rictor-mTOR complex integrity and regulates Akt phosphorylation and substrate specificity." Cell **127**(1): 125-137.

Jacinto, E. and A. Lorberg (2008). "TOR regulation of AGC kinases in yeast and mammals." Biochem J **410**(1): 19-37.

Janku, F., T. A. Yap and F. Meric-Bernstam (2018). "Targeting the PI3K pathway in cancer: are we making headway?" Nat Rev Clin Oncol **15**(5): 273-291.

Jean, S. and A. A. Kiger (2014). "Classes of phosphoinositide 3-kinases at a glance." J Cell Sci **127**(Pt 5): 923-928.

Jia, S., Z. Liu, S. Zhang, P. Liu, L. Zhang, S. H. Lee, J. Zhang, S. Signoretti, M. Loda, T. M. Roberts and J. J. Zhao (2008). "Essential roles of PI(3)K-p110beta in cell growth, metabolism and tumorigenesis." Nature **454**(7205): 776-779.

Kalimutho, M., K. Parsons, D. Mittal, J. A. Lopez, S. Srihari and K. K. Khanna (2015). "Targeted Therapies for Triple-Negative Breast Cancer: Combating a Stubborn Disease." Trends Pharmacol Sci **36**(12): 822-846.

Kao, J., K. Salari, M. Bocanegra, Y. L. Choi, L. Girard, J. Gandhi, K. A. Kwei, T. Hernandez-Boussard, P. Wang, A. F. Gazdar, J. D. Minna and J. R. Pollack (2009). "Molecular profiling of breast cancer cell lines defines relevant tumor models and provides a resource for cancer gene discovery." PLoS One **4**(7): e6146.

Kawazu, M., T. Ueno, K. Kontani, Y. Ogita, M. Ando, K. Fukumura, A. Yamato, M. Soda, K. Takeuchi, Y. Miki, H. Yamaguchi, T. Yasuda, T. Naoe, Y. Yamashita, T. Katada, Y. L. Choi and H. Mano (2013). "Transforming mutations of RAC guanosine triphosphatases in human cancers." Proc Natl Acad Sci U S A **110**(8): 3029-3034.

King, W. G., M. D. Mattaliano, T. O. Chan, P. N. Tsichlis and J. S. Brugge (1997). "Phosphatidylinositol 3-kinase is required for integrin-stimulated AKT and Raf-1/mitogen-activated protein kinase pathway activation." Mol Cell Biol **17**(8): 4406-4418.

Kirchner, M. and S. Schneider (2015). "CRISPR-Cas: From the Bacterial Adaptive Immune System to a Versatile Tool for Genome Engineering." Angew Chem Int Ed Engl **54**(46): 13508-13514.

Knudsen, E. S., T. F. Pajak, M. Qeenan, A. K. McClendon, B. D. Armon, G. F. Schwartz and A. K. Witkiewicz (2012). "Retinoblastoma and phosphate and tensin homolog tumor suppressors: impact on ductal carcinoma in situ progression." J Natl Cancer Inst **104**(23): 1825-1836.

Kobayashi, S., T. J. Boggon, T. Dayaram, P. A. Janne, O. Kocher, M. Meyerson, B. E. Johnson, M. J. Eck, D. G. Tenen and B. Halmos (2005). "EGFR mutation and resistance of non-small-cell lung cancer to gefitinib." N Engl J Med **352**(8): 786-792.

Kolch, W., M. Calder and D. Gilbert (2005). "When kinases meet mathematics: the systems biology of MAPK signalling." FEBS Lett **579**(8): 1891-1895.

Kolch, W. and D. Fey (2017). "Personalized Computational Models as Biomarkers." J Pers Med **7**(3).

Kolch, W., M. Halasz, M. Granovskaya and B. N. Kholodenko (2015). "The dynamic control of signal transduction networks in cancer cells." Nat Rev Cancer **15**(9): 515-527.

Krieg, J., J. Hofsteenge and G. Thomas (1988). "Identification of the 40 S ribosomal protein S6 phosphorylation sites induced by cycloheximide." J Biol Chem **263**(23): 11473-11477.

Kwitkowski, V. E., T. M. Prowell, A. Ibrahim, A. T. Farrell, R. Justice, S. S. Mitchell, R. Sridhara and R. Pazdur (2010). "FDA approval summary: temsirolimus as treatment for advanced renal cell carcinoma." Oncologist **15**(4): 428-435.

Labun, K., T. G. Montague, J. A. Gagnon, S. B. Thyme and E. Valen (2016). "CHOPCHOP v2: a web tool for the next generation of CRISPR genome engineering." Nucleic Acids Res **44**(W1): W272-276.

Lee, J. S., H. S. Kim, Y. B. Kim, M. C. Lee, C. S. Park and K. W. Min (2004). "Reduced PTEN expression is associated with poor outcome and angiogenesis in invasive ductal carcinoma of the breast." Appl Immunohistochem Mol Morphol **12**(3): 205-210.

Lee, M. J., A. S. Ye, A. K. Gardino, A. M. Heijink, P. K. Sorger, G. MacBeath and M. B. Yaffe (2012). "Sequential application of anticancer drugs enhances cell death by rewiring apoptotic signaling networks." Cell **149**(4): 780-794.

Lee, Y. R., M. Chen and P. P. Pandolfi (2018). "The functions and regulation of the PTEN tumour suppressor: new modes and prospects." Nat Rev Mol Cell Biol **19**(9): 547-562.

Lehmann, B. D., J. A. Bauer, X. Chen, M. E. Sanders, A. B. Chakravarthy, Y. Shyr and J. A. Pietenpol (2011). "Identification of human triple-negative breast cancer subtypes and preclinical models for selection of targeted therapies." J Clin Invest **121**(7): 2750-2767.

Lehmann, B. D., J. A. Bauer, J. M. Schafer, C. S. Pendleton, L. Tang, K. C. Johnson, X. Chen, J. M. Balko, H. Gomez, C. L. Arteaga, G. B. Mills, M. E. Sanders and J. A. Pietenpol (2014). "PIK3CA mutations in androgen receptor-positive triple negative breast cancer confer sensitivity to the combination of PI3K and androgen receptor inhibitors." Breast Cancer Res **16**(4): 406.

Lehr, S., J. Kotzka, H. Avci, A. Sickmann, H. E. Meyer, A. Herkner and D. Muller-Wieland (2004). "Identification of major ERK-related phosphorylation sites in Gab1." Biochemistry **43**(38): 12133-12140.

Li, S., Y. Shen, M. Wang, J. Yang, M. Lv, P. Li, Z. Chen and J. Yang (2017). "Loss of PTEN expression in breast cancer: association with clinicopathological characteristics and prognosis." Oncotarget **8**(19): 32043-32054.

Li, X., Y. Huang, J. Jiang and S. J. Frank (2008). "ERK-dependent threonine phosphorylation of EGF receptor modulates receptor downregulation and signaling." Cell Signal **20**(11): 2145-2155.

Li, X. M., A. Mohammad-Djafari, M. Dumitru, S. Dulong, E. Filipski, S. Siffroi-Fernandez, A. Mteyrek, F. Scaglione, C. Guettier, F. Delaunay and F. Levi (2013). "A circadian clock transcription model for the personalization of cancer chronotherapy." Cancer Res **73**(24): 7176-7188.

Li, Z., X. Dong, Z. Wang, W. Liu, N. Deng, Y. Ding, L. Tang, T. Hla, R. Zeng, L. Li and D. Wu (2005). "Regulation of PTEN by Rho small GTPases." Nat Cell Biol **7**(4): 399-404.

Lietzke, S. E., S. Bose, T. Cronin, J. Klarlund, A. Chawla, M. P. Czech and D. G. Lambright (2000). "Structural basis of 3-phosphoinositide recognition by pleckstrin homology domains." Mol Cell **6**(2): 385-394.

Ling, X. and R. B. Arlinghaus (2005). "Knockdown of STAT3 expression by RNA interference inhibits the induction of breast tumors in immunocompetent mice." Cancer Res **65**(7): 2532-2536.

Longley, D. B. and P. G. Johnston (2005). "Molecular mechanisms of drug resistance." J Pathol **205**(2): 275-292.

Lu, X. J., X. Qi, D. H. Zheng and L. J. Ji (2015). "Modeling cancer processes with CRISPR-Cas9." Trends Biotechnol **33**(6): 317-319.

Maehama, T. and J. E. Dixon (1998). "The tumor suppressor, PTEN/MMAC1, dephosphorylates the lipid second messenger, phosphatidylinositol 3,4,5-trisphosphate." J Biol Chem **273**(22): 13375-13378.

Malek, M., A. Kielkowska, T. Chessa, K. E. Anderson, D. Barneda, P. Pir, H. Nakanishi, S. Eguchi, A. Koizumi, J. Sasaki, V. Juvin, V. Y. Kiselev, I. Niewczas, A. Gray, A. Valayer, D. Spensberger, M. Imbert, S. Felisbino, T. Habuchi, S. Beinke, S. Cosulich, N. Le Novere, T. Sasaki, J. Clark, P. T. Hawkins and L. R. Stephens (2017). "PTEN Regulates PI(3,4)P2 Signaling Downstream of Class I PI3K." Mol Cell **68**(3): 566-580 e510.

Malhotra, G. K., X. Zhao, H. Band and V. Band (2010). "Histological, molecular and functional subtypes of breast cancers." Cancer Biol Ther **10**(10): 955-960.

Man, K. F., K. S. Tang and S. Kwong (1996). "Genetic algorithms: concepts and applications [in engineering design]." IEEE Transactions on Industrial Electronics **43**(5): 519-534.

Manning, B. D. and L. C. Cantley (2007). "AKT/PKB signaling: navigating downstream." Cell **129**(7): 1261-1274.

Marotta, L. L., V. Almendro, A. Marusyk, M. Shipitsin, J. Schemme, S. R. Walker, N. Bloushtain-Qimron, J. J. Kim, S. A. Choudhury, R. Maruyama, Z. Wu, M. Gonen, L. A. Mulvey, M. O. Bessarabova, S. J. Huh, S. J. Silver, S. Y. Kim, S. Y. Park, H. E. Lee, K. S. Anderson, A. L. Richardson, T. Nikolskaya, Y. Nikolsky, X. S. Liu, D. E. Root, W. C. Hahn, D. A. Frank and K. Polyak (2011). "The JAK2/STAT3 signaling pathway is required for growth of CD44(+)CD24(-) stem cell-like breast cancer cells in human tumors." J Clin Invest **121**(7): 2723-2735.

Martini, M., E. Ciraolo, F. Gulluni and E. Hirsch (2013). "Targeting PI3K in Cancer: Any Good News?" Front Oncol **3**: 108.

Marty, B., V. Maire, E. Gravier, G. Rigaill, A. Vincent-Salomon, M. Kappler, I. Lebigot, F. Djelti, A. Tourdes, P. Gestraud, P. Hupe, E. Barillot, F. Cruzalegui, G. C. Tucker, M. H. Stern, J. P. Thiery, J. A. Hickman and T. Dubois (2008). "Frequent PTEN genomic alterations and activated phosphatidylinositol 3-kinase pathway in basal-like breast cancer cells." Breast Cancer Res **10**(6): R101.

Massacesi, C., E. di Tomaso, N. Fretault and S. Hirawat (2013). "Challenges in the clinical development of PI3K inhibitors." Ann N Y Acad Sci **1280**: 19-23.

Masuda, H., D. Zhang, C. Bartholomeusz, H. Doihara, G. N. Hortobagyi and N. T. Ueno (2012). "Role of epidermal growth factor receptor in breast cancer." Breast Cancer Res Treat **136**(2): 331-345.

Matkar, S., C. An and X. Hua (2017). "Kinase inhibitors of HER2/AKT pathway induce ERK phosphorylation via a FOXO-dependent feedback loop." Am J Cancer Res **7**(7): 1476-1485.

McCubrey, J. A., L. S. Steelman, W. H. Chappell, S. L. Abrams, E. W. Wong, F. Chang, B. Lehmann, D. M. Terrian, M. Milella, A. Tafuri, F. Stivala, M. Libra, J. Basecke, C. Evangelisti, A. M. Martelli and R. A. Franklin (2007). "Roles of the Raf/MEK/ERK pathway in cell growth, malignant transformation and drug resistance." Biochim Biophys Acta **1773**(8): 1263-1284.

Mendoza, M. C., E. E. Er and J. Blenis (2011). "The Ras-ERK and PI3K-mTOR pathways: cross-talk and compensation." Trends Biochem Sci **36**(6): 320-328.

Meric-Bernstam, F., A. Akcakanat, H. Chen, K. A. Do, T. Sangai, F. Adkins, A. M. Gonzalez-Angulo, A. Rashid, K. Crosby, M. Dong, A. T. Phan, R. A. Wolff, S. Gupta, G. B. Mills and J. Yao (2012). "PIK3CA/PTEN mutations and Akt activation as markers of sensitivity to allosteric mTOR inhibitors." Clin Cancer Res **18**(6): 1777-1789.

Mirzoeva, O. K., D. Das, L. M. Heiser, S. Bhattacharya, D. Siwak, R. Gendelman, N. Bayani, N. J. Wang, R. M. Neve, Y. Guan, Z. Hu, Z. Knight, H. S. Feiler, P. Gascard, B. Parvin, P. T. Spellman, K. M. Shokat, A. J. Wyrobek, M. J. Bissell, F. McCormick, W. L. Kuo, G. B. Mills, J. W. Gray and W. M. Korn (2009). "Basal subtype and MAPK/ERK kinase (MEK)-phosphoinositide 3-kinase feedback signaling determine susceptibility of breast cancer cells to MEK inhibition." Cancer Res **69**(2): 565-572.

Mojica, F. J., C. Diez-Villasenor, J. Garcia-Martinez and E. Soria (2005). "Intervening sequences of regularly spaced prokaryotic repeats derive from foreign genetic elements." J Mol Evol **60**(2): 174-182.

Moon, S. H., D. K. Kim, Y. Cha, I. Jeon, J. Song and K. S. Park (2013). "PI3K/Akt and Stat3 signaling regulated by PTEN control of the cancer stem cell population, proliferation and senescence in a glioblastoma cell line." Int J Oncol **42**(3): 921-928.

Mortality, G. B. D. and C. Causes of Death (2016). "Global, regional, and national life expectancy, all-cause mortality, and cause-specific mortality for 249 causes of death, 1980-2015: a systematic analysis for the Global Burden of Disease Study 2015." Lancet **388**(10053): 1459-1544.

Moscatello, D. K., R. B. Montgomery, P. Sundareshan, H. McDanel, M. Y. Wong and A. J. Wong (1996). "Transformational and altered signal transduction by a naturally occurring mutant EGF receptor." Oncogene **13**(1): 85-96.

Mundi, P. S., J. Sachdev, C. McCourt and K. Kalinsky (2016). "AKT in cancer: new molecular insights and advances in drug development." Br J Clin Pharmacol **82**(4): 943-956.

Myers, M. P., J. P. Stolarov, C. Eng, J. Li, S. I. Wang, M. H. Wigler, R. Parsons and N. K. Tonks (1997). "P-TEN, the tumor suppressor from human chromosome 10q23, is a dual-specificity phosphatase." Proc Natl Acad Sci U S A **94**(17): 9052-9057.

Nagata, Y., K. H. Lan, X. Zhou, M. Tan, F. J. Esteva, A. A. Sahin, K. S. Klos, P. Li, B. P. Monia, N. T. Nguyen, G. N. Hortobagyi, M. C. Hung and D. Yu (2004). "PTEN activation contributes to tumor inhibition by trastuzumab, and loss of PTEN predicts trastuzumab resistance in patients." Cancer Cell **6**(2): 117-127.

Nakanishi, Y., K. Walter, J. M. Spoerke, C. O'Brien, L. Y. Huw, G. M. Hampton and M. R. Lackner (2016). "Activating Mutations in PIK3CB Confer Resistance to PI3K Inhibition and Define a Novel Oncogenic Role for p110beta." Cancer Res **76**(5): 1193-1203.

Nazarian, R., H. Shi, Q. Wang, X. Kong, R. C. Koya, H. Lee, Z. Chen, M. K. Lee, N. Attar, H. Sazegar, T. Chodon, S. F. Nelson, G. McArthur, J. A. Sosman, A. Ribas and R. S. Lo (2010). "Melanomas acquire resistance to B-RAF(V600E) inhibition by RTK or N-RAS upregulation." Nature **468**(7326): 973-977.

Nguyen, L. K. (2016). "Dynamics of ubiquitin-mediated signalling: insights from mathematical modelling and experimental studies." Brief Bioinform **17**(3): 479-493.

Nguyen, L. K. and B. N. Kholodenko (2015). "Feedback regulation in cell signalling: Lessons for cancer therapeutics." Semin Cell Dev Biol(50): 85-94.

Nguyen, L. K. and B. N. Kholodenko (2016). "Feedback regulation in cell signalling: Lessons for cancer therapeutics." Seminars in Cell & Developmental Biology **50**: 85-94.

Nguyen, L. K. and B. N. Kholodenko (2016). "Feedback regulation in cell signalling: Lessons for cancer therapeutics." Semin Cell Dev Biol **50**: 85-94.

Nguyen, L. K., D. Matallanas, D. R. Croucher, A. von Kriegsheim and B. N. Kholodenko (2013). "Signalling by protein phosphatases and drug development: a systems-centred view." FEBS J **280**(2): 751-765.

Ni, J., Q. Liu, S. Xie, C. Carlson, T. Von, K. Vogel, S. Riddle, C. Benes, M. Eck, T. Roberts, N. Gray and J. Zhao (2012). "Functional characterization of an isoform-selective inhibitor of PI3K-p110beta as a potential anticancer agent." Cancer Discov **2**(5): 425-433.

Nylander, S., B. Kull, J. A. Bjorkman, J. C. Ulvinge, N. Oakes, B. M. Emanuelsson, M. Andersson, T. Skarby, T. Inghardt, O. Fjellstrom and D. Gustafsson (2012). "Human target validation of phosphoinositide 3-kinase (PI3K)beta: effects on platelets and insulin sensitivity, using AZD6482 a novel PI3Kbeta inhibitor." J Thromb Haemost **10**(10): 2127-2136.

O'Brien, N. A., K. McDonald, L. Tong, E. von Euw, O. Kalous, D. Conklin, S. A. Hurvitz, E. di Tomaso, C. Schnell, R. Linnartz, R. S. Finn, S. Hirawat and D. J. Slamon (2014). "Targeting PI3K/mTOR overcomes resistance to HER2-targeted therapy independent of feedback activation of AKT." Clin Cancer Res **20**(13): 3507-3520.

O'Reilly, K. E., F. Rojo, Q. B. She, D. Solit, G. B. Mills, D. Smith, H. Lane, F. Hofmann, D. J. Hicklin, D. L. Ludwig, J. Baselga and N. Rosen (2006). "mTOR inhibition induces upstream receptor tyrosine kinase signaling and activates Akt." Cancer Res **66**(3): 1500-1508.

Oda, K., D. Stokoe, Y. Taketani and F. McCormick (2005). "High frequency of coexistent mutations of PIK3CA and PTEN genes in endometrial carcinoma." Cancer Res **65**(23): 10669-10673.

Papa, A., L. Wan, M. Bonora, L. Salmena, M. S. Song, R. M. Hobbs, A. Lunardi, K. Webster, C. Ng, R. H. Newton, N. Knoblauch, J. Guarnerio, K. Ito, L. A. Turka, A. H. Beck, P. Pinton, R. T. Bronson, W. Wei and P. P. Pandolfi (2014). "Cancer-associated PTEN mutants act in a dominant-negative manner to suppress PTEN protein function." Cell **157**(3): 595-610.

Pazarentzos, E., P. Giannikopoulos, G. Hrustanovic, J. St John, V. R. Olivas, M. A. Gubens, R. Balassanian, J. Weissman, W. Polkinghorn and T. G. Bivona (2015). "Oncogenic activation of the PI3-kinase p110β isoform via the tumor-derived PIK3CβD1067V kinase domain mutation." Oncogene **35**: 1198.

Pellegrini, S. and I. Dusanter-Fourt (1997). "The structure, regulation and function of the Janus kinases (JAKs) and the signal transducers and activators of transcription (STATs)." Eur J Biochem **248**(3): 615-633.

Perou, C. M., T. Sorlie, M. B. Eisen, M. van de Rijn, S. S. Jeffrey, C. A. Rees, J. R. Pollack, D. T. Ross, H. Johnsen, L. A. Akslen, O. Fluge, A. Pergamenschikov, C. Williams, S. X. Zhu, P. E. Lonning, A. L. Borresen-Dale, P. O. Brown and D. Botstein (2000). "Molecular portraits of human breast tumours." Nature **406**(6797): 747-752.

Pires, M. M., B. D. Hopkins, L. H. Saal and R. E. Parsons (2013). "Alterations of EGFR, p53 and PTEN that mimic changes found in basal-like breast cancer promote transformation of human mammary epithelial cells." Cancer Biol Ther **14**(3): 246-253.

Prat, A., J. S. Parker, O. Karginova, C. Fan, C. Livasy, J. I. Herschkowitz, X. He and C. M. Perou (2010). "Phenotypic and molecular characterization of the claudin-low intrinsic subtype of breast cancer." Breast Cancer Res **12**(5): R68.

Qin, J. J., L. Yan, J. Zhang and W. D. Zhang (2019). "STAT3 as a potential therapeutic target in triple negative breast cancer: a systematic review." J Exp Clin Cancer Res **38**(1): 195.

Rabinovsky, R., P. Pochanard, C. McNear, S. M. Brachmann, J. S. Duke-Cohan, L. A. Garraway and W. R. Sellers (2009). "p85 Associates with unphosphorylated PTEN and the PTEN-associated complex." Mol Cell Biol **29**(19): 5377-5388.

Rakha, E. A., D. S. Tan, W. D. Foulkes, I. O. Ellis, A. Tutt, T. O. Nielsen and J. S. Reis-Filho (2007). "Are triple-negative tumours and basal-like breast cancer synonymous?" Breast Cancer Res **9**(6): 404; author reply 405.

Razis, E., M. Bobos, V. Kotoula, A. G. Eleftheraki, H. P. Kalofonos, K. Pavlakis, P. Papakostas, G. Aravantinos, G. Rigakos, I. Efstratiou, K. Petraki, D. Bafaloukos, I. Kostopoulos, D. Pectasides, K. T. Kalogeras, D. Skarlos and G. Fountzilas (2011). "Evaluation of the association of PIK3CA mutations and PTEN loss with efficacy of trastuzumab therapy in metastatic breast cancer." Breast Cancer Res Treat **128**(2): 447-456.

Reali, F., C. Priami and L. Marchetti (2017). "Optimization Algorithms for Computational Systems Biology." Frontiers in Applied Mathematics and Statistics **3**(6).

Recupero, D., L. Daniele, C. Marchio, L. Molinaro, I. Castellano, P. Cassoni, A. Righi, F. Montemurro, P. Sismondi, N. Biglia, G. Viale, M. Risio and A. Sapino (2013). "Spontaneous and pronase-induced HER2 truncation increases the trastuzumab binding capacity of breast cancer tissues and cell lines." J Pathol **229**(3): 390-399.

Rexer, B. N., S. Chanthaphaychith, K. Dahlman and C. L. Arteaga (2014). "Direct inhibition of PI3K in combination with dual HER2 inhibitors is required for optimal antitumor activity in HER2+ breast cancer cells." Breast Cancer Res **16**(1): R9.

Rinehart, J., A. A. Adjei, P. M. Lorusso, D. Waterhouse, J. R. Hecht, R. B. Natale, O. Hamid, M. Varterasian, P. Asbury, E. P. Kaldjian, S. Gulyas, D. Y. Mitchell, R. Herrera, J. S. Sebolt-Leopold and M. B. Meyer (2004). "Multicenter phase II study of the oral MEK inhibitor, CI-1040, in patients with advanced non-small-cell lung, breast, colon, and pancreatic cancer." J Clin Oncol **22**(22): 4456-4462.

Rodrigues, G. A., M. Falasca, Z. Zhang, S. H. Ong and J. Schlessinger (2000). "A novel positive feedback loop mediated by the docking protein Gab1 and phosphatidylinositol 3-kinase in epidermal growth factor receptor signaling." Mol Cell Biol **20**(4): 1448-1459.

Rodriguez-Rodriguez, D. R., R. Ramirez-Solis, M. A. Garza-Elizondo, M. L. Garza-Rodriguez and H. A. Barrera-Saldana (2019). "Genome editing: A perspective on the application of CRISPR/Cas9 to study human diseases (Review)." Int J Mol Med **43**(4): 1559-1574.

Rodriguez-Viciana, P., C. Sabatier and F. McCormick (2004). "Signaling specificity by Ras family GTPases is determined by the full spectrum of effectors they regulate." Mol Cell Biol **24**(11): 4943-4954.

Romano, D., L. K. Nguyen, D. Matallanas, M. Halasz, C. Doherty, B. N. Kholodenko and W. Kolch (2014). "Protein interaction switches coordinate Raf-1 and MST2/Hippo signalling." Nat Cell Biol **16**(7): 673-684.

Roskoski, R., Jr. (2019). "Properties of FDA-approved small molecule protein kinase inhibitors." Pharmacol Res **144**: 19-50.

Rubin, C., V. Litvak, H. Medvedovsky, Y. Zwang, S. Lev and Y. Yarden (2003). "Sprouty fine-tunes EGF signaling through interlinked positive and negative feedback loops." Curr Biol **13**(4): 297-307.

Rueff, J. and A. S. Rodrigues (2016). "Cancer Drug Resistance: A Brief Overview from a Genetic Viewpoint." Methods Mol Biol **1395**: 1-18.

Ruiz-Saenz, A., C. Dreyer, M. R. Campbell, V. Steri, N. Gulizia and M. M. Moasser (2018). "HER2 Amplification in Tumors Activates PI3K/Akt Signaling Independent of HER3." Cancer Res **78**(13): 3645-3658.

Ruvinsky, I. and O. Meyuhas (2006). "Ribosomal protein S6 phosphorylation: from protein synthesis to cell size." Trends Biochem Sci **31**(6): 342-348.

Saal, L. H., S. K. Gruvberger-Saal, C. Persson, K. Lovgren, M. Jumppanen, J. Staaf, G. Jonsson, M. M. Pires, M. Maurer, K. Holm, S. Koujak, S. Subramaniyam, J. Vallon-Christersson, H. Olsson, T. Su, L. Memeo, T. Ludwig, S. P. Ethier, M. Krogh, M. Szabolcs, V. V. Murty, J. Isola, H. Hibshoosh, R. Parsons and A. Borg (2008). "Recurrent gross mutations of the PTEN tumor suppressor gene in breast cancers with deficient DSB repair." Nat Genet **40**(1): 102-107.

Saal, L. H., K. Holm, M. Maurer, L. Memeo, T. Su, X. Wang, J. S. Yu, P. O. Malmstrom, M. Mansukhani, J. Enoksson, H. Hibshoosh, A. Borg and R. Parsons (2005). "PIK3CA mutations correlate with hormone receptors, node metastasis, and ERBB2, and are mutually exclusive with PTEN loss in human breast carcinoma." Cancer Res **65**(7): 2554-2559.

Sanchez-Vega, F., M. Mina, J. Armenia, W. K. Chatila, A. Luna, K. C. La, S. Dimitriadoy, D. L. Liu, H. S. Kantheti, S. Saghafinia, D. Chakravarty, F. Daian, Q. Gao, M. H. Bailey, W. W. Liang, S. M. Foltz, I. Shmulevich, L. Ding, Z. Heins, A. Ochoa, B. Gross, J. Gao, H. Zhang, R. Kundra, C. Kandoth, I. Bahceci, L. Dervishi, U. Dogrusoz, W. Zhou, H. Shen, P. W. Laird, G. P. Way, C. S. Greene, H. Liang, Y. Xiao, C. Wang, A. Iavarone, A. H. Berger, T. G. Bivona, A. J. Lazar, G. D. Hammer, T. Giordano, L. N. Kwong, G. McArthur, C. Huang, A. D. Tward, M. J. Frederick, F. McCormick, M. Meyerson, N. Cancer Genome Atlas Research, E. M. Van Allen, A. D. Cherniack, G. Ciriello, C. Sander and N. Schultz (2018). "Oncogenic Signaling Pathways in The Cancer Genome Atlas." Cell **173**(2): 321-337 e310.

Sarbassov, D. D., D. A. Guertin, S. M. Ali and D. M. Sabatini (2005). "Phosphorylation and regulation of Akt/PKB by the rictor-mTOR complex." Science **307**(5712): 1098-1101.

Sato, N., M. Wakabayashi, M. Nakatsuji, H. Kashiwagura, N. Shimoji, S. Sakamoto, A. Ishida, J. Lee, B. Lim, N. T. Ueno, H. Ishihara and T. Inui (2017). "MEK and PI3K catalytic activity as predictor of the response to molecularly targeted agents in triple-negative breast cancer." Biochem Biophys Res Commun **489**(4): 484-489.

Schwartz, S., J. Wongvipat, C. B. Trigwell, U. Hancox, B. S. Carver, V. Rodrik-Outmezguine, M. Will, P. Yellen, E. de Stanchina, J. Baselga, H. I. Scher, S. T. Barry, C. L. Sawyers, S. Chandarlapaty and N. Rosen (2015). "Feedback suppression of PI3Kalpha signaling in PTEN-mutated tumors is relieved by selective inhibition of PI3Kbeta." Cancer Cell **27**(1): 109-122.

Schwarz, L. J., K. E. Hutchinson, B. N. Rexer, M. V. Estrada, P. I. Gonzalez Ericsson, M. E. Sanders, T. C. Dugger, L. Formisano, A. Guerrero-Zotano, M. Red-Brewer, C. D. Young, J. Lantto, M. W. Pedersen, M. Kragh, I. D. Horak and C. L. Arteaga (2017). "An ERBB1-3 Neutralizing Antibody Mixture With High Activity Against Drug-Resistant HER2+ Breast Cancers With ERBB Ligand Overexpression." J Natl Cancer Inst **109**(11).

Serra, V., M. Scaltriti, L. Prudkin, P. J. Eichhorn, Y. H. Ibrahim, S. Chandarlapaty, B. Markman, O. Rodriguez, M. Guzman, S. Rodriguez, M. Gili, M. Russillo, J. L. Parra, S. Singh, J. Arribas, N. Rosen and J. Baselga (2011). "PI3K inhibition results in enhanced HER signaling and acquired ERK dependency in HER2-overexpressing breast cancer." Oncogene **30**(22): 2547-2557.

Shah, N. P., C. Tran, F. Y. Lee, P. Chen, D. Norris and C. L. Sawyers (2004). "Overriding imatinib resistance with a novel ABL kinase inhibitor." Science **305**(5682): 399-401.

Shapiro, P. (2002). "Ras-MAP kinase signaling pathways and control of cell proliferation: relevance to cancer therapy." Crit Rev Clin Lab Sci **39**(4-5): 285-330.

Shin, S.-Y. and L. K. Nguyen (2016). "Unveiling Hidden Dynamics of Hippo Signalling: A Systems Analysis." Genes **7**(8): 44.

Shin, S.-Y. and L. K. Nguyen (2017). Dissecting cell-fate determination through integrated mathematical modeling of the ERK/MAPK signaling pathway. Methods in Molecular Biology, Humana Press. **1487:** 409-432.

Shin, S., A. K. Muller, N. Verma, S. Lev and L. K. Nguyen (2018). "Systems modelling of the EGFR-PYK2-c-Met interaction network predicts and prioritizes synergistic drug combinations for triple-negative breast cancer." PLOS Computational Biology **14**(6): e1006192.

Shin, S. and L. K. Nguyen (2016). Dissecting cell-fate determination through integrated modelling of the ERK/MAPK signalling pathway. ERK Signaling. G. Jimenez, Methods Molecular Biology. **1487**.

Shin, S. Y., T. Kim, H. S. Lee, J. H. Kang, J. Y. Lee, K. H. Cho and H. Kim do (2014). "The switching role of β-adrenergic receptor signalling in cell survival or death decision of cardiomyocytes." Nat Commun **5**: 5777.

Shin, S. Y., A. K. Muller, N. Verma, S. Lev and L. K. Nguyen (2018). "Systems modelling of the EGFR-PYK2-c-Met interaction network predicts and prioritizes synergistic drug combinations for triple-negative breast cancer." PLoS Comput Biol **14**(6): e1006192.

Shin, S. Y., O. Rath, S. M. Choo, F. Fee, B. McFerran, W. Kolch and K. H. Cho (2009). "Positive- and negative-feedback regulations coordinate the dynamic behavior of the Ras-Raf-MEK-ERK signal transduction pathway." Journal of Cell Science **122**(3): 425-435.

Shoelson, S. E. (1997). "SH2 and PTB domain interactions in tyrosine kinase signal transduction." Curr Opin Chem Biol **1**(2): 227-234.

Shoman, N., S. Klassen, A. McFadden, M. G. Bickis, E. Torlakovic and R. Chibbar (2005). "Reduced PTEN expression predicts relapse in patients with breast carcinoma treated by tamoxifen." Mod Pathol **18**(2): 250-259.

Singh, B., M. M. Ittmann and J. J. Krolewski (1998). "Sporadic breast cancers exhibit loss of heterozygosity on chromosome segment 10q23 close to the Cowden disease locus." Genes Chromosomes Cancer **21**(2): 166-171.

Sirkisoon, S. R., R. L. Carpenter, T. Rimkus, A. Anderson, A. Harrison, A. M. Lange, G. Jin, K. Watabe and H. W. Lo (2018). "Interaction between STAT3 and GLI1/tGLI1 oncogenic transcription factors promotes the aggressiveness of triple-negative breast cancers and HER2-enriched breast cancer." Oncogene **37**(19): 2502-2514.

Smalley, K. S. (2003). "A pivotal role for ERK in the oncogenic behaviour of malignant melanoma?" Int J Cancer **104**(5): 527-532.

Smith, S. E., P. Mellor, A. K. Ward, S. Kendall, M. McDonald, F. S. Vizeacoumar, F. J. Vizeacoumar, S. Napper and D. H. Anderson (2017). "Molecular characterization of breast cancer cell lines through multiple omic approaches." Breast Cancer Res **19**(1): 65.

Sorlie, T., C. M. Perou, R. Tibshirani, T. Aas, S. Geisler, H. Johnsen, T. Hastie, M. B. Eisen, M. van de Rijn, S. S. Jeffrey, T. Thorsen, H. Quist, J. C. Matese, P. O. Brown, D. Botstein, P. E. Lonning and A. L. Borresen-Dale (2001). "Gene expression patterns of breast carcinomas distinguish tumor subclasses with clinical implications." Proc Natl Acad Sci U S A **98**(19): 10869-10874.

Sorlie, T., R. Tibshirani, J. Parker, T. Hastie, J. S. Marron, A. Nobel, S. Deng, H. Johnsen, R. Pesich, S. Geisler, J. Demeter, C. M. Perou, P. E. Lonning, P. O. Brown, A. L. Borresen-Dale and D. Botstein (2003). "Repeated observation of breast tumor subtypes in independent gene expression data sets." Proc Natl Acad Sci U S A **100**(14): 8418-8423.

Soule, H. D., T. M. Maloney, S. R. Wolman, W. D. Peterson, Jr., R. Brenz, C. M. McGrath, J. Russo, R. J. Pauley, R. F. Jones and S. C. Brooks (1990). "Isolation and characterization of a spontaneously immortalized human breast epithelial cell line, MCF-10." Cancer Res **50**(18): 6075-6086.

Stambolic, V., A. Suzuki, J. L. de la Pompa, G. M. Brothers, C. Mirtsos, T. Sasaki, J. Ruland, J. M. Penninger, D. P. Siderovski and T. W. Mak (1998). "Negative regulation of PKB/Akt-dependent cell survival by the tumor suppressor PTEN." Cell **95**(1): 29-39.

Stemke-Hale, K., A. M. Gonzalez-Angulo, A. Lluch, R. M. Neve, W. L. Kuo, M. Davies, M. Carey, Z. Hu, Y. Guan, A. Sahin, W. F. Symmans, L. Pusztai, L. K. Nolden, H. Horlings, K. Berns, M. C. Hung, M. J. van de Vijver, V. Valero, J. W. Gray, R. Bernards, G. B. Mills and B. T. Hennessy (2008). "An integrative genomic and proteomic analysis of PIK3CA, PTEN, and AKT mutations in breast cancer." Cancer Res **68**(15): 6084-6091.

Stratikopoulos, E. E., M. Dendy, M. Szabolcs, A. J. Khaykin, C. Lefebvre, M. M. Zhou and R. Parsons (2015). "Kinase and BET Inhibitors Together Clamp Inhibition of PI3K Signaling and Overcome Resistance to Therapy." Cancer Cell **27**(6): 837-851.

Stuhlmiller, T. J., S. M. Miller, J. S. Zawistowski, K. Nakamura, A. S. Beltran, J. S. Duncan, S. P. Angus, K. A. Collins, D. A. Granger, R. A. Reuther, L. M. Graves, S. M. Gomez, P. F. Kuan, J. S. Parker, X. Chen, N. Sciaky, L. A. Carey, H. S. Earp, J. Jin and G. L. Johnson (2015). "Inhibition of Lapatinib-Induced Kinome Reprogramming in ERBB2-Positive Breast Cancer by Targeting BET Family Bromodomains." Cell Rep **11**(3): 390-404.

Sun, S. and B. M. Steinberg (2002). "PTEN is a negative regulator of STAT3 activation in human papillomavirus-infected cells." J Gen Virol **83**(Pt 7): 1651-1658.

Tamguney, T. and D. Stokoe (2007). "New insights into PTEN." J Cell Sci **120**(Pt 23): 4071-4079.

Teng, Y. H., W. J. Tan, A. A. Thike, P. Y. Cheok, G. M. Tse, N. S. Wong, G. W. Yip, B. H. Bay and P. H. Tan (2011). "Mutations in the epidermal growth factor receptor (EGFR) gene in triple negative breast cancer: possible implications for targeted therapy." Breast Cancer Res **13**(2): R35.

Thorpe, L. M., H. Yuzugullu and J. J. Zhao (2015). "PI3K in cancer: divergent roles of isoforms, modes of activation and therapeutic targeting." Nat Rev Cancer **15**(1): 7-24.

Tiong, K. H., L. Y. Mah and C. O. Leong (2013). "Functional roles of fibroblast growth factor receptors (FGFRs) signaling in human cancers." Apoptosis **18**(12): 1447-1468.

Tokunaga, E., E. Oki, A. Egashira, N. Sadanaga, M. Morita, Y. Kakeji and Y. Maehara (2008). "Deregulation of the Akt pathway in human cancer." Curr Cancer Drug Targets **8**(1): 27-36.

Torbett, N. E., A. Luna-Moran, Z. A. Knight, A. Houk, M. Moasser, W. Weiss, K. M. Shokat and D. Stokoe (2008). "A chemical screen in diverse breast cancer cell lines reveals genetic enhancers and suppressors of sensitivity to PI3K isoform-selective inhibition." Biochem J **415**(1): 97-110.

Torre, L. A., F. Bray, R. L. Siegel, J. Ferlay, J. Lortet-Tieulent and A. Jemal (2015). "Global cancer statistics, 2012." CA Cancer J Clin **65**(2): 87-108.

Torres, J. and R. Pulido (2001). "The tumor suppressor PTEN is phosphorylated by the protein kinase CK2 at its C terminus. Implications for PTEN stability to proteasome-mediated degradation." J Biol Chem **276**(2): 993-998.

Turke, A. B., Y. Song, C. Costa, R. Cook, C. L. Arteaga, J. M. Asara and J. A. Engelman (2012). "MEK inhibition leads to PI3K/AKT activation by relieving a negative feedback on ERBB receptors." Cancer Res **72**(13): 3228-3237.

Vanhaesebroeck, B., J. Guillermet-Guibert, M. Graupera and B. Bilanges (2010). "The emerging mechanisms of isoform-specific PI3K signalling." Nat Rev Mol Cell Biol **11**(5): 329-341.

Vanhaesebroeck, B., L. Stephens and P. Hawkins (2012). "PI3K signalling: the path to discovery and understanding." Nat Rev Mol Cell Biol **13**(3): 195-203.

Varusai, T. M. and L. K. Nguyen (2018). "Dynamic modelling of the mTOR signalling network reveals complex emergent behaviours conferred by DEPTOR." Sci Rep **8**(1): 643.

Vazquez, F. and P. Devreotes (2006). "Regulation of PTEN function as a PIP3 gatekeeper through membrane interaction." Cell Cycle **5**(14): 1523-1527.

Verma, N., A. K. Muller, C. Kothari, E. Panayotopoulou, A. Kedan, M. Selitrennik, G. B. Mills, L. K. Nguyen, S. Shin, T. Karn, U. Holtrich and S. Lev (2017). "Targeting of PYK2 Synergizes with EGFR Antagonists in Basal-like TNBC and Circumvents HER3-Associated Resistance via the NEDD4-NDRG1 Axis." Cancer Res **77**(1): 86-99.

Villanueva, J., A. Vultur, J. T. Lee, R. Somasundaram, M. Fukunaga-Kalabis, A. K. Cipolla, B. Wubbenhorst, X. Xu, P. A. Gimotty, D. Kee, A. E. Santiago-Walker, R. Letrero, K. D'Andrea, A. Pushparajan, J. E. Hayden, K. D. Brown, S. Laquerre, G. A. McArthur, J. A. Sosman, K. L. Nathanson and M. Herlyn (2010). "Acquired resistance to BRAF inhibitors mediated by a RAF kinase switch in melanoma can be overcome by cotargeting MEK and IGF-1R/PI3K." Cancer Cell **18**(6): 683-695.

Vincent, E. E., D. J. Elder, E. C. Thomas, L. Phillips, C. Morgan, J. Pawade, M. Sohail, M. T. May, M. R. Hetzel and J. M. Tavare (2011). "Akt phosphorylation on Thr308 but not on Ser473 correlates with Akt protein kinase activity in human non-small cell lung cancer." Br J Cancer **104**(11): 1755-1761.

Vitolo, M. I., M. B. Weiss, M. Szmacinski, K. Tahir, T. Waldman, B. H. Park, S. S. Martin, D. J. Weber and K. E. Bachman (2009). "Deletion of PTEN promotes tumorigenic signaling, resistance to anoikis, and altered response to chemotherapeutic agents in human mammary epithelial cells." Cancer Res **69**(21): 8275-8283.

Vultur, A., J. Cao, R. Arulanandam, J. Turkson, R. Jove, P. Greer, A. Craig, B. Elliott and L. Raptis (2004). "Cell-to-cell adhesion modulates Stat3 activity in normal and breast carcinoma cells." Oncogene **23**(15): 2600-2616.

Walker, S. R., M. Xiang and D. A. Frank (2014). "Distinct roles of STAT3 and STAT5 in the pathogenesis and targeted therapy of breast cancer." Mol Cell Endocrinol **382**(1): 616-621.

Wee, P. and Z. Wang (2017). "Epidermal Growth Factor Receptor Cell Proliferation Signaling Pathways." Cancers (Basel) **9**(5).

Wee, S., D. Wiederschain, S. M. Maira, A. Loo, C. Miller, R. deBeaumont, F. Stegmeier, Y. M. Yao and C. Lengauer (2008). "PTEN-deficient cancers depend on PIK3CB." Proc Natl Acad Sci U S A **105**(35): 13057-13062.

Weigelt, B., F. L. Baehner and J. S. Reis-Filho (2010). "The contribution of gene expression profiling to breast cancer classification, prognostication and prediction: a retrospective of the last decade." J Pathol **220**(2): 263-280.

Wen, W. S., Z. M. Yuan, S. J. Ma, J. Xu and D. T. Yuan (2016). "CRISPR-Cas9 systems: versatile cancer modelling platforms and promising therapeutic strategies." Int J Cancer **138**(6): 1328-1336.

Weng, Q., M. Zhao, J. Zheng, L. Yang, Z. Xu, Z. Zhang, J. Wang, J. Wang, B. Yang, Q. Richard Lu, M. Ying and Q. He (2019). "STAT3 dictates beta-cell apoptosis by modulating PTEN in streptozocin-induced hyperglycemia." Cell Death Differ.

Will, M., A. C. Qin, W. Toy, Z. Yao, V. Rodrik-Outmezguine, C. Schneider, X. Huang, P. Monian, X. Jiang, E. de Stanchina, J. Baselga, N. Liu, S. Chandarlapaty and N. Rosen (2014). "Rapid induction of apoptosis by PI3K inhibitors is dependent upon their transient inhibition of RAS-ERK signaling." Cancer Discov **4**(3): 334-347.

Yang, J., J. Nie, X. Ma, Y. Wei, Y. Peng and X. Wei (2019). "Targeting PI3K in cancer: mechanisms and advances in clinical trials." Mol Cancer **18**(1): 26.

Yap, T. A., A. Omlin and J. S. de Bono (2013). "Development of therapeutic combinations targeting major cancer signaling pathways." J Clin Oncol **31**(12): 1592-1605.

Yart, A., M. Laffargue, P. Mayeux, S. Chretien, C. Peres, N. Tonks, S. Roche, B. Payrastre, H. Chap and P. Raynal (2001). "A critical role for phosphoinositide 3-kinase upstream of Gab1 and SHP2 in the activation of ras and mitogen-activated protein kinases by epidermal growth factor." J Biol Chem **276**(12): 8856-8864.

Yoon, Y. K., H. P. Kim, S. W. Han, H. S. Hur, D. Y. Oh, S. A. Im, Y. J. Bang and T. Y. Kim (2009). "Combination of EGFR and MEK1/2 inhibitor shows synergistic effects by suppressing

EGFR/HER3-dependent AKT activation in human gastric cancer cells." Mol Cancer Ther **8**(9): 2526-2536.

Youlden, D. R., S. M. Cramb, C. H. Yip and P. D. Baade (2014). "Incidence and mortality of female breast cancer in the Asia-Pacific region." Cancer Biol Med **11**(2): 101-115.

Yu, C. F., Z. X. Liu and L. G. Cantley (2002). "ERK negatively regulates the epidermal growth factor-mediated interaction of Gab1 and the phosphatidylinositol 3-kinase." J Biol Chem **277**(22): 19382-19388.

Yu, H. and R. Jove (2004). "The STATs of cancer--new molecular targets come of age." Nat Rev Cancer **4**(2): 97-105.

Yu, H., H. Lee, A. Herrmann, R. Buettner and R. Jove (2014). "Revisiting STAT3 signalling in cancer: new and unexpected biological functions." Nat Rev Cancer **14**(11): 736-746.

Yu, X., L. He, P. Cao and Q. Yu (2015). "Eriocalyxin B Inhibits STAT3 Signaling by Covalently Targeting STAT3 and Blocking Phosphorylation and Activation of STAT3." PLoS One **10**(5): e0128406.

Yusoff, P., D. H. Lao, S. H. Ong, E. S. Wong, J. Lim, T. L. Lo, H. F. Leong, C. W. Fong and G. R. Guy (2002). "Sprouty2 inhibits the Ras/MAP kinase pathway by inhibiting the activation of Raf." J Biol Chem **277**(5): 3195-3201.

Zawistowski, J. S., S. M. Bevill, D. R. Goulet, T. J. Stuhlmiller, A. S. Beltran, J. F. Olivares-Quintero, D. Singh, N. Sciaky, J. S. Parker, N. U. Rashid, X. Chen, J. S. Duncan, M. C. Whittle, S. P. Angus, S. H. Velarde, B. T. Golitz, X. He, C. Santos, D. B. Darr, K. Gallagher, L. M. Graves, C. M. Perou, L. A. Carey, H. S. Earp and G. L. Johnson (2017). "Enhancer Remodeling during Adaptive Bypass to MEK Inhibition Is Attenuated by Pharmacologic Targeting of the P-TEFb Complex." Cancer Discov **7**(3): 302-321.

Zhang, J., X. Gao, F. Schmit, G. Adelmant, M. J. Eck, J. A. Marto, J. J. Zhao and T. M. Roberts (2017). "CRKL Mediates p110beta-Dependent PI3K Signaling in PTEN-Deficient Cancer Cells." Cell Rep **20**(3): 549-557.

Zhang, J., Z. Gao, J. Yin, M. J. Quon and J. Ye (2008). "S6K directly phosphorylates IRS-1 on Ser-270 to promote insulin resistance in response to TNF-(alpha) signaling through IKK2." J Biol Chem **283**(51): 35375-35382.

Zhang, X. H., L. Y. Tee, X. G. Wang, Q. S. Huang and S. H. Yang (2015). "Off-target Effects in CRISPR/Cas9-mediated Genome Engineering." Mol Ther Nucleic Acids **4**: e264.

Zhao, L. and P. K. Vogt (2008). "Class I PI3K in oncogenic cellular transformation." Oncogene **27**(41): 5486-5496.

Zhong, Z., Z. Wen and J. E. Darnell, Jr. (1994). "Stat3: a STAT family member activated by tyrosine phosphorylation in response to epidermal growth factor and interleukin-6." Science **264**(5155): 95-98.

Zhou, J., J. Wulfkuhle, H. Zhang, P. Gu, Y. Yang, J. Deng, J. B. Margolick, L. A. Liotta, E. Petricoin, 3rd and Y. Zhang (2007). "Activation of the PTEN/mTOR/STAT3 pathway in breast cancer stem-like cells is required for viability and maintenance." Proc Natl Acad Sci U S A **104**(41): 16158-16163.

Appendix 1

Please find my recently published review paper which we conceived on the topic of adaptive resistance mechanisms to targeted inhibition of two major oncogenic signalling axes frequently dysregulated in breast cancer, the PI3K-AKT-mTOR and RAS-MAPK signalling pathways. In this review we discuss the potential combination treatment strategies that overcome such resistance, and we also highlight application of quantitative and computational modelling as a novel integrative and powerful approach to gain network-level understanding of network rewiring, and rationally identify and prioritise effective drug combinations.

Cremers *et al*. *Cancer Drug Resist* 2019;2:[Online First]
DOI: 10.20517/cdr.2019.60

Cancer Drug Resistance

Review

Open Access

Network rewiring, adaptive resistance and combating strategies in breast cancer

Constance Gaya Cremers[1,2], Lan K. Nguyen[1,2]

[1]Department of Biochemistry and Molecular Biology, School of Biomedical Sciences, Monash University, Clayton, Victoria 3800, Australia.
[2]Biomedicine Discovery Institute, Monash University, Clayton, Victoria 3800, Australia.

Correspondence to: Dr. Lan K. Nguyen, Biomedicine Discovery Institute, Monash University, Clayton, Victoria 3800, Australia. E-mail: lan.k.nguyen@monash.edu

How to cite this article: Cremers CG, Nguyen LK. Network rewiring, adaptive resistance and combating strategies in breast cancer. *Cancer Drug Resist* 2019;2:[Online First]. http://dx.doi.org/10.20517/cdr.2019.60

Received: 11 Jul 2019 **First Decision:** 18 Sep 2019 **Revised:** 23 Sep 2019 **Accepted:** 15 Oct 2019 **Published:** 24 Oct 2019

Science Editor: Godefridus J. Peters **Copy Editor:** Cai-Hong Wang **Production Editor:** Tian Zhang

Abstract

Resistance to targeted anti-cancer drugs is a complex phenomenon and a major challenge in cancer treatment. It is becoming increasingly evident that a form of acquired drug resistance known as "adaptive resistance" is a common cause of treatment failure and patient relapse in many cancers. Unlike classical resistance mechanisms that are acquired via genomic alterations, adaptive resistance is instead driven by non-genomic changes involving rapid and dynamic rewiring of signalling and/or transcriptional networks following therapy, enabled by complex pathway crosstalk and feedback regulation. Such network rewiring allows tumour cells to adapt to the drug treatment, circumvent the initial drug challenge and continue to survive in the presence of the drug. Despite its great clinical importance, adaptive resistance remains largely under-studied and poorly defined. This review is focused on recent findings which provide new insights into the mechanisms underlying adaptive resistance in breast cancer, highlighting how breast tumour cells rewire intracellular signalling pathways to overcome the stress of initial targeted therapy. In particular, we investigate adaptive resistance to targeted inhibition of two major oncogenic signalling axes frequently dysregulated in breast cancer, the PI3K-AKT-mTOR and RAS-MAPK signalling pathways; and discuss potential combination treatment strategies that overcome such resistance. In addition, we highlight application of quantitative and computational modelling as a novel integrative and powerful approach to gain network-level understanding of network rewiring, and rationally identify and prioritise effective drug combinations.

Keywords: Network rewiring, adaptive resistance, PI3K signalling, MAPK signalling, breast cancer, mathematical modelling, systems analysis

© The Author(s) 2019. **Open Access** This article is licensed under a Creative Commons Attribution 4.0 International License (https://creativecommons.org/licenses/by/4.0/), which permits unrestricted use, sharing, adaptation, distribution and reproduction in any medium or format, for any purpose, even commercially, as long as you give appropriate credit to the original author(s) and the source, provide a link to the Creative Commons license, and indicate if changes were made.

ADAPTIVE RESISTANCE TO ANTI-CANCER MONOTHERAPY

Cancer is a complex network disease in which cells have acquired the ability to divide and grow uncontrollably, usually through genetic alterations in specific genes[1]. The discovery of molecular drivers of cancer and development of targeted drugs against these molecules have truly transformed the treatment of cancer. Imatinib (Gleevec), an inhibitor that blocks the BCR-Abelson murine leukemia viral oncogene homolog 1 (ABL1) tyrosine kinase activated in chronic myeloid leukemia (CML), is an outstanding example of an effective targeted therapy. Despite initial successes however, the overall progress of targeted therapy in the clinic has been hampered by the emergence of drug resistance, especially to those administered as single-agents, often referred to as monotherapy.

Drug resistance is a complex phenomenon and a major cause of cancer treatment failure, leading to patient relapse, disease progression and death[2]. Broadly, resistance to anti-cancer therapies can be divided into 2 categories: intrinsic or acquired. The former indicates the pre-existence of resistance-inducing factors in the tumour even before drug administration, and thus the treatment is ineffective from the start. In contrast, acquired resistance develops during the course of treatment, typically following an initial period when the treatment is effective. To date, multiple direct and indirect mechanisms underlying drug resistance have been identified, including - poor drug influx or excessive efflux, inherent cellular heterogeneity within the tumour, drug inactivation and alterations of the drug targets, which can act independently or in combination to limit drug efficacy[3].

Among the mechanisms of acquired resistance, development of secondary mutations of the drug targets that compromise binding or inhibition of the drug to the target has been probably the most well studied. Notable examples include the emergence of T790M mutation in epidermal growth factor receptor (EGFR) leading to resistance to gefitinib in EGFR-mutant lung cancer[4], T315 in ABL1 causing imatinib/dasatinib resistance in acute lymphocytic leukemia and CML[5,6]; and ERBB2/HER2 truncation leading to trastuzumab resistance in ERBB2-positive breast cancer[7]. In addition to these genetic mechanisms, it has become increasingly clear that tumour cells also rely on a non-genetic and highly adaptive mechanism involving dynamic rewiring of cell signalling networks to circumvent the initial drug blockade. A distinguishing and remarkable feature of drug-induced "network rewiring" and ensuing "adaptive resistance", compared to classical resistance mechanisms, is that they can occur extremely quickly and have been commonly observed within hours or days following drug treatment in cell and animal tumour models[8] as well as in cancer patients[9].

Given the great relevance of network-mediated adaptive resistance, an increasing number of studies have been undertaken that have shed new light on the underlying mechanisms of drug-induced network rewiring and illuminated common themes behind the cause of adaptive resistance. Here, we review recent and notable experimental studies in this area with a special focus on this adaptive resistance phenomenon to kinase inhibitors targeting the phosphoinositide 3-kinases (PI3Ks)/AKT/mTOR and receptor tyrosine kinase (RTK)/rapidly accelerated fibrosarcoma (RAS)-MAPK signalling pathways in breast cancer (BC). We discuss potential combination treatment strategies where additional targeted drugs are combined with the initial agent to overcome adaptive resistance caused by treatment of the latter alone. Furthermore, as signalling networks are highly complex systems due to an abundance of feedback regulation, pathway crosstalk and intricate post-translational modifications, in-depth understanding of signalling network rewiring requires new integrative and quantitative approaches that extend beyond experimental work alone. The rapid development of adaptive resistance under typically short-time scales also begs for a new perspective to interrogate drug response dynamically rather than just obtaining a static snapshot. To this end, we will highlight the application of systems-based approaches combining computational modelling with lab based experiment to cope with these challenges and advance the discovery of effective combination therapies.

PI3K-AKT-MTOR AND RAS-MAPK SIGNALLING PATHWAYS IN BC: KEY DRIVERS OF ONCOGENESIS

BC is the most common cancer among women, which accounts for about a quarter of all diagnosed human tumours[10]. Although early diagnosis and enhanced therapies have greatly improved the overall survival time, BC is still a leading cause of cancer-related death worldwide[10]. While BC is a common term referring to tumours originating from the breast, it is an extremely heterogeneous disease with multiple subtypes that are distinct in molecular characteristics, level of aggressiveness and association with patient outcome[11]. Depending on the molecular data and measuring techniques used, the subtyping of BC may differ slightly, but it is usually classified into several major subtypes based primarily on the status of 3 major cell-surface receptors: luminal A [estrogen receptor (ER) and/or progestogen receptor (PR) positive, HER2 negative]; luminal B (ER+ and/or PR+, HER2+); HER2-amplified (ER-, PR-, HER2+), and triple-negative BC (Basal-like or TNBC, ER-, PR-, HER2-)[12]. Targeted therapies are available for luminal A/B and HER2+ BC, however due to the lack of all three receptors TNBC currently has no targeted treatment options.

Advances in DNA sequencing over the past decade has enabled us to systematically study genetic alterations and their frequencies in cancer patients, leading to a better understanding of key cancer-driving signalling pathways. The PI3K-AKT-mTOR and RAS-MAPK signalling pathways are among the most frequently altered pathways across different cancer types including BC[13]. Located downstream of various RTKs, these are 2 major independent, yet highly interconnected, signalling cascades that critically regulate oncogenesis, reflected by their central roles in normal cell physiology[14]. The PI3K pathway is a prototypic survival pathway and is the most frequently dysregulated pathway in BC[15], through a variety of genetic disruptions such as deletion of the tumour suppressor PTEN, oncogenic mutations in phosphatidylinositol-4,5-bisphosphate 3-kinase catalytic subunit alpha mutation (PIK3CA), and/or HER2 amplification[16]. Altered PI3K signalling, defined by alternation of one or more genes within the pathway, occurs across different BC subtypes, but most frequently in Luminal A, HER2+ and Basal-like BC (62%, 60% and 53%, respectively)[13]. The most common genetic alteration of this pathway are activating mutations in PIK3CA gene which encodes the p110α catalytic subunit of PI3K. Data compiled on the alteration frequencies using the CBioPortal Cancer Genomics shows that ~40% of BC patients had PIK3CA alterations, followed by 11% having PTEN deletion [Figure 1A]. Interestingly, while alterations in PIK3CA are primarily missense mutations and occur mostly in luminal A/B or HER2+ patients, loss of PTEN prominently happens in Basal-like/TNBC patients[17].

Disruptive activation of the RAS-MAPK pathway, on the other hand, occurs in more than 30% of human cancers and is associated with increased risk of metastasis[18]. Activation of the pathway can be brought about by mutations in the core members RAS and RAF, but more often is due to alterations of upstream RTKs such as the ERBB family receptors, fibroblast growth factor receptor (FGFR) or MET. When this was taken into account, among the 10 most common oncogenic signalling pathways the RTK-RAS-MAPK pathway had the highest median frequency of alterations (46%) across all cancer types[13]. Of these, HER2+ BC has the third highest alteration rate in this pathway (82%), after only melanoma (94% altered) and the genomically-stable subtype of colorectal cancer (88%)[13]. EGFR, the most well-known upstream RTK of RAS-MAPK signalling, is frequently amplified in TNBC/basal-like subtype[19,20], leading to pathway activation in ~50% of these patient groups[21].

Due to their frequent alterations, targeting the receptor and protein kinase components of the PI3K and RAS-MAPK signalling pathways have been attractive therapeutic approaches for BC, reflected by an increasing array of targeted agents under active development and clinical testing[22,23] [Figure 1B]. Yet, network rewiring and adaptive resistance represent major obstacles that limit the full clinical potential of these inhibitors. Below, we will first discuss these phenomenon observed for inhibitors targeting the RAS-MAPK pathway, followed by those targeting the PI3K pathway.

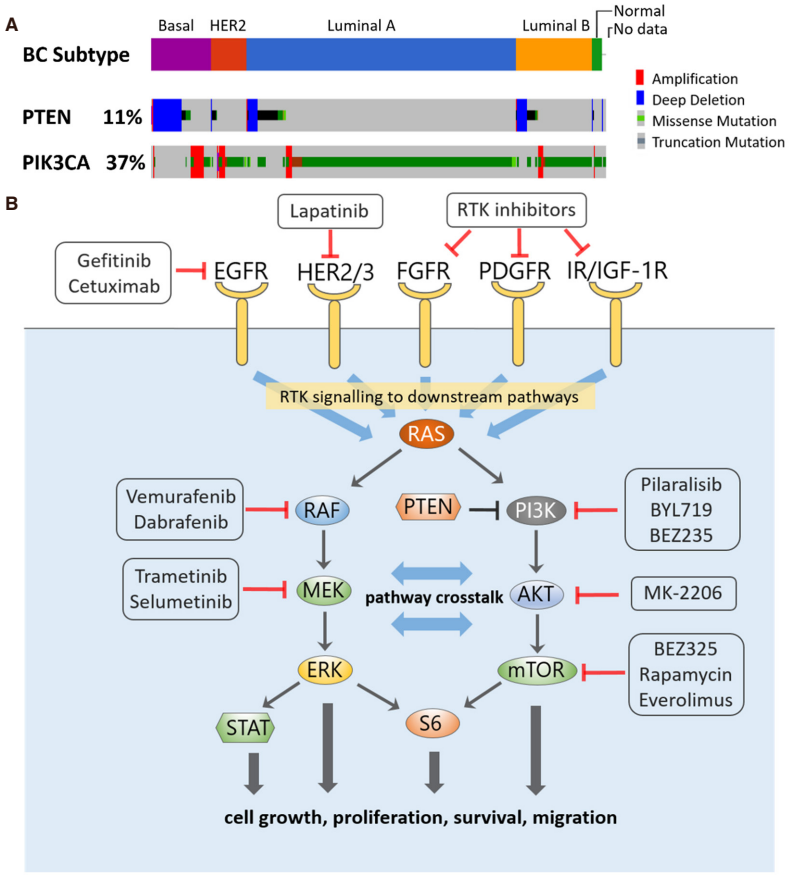

Figure 1. A: Frequency of alterations of PTEN and PIK3CA in breast cancer patients by subtype, analysed using the Pan-cancer Atlas dataset (n = 994) from The Cancer Genome Atlas Program (www.cbioportal.org); B: Signalling crosstalk between the PI3K and MAPK signalling pathways, with examples of targeted inhibitors directed at the network nodes

NETWORK REWIRING IN RESPONSE TO RAS-MAPK PATHWAY INHIBITION: ADAPTIVE RESISTANCE MECHANISMS AND PROPOSED COMBINATION THERAPIES

MEK inhibition activates PI3K-AKT signalling by relieving negative feedback on ERBBs

As a central node within the RAS-MAPK signalling cascade, MEK represents a promising therapeutic target; however clinical studies of MEK inhibitors (MEKi) have shown only limited anti-tumour activity[24,25]. The earliest evidence of adaptive response to MEK inhibition in BC was reported almost a decade ago by independent groups[26,27], where they found inhibition of MEK led to unexpected and rapid activation of PI3K-AKT signalling. To determine how this actually happened, Mirzoeva *et al.*[27] performed a targeted reverse-phase protein array (RPPA) allowing for temporal response of ~30 pan-pathway signalling nodes to the MEK inhibitor U0126, using the TNBC MDA-MB-231 cells as a model system. Besides activated AKT which occurred as soon as 1 hour after drug treatment, RPPA revealed the inhibitor also induced marked activation of EGFR within the same time frame, which was even more pronounced in the presence of epidermal growth factor (EGF). MEK inhibition-induced AKT activation was confirmed in 5 (out of 8 tested) cell lines including TNBC and luminal lines, suggesting this is a common, yet cell-specific phenomenon. Since EGFR is an upstream input of PI3K signalling and ERK is a known negative regulator of EGFR[28], the authors hypothesized that resistance to MEK inhibition is mediated by feedback activation of the PI3K pathway following relief of a negative feedback from MEK/ERK to PI3K/AKT via EGFR. Such feedback has been described previously[29]. In further support of this hypothesis, inhibition of EGFR effectively abolished the adverse AKT activation caused by MEK inhibition alone; and combined MEK-PI3K inhibition synergistically suppressed growth in 4 of the 11 BC cell lines tested[27].

Similar findings were reported around the same time by Hoeflich *et al.*[26], who provided additional *in vivo* evidence that dual MEK-PI3K inhibition was synergistic in reducing tumour growth in a MDA-MB-231 derived xenograft model of TNBC. A common conclusion reached by both studies was that basal-like/ TNBC is particularly susceptible to MEK inhibition as compared to other BC subtypes, this however, seemed to be a weak association rather than a general rule as several TNBC cell lines, including MDA-MB-231, were among the most resistant cell lines against MEKi[26,27]. Lack of PTEN, which occurs in a subset of TNBC cell lines and promotes basal PI3K-AKT signalling, was attributed to enhanced resistance to MEKi-based therapy[26]. While MEKi-induced AKT activation tends to occur in BC cell lines having normal PTEN in these studies, it remains unclear if such adaptive response also happens in a PTEN-null background or if the already enhanced basal AKT activation would buffer the potential effect coming from breaking the MEK-EGFR-PI3K negative feedback.

The network rewiring induced by MEK inhibition that led to AKT activation is not exclusive to TNBC or HER2-negative BC. A few years later, a study from the Engelman group showed that this signalling remodelling also occurs in a range of HER2-driven cancers[30], including breast and lung cancer. Importantly, this work provided critical mechanistic insights into the functioning of the MEK/ERK-to-PI3K feedback loop, which turned out to be mediated by ERRB3 (HER3), rather than EGFR directly. Specifically, MEK inhibition (by AZD6244/ selumetinib) activates AKT by inhibiting ERK activity, which blocks an ERK-mediated inhibitory threonine phosphorylation on the juxtamembrane domains of EGFR (T669) and HER2 (T677). Relief of this negative regulation by MEKi led to dramatic activation of HER3, enhanced binding of HER3 to GAB1 and PI3K, and AKT phosphorylation. Consistently, knockdown of HER3 abrogates this feedback and re-sensitises cancer cells to AZD6244 treatment. Although the previous studies did not examine HER3[26,27], in hindsight the feedback activation of AKT seen in these works was also likely to be mediated by HER3, in addition to EGFR.

The above findings, collectively, may suggest that feedback activation of AKT is a common theme among breast and other cancers addicted to EGFR/HER2 and/or displaying over-activation of ERK signalling[26,27,31] , this however, is not the case. Indeed, when treating a panel of KRAS-mutant cell lines to MEK inhibitor, Turke *et al.*[30] found that AKT was not adversely activated despite potent upregulation of phosphorylated ERBB3/HER3, indicating the MEK/ERK-ERBB3-PI3K feedback loop was not working under these conditions. This may be due to low levels of EGFR and HER2 in these cells, which were insufficient to transactivate ERBB3 to a level high enough for AKT activation. Another reason may be because the network circuitry is different and ERBB3 did not drive PI3K in these KRAS-mutant cell lines. In support of this, IGF-IR/IRS has been shown to be the major PI3K input in these cells[32]. While the exact cause(s) for the disconnect between ERBB3 and AKT activation requires further investigation, the above studies have demonstrated a highly dynamic and context-specific network rewiring mechanism to MEK inhibition involving the PI3K/AKT pathway, which underlies adaptive resistance to MEKi-based therapy.

MEK inhibition drives extensive rewiring of the kinome and epigenomic networks

While inhibition of MEK had been known to acutely reprogram specific signalling networks, the extent and complexity of such reprogramming was only truly revealed in a seminal study in 2013[8], thanks to advances in mass-spectrometry (MS)-based proteomics. Using a chemical proteomics approach that coupled kinase affinity capture with quantitative mass spectrometry, Duncan *et al.*[8] was able to elucidate for the first time the kinome changes in response to MEK inhibition at a global level, in both cultured cells and genetically modified mouse models of TNBC. Remarkably, MEK inhibition by AZD6244 (and U0126) induced an extensive and dynamic remodelling of the cell signalling systems that extended far beyond ERBB/PI3K signalling, evident by large changes in expression and/or activation of > 140 kinases, from all major kinase subfamilies, within 24 h of treatment. These include a variety of pro-survival RTKs; PDGFRβ,

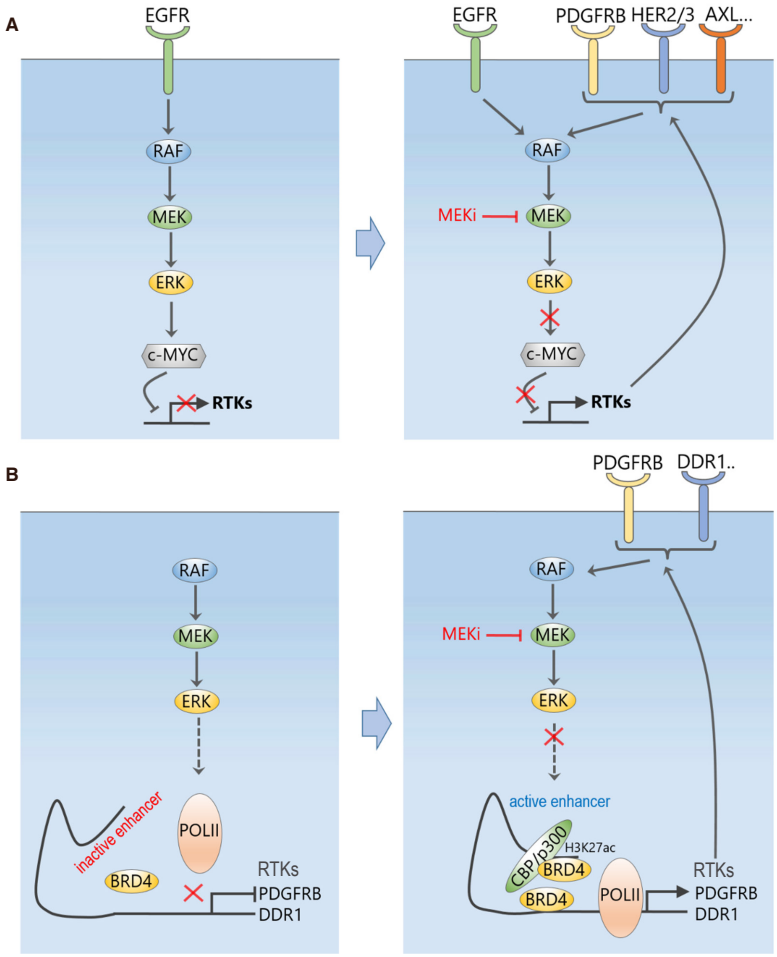

Figure 2. MEK inhibition dynamically reprograms the kinome and RTK signalling network. A: Inhibition of MEK disrupts a repressing transcriptional program exerted by the transcriptional factor c-Myc on the RTKs, which leads to induced expression and activation of an array of RTKs; B: MEK inhibition triggers a dynamic genome-wide enhancer formation with pronounced BRD4 density co-occupied with typical enhancer marks, causing increased expression and subsequent activation of RTKs, including PDGFRB, FGFR2, and DDR1

VEGFR, AXL, HER2/3 and discoidin domain receptor family, member 1 (DDR1), and this inhibitor-induced RTK remodelling was accompanied by increased oncogenic signalling through the PI3K/AKT, JAK/STAT and MEK/ERK pathways, consistent with previous observations[27]. The results by Duncan *et al.*[8] were significant as it revealed that selective perturbation of even a single node can trigger an extensive and rapid global response by the cancer cell signalling machinery, which counteracts the inhibitor's effect.

While defining the changes of signalling responses to targeted inhibitors is, nowadays, relatively straightforward with modern MS-based technologies like quantitative chemical proteomics, elucidating the underlying mechanisms of network rewiring is, however, more challenging. In addressing this, Duncan *et al.*[8] found that the induced RTK expression/activation was due to disruption of a repressing transcriptional program exerted by the transcriptional factor c-Myc on the RTKs [Figure 2A]. As ERK phosphorylates c-Myc on S62 and enhances its stability, acute loss of ERK activity by MEKi treatment led to rapid c-Myc degradation and hence transcriptional de-repression of RTKs and their ligands that are negatively regulated by c-Myc. In support of this, RNAi-mediated knockdown of ERK or c-Myc induced similar RTKs as seen with MEKi, and blocking c-Myc degradation prevented the kinome reprogramming. Given c-Myc is not the only transcription factor regulating the induced RTKs, it is unlikely c-Myc degradation is the sole mechanism responsible for their transcriptional induction, yet this mechanistic

insight offered valuable guidance for rational choice of combination therapy. For example, future selective inhibition of the E3 ligase(s) responsible for c-Myc degradation may help stabilize c-Myc and thus revert the MEKi-induced kinome remodelling. Until this is possible, the authors demonstrated proof of principle that combined treatment of MEK inhibitor selumetinib (AZD6244) with a pan-RTK inhibitor sorafenib synergistically reduced tumour growth in a mouse model of TNBC; albeit this combination is unlikely to be clinically useful due to the extensive off-target profile of sorafenib, which also targets RAF kinases.

To overcome this issue, a recent follow-up study[9] has demonstrated that rather than trying to combat RTK upregulation using a secondary kinase inhibitor like sorafenib, the use of bromodomain and extra-terminal motif (BET) inhibitors (BETi), which targets bromodomain-containing proteins 2, 3 and 4 (BRD2/3/4), effectively and broadly prevented MEKi-induced transcriptional adaptation. This happened not only in TNBC cell lines, but also in patients following a small 7-day window-of-opportunity clinical trial of MEKi trametinib treatment, highlighting the significant clinical relevance of the findings. Mechanistically, the authors found MEKi induced an expansive, genome-wide and rapid remodelling of the epigenomic landscape[9]. BET family bromodomain proteins such as BRD4, bind to acetylated lysines of histone subunits or transcriptional factors to regulate transcriptional elongation through recruitment of positive transcription elongation factor (P-TEFb), an RNA polymerase II complex containing cyclin-dependent kinase 9 (CDK9) and Cyclin T1. Within 1-4 h of trametinib treatment, enhancers with pronounced BRD4 density co-occupied with typical enhancer marks were formed genome-wide, including at sites proximal to RTK loci such as *PDGFRB*, *FGFR2*, and *DDR1*, explaining their induced upregulation [Figure 2B]. Remarkably, BETi reduced the total number of MEKi-induced enhancers near baseline level; and BETi JQ1 combined with trametinib durably and synergistically inhibited tumour growth in both orthotropic and syngeneic mouse models of TNBC[9]. Consistent with the proposed model of RTK upregulation, small-molecule inhibition of P-TEFb constituent CDK9, or BRD4-associated factor p300 abrogated adaptive RTK induction.

Overall, the above studies together have unveiled extraordinary adaptive reprogramming of cancer cells to targeted MEK inhibition at both epigenomic and signalling levels, the former initially triggered the latter, which in turn likely fuelled further epigenomic changes in a positive-feedback manner. Although they have provided major insights in our understanding of inhibitor-induced acute adaptation, key questions remain to be answered. For example, given that the discussed work has utilised only a handful of TNBC cell models, are the observed rewiring mechanisms conserved across different TNBC cells, and if so do they occur to a similar extent? Clues to these questions came from[9] where it found that TNBC cells of a basal-like subtype failed to remodel the BRD4 epigenome following MEK inhibition, while cells of the claudin-low subtype displayed comprehensive *de novo* enhancer formation, suggesting remodelling is likely cell type and context specific. Are the observed transcriptional and signalling rewiring and their mechanisms unique to MEKi? Or will different sets of RTKs be induced by inhibitors targeting other kinases, e.g., PI3K or mTOR? We believe in-depth answers to these questions will require more systematic efforts involving the use of large cell line panels and diverse drug agents, which will better illuminate the level and extent of tumour context-specific plasticity in response to targeted treatment.

SHP2 drives adaptive resistance in KRAS-mutant and ERK-dependent tumours

In addition to overcoming MEK inhibitor resistance by targeting the induced RTKs directly with polypharmacology-based agents or preventing their transcriptional induction using BETi, inhibition of the convergent signalling "hubs" downstream of these RTKs also presents an attractive therapeutic strategy. This logic was successfully applied to Src homology region 2 (SH2)-containing protein tyrosine phosphatase 2 (Shp2), a phosphatase encoded by the gene *PTPN11*, which sits downstream of multiple RTKs and is critical for RAS activation. In 2018 and early 2019, five independent studies demonstrated that combining MEK inhibitor with a SHP2 inhibitor (SHP099) effectively abolished the adaptive resistance caused by single-

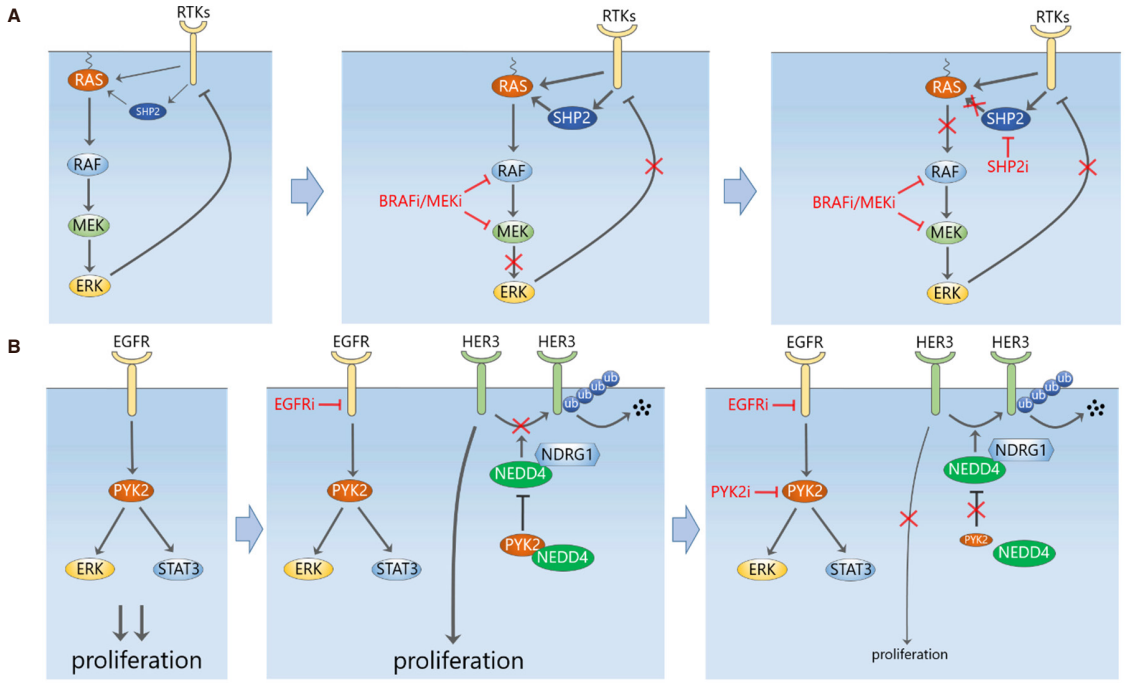

Figure 3. Adaptive upregulation of compensatory signalling limits the efficacy of EGFR-MAPK pathway inhibition. A: SHP2 is a convergent signalling node downstream of multiple RTKs. Inhibition of MEK induces SHP2 activation through increased RTK signalling and possibly other direct mechanisms, leading to ERK activity rebound. Inhibition of SHP2 prevents MEKi-induced ERK rebound through limiting the activity of RAS; B: upregulation of HER3 mediates adaptive resistance to EGFR in TNBC cells. PYK2 normally binds to the E3 ligase NEDD4 to inhibit it from degrading HER3. Inhibition of PYK2 destabilizes HER3 and resensitizes TBNC cells to EGFR inhibitors

agent MEKi treatment in a wide variety of RAS-mutant/amplified cancers, including pancreatic, lung and gastric cancer[33-37]. Biochemically, SHP2i prevents MEKi-induced ERK rebound through limiting the induced RAS-GTP loading mediated by the upstream RTKs[37] [Figure 3A]. Interestingly, Fedele *et al.*[37] further showed that this combined treatment also overcame adaptive resistance in RAS-normal TNBC cells. The effect on TNBC was subsequently solidified by Ahmed *et al.*[36], who found the dual MEK-SHP2 inhibition profoundly inhibited both ERK signaling and cell growth in a panel of TNBC cell lines, including RAS-mutant and RTK-overexpressing TNBC cells, suggesting this combination provides a potential therapeutic strategy for TNBC patients. These results are in line with a previous finding that SHP2 promotes basal-like and TNBC[38]. Interestingly, not only MEK inhibition induced SHP2 activity, but also treatment of SHP2i alone was found to trigger a rebound of ERK[37]. This finding and evidence that SHP2 also acts upstream of RTKs (e.g., EGFR, MET and FGFR[38]) suggest the RTKs-SHP2-ERK circuitry is probably far more complex than currently known, and certainly more work is required for better mechanistic understanding.

While the collective evidence supporting MEK-SHP2 dual inhibition in KRAS-driven tumours is overwhelming, it is clear that this combination also works in additional tumour contexts, including those driven by ERK signalling either via BRAF mutations, overexpressed RTKs, or even under wild-type KRAS background[33-37]. The next key challenge in translating this combination therapy into the clinic will be identification of predictive biomarkers to guide patient selection for clinical trials. It appeared that patients having mutated RAS with high intrinsic GTPase activity (e.g., RAS G12C/S/A) are more sensitive to MEK-SHP2 co-targeting, while those with low GTPase-activity RAS mutants (e.g., Q61X) are more refractory to the regimen. Further, a high baseline level of phosphorylated SHP2 (e.g., pY542, indicative of SHP2 activity) seemed predictive of treatment sensitivity[37]; but as it remains unclear whether SHP2's catalytic activity, its scaffolding function, or both are important for ERK rebound, the abundance of SHP2 may also serve as a good biomarker in certain contexts. Due to the complexity of the target network and highly

context-dependent activity of MEK-SHP2 co-targeting strategy, determinants of its efficacy are probably multi-factorial and optimal companion biomarkers will likely involve multiple gene/protein indicators. We believe this issue is not unique to the MEKi+SHP2i combination, but rather will be a general rule for combination therapies.

Extracellular RTK shedding contributes to adaptation to ERK signalling inhibition

Studies to date have primarily shown that tumour cells rewire their intracellular communication networks to adapt to drug challenge, extracellular mechanisms however, also contribute to such adaptive response. A variety of transmembrane receptors, including RTKs are known to undergo proteolysis via cleavage at extracellular sites mediated by metalloproteinases, such as A Disintegrin And Metalloproteinases 10 and 17 (ADAM10/17). Miller *et al.*[39] found that MEK inhibition reduced the proteolytic shedding of multiple RTKs, including HER4, MET and most prominently AXL (an ADAM10/17 substrate) in melanoma and TNBC cells. Reduced RTK shedding increased the accumulation of full-length, signalling-competent RTKs on the tumour cell surface, which led to enhanced mitogenic signalling through downstream signalling such as the JNK/cJun pathway, thus evading the initial MEK inhibition. Consequently, combination of MEKi trametinib and AXL inhibitor R428 synergistically reduced tumour growth and metastasis in orthotopic TNBC (and melanoma) xenograft models derived from cell lines that showed increased surface AXL following MEKi. The findings by Miller *et al.*[39] add an extra layer of complexity to the adaptation of cancer cells to targeted agents, and suggest that reduced RTK shedding may complement other bypassing mechanisms to reactivate oncogenic signalling. This is because many RTKs previously seen transcriptionally upregulated by MEKi, including PDGFRβ and VEGFR2, are also subject to shedding[8]. Figuring out which and how these different bypassing mechanisms co-operate under specific tumour contexts will be crucial in developing effective combination strategies to overcome them.

TNBC circumvents EGFR inhibition through post-translational upregulation of ERBB3

It has been found that in TNBC patients EGFR inhibition is circumvented through HER3 upregulation[40]. Verma *et al.*[41] recently showed that this HER3-mediated drug resistance was abolished by inhibition of the non-receptor tyrosine kinase proline-rich tyrosine kinase 2 (PYK2), thereby preventing the adaptive resistance to EGFR inhibition. They demonstrated that high expression of both PYK2 and EGFR is significantly associated with poor clinical outcome in TNBC patients, and combined targeting of EGFR and PYK2 was synergistic in blocking proliferation and inducing cell death of basal-like TNBC cells. Dual inhibition of EGFR and PYK2/FAK blocked key growth and survival pathways mediated by AKT, S6K, STAT3 and ERK1/2 activation. Importantly, the authors validated this drug combination *in vivo* by demonstrating it was able to attenuate tumour growth in a mouse xenograft model. These data suggest that EGFR-PYK2 co-inhibition provide a potential effective treatment for a subset of basal-like TNBC.

In addressing the mechanism underlying why PYK2 was a good EGFR co-target, the authors found that N-Myc Downstream Regulated 1 (NDRG1) enhanced the interaction of HER3 with the ubiquitin ligase neural precursor cell expressed developmentally down-regulated protein 4 (NEDD4), while PYK2, which interacts with NEDD4 and HER3, disrupted this NEDD4-HER3 binding. Inhibition of PYK2 thus facilitated the proteosomal degradation of HER3 and counteracted the increase in HER3 expression caused by EGFR antagonists [Figure 3B]. This provides a novel post-translational mechanism for drug-induced HER3 upregulation that is distinct from the previously discussed transcriptional induction of RTKs.

NETWORK REWIRING IN RESPONSE TO PI3K PATHWAY INHIBITION: ADAPTIVE RESISTANCE MECHANISMS AND PROPOSED COMBINATION THERAPIES

Non-redundant functional roles of PI3K isoforms in normal and transformed cells

The PI3Ks generate lipid second messengers inside cells, which are essential for controlling cellular functions, including cell survival, proliferation, metabolism and migration. The complexity of PI3K

signalling is, in part, due to existence of a large number (eight) of PI3K isoforms, grouped into three classes: class I, II and III, each generates different lipids - and controls different - biological aspects within the cell. While the reason(s) remain unclear, class I PI3Ks are the main PI3K genes found to be mutated in cancer, often at high frequency, and thus are the main PI3K isoforms currently pursued in anti-cancer drug development[42]. These PI3Ks are stimulated by tyrosine kinases, RAS and G protein-coupled receptors; and as such are often recruited by tyrosine kinase-based signalling networks, such as those activated by insulin and EGF. The class IA PI3Ks (PIK3Cα, PIK3Cβ, PIK3Cδ) exist as heterodimeric proteins made up of a regulatory p85 subunit (derived from three genes, *p85a, p85b* and *p55*) bound to one of three p110 catalytic subunits (p110α, p110β or p110δ, encoded by *PIK3CA*, *PIK3CB*, and *PIK3CD*, respectively).

The critical role of PI3K signalling in normal physiology and its frequent disruption in cancer has led to a major effort in developing inhibitors targeting the key kinase components of this pathway, in particular class I PI3Ks, AKT and mammalian target of rapamycin complex 1/2. To date, over 40 PI3K-signalling targeted inhibitors have been developed, which include isoform-selective PI3K inhibitors, pan-PI3K inhibitors, dual pan-PI3K and mTORC1/2 inhibitors, as well as specific inhibitors of mTORC1 and AKT. Although some of these agents such as the mTOR inhibitors (temsirolimus and everolimus) have already been approved for use in a number of cancers[43,44], undue toxicities and emergence of resistance, including adaptive resistance to these inhibitors have significantly hampered their full clinical potential as single-agent therapies[45]. Clinical translation is further complicated by the poorly-understood observations that different p110 isozymes play non-redundant roles in cell transformation. For examples, while p110α is predominantly required for growth of tumours driven by RTKs, mutant RAS, and/or PIK3CA mutations, p110β is the dominant isoform in PTEN-deficient tumours[46,47]. Thus, compared to pan-PI3K inhibitors, isoform-selective PI3K inhibitors are likely less toxic to normal tissues. Although differing toxicities are associated with various classes of PI3K pathway inhibitors, common adverse events in BC include stomatitis, non-infectious pneumonitis, rash, hyperglycemia, and immunosuppression[48]. On the downside, the use of isoform-selective inhibitors may lead to compensatory upregulation of other PI3K isoforms that reactivate the pathway and limit the drug efficacy. Striking the right balance between efficacy and toxicity is a major challenge in translating PI3K inhibitors into the clinic.

PI3K pathway inhibition reactivates AKT signalling through feedback upregulation of HER3 and other RTKs

In 2006, O'Reilly *et al.*[49] provided one of the first pieces of evidence of a feedback bypass mechanism in response to PI3K signalling inhibition[49]. They showed that in BC cell lines with hyper-activated PI3K signalling, mTOR inhibition by rapamycin released the mTORC1-dependent suppression of insulin-like growth factor 1 receptor (IGF1R) and insulin receptor (IR), thus upregulating insulin receptor substrate 1 and restoring PI3K/AKT signalling[49]. This drug-induced relief of the mTORC1-to-IRS1 negative feedback largely explained the modest anti-tumour activity by rapamycin and mTOR inhibitor analogues seen in the clinic. A few years later, Chakrabarty *et al.*[50] demonstrated that inhibition of PI3K by XL147 (pilaralisib), a highly selective pan-inhibitor of class 1A PI3Ks (α, β, γ, and δ), induced upregulation and activation of HER3 and other RTKs, including IR, IGF1R and FGFRs in HER2-overexpressing BC cell lines, which eventually reactivated PI3K/AKT signalling. The same changes were not due to off-target effects as they were also observed with another pan-PI3K inhibitor BKM120. The induction of these RTKs is explained in part by the relief of negative feedback from AKT to the RTKs via the forkhead box O (FOXO) family of transcription factors. Specifically, since AKT phosphorylates and inhibits FOXO via cytoplasmic sequestration[51], AKT inhibition by XL147 released FOXO to the nucleus which was then able to transcribe the RTKs[50]. Importantly, because in HER2+ cell lines, HER2 is a major activator of HER3, the upregulation of HER3 expression resulted in significant HER2-mediated increase in its activity, ultimately triggering PI3K reactivation and limiting XL147's efficacy. The authors went on to show that combinations of XL147 with HER2 antagonists (trastuzumab or lapatinib) were synergistic in delaying tumour growth in mice bearing xenografts derived from BT474, a HER2+/PIK3CA-mutant BC cell line. By utilising the same BC

experimental models, very similar observations were also reported by Chandarlapaty *et al.*[52], but using AKT inhibitors instead of pan-class I PI3K inhibitors as in[50]. This similarity probably came from the fact that AKT is a common downstream node of the class I PI3Ks. While the above studies both suggested HER2 induced PI3K signalling via HER3, recent work showed HER2, when overexpressed, can directly activate PI3K/AKT signalling independent of HER3[53]. Regardless, these studies together highlight that combined PI3K/HER2 inhibition may be a potentially effective treatment for HER2-overexpresing BC patients.

Would PI3K/HER2 co-inhibition be useful even in non HER2-dependent tumours? There are several clues to this question. First, PI3K/AKT and FOXO-dependent upregulation of HER3 was found even following HER2 inhibition by lapatinib[50,54]. Remarkably, even dual blockade of HER2 with trastuzumab and lapatinib did not entirely eliminate the compensatory upregulation of HER3[55]. These studies suggest that - low levels of residual HER2 comparable to that in non-HER2-amplified tumours may be sufficient to phosphorylate and activate HER3, subsequently causing PI3K/AKT activation after PI3K/AKT or HER2 inhibition. Further, strong induction of common RTKs including IGF-1R, IR, HER3, Ephrin type-A receptor 7 (EphA7), and rearranged during transfection (RET) were seen following AKT inhibition in both HER2+ and non-HER2+ cell lines[52]. Collectively, these findings suggest that dual blockade of AKT and HER2 signalling may also be useful in non-HER2+ contexts. Indeed, combined AKT/HER2 inhibition was synergistic in suppressing tumour growth in mice bearing xenograft established from NCI-H292, a non-HER2 amplified lung tumour cell lines[52]. Provided toxicity is tolerable, dual combination of either PI3K or AKT inhibitors with HER3-neutralizing monoclonal antibody, or triple combination of PI3K/AKT, HER2 inhibitors and a HER3 antibody may be fruitful therapeutics for HER2+ as well as non-HER2+ cancers, as these combinations would more completely eliminate HER2-mediated HER3 activation. In support of this notion, combination of LJM716 (a HER3 neutralizing antibody) and BYL719 (a PI3Kα-specific inhibitor) inhibited AKT phosphorylation more potently than LJM716 or BYL719 alone and synergistically inhibited growth in a panel of HER2-overexpressing breast and gastric cancer cells[56]. Furthermore, in HER2-normal tumours where PI3K signalling is likely not driven by HER2 alone, depending on which upregulated RTKs, discussed above, are the primary input into PI3K/AKT signalling, co-inhibition of PI3K/AKT and such RTK(s) could also provide potentially effective therapies. Nonetheless such avenues clearly warrant further investigation in future research.

What about BC with co-alteration of HER2 and PI3K? Our analysis of data from TCGA (using Cbioportal) showed that almost one third of HER2-amplified BC patients also harbour PIK3CA mutation and/or amplification[57]. In another important study[54], Chakrabarty *et al.*[54] found that expression of H1047R PI3K (the most common PI3K mutation) in MCF10A human mammary epithelial cells, but not E545K PI3K, markedly upregulated the HER3/HER4 ligand heregulin (HRG). This provides, yet another mechanism where specific PI3K mutations further fuel the activation of HER3 mediated by HER2. As expected, the PI3K inhibitor BEZ235 markedly inhibited HRG and phospho-AKT (pAKT) levels and, in combination with lapatinib, completely inhibited growth of cells expressing H1047R PI3K[54]. These findings suggest that selection of drug combinations would need to take into account the specific mutation status of PIK3CA, as direct PI3K inhibitors may be required to inhibit the unwanted mutation-induced upregulation of ERBB ligands[58]. These results also point to the combined use of PI3K inhibitors and ERBB1-3-neutralizing antibody mixtures, such as pan-HER/ERBB which can simultaneously block targeted ERBB receptors and ligands[59], as a potential therapy for BC tumours with HER2/PIK3CA co-alteration.

PI3K pathway inhibition rewires ERK signalling through multiple mechanisms

While the above studies have primarily demonstrated that the PI3K/AKT pathway itself is a major escape mechanism to inhibitors targeting PI3K signalling, other studies also found that compensatory activation of ERK signalling provides another escape route. First, Carracedo *et al.*[60] showed that inhibition of mTORC1 with rapamycin not only activated PI3K-AKT signalling, but also induced ERK phosphorylation in BC cell lines and tumour biopsies from patients treated with the drug. Rapamycin-induced ERK

activation occurred in both normal and cancer cells lines, due to interference of a negative feedback from mTORC1/S6K to PI3K/RAS, most likely mediated via IRS1[60]. Later, Serra *et al.*[61] demonstrated treatment of BEZ235, a dual PI3K/mTOR inhibitor, in HER2+ BC cells also led to potent ERK activation, but primarily through upregulation of the RTKs, particularly ERBB signalling. This mechanism of ERBB-induced ERK activity was confirmed as BEZ235 treatment combined with HER2/3 antagonists (lapatinib or trastuzumab) or MEK inhibitor (selumetinib) led to decreased ERK activity and improved anti-tumour activity *in vivo* compared to BEZ235 treatment alone[60].

Does ERK activation depend on the inhibitor target? While BEZ235 was mainly used, Serra *et al.*[61] also demonstrated ERK activation in response to a diverse range of agents such as pan-PI3K inhibitor (GDC-0941), p110α inhibitor (PIK-90), AKT inhibitor (MK-2206), as well as mTOR inhibitors (RAD001 and Torin1) in a couple of HER2+ BC cell lines including BT474, suggesting ERK activation is a broad consequence of PI3K signalling inhibition regardless of the targeted node[61]. This, however, is at odds with results from[50], which reported no consistent ERK activation in the BT474 cell line in response to pan-PI3K inhibition. Because the data related to ERK activation in BT474 cells was discussed but "not shown" in[60], we could not further analyse these findings. Additional clues to the above question came from Will *et al.*[62] who showed that inhibition of PI3K, but not AKT, leads to the rapid, but transient inhibition of the RAS-ERK signalling axis in HER2+ BC cells; and this inhibition, though transient, is critical for the enhanced cell death caused by PI3K over AKT inhibitors. The authors posited that inhibiting PI3K causes the rapid inhibition of both AKT-mTOR and RAS-ERK signalling, whereas AKT inhibitors suppress only the former and, in fact, activate the latter. The discrepancies among the above studies deserve more investigation, which will offer more clarity on how dependent ERK activation is with regard to the specific inhibitors and/or the targets they inhibit.

In line with the above observations, a more recent study also reported induced ERK activation following prolonged HER2 inhibition with lapatinib in HER2+ BC cells, which was partially dependent on FOXO transcription factors[63]. Interestingly, the lapatinib-induced increase in ERK phosphorylation correlated with increased stability of c-Myc, suggesting that in this case, ERK activation was probably due to disruption of both the AKT/FOXO and ERK/c-Myc negative feedbacks to the ERBB receptor family caused by lapatinib-mediated acute AKT and ERK inhibition. Further, compensatory ERK activation was observed *in vivo* in a genetically modified mouse model of HER2+ breast tumour with co-existing PIK3CA (H1047R) mutation following inactivation of the oncogenic PI3K[64]. Collectively, the studies discussed here provide a strong rationale for targeting both the PI3K and ERK pathways in HER2+ BC. Activation status of these pathways, including whether or not the tumours harbour loss of PTEN and/or RTK overexpression, can influence therapeutic response and serve as useful biomarkers for therapy selection[65].

Network rewiring in response to PI3K isoform-specific inhibition

The above studies have demonstrated adaptive resistance to pan-PI3K inhibitors, this however also occurred with more recently developed PI3K isoform-selective inhibitors. Schwartz *et al.*[66] showed that PI3Kβ inhibition by AZD8186 only transiently suppressed PI3K signalling in PTEN-deficient breast (and prostate) cancer cells, with rapid rebound of PI3K/AKT signalling observed just 2 h after drug treatment. Interestingly, it was found that the rebound depended on activation of the PI3Kα isoform, which was caused by feedback upregulation of its activators IRS1 and IGF1R [Figure 4A]. Combination of AZD8186 with a PI3Kα isoform inhibitor (BYL719) or IGF1R/IR inhibitor (OSI-906) both significantly attenuated this AKT rebound and efficiently suppressed cancer cell growth[66]. In the same vein, the work by Costa *et al.*[67] showed that PI3Kα inhibition by BYL719 initially abrogated PI3K signalling, but within 24 h induced a rebound in PI3K activation (indicated by the elevated phosphoinositide PIP3 level) in HER2+ or PIK3CA-mutant luminal BC cells[67]. Further analysis revealed that the elevated PIP3 was due to increased recruitment of

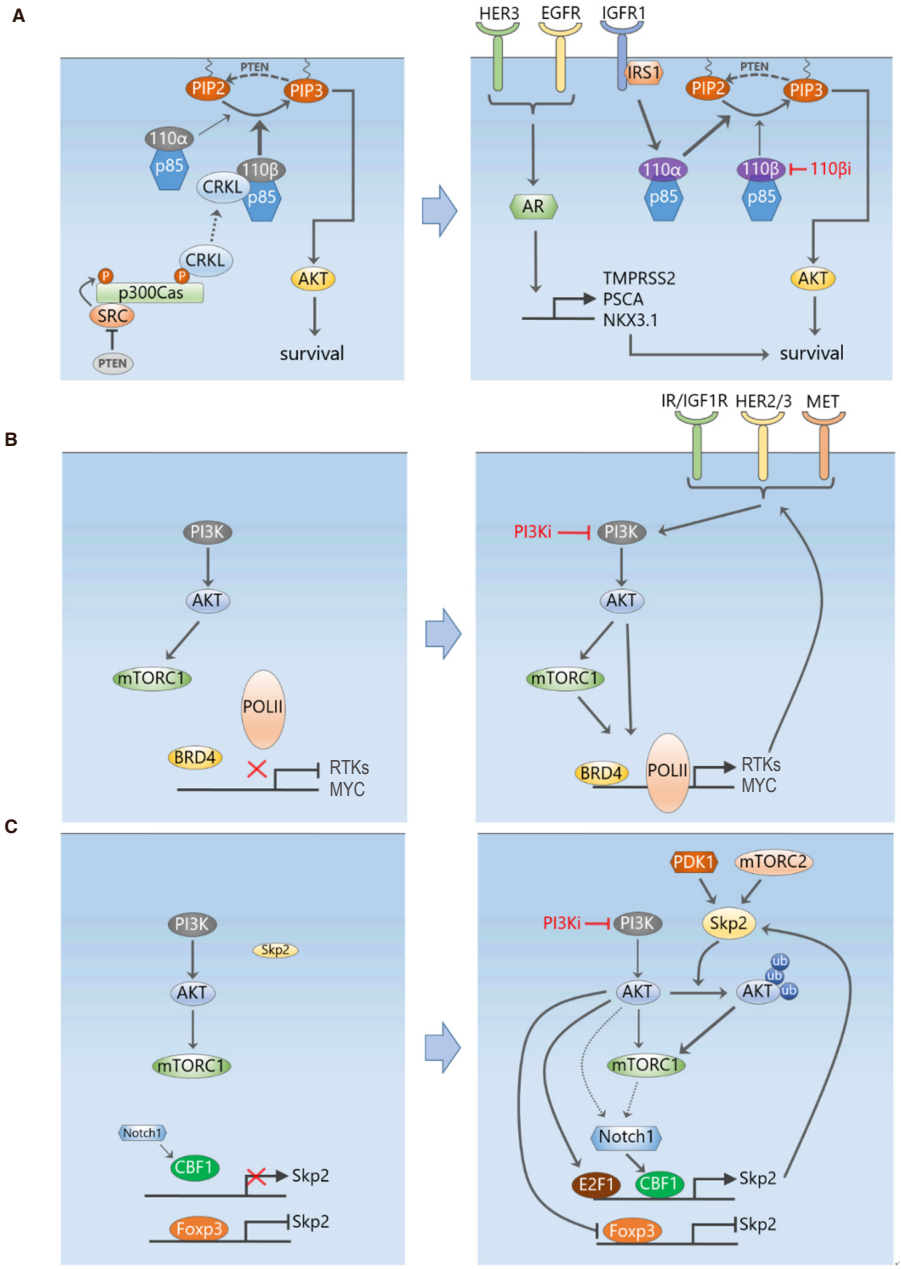

Figure 4. Selective adaptive resistance mechanisms in response to PI3K pathway inhibition. A: A PTEN/Src/p130Cas signalling axis activates CRKL/p110β in PTEN-deficient tumour cells, providing a link between PTEN loss and activation of p110β in these cells (left). Specific PI3Kβ inhibition cause feedback upregulation of IRS1 and IGF1R which then activates the PI3Kα isoform and results in a rebound of PI3K signalling following transient suppression (right). The androgen receptor downstream of several RTKs also provides another escape mechanism for continued survival following PI3K inhibition; B: similar to MEK inhibition, PI3K inhibition also reprograms the transcriptional machinery controlled by BRD4, leading to induced upregulation of multiple RTKs and MYC; C: a ubiquitin-based mechanism of adaptive resistance to PI3K inhibition mediated by the E3 ubiquitin ligase Skp2. PI3K inhibition leads to increased Skp2 expression and activity, which ubiquitinates and enhances the activation of AKT

the PI3Kβ isoform to HER3. As in[66], co-inhibition of both PI3Kα and β significantly enhanced BC cell death and induced tumour regression *in vivo*[67]. These reciprocal feedback regulation among the PI3K isoforms highlight another intricate layer of the feedback circuitry controlling the PI3K signalling pathway. Systems-level understanding of complex feedback mechanisms and isoform-specific PI3K signalling will be important in identifying tumours susceptible to individual isoform inhibition, and informing appropriate combination therapy.

While it has been long known that in PTEN-deficient cancer cells PI3K signalling is driven by PI3Kβ, the mechanism linking PTEN loss with preferential p110β activation was only recently illuminated. Zhang *et al.*[56] reported a role for the Crk-like adaptor protein (CRKL) in associating with and regulating p110β-dependent PI3K activity in PTEN-null cancer cells. Mechanistically, loss of PTEN activates Src, which in turn tyrosine phosphorylates the scaffolding protein p130Cas and phosphorylated p130Cas provides a platform for recruitment of CRKL that preferentially binds to p110β over p110α. Thus, a PTEN/Src/p130Cas axis activates CRKL/p110β in PTEN-null cancer cells [Figure 4A]. In support of this notion, the authors showed that Src inhibition co-operates with PI3K or p110β inhibition to suppress the growth of PTEN-null breast and prostate tumour cells[56]. However, further animal testing of these combinations are needed to confirm their synergistic effects in an *in vivo* setting.

To identify drugs that can be effectively combined with PI3Kβ inhibitor to comprehensively suppress PI3K signalling in PTEN-null tumours, Lynch *et al.*[68] performed a cell proliferation based drug combination screen in a panel of PTEN-null TNBC, prostate, and renal cancer cell lines. Among the inhibitors targeting kinases known to be associated with resistance or feedback reactivation (e.g., mTOR, P13K, AKT, MEK and IGF-1R), the mTOR inhibitor vistusertib was found most effective when combined with the PI3Kβ inhibitor AZD8186 in suppressing cell proliferation. This combination also potently suppressed tumour growth *in vivo* in PTEN-null human tumour xenograft models[68]. Biochemically, combined mTOR/PI3Kβ inhibition efficiently inhibited PI3K/AKT signalling and cellular glucose uptake in the tested cell and animal models, which explained their superior efficacy. However, given the compensatory ERK activation is a known feature of PI3Ki-associated adaptive resistance, it was unclear if this happened in response to PI3Kβ inhibition and if the combined mTOR/PI3Kβ inhibition was also effective in eliminating it. More work is required to clarify this issue. Another point to note was that despite being deficient in PTEN, the TNBC cell line MDA-MB-468 failed to show similar synergistic anti-tumour benefit from the combined mTOR/PI3Kβ inhibition, the reason for which is unclear. This suggests that PTEN loss is not a sufficient biomarker *per se*, and more accurate biomarkers are required for PI3Kβ-based combination therapy.

As mentioned previously, unlike PTEN-null BC, in PIK3CA-mutant BC the p110α isoform predominantly drives PI3K signalling instead of p110β, leading to investigation of PI3Kα inhibitors such as BYL719 as potential therapeutics for these tumours. Elkabets and co-authors found that persistently active mTORC1 signalling was responsible for resistance to BYL719 despite efficient inhibition of AKT phosphorylation by the agent[69]. Inhibition of mTORC1 reduced resistance to PI3Kα inhibitors in *in vitro* and *in vivo*[69]. Shortly after, the same group further showed that PIK3CA-mutant cancer cells sensitive to BYL719 tend to potently inhibit phosphorylation of retinoblastoma protein (RB), a substrate of CDK4/6, whereas resistant cells failed to do so[70]. As expected, combined PI3K-CDK4/6 inhibition overcame BYL719 resistance, leading to tumour regressions in PIK3CA mutant xenografts. It is important to note, however, that both of these studies relied on resistant cell models established from prolonged exposure to BYL719, and so the observed resistance may involve epigenetic changes beyond adaptive network rewiring. Whether mTORC1 activation and/or RB phosphorylation take place dynamically in treatment-naïve PIK3CA-mutant cancer cells following p110α inhibition is unclear and requires further study.

Overcoming adaptive kinome response to PI3K inhibition through BET inhibition

It has become clear from the above studies that similar to MEK inhibition, inhibition of the PI3K signalling pathway also triggers induction of a whole host of RTKs, many of which are also induced by MEKi. In light of the effectiveness of BET inhibition as a way to prevent RTK programming following MEKi, the use of BET inhibitors as part of combination therapies have been also explored in PI3K-driven tumours. Consistent with previous work, Stratikopoulos *et al.*[71] showed that PI3K inhibition induces feedback activation of upstream RTKs and quick rebound of PI3K pathway activity. Importantly, they showed that BRD4 is key for these RTKs activation, with increased BRD4 occupancy observed at conserved regions

upstream from the transcriptional start site of multiple RTKs and *MYC*, which was blocked by treatment with the BET inhibitor MS417 [Figure 4B]. Consequently, BET inhibitors inhibited the activation of AKT, mTOR, and MYC due to PI3K inhibition, and combined PI3K-BET inhibition sustained PI3K pathway inhibition and enhanced tumour cell killing in a variety of tumour models, including prostate cancer, melanoma and TNBC[71]. In another study, BET inhibition was also able to suppress lapatinib-induced transcriptional induction of a large portion of tyrosine kinases including those identified to contribute to growth (HER3, DDR1, FGFR2 and MET) in HER2+ BC cells[72], preventing downstream SRC/FAK signalling and AKT reactivation.

Taken together, these findings suggest that combined kinase and epigenetic targeting can be a broader, more efficacious strategy to circumvent feedback-mediated resistance from inhibition of other kinases besides PI3K. This approach prevents adaptive resistance via kinome reprogramming by blocking transcription, generating the necessary sustained pathway inhibition, as well as overcoming the issue of heterogeneity in the adaptive kinome reprogramming response. Despite these promising results, further work will be required in additional models and in human clinical trials to determine the efficacy and safety of combining BET and PI3K inhibitors.

Other adaptive resistance mechanisms to PI3K-AKT-mTOR signalling inhibition

Besides the PI3K and ERK pathways, other signalling pathways have been implicated in mediating network remodelling and adaptive resistance to PI3K signalling inhibition. Dual PI3K/mTOR inhibition using BE2235 was shown to induce IRS1-dependent activation of JAK2/STAT5 signalling, possibly via disruption of the mTORC1-IRS1 negative feedback[73]. In addition, BE2235 led to secretion of the pro-metastatic cytokine IL-8 that further activates JAK2/STAT5, driving resistance in TNBC. Accordingly, co-inhibition of PI3K/mTOR and JAK2 synergistically reduced cancer cell number and tumour growth, and also decreased tumour metastatic spread. In line with this finding, another study revealed that acquired resistance to PI3K inhibitors is mediated by feedback activation of IL6-STAT3 signalling, which triggered EMT and metastatic potential in human BC cells[74].

In ER-positive BC, it has been recently shown that ER drives PI3K/AKT feedback activation induced by mTORC1 inhibition[75]. Inhibition of ER, IGF-1R/IR, or IRS-1/2 prevented the mTORC1 inhibition-induced AKT activation. This work suggests a strong rationale for combinations of anti-estrogens and mTORC1 inhibitors for ER-driven BC. Indeed, everolimus has been approved for treatment of recurrent/metastatic ER+ BC together with the aromatase inhibitor (AI) exemestane[76].

While most of the adaptive resistance mechanisms discussed so far, are related to compensatory signalling activation mediated by phosphorylation, Clement *et al.*[77] recently discovered a novel ubiquitin-based mechanism of adaptive resistance to PI3K inhibition. They found that in a subset of TNBC cell lines, PI3K inhibition, by BKM120 or PIK3CA depletion, ultimately promoted AKT reactivation in a manner partially dependent on the E3 ubiquitin ligase Skp2. Importantly, Skp2 expression robustly increased following PI3K inhibition, and levels of both Skp2 expression and AKT ubiquitination correlated with resistance to PI3K inhibitors. Depletion of Skp2 reduced AKT ubiquitination and activity, and inhibited the progression of BKM120-resistant BC xenografts[77]. Although the exact reason for PI3K inhibition-induced Skp2 expression is not yet clear, this could be due to inactivation of FOXO-mediated suppression or Skp2, and/or activation of Notch1, a known inducer of Skp2 [Figure 4C]. Given the complex feedback structure of this network, what is also unclear is the order of events leading to AKT reactivation following BKM120 treatment. Nevertheless, this study has unveiled a new PI3K-independent mechanism of adaptive resistance involving ubiquitin signalling. As ubiquitin is a major mediator of non-proteolytic cell signalling, we suspect this finding is only the tip of an iceberg of ubiquitin-related resistance mechanisms still to be discovered.

APPLICATION OF COMPUTATIONAL SYSTEMS MODELLING TO DECIPHER DRUG-INDUCED NETWORK REWIRING AND IDENTIFY EFFECTIVE DRUG COMBINATIONS

The experimental studies above (and others not discussed here due to space limitation), have revealed remarkable complexity into the mechanisms of targeted drug-induced network rewiring, which are highly diverse, dynamic and context-specific. This phenomenon reflects, in part, the presence of complex pathway crosstalk, intertwined positive and negative feedback loops, and post-translational modifications that together make signalling networks incredibly plastic and highly nonlinear. In-depth understanding of network remodelling therefore requires an ability to quantitatively describe drug-affected signalling-transcriptional networks and their dynamic behaviours overtime, which extends beyond experimental approaches alone. To this end, we believe systems-based approaches that integrate mathematical network modelling with experimental work will be essential for systematic interrogation of feedback and crosstalk disruption, dynamic drug response and ultimately drug-mediated network rewiring[78-83]. Mathematical models offer useful abstractions and powerful quantitative frameworks that enable us to validate our intuitive understanding, and gain new insights into these complex processes through formal analysis and predictive simulations[84-87].

Moreover, mathematical modelling and model-based analysis can rationally inform suitable therapeutic targets and new drug combinations. While it is much more costly and practically challenging to screen vast number of possible target/drug combinations experimentally, predictive modelling, in principle, can be exploited to narrow down myriad possibilities and prioritise optimal combinations, thereby focusing experimental efforts only on these lead candidates[88]. We have recently demonstrated the validity of these concepts through model-based analysis of drug-induced signalling rebound in TNBC cells, and development of a computational drug combinations identication pipeline that enables *in silico* screening of numerous pair-wise drug combinations directed at signalling nodes and the ability to rank them by synergistic potential[89]. Applying this pipeline to a new mathematical model of EGFR signalling in TNBC led to predictions that combined inhibition of EGFR with PYK2, and to a lesser extent MET, displayed potent synergistic effects in suppressing oncogenic signalling. Experimental validation in TNBC cell lines and tumour xenograft confirmed these model predictions[41,89]. Further, unlike machine learning based approaches to drug combination discovery which often treat the target system as black-boxes[90], dynamic modelling has the ability to offer mechanistic reasoning behind the synergistic effect of effective drug combinations, which are critical for assessing their application under different cellular contexts. Indeed, time-course simulations showed that EGFR-PYK2 co-inhibition was synergistic because it eliminated the adverse network rewiring and reactivation of STAT3 and ERK caused by either EGFR or PYK2 inhibition alone[89].

The heterogeneity between cancer patients and their tumours leading to heterogeneous drug-induced network response poses a significant challenge for personalised cancer treatment. Here, mathematical modelling of biochemical networks further provides an effective approach to capture the patient-to-patient heterogeneity through incorporation of patient-specific - omics data and generation of patient-specific models[91,92]. These models can then be used to predict drug response[91,93,94], design rational drug combinations[92,95] and identify potential predictive biomarkers[91,92] in a personalised manner. More interestingly, dynamic outputs from these computational network models can themselves serve as biomarkers[96] that may be integrated with classical genes or protein-centric biomarkers for better personalisation of the treatment options. While mathematical modelling has been a highly useful tool for gaining systems-level understanding of signalling networks over the past decade, we believe future research priority should be placed on harnessing the translational capability of these models.

CONCLUDING REMARKS

This review has provided an integrative summary on the known mechanisms of adaptive resistance to inhibitors targeting the PI3K and RAS-MAPK pathways in BC (see Table 1 for a list of the major studies

Table 1. Summary of selected network rewiring mechanisms in response to targeted inhibition discussed in this review

Targets	Drug agents	Rewiring mechanisms	Resistance-overcoming strategies	Ref.
MEK	U0126	Activated PI3K/AKT signalling, via MEK-EGFR-PI3K negative feedback	Combined MEK + PI3K inhibition	[26,27]
MEK	Selumetinib	Activated AKT signalling, via MEK/ERK-ERBB3-PI3K negative feedback	Combined MEK + ERBB3 inhibition	[30]
MEK	Trametinib	Upregulation/activation of multiple RTKs, via c-Myc degradation	Combined MEK + RTKs inhibition	[8]
MEK	Trametinib	Increased genome-wide BRD4-density enhancers leading to upregulation of multiple RTKs	Combined MEK + BET inhibition	[9]
MEK	MEK inhibitors	Activation of SHP2 signalling	Combined MEK + SHP2 inhibition	[33-37]
MEK	Trametinib	Reduced proteolytic shedding of multiple RTKs (AXL, HER4, MET), leading to incresed mitogenic signaling	Combined MEK + AXL inhibition	[39]
EGFR	Gefitinib	Enhanced HER3 signalling via PYK2	Combined EGFR + PYK2 inhibition	[41]
mTOR	Rapamycin	Activated IGF1R/IR via mTORC1-IRS1 negative feedback	Combined mTORC1 + IGF1R inhibition	[49]
PI3K/AKT	XL147 (Pilaralisib), BKM120 or AKT inhibitors	Upregulation and activation of RTKs (HER3, IR, IGF1R and FGFRs), partly via AKT-FOXO-RTKs negative feedback	Combined PI3K + specific RTK (e.g., HER3) inhibition	[50,52]
mTOR	Rapamycin	ERK activation via mTORC1-PI3K-Ras feedback	Combined mTORC1 and MAPK inhibition	[60]
PI3K/mTOR	BEZ235	ERK activation via ERBBs	Combined PI3K/mTOR and HER2/3 antagonists	[61]
PI3Kβ	AZD8186	IGF1R	Combined PI3Kβ + PI3Kα or PI3Kβ + IGF1R/IR inhibition	[66]
PI3K	PI3K inhibitors	Increased BRD4 occupancy at conserved regions upstream from the transcriptional start site of multiple RTKs and MYC	Combined PI3K + BET inhibition	[71]
PI3K/mTOR	BEZ235	IRS1-dependent activation of JAK2/STAT5 signalling	Combined PI3K/mTOR and JAK2	[73]
PI3K	BKM120	AKT reactivation via Skp2	Combined PI3K + Skp2 inhibition	[77]

discussed). While these mechanisms appeared diverse in nature, several key themes have emerged. First, adaptive resistance occurs extremely quickly. Network-mediated activation of compensatory oncogenic signalling typically happens within hours of drug treatment in cancer cell lines. Although more work is required to monitor drug response *in vivo*, drug-induced network rewiring likely occurs in hours to days in animal models or patients, which is still much more rapid relative to the time typically needed for development of resistance due to genetic changes. This highlights the importance of the timing of drug combinations, which have been under-appreciated and under-studied so far. The fast timescale associated with adaptive resistance also implies the "wait-and-see" treatment strategies are not appropriate, and instead new treatments, such as combinatorial therapy, should predictively and pre-emptively prevent network adaptation before it takes place. Second, upregulation of RTKs is a recurring theme that applies to inhibitors targeting both pathways. Remarkably, common sets of RTKs tend to be induced by distinct inhibitors, indicating different inhibitors may utilise similar transcriptional machinery for RTK induction. Supporting this notion, combination of kinase inhibitors with epigenetic inhibitors such as those targeting BET have been shown to yield broad efficacy. It is likely that BET inhibitors may also be useful as part of combination treatments along with inhibitors for kinases other than those in the PI3K or ERK pathways. Third, adaptive resistance is primarily mediated by disruption of negative feedback loops. These feedbacks may have evolved to control important aspects of cell biology in non-transformed contexts[97], but are hijacked by cancer cells to evade the drug effect. Moreover, although the studies reviewed here tend to focus on isolated feedback mechanisms, it is almost certain that they work together in any specific tumour setting, likely at differing intensities. Understanding which feedback (or combination of feedbacks) is dominant under which context(s) in mediating resistance will be critical in designing effective combination therapy to overcome it.

In addition to sharing common features, specific mechanisms of adaptive resistance also display distinct properties depending on the targets and/or specific inhibitors used. For example, PI3K and AKT inhibition may trigger very different rewiring mechanisms by invoking different feedback loops. Importantly, many of the issues raised here can only be understood at the network level aided by mathematical

and computational models of these networks. Thus, systems approaches that embrace predictive and quantitative modelling will be essential for future research into understanding network-mediated adaptive resistance and developing therapeutic strategies to combat adaptive resistance.

DECLARATIONS

Authors' contributions

Conceived the review: Nguyen LK
Wrote the manuscript: Cremers CG, Nguyen LK

Availability of data and materials

Not applicable.

Financial support and sponsorship

This work was supported by the Victorian Cancer Agency Mid-Career Research Fellowship (MCRF18026) and the Cancer Council Victoria Grant in Aid, Ref. No. 1123892CC awarded to Lan K Nguyen (Nguyen LK).

Conflicts of interest

Both authors declared that there are no conflicts of interest.

Ethical approval and consent to participate

Not applicable.

Consent for publication

Not applicable.

Copyright

© The Author(s) 2019.

REFERENCES

1. Hanahan D, Weinberg RA. Hallmarks of cancer: the next generation. Cell 2011;144:646-74.
2. Rueff J, Rodrigues AS. Cancer drug resistance: a brief overview from a genetic viewpoint. Methods Mol Biol 2016;1395:1-18.
3. Housman G, Byler S, Heerboth S, Lapinska K, Longacre M, et al. Drug resistance in cancer: an overview. Cancers (Basel) 2014;6:1769-92.
4. Kobayashi S, Boggon TJ, Dayaram T, Janne PA, Kocher O, et al. EGFR mutation and resistance of non-small-cell lung cancer to gefitinib. N Engl J Med 2005;352:786-92.
5. Shah NP, Tran C, Lee FY, Chen P, Norris D, et al. Overriding imatinib resistance with a novel ABL kinase inhibitor. Science 2004;305:399-401.
6. Gorre ME, Mohammed M, Ellwood K, Hsu N, Paquette R, et al. Clinical resistance to STI-571 cancer therapy caused by BCR-ABL gene mutation or amplification. Science 2001;293:876-80.
7. Recupero D, Daniele L, Marchio C, Molinaro L, Castellano I, et al. Spontaneous and pronase-induced HER2 truncation increases the trastuzumab binding capacity of breast cancer tissues and cell lines. J Pathol 2013;229:390-9.
8. Duncan JS, Whittle MC, Nakamura K, Abell AN, Midland AA, et al. Dynamic reprogramming of the kinome in response to targeted MEK inhibition in triple-negative breast cancer. Cell 2012;149:307-21.
9. Zawistowski JS, Bevill SM, Goulet DR, Stuhlmiller TJ, Beltran AS, et al. Enhancer remodeling during adaptive bypass to MEK inhibition is attenuated by pharmacologic targeting of the P-TEFb complex. Cancer Discov 2017;7:302-21.
10. Tao Z, Shi A, Lu C, Song T, Zhang Z, et al. Breast cancer: epidemiology and etiology. Cell Biochem Biophys 2015;72:333-8.
11. Sorlie T, Perou CM, Tibshirani R, Aas T, Geisler S, et al. Gene expression patterns of breast carcinomas distinguish tumor subclasses with clinical implications. Proc Natl Acad Sci U S A 2001;98:10869-74.
12. Perou CM, Sorlie T, Eisen MB, van de Rijn M, Jeffrey SS, et al. Molecular portraits of human breast tumours. Nature 2000;406:747-52.
13. Sanchez-Vega F, Mina M, Armenia J, Chatila WK, Luna A, et al. Oncogenic signaling pathways in the cancer genome Atlas. Cell 2018;173:321-37.e10.
14. Lemmon MA, Schlessinger J. Cell signaling by receptor tyrosine kinases. Cell 2010;141:1117-34.
15. Tokunaga E, Oki E, Egashira A, Sadanaga N, Morita M, et al. Deregulation of the Akt pathway in human cancer. Curr Cancer Drug Targets 2008;8:27-36.

16. Lopez-Knowles E, O'Toole SA, McNeil CM, Millar EK, Qiu MR, et al. PI3K pathway activation in breast cancer is associated with the basal-like phenotype and cancer-specific mortality. Int J Cancer 2010;126:1121-31.
17. Stephens PJ, Tarpey PS, Davies H, Van Loo P, Greenman C, et al. The landscape of cancer genes and mutational processes in breast cancer. Nature 2012;486:400-4.
18. Shapiro P. Ras-MAP kinase signaling pathways and control of cell proliferation: relevance to cancer therapy. Crit Rev Clin Lab Sci 2002;39:285-330.
19. Corkery B, Crown J, Clynes M, O'Donovan N. Epidermal growth factor receptor as a potential therapeutic target in triple-negative breast cancer. Ann Oncol 2009;20:862-7.
20. Hoadley KA, Weigman VJ, Fan C, Sawyer LR, He X, et al. EGFR associated expression profiles vary with breast tumor subtype. BMC Genomics 2007;8:258.
21. Dent R, Trudeau M, Pritchard KI, Hanna WM, Kahn HK, et al. Triple-negative breast cancer: clinical features and patterns of recurrence. Clin Cancer Res 2007;13:4429-34.
22. Crown J, O'Shaughnessy J, Gullo G. Emerging targeted therapies in triple-negative breast cancer. Ann Oncol 2012;23 Suppl 6:vi56-65.
23. Kalimutho M, Parsons K, Mittal D, Lopez JA, Srihari S, et al. Targeted therapies for triple-negative breast cancer: combating a stubborn disease. Trends Pharmacol Sci 2015;36:822-46.
24. Rinehart J, Adjei AA, Lorusso PM, Waterhouse D, Hecht JR, et al. Multicenter phase II study of the oral MEK inhibitor, CI-1040, in patients with advanced non-small-cell lung, breast, colon, and pancreatic cancer. J Clin Oncol 2004;22:4456-62.
25. Adjei AA, Cohen RB, Franklin W, Morris C, Wilson D, et al. Phase I pharmacokinetic and pharmacodynamic study of the oral, small-molecule mitogen-activated protein kinase kinase 1/2 inhibitor AZD6244 (ARRY-142886) in patients with advanced cancers. J Clin Oncol 2008;26:2139-46.
26. Hoeflich KP, O'Brien C, Boyd Z, Cavet G, Guerrero S, et al. In vivo antitumor activity of MEK and phosphatidylinositol 3-kinase inhibitors in basal-like breast cancer models. Clin Cancer Res 2009;15:4649-64.
27. Mirzoeva OK, Das D, Heiser LM, Bhattacharya S, Siwak D, et al. Basal subtype and MAPK/ERK kinase (MEK)-phosphoinositide 3-kinase feedback signaling determine susceptibility of breast cancer cells to MEK inhibition. Cancer Res 2009;69:565-72.
28. Li X, Huang Y, Jiang J, Frank SJ. ERK-dependent threonine phosphorylation of EGF receptor modulates receptor downregulation and signaling. Cell Signal 2008;20:2145-55.
29. Yu CF, Liu ZX, Cantley LG. ERK negatively regulates the epidermal growth factor-mediated interaction of Gab1 and the phosphatidylinositol 3-kinase. J Biol Chem 2002;277:19382-8.
30. Turke AB, Song Y, Costa C, Cook R, Arteaga CL, et al. MEK inhibition leads to PI3K/AKT activation by relieving a negative feedback on ERBB receptors. Cancer Res 2012;72:3228-37.
31. Yoon YK, Kim HP, Han SW, Hur HS, Oh DY, et al. Combination of EGFR and MEK1/2 inhibitor shows synergistic effects by suppressing EGFR/HER3-dependent AKT activation in human gastric cancer cells. Mol Cancer Ther 2009;8:2526-36.
32. Ebi H, Corcoran RB, Singh A, Chen Z, Song Y, et al. Receptor tyrosine kinases exert dominant control over PI3K signaling in human KRAS mutant colorectal cancers. J Clin Invest 2011;121:4311-21.
33. Wong GS, Zhou J, Liu JB, Wu Z, Xu X, et al. Targeting wild-type KRAS-amplified gastroesophageal cancer through combined MEK and SHP2 inhibition. Nat Med 2018;24:968-77.
34. Mainardi S, Mulero-Sanchez A, Prahallad A, Germano G, Bosma A, et al. SHP2 is required for growth of KRAS-mutant non-small-cell lung cancer in vivo. Nat Med 2018;24:961-7.
35. Ruess DA, Heynen GJ, Ciecielski KJ, Ai J, Berninger A, et al. Mutant KRAS-driven cancers depend on PTPN11/SHP2 phosphatase. Nat Med 2018;24:954-60.
36. Ahmed TA, Adamopoulos C, Karoulia Z, Wu X, Sachidanandam R, et al. SHP2 Drives Adaptive Resistance to ERK Signaling Inhibition in Molecularly Defined Subsets of ERK-Dependent Tumors. Cell Rep 2019;26:65-78.e5.
37. Fedele C, Ran H, Diskin B, Wei W, Jen J, et al. SHP2 inhibition prevents adaptive resistance to MEK inhibitors in multiple cancer models. Cancer Discov 2018;8:1237-49.
38. Matalkah F, Martin E, Zhao H, Agazie YM. SHP2 acts both upstream and downstream of multiple receptor tyrosine kinases to promote basal-like and triple-negative breast cancer. Breast Cancer Res 2016;18:2.
39. Miller MA, Oudin MJ, Sullivan RJ, Wang SJ, Meyer AS, et al. Reduced proteolytic shedding of receptor tyrosine kinases is a post-translational mechanism of kinase inhibitor resistance. Cancer Discov 2016;6:382-99.
40. Tao JJ, Castel P, Radosevic-Robin N, Elkabets M, Auricchio N, et al. Antagonism of EGFR and HER3 enhances the response to inhibitors of the PI3K-Akt pathway in triple-negative breast cancer. Sci Signal 2014;7:ra29.
41. Verma N, Muller AK, Kothari C, Panayotopoulou E, Kedan A, et al. Targeting of PYK2 synergizes with EGFR antagonists in basal-like TNBC and circumvents HER3-associated resistance via the NEDD4-NDRG1 Axis. Cancer Res 2017;77:86-99.
42. Vanhaesebroeck B, Guillermet-Guibert J, Graupera M, Bilanges B. The emerging mechanisms of isoform-specific PI3K signalling. Nat Rev Mol Cell Biol 2010;11:329-41.
43. Roskoski R Jr. Properties of FDA-approved small molecule protein kinase inhibitors. Pharmacol Res 2019;144:19-50.
44. Kwitkowski VE, Prowell TM, Ibrahim A, Farrell AT, Justice R, et al. FDA approval summary: temsirolimus as treatment for advanced renal cell carcinoma. Oncologist 2010;15:428-35.
45. Massacesi C, di Tomaso E, Fretault N, Hirawat S. Challenges in the clinical development of PI3K inhibitors. Ann N Y Acad Sci 2013;1280:19-23.
46. Wee S, Wiederschain D, Maira SM, Loo A, Miller C, et al. PTEN-deficient cancers depend on PIK3CB. Proc Natl Acad Sci U S A 2008;105:13057-62.
47. Torbett NE, Luna-Moran A, Knight ZA, Houk A, Moasser M, et al. A chemical screen in diverse breast cancer cell lines reveals genetic enhancers and suppressors of sensitivity to PI3K isoform-selective inhibition. Biochem J 2008;415:97-110.

48. Chia S, Gandhi S, Joy AA, Edwards S, Gorr M, et al. Novel agents and associated toxicities of inhibitors of the pi3k/Akt/mtor pathway for the treatment of breast cancer. Curr Oncol 2015;22:33-48.
49. O'Reilly KE, Rojo F, She QB, Solit D, Mills GB, et al. mTOR inhibition induces upstream receptor tyrosine kinase signaling and activates Akt. Cancer Res 2006;66:1500-8.
50. Chakrabarty A, Sanchez V, Kuba MG, Rinehart C, Arteaga CL. Feedback upregulation of HER3 (ErbB3) expression and activity attenuates antitumor effect of PI3K inhibitors. Proc Natl Acad Sci U S A 2012;109:2718-23.
51. Brunet A, Bonni A, Zigmond MJ, Lin MZ, Juo P, et al. Akt promotes cell survival by phosphorylating and inhibiting a Forkhead transcription factor. Cell 1999;96:857-68.
52. Chandarlapaty S, Sawai A, Scaltriti M, Rodrik-Outmezguine V, Grbovic-Huezo O, et al. AKT inhibition relieves feedback suppression of receptor tyrosine kinase expression and activity. Cancer Cell 2011;19:58-71.
53. Ruiz-Saenz A, Dreyer C, Campbell MR, Steri V, Gulizia N, et al. HER2 amplification in tumors activates PI3K/Akt signaling independent of HER3. Cancer Res 2018;78:3645-58.
54. Chakrabarty A, Rexer BN, Wang SE, Cook RS, Engelman JA, et al. H1047R phosphatidylinositol 3-kinase mutant enhances HER2-mediated transformation by heregulin production and activation of HER3. Oncogene 2010;29:5193-203.
55. Garrett JT, Sutton CR, Kuba MG, Cook RS, Arteaga CL. Dual blockade of HER2 in HER2-overexpressing tumor cells does not completely eliminate HER3 function. Clin Cancer Res 2013;19:610-9.
56. Zhang J, Gao X, Schmit F, Adelmant G, Eck MJ, et al. CRKL mediates p110β-dependent PI3K signaling in PTEN-deficient cancer cells. Cell Rep 2017;20:549-57.
57. Cancer Genome Atlas Research Network, Weinstein JN, Collisson EA, Mills GB, Shaw KR, et al. The cancer genome Atlas Pan-cancer analysis project. Nat Genet 2013;45:1113-20.
58. Rexer BN, Chanthaphaychith S, Dahlman K, Arteaga CL. Direct inhibition of PI3K in combination with dual HER2 inhibitors is required for optimal antitumor activity in HER2+ breast cancer cells. Breast Cancer Res 2014;16:R9.
59. Schwarz LJ, Hutchinson KE, Rexer BN, Estrada MV, Gonzalez Ericsson PI, et al. An ERBB1-3 neutralizing antibody mixture with high activity against drug-resistant HER2+ breast cancers with ERBB ligand overexpression. J Natl Cancer Inst 2017;109.
60. Carracedo A, Ma L, Teruya-Feldstein J, Rojo F, Salmena L, et al. Inhibition of mTORC1 leads to MAPK pathway activation through a PI3K-dependent feedback loop in human cancer. J Clin Invest 2008;118:3065-74.
61. Serra V, Scaltriti M, Prudkin L, Eichhorn PJ, Ibrahim YH, et al. PI3K inhibition results in enhanced HER signaling and acquired ERK dependency in HER2-overexpressing breast cancer. Oncogene 2011;30:2547-57.
62. Will M, Qin AC, Toy W, Yao Z, Rodrik-Outmezguine V, et al. Rapid induction of apoptosis by PI3K inhibitors is dependent upon their transient inhibition of RAS-ERK signaling. Cancer Discov 2014;4:334-47.
63. Matkar S, An C, Hua X. Kinase inhibitors of HER2/AKT pathway induce ERK phosphorylation via a FOXO-dependent feedback loop. Am J Cancer Res 2017;7:1476-85.
64. Cheng H, Liu P, Ohlson C, Xu E, Symonds L, et al. PIK3CA(H1047R)- and Her2-initiated mammary tumors escape PI3K dependency by compensatory activation of MEK-ERK signaling. Oncogene 2016;35:2961-70.
65. Sato N, Wakabayashi M, Nakatsuji M, Kashiwagura H, Shimoji N, et al. MEK and PI3K catalytic activity as predictor of the response to molecularly targeted agents in triple-negative breast cancer. Biochem Biophys Res Commun 2017;489:484-9.
66. Schwartz S, Wongvipat J, Trigwell CB, Hancox U, Carver BS, et al. Feedback suppression of PI3Kalpha signaling in PTEN-mutated tumors is relieved by selective inhibition of PI3Kbeta. Cancer Cell 2015;27:109-22.
67. Costa C, Ebi H, Martini M, Beausoleil SA, Faber AC, et al. Measurement of PIP3 levels reveals an unexpected role for p110beta in early adaptive responses to p110alpha-specific inhibitors in luminal breast cancer. Cancer Cell 2015;27:97-108.
68. Lynch JT, Polanska UM, Hancox U, Delpuech O, Maynard J, et al. Combined inhibition of PI3Kbeta and mTOR inhibits growth of PTEN-null tumors. Mol Cancer Ther 2018;17:2309-19.
69. Elkabets M, Vora S, Juric D, Morse N, Mino-Kenudson M, et al. mTORC1 inhibition is required for sensitivity to PI3K p110alpha inhibitors in PIK3CA-mutant breast cancer. Sci Transl Med 2013;5:196ra99.
70. Vora SR, Juric D, Kim N, Mino-Kenudson M, Huynh T, et al. CDK 4/6 inhibitors sensitize PIK3CA mutant breast cancer to PI3K inhibitors. Cancer Cell 2014;26:136-49.
71. Stratikopoulos EE, Dendy M, Szabolcs M, Khaykin AJ, Lefebvre C, et al. Kinase and BET inhibitors together clamp inhibition of PI3K signaling and overcome resistance to therapy. Cancer Cell 2015;27:837-51.
72. Stuhlmiller TJ, Miller SM, Zawistowski JS, Nakamura K, Beltran AS, et al. Inhibition of lapatinib-induced kinome reprogramming in ERBB2-positive breast cancer by targeting BET family bromodomains. Cell Rep 2015;11:390-404.
73. Britschgi A, Andraos R, Brinkhaus H, Klebba I, Romanet V, et al. JAK2/STAT5 inhibition circumvents resistance to PI3K/mTOR blockade: a rationale for cotargeting these pathways in metastatic breast cancer. Cancer Cell 2012;22:796-811.
74. Yang L, Han S, Sun Y. An IL6-STAT3 loop mediates resistance to PI3K inhibitors by inducing epithelial-mesenchymal transition and cancer stem cell expansion in human breast cancer cells. Biochem Biophys Res Commun 2014;453:582-7.
75. Yang W, Schwartz GN, Marotti JD, Chen V, Traphagen NA, et al. Estrogen receptor alpha drives mTORC1 inhibitor-induced feedback activation of PI3K/AKT in ER+ breast cancer. Oncotarget 2018;9:8810-22.
76. Yardley DA, Noguchi S, Pritchard KI, Burris HA 3rd, Baselga J, et al. Everolimus plus exemestane in postmenopausal patients with HR(+) breast cancer: BOLERO-2 final progression-free survival analysis. Adv Ther 2013;30:870-84.
77. Clement E, Inuzuka H, Nihira NT, Wei W, Toker A. Skp2-dependent reactivation of AKT drives resistance to PI3K inhibitors. Sci Signal 2018;11.
78. Nguyen LK, Kholodenko BN. Feedback regulation in cell signalling: lessons for cancer therapeutics. Semin Cell Dev Biol 2016;50:85-94.
79. Fabian Z, Taylor CT, Nguyen LK. Understanding complexity in the HIF signaling pathway using systems biology and mathematical

modeling. J Mol Med (Berl) 2016;94:377-90.
80. Nguyen LK. Dynamics of ubiquitin-mediated signalling: insights from mathematical modelling and experimental studies. Brief Bioinform 2016;17:479-93.
81. Shin S, Nguyen LK. Dissecting cell-fate determination through integrated modelling of the ERK/MAPK signalling pathway. ERK Signaling: Methods Molecular Biology; 2016.
82. Kolch W, Halasz M, Granovskaya M, Kholodenko BN. The dynamic control of signal transduction networks in cancer cells. Nat Rev Cancer 2015;15:515-27.
83. Claas AM, Atta L, Gordonov S, Meyer AS, Lauffenburger DA. Systems modeling identifies divergent receptor tyrosine kinase reprogramming to MAPK pathway inhibition. Cell Mol Bioeng 2018;11:451-69.
84. Romano D, Nguyen LK, Matallanas D, Halasz M, Doherty C, et al. Protein interaction switches coordinate Raf-1 and MST2/Hippo signalling. Nat Cell Biol 2014;16:673-84.
85. Byrne KM, Monsefi N, Dawson JC, Degasperi A, Bukowski-Wills JC, et al. Bistability in the Rac1, PAK, and RhoA signaling network drives actin cytoskeleton dynamics and cell motility switches. Cell Syst 2016;2:38-48.
86. Shin SY, Nguyen LK. Unveiling hidden dynamics of hippo signalling: a systems analysis. Genes 2016;7:44.
87. Varusai TM, Nguyen LK. Dynamic modelling of the mTOR signalling network reveals complex emergent behaviours conferred by DEPTOR. Sci Rep 2018;8:643.
88. Fitzgerald JB, Schoeberl B, Nielsen UB, Sorger PK. Systems biology and combination therapy in the quest for clinical efficacy. Nat Chem Biol 2006;2:458-66.
89. Shin SY, Muller AK, Verma N, Lev S, Nguyen LK. Systems modelling of the EGFR-PYK2-c-Met interaction network predicts and prioritizes synergistic drug combinations for triple-negative breast cancer. PLoS Comput Biol 2018;14:e1006192.
90. Feala JD, Cortes J, Duxbury PM, Piermarocchi C, McCulloch AD, et al. Systems approaches and algorithms for discovery of combinatorial therapies. Wiley Interdiscip Rev Syst Biol Med 2010;2:181-93.
91. Fey D, Halasz M, Dreidax D, Kennedy SP, Hastings JF, et al. Signaling pathway models as biomarkers: patient-specific simulations of JNK activity predict the survival of neuroblastoma patients. Sci Signal 2015;8:ra130.
92. Shin SY, Müller AK, Verma N, Lev S, Nguyen LK. Systems modelling of the EGFR-PYK2-c-Met interaction network predicts and prioritizes synergistic drug combinations for triple-negative breast cancer. PLoS Comput Biol 2018;14:e1006192.
93. Li XM, Mohammad-Djafari A, Dumitru M, Dulong S, Filipski E, et al. A circadian clock transcription model for the personalization of cancer chronotherapy. Cancer Res 2013;73:7176-88.
94. Faratian D, Goltsov A, Lebedeva G, Sorokin A, Moodie S, et al. Systems biology reveals new strategies for personalizing cancer medicine and confirms the role of PTEN in resistance to trastuzumab. Cancer Res 2009;69:6713-20.
95. Nguyen LK, Matallanas D, Croucher DR, von Kriegsheim A, Kholodenko BN. Signalling by protein phosphatases and drug development: a systems-centred view. FEBS J 2013;280:751-65.
96. Kolch W, Fey D. Personalized computational models as biomarkers. J Pers Med 2017;7:E9.
97. Nguyen LK, Kholodenko BN. Feedback regulation in cell signalling: Lessons for cancer therapeutics. Semin Cell Dev Biol 2016;50:85-94.